

UNIVERSITA' DEGLI STUDI DI NAPOLI
"FEDERICO II"



DOTTORATO DI RICERCA IN "SCIENZA DEL FARMACO"
XXIV CICLO 2008-2011

ISOLATION AND STRUCTURE ELUCIDATION OF
BIOACTIVE SECONDARY METABOLITES
FROM MARINE AND TERRESTRIAL ORGANISMS

Dr. Giuseppina Chianese

Tutor

Prof. O. Taglialatela-Scafati

Coordinatore

Prof.ssa M. V. D'Auria

INDEX

Abstract (English)	page 5
Abstract (Italian)	page 7
CHAPTER I - INTRODUCTION	page 9
1.1. Natural Products Chemistry	page 9
1.1.1 An historical perspective.....	page 10
1.1.2 Marine Natural Products	page 13
1.2. Structural determination methods	page 14
1.2.1 Mass spectrometry	page 15
1.2.2 Nuclear Magnetic Resonance.....	page 17
1.3. Methods for configuration determination	page 18
1.3.1 Circular Dichroism.....	page 19
1.3.2 Computational methods for configuration determination.....	page 20
References	page 22
Publication of the candidate during the Ph.D. period	page 24
CHAPTER II - CANNABINOIDS: ISOLATION AND SYNTHESIS OF NEW COMPOUNDS	page 26
2.1. Phytochemistry and Medicinal Chemistry of Cannabinoids	page 26
2.1.1 Cannabigerol-type.....	page 30
2.1.2 Cannabichromene- and cannabicyclol-type	page 31
2.1.3 Cannabidiol- cannabielsoin- and cannabimovone-type	page 31
2.1.4 Tetrahydrocannabinol-type	page 34

2.1.5 Cannabicumaronone- and cannabichromanone-type	page 35
2.2. Cannabinoid receptors.....	page 36
2.3. Cannabioxepane, a novel tetracyclic cannabinoid from hemp, <i>Cannabis</i>	
<i>sativa</i> L.	page 41
2.3.1 An ancient plant	page 41
2.3.2 Extraction, isolation and structure elucidation.....	page 43
2.3.3 Affinity of the cannabioxepane for cannabinoid receptors	page 49
2.3.4 Experimental	page 51
2.4. Steroidal CB receptor ligands from the Indonesian sponge <i>Dasychalina</i>	
sp.....	page 53
2.4.1 Introduction.....	page 53
2.4.2 Extraction, isolation and structure elucidation.....	page 54
2.4.3 Preparation of semisynthetic derivatives of haplosamate A	page 56
2.4.4 Experimental	page 59
References	page 62

CHAPTER III - ISOLATION AND SYNTHESIS OF NEW	
ANTIMALARIAL COMPOUNDS	page 67
3.1. Malaria	page 67
3.2. Antimalarial endoperoxides	page 70
3.3. Synthesis of simplified antimalarial endoperoxides.....	page 78
3.3.1 <i>In vitro</i> antimalarial activity.....	page 84
3.3.2 Reaction with Fe(II) chloride.....	page 85
3.3.3 Structure-Activity Relationship Studies	page 88
3.3.4 Experimental	page 90

3.4. Antimalarial limonoids from the neem plant (<i>Azadirachta indica</i>)	page 99
3.4.1 Isolation and structure elucidation of new secondary metabolites	
.....	page 101
3.4.2 Pharmacological activity.....	page 106
3.4.3 Experimental	page 108
References	page 110

CHAPTER IV - DITERPENOIDS FROM PLANTS OF THE FAMILY

EUPHORBIACEAE

4.1. Secondary metabolites from root barks of *Jatropha curcas*.....

4.1.1 Introduction.....	page 120
4.1.2 Isolation and structure elucidation of new secondary metabolites	
.....	page 121
4.1.3 Spirocurcasone, a diterpenoid with a novel carbon skeleton	page 123
4.1.4 Pharmacological activity.....	page 127
4.1.5 Experimental	page 127

4.2. Diterpenoids from the Iranian plant *Euphorbia macroclada* Boiss. page 132

4.2.1 Introduction.....	page 132
4.2.2 Pre-myrsinane derivates	page 132
4.2.3 Tigliane derivates	page 136
4.2.4 Experimental	page 140

4.3. Diterpenoids from the Iranian plant *Euphorbia bungei* Boiss.

4.3.1 Introduction.....	page 145
4.3.2 Structure elucidation	page 145
4.3.3 Experimental	page 152

References

page 154

CHAPTER V – SUPPORTING DATA	page 157
5.1. General methods	page 157
5.2. NMR spectra	page 158
5.3. Computational details of compounds 57-63	page 176
5.4. Computational details of compound 76	page 178
ACKNOWLEDGMENTS	page 180

ABSTRACT

Natural products have historically been a rich source of “lead compounds” in drug discovery. The investigation of terrestrial plants and marine organisms aimed at searching new biologically active compounds is a central issue of this kind of studies, through structure elucidation combined with biological tests. My research work, described in this PhD thesis, is included in this research topic and was addressed at three different topics: - cannabinoids from *Cannabis sativa* and from the Indonesian sponge *Dasychalina* sp.; - isolation and synthesis of antimalarial compounds; - metabolites isolated from plants belonging to the Euphorbiaceae family (*Jatropha curcas*, *Euphorbia macroclada* and *Euphorbia bungei*).

A phytochemical investigation of the fibre cultivar of *Cannabis sativa* derived from the historical *Carmagnola* variety led to isolation of the novel spiranic stilbenoid isocannabispiradienone and the biphenyl-type cannabinoid cannabioxepane (CBX), a tetracyclic compound characterized by an unprecedented C-5/C-8' oxygen bridge and devoid of cannabinoid activity. In the same area, from the polar organic extract of the Indonesian sponge *Dasychalina* sp., I have isolated haplosamate A, a unique C₂₈ sterol containing a sulfate group at C-3 and a methyl phosphate at C-15, along with its new desulfo analogue. Both compounds, as well as their semi-synthetic analogues, have been evaluated for interaction with CB₁ and CB₂ receptors through a binding test. Desulfohaplosamate showed a selective affinity for CB₂ receptors in the low μM range. Haplosamate derivatives represent the first CB receptor ligands belonging to the class of steroids.

The search for antimalarial lead compounds is another main topic of my Ph.D. activity discussed in this thesis. On the basis of the previously developed pharmacophore of plakortin antimalarials, in this thesis I report a synthesis of a new series of simple endoperoxides, characterized by a 3-methoxy-1,2-dioxane scaffold. In particular, I have contributed to the design, the synthesis, the biological evaluation of a novel series of compounds obtained by means of an efficient one-pot three-component Mn(III)-mediated synthesis which utilizes cheap starting materials. The obtained molecules are 3,6,6-trisubstituted 3-

methoxy-1,2-dioxanes with simple alkyl chains and bearing an ester group at position 4, which were tested against *Pf*.

As part of the ongoing research aimed at finding new antimalarial leads from natural sources, I have carried out a detailed phytochemical investigation of the fruit of an African sample of *Azadirachta indica*, collected in Burkina Faso. Eight known and two new triterpenoid derivatives, named neemfruitins A and B, have been isolated from the fruits of neem, *Azadirachta indica* A. Juss., a traditional antimalarial plant used by Asian and African populations. *In vitro* antiplasmodial tests carried out with the isolated metabolites evidenced a significant activity of the known gedunin and azadirone and the new neemfruitin A, and provided useful information about the structure-antimalarial activity relationships in the limonoid class.

Finally, the chemical investigation of Euforbiaceae plants carried out during my Ph.D., and described in this thesis, led to isolation of many diterpenoids. From the root barks of *Jatropha curcas* I isolated spirocurcasone, a diterpenoid possessing the unprecedented “spirorhamnofolane” skeleton, along with 11 known and two other new diterpenoids. The absolute configuration of spirocurcasone was established using quantum mechanical calculation of the electronic circular dichroic (ECD) spectrum. Some of the isolated diterpenoids showed a potent activity against L5178Y, a mouse lymphoma cell line. The phytochemical investigation of *Euphorbia macroclada* Boiss. and *Euphorbia bungei*, led to isolation of many new diterpenoids belonging to the jatrophane and pre-myrsinane classes. The main interest in these compounds is related to their biological activity as glycoprotein-P inhibitors and so modulators of multidrug resistance in cancer chemotherapy.

The structures of all new compounds were elucidated using modern spectroscopic methods including 2D NMR and HRMS.

ABSTRACT (IN ITALIAN)

Le sostanze naturali sono da sempre una ricca fonte di composti guida per la scoperta di nuovi farmaci. Lo studio chimico di piante terrestri e organismi marini attraverso la determinazione stereostutturale di nuovi metaboliti in combinazione con la valutazione della loro attività biologica costituisce il fulcro della Chimica delle Sostanze Naturali. In tale ambito, l'attività di ricerca condotta durante il corso di Dottorato, i cui risultati sono riportati nella seguente tesi, è stata focalizzata su tre tematiche: - isolamento e semisintesi di composti attivi sui recettori dei cannabinoidi; - isolamento e sintesi di molecole dotate di azione antimalarica; - diterpeni bioattivi da piante appartenenti alla famiglia delle Euforbiaceae.

Nell'ambito della prima tematica di ricerca è stata analizzata una varietà da fibra di *Cannabis sativa*, denominata varietà *Carma*, ottenendo l'isolamento di un fitocannabinoide, denominato cannabioxepane (CBX), caratterizzato da un nuovo tipo di scheletro tetraciclico, privo di attività cannabinoide. Nella stessa area di ricerca è stato analizzato un estratto polare della spugna *Dasychalina* sp. isolando l'haplosamato A, un C₂₈ sterolo contenente un gruppo solfato ed un metilfosfato, insieme al suo nuovo desulfo-derivato. Quest'ultimo composto ha mostrato un'attività selettiva sul recettore CB₂, definendo in tal modo un nuovo chemotipo di ligandi di tale recettore.

La ricerca di nuovi composti antimalarici alternativi agli attuali farmaci in commercio è una delle principali tematiche della mia attività di ricerca, inserendomi in un ambito già avviato dal mio gruppo di ricerca. È stata dunque, progettata e realizzata una sintesi semplice ed economica, basata sull'azione catalitica di composti a base di Mn(III), di derivati 1,2-diossani dotati di buona attività antimalarica. Sono stati ottenuti una serie di derivati con una buona variabilità stereostutturale intorno al nucleo endoperossidico, requisito farmacoforico. Tutti i prodotti sono stati saggiati su ceppi di *P. falciparum* CQ-S e CQ-R. L'analisi fitochimica dei frutti di *Azadiractha indica*, una pianta tradizionale utilizzata da popolazioni asiatiche e africane, ha portato all'ottenimento di dieci limonoidi (di cui due nuovi, denominati neenfriutina A e B). Tre dei metaboliti isolati

(gedunina, azadirone e neemfruitina A) hanno mostrato un'ottima attività, fornendo inoltre preziose informazioni sulle relazioni struttura attività nella classe dei limonoidi.

Infine, nell'ambito dello studio di diterpeni da piante appartenenti alla famiglia delle Euphorbiaceae, sono state analizzate due piante appartenenti al genere *Euphorbia* (*E. macroclada* e *E. bungei*) ed una del genere *Jatropha* (*J. curcas*). L'analisi fitochimica delle prime due piante ha condotto all'isolamento di numerosi nuovi diterpeni a scheletro jatrofanico e premirsinamico, molecole biologicamente interessanti in quanto inibitori delle glicoproteina-P e quindi potenziali modulatori della multi-drug resistance nella terapia anticancro. Dall'estratto apolare di *Jatropha curcas* sono stati isolati più di dieci metaboliti, tra i quali lo spirocurcasone, un diterpene caratterizzato da un nuovo scheletro carbonioso, che è stato denominato spiro-rhamnfolano. La stereochimica di tale composto è stata valutata attraverso calcoli quantomeccanici dello spettro di dicroismo circolare elettronico (ECD). Alcuni dei diterpeni ottenuti hanno mostrato una potente attività antiproliferativa su una linea cellulare di linfoma di ratto (IC₅₀ nell'ordine nM).

La caratterizzazione stereostutturale di tutti i composti isolati o sintetizzati è stata effettuata mediante indagini spettroscopiche (UV, IR, NMR mono- e bidimensionale) e spettrometriche (ESI-MS), talvolta includendo derivatizzazioni chimiche.

CHAPTER I

INTRODUCTION

1.1. NATURAL PRODUCTS CHEMISTRY

Nature represents an endless arsenal of new bioactive molecules and the study of these metabolites has historically proven of immense benefit in the drug discovery process. The history of terrestrial natural products chemistry can readily be traced back to the beginning of the XIX century with the first investigation of terrestrial plants aimed at finding the molecules responsible of the biological activities of the extracts. This is in distinct contrast to the natural products chemistry associated with marine species which has emerged only over the past 65 years mainly as a result in the improvement of collection techniques, as SCUBA diving. Furthermore, the improvements in spectroscopic methods have historically stimulated natural products chemistry and the efforts to examine new compounds from unusual organisms rapidly and systematically. Nevertheless, natural products chemistry suffered a decline from the mid 1990's when major pharmaceutical companies disinvested in this area and switched to more "rational" combi-chem approaches.¹ In recent years Natural products chemistry began to flourish also through chemical biology and chemical genetics and the realization that natural product structures often explore structural space unavailable to combi-chem approaches. Summarizing, simple natural organisms are able to create new structures in a multitude of different ways and, thus, natural products constitute a potentially infinite source of molecular diversity, unmatched by any synthetic chemical collection or combinatorial chemistry.

Natural products have historically been a rich source of lead molecules in drug discovery. The searches for new biologically active compounds are based on microbial, plant and marine sources. The central issue of such type of studies is the structure elucidation combined with biological tests.

The research work described in this PhD thesis has been performed at the Dipartimento di Chimica delle Sostanze Naturali of Università di Napoli

"Federico II", and was addressed at different aspects of the research on marine and terrestrial natural products. My research was directed to the "core activity" of natural product chemistry, i.e. isolation and structure elucidation of new compounds accompanied by semisynthesis or total synthesis on the most interesting compounds. In particular, my research activity was addressed at three different fields:

- a) metabolites isolated from plants belonging to the Euphorbiaceae family (*Jatropha curcas*, *Euphorbia macroclada* and *Euphorbia bungei*);
- b) cannabinoids from *Cannabis sativa* and from the Indonesian sponge *Dasychalina* sp.
- c) isolation and synthesis of antimalarial compounds, c1) a phytochemical investigation of the fruit of an African sample of *Azadirachta indica*, a plant of used by African populations against malaria fever; c2) synthesis of monocyclic 1,2-dioxane derivatives, based on the plakortin scaffold. Plakortin is an endoperoxide polyketide with interesting antimalarial properties which was isolated from the marine sponge *Plakortis simplex*.

The results obtained during my Ph.D. have been reported in ten papers (listed at the end of this chapter) already published or sent for publication.

1.1.1. *An historical perspective*²⁻⁴

For centuries China led the world in the use of natural products for healing. The oldest compilation of Chinese herbs is Shen Nung Pen Ts'ao, which lists 385 materials. Pen Ts'ao Ma catalogue, written by Li-Chen during the Ming Dynasty, (1573–1620) mentions 1898 herbal drugs and 8160 prescriptions. The number of medicinal herbs used in 1979 in China numbered 5967. One of the most famous of the Chinese folk herbs is the ginseng root *Panax ginseng*, used for health maintenance and treatment of various diseases. The active principles were thought to be the saponins called ginsenosides. Another popular folk drug, the extract of the Ginkgo tree, *Ginkgo biloba* L. which can improve memory and sharpen mental alertness. Numerous psychedelic plants have been used since ancient times, producing visions, mystical fantasies, sensation of flying, etc. The Indian hemp plant, *Cannabis sativa*, has been used since 3000 BC, and it is also used as

marijuana or hashish. Its constituent, Δ^1 -THC (tetrahydrocannabinol) is responsible for its mind-altering effect. Mechoulam⁵ has been the principal worker in the cannabinoids, including structure determination and synthesis of Δ^9 -THC. During the 17th century, the Jesuits brought with them from South America the bark of the cinchona *Cinchona officinalis* (called quina-quina by the Indians) for the treatment of malaria. In 1820, Pelletier and Caventou isolated from the China tree the active compound, quinine. Alkaloids are the major constituents of the herbal plants and the extracts used for centuries, but it was not until the early nineteenth century that the active principles were isolated in pure form, for example morphine (1816), atropine (1819). It was a century later that the structures of these compounds were finally elucidated. Modern methods used to separate complex organic mixtures utilizing gas-liquid chromatography (GLC), high-pressure liquid chromatography (HPLC), and droplet counter-current (DCC) chromatography can separate samples rapidly and efficiently in the picogram range. This has been impossible until recently. Among the recent outstanding contributions to the chemistry of natural products is the conformational analysis designed by Derek Barton. Using conformational analysis, he determined the structures of many key terpenoids such as β -amyrin and cycloartenol. Robert B. Woodward was involved in the structural determinations of penicillin, strychnine, patalin, terramycin, aureomycin and the synthesis of Vitamin B12. His paper published in 1941-42 on empirical rules for estimating the absorption maxima of enones and dienes made the general organic chemical community realize that UV could be used for structural studies, thus launching the beginning of the spectroscopic revolution which soon brought on the applications of IR, NMR and MS. As chemical techniques improved, the active constituents were isolated from plants, were structurally characterized, and in due course, many were synthesized in the laboratory. Sometimes, more active better tolerated drugs were produced by chemical modification (semi-synthesis), or by total synthesis of analogues of the active principles.

The investigation on the biosynthesis, a metabolic sequences leading to various selected classes of natural products, is of pivotal importance in Natural Product Chemistry. The term natural product is generally used to mean a secondary metabolite: a small molecule that is not essential to the growth and development of the producing organism. Such compounds are found only in specific organisms,

or group of organisms, and are an expression of the individuality of species. Well over 300,000 secondary metabolites probably exist, generally classified into five categories: terpenoids and steroids, fatty acid-derived substances and polyketides, alkaloids, nonribosomal polypeptides, and shikimate derived compounds. Unraveling the biosynthetic pathways by which natural products are made is difficult and time-consuming work, but is fundamental to understand how organisms function at the molecular level. The molecules are sometimes complex, but the building blocks for their biosynthesis derived from primary metabolism. It has been established that the primary synthetic process in nature is photosynthesis by which green plants utilize the energy of the sun for the production of organic compounds from carbon dioxide. The initial products of photosynthesis are carbohydrates. Further metabolic alterations lead to the formation of a pool of organic compounds of low molecular weight and simple structures such as carboxylic- and amino acids, which are vital for the living organisms. They form the synthetic starting materials for specific, genetically controlled, enzymatically catalyzed reactions that lead to the complex compounds that characterize the secondary metabolism of plants and mammals. In many cases, a suitable cofactor, e.g. NAD^+ , PLP, HSCoA, as well as the substrate, may also be bound to participate in the transformation. Enzymes have the power to effect these transformation more efficiently and more rapidly than the chemical analogy, and also under very much milder conditions. Where relevant, they also carry out reactions in stereospecific manner. Some of the important reaction frequently encountered are alkylation, oxidation and reduction, decarboxylation, aldol and Claisen reactions.

The reaction pathway leading to a particular natural product is called the biosynthetic pathway and the corresponding event is known as biogenesis. By far the most important building blocks employed in the biosynthesis of secondary metabolites are derived from the intermediates acetyl coenzyme A (acetyl-CoA), shikimic acid, mevalonic acid, and 1-deoxyxylulose 5-phosphate. These are utilized respectively in the acetate, shikimate, mevalonate, and deoxyxylulose phosphate pathways.

1.1.2. *Marine Natural Products*

The study of marine natural products is considerably far behind that of compounds of terrestrial origin due to the difficulty in collection and identification of marine organisms. However, in spite of these difficulties, the marine environment has proven to be a very rich source of extremely potent compounds that have demonstrated significant activities in antitumor, anti-inflammatory, analgesia, immuno-modulation, allergy, and anti-viral assays.⁶ To date, more than 25,000 marine natural products have been isolated from 3,000 marine organisms and reported in about 8,000 publications (these data are referred to early 2009). Bioactive products have been isolated from animalia and plantae as well as from marine microorganisms such as bacteria and fungi, protozoa and chromista.

The oceans cover more than 70% of the earth's surface and contain more than 300,000 described species of plants and animals.^{7,8} Macroscopic plants and animals have adapted to all regions of the oceans, including polar, temperate, and tropical areas. The diversity in species is extraordinarily rich on coral reefs, where there are around 1,000 species per m² in some areas, and the Indo-Pacific Ocean has the world's greatest tropical marine biodiversity. The number and the activity of the natural products is directly related to the level of biodiversity of a marine area. The most interesting and promising marine natural products are small- to medium- molecular weight compounds produced principally by marine invertebrates (sponges, tunicates, soft corals) and microbes that have stimulated interdisciplinary studies by chemists, biologists and pharmacologists. The incredible potential of even a single marine organism to produce a large array of secondary metabolites can be interpreted by considering the common features of the secondary metabolism in all the living organisms as well as some peculiar features of the marine environment. Secondary metabolites play an essential role for the adaptation of the producer organism to the environment, mainly, but not uniquely, in terms of defence; they are practically the sole tool in the hands of organisms at lower evolutionary levels or lacking of mechanical or morphological way for protecting themselves (this is the case of sessile organisms as plants, algae, and the marine invertebrates sponges, tunicates, and bryozoans). It is now generally accepted that metabolic pathways of the secondary metabolism are intrinsically different from those characterizing the primary metabolism.

For all the reasons above summarized, it is not surprising that a thorough chemical analysis of a single marine invertebrate, carried out with non-destructive modern spectroscopic techniques (allowing the stereostructure elucidation of molecules isolated in the low milligram range) can afford tens, when not hundreds, of secondary metabolites. These products provide a rich source of chemical diversity that can be fruitfully used as a “natural combinatorial library”, frequently more rich and chemically diverse than the libraries obtained through the use of synthetic combinatorial chemistry. Ideally, this “natural library” can be screened in order to find lead compounds to be used as inspiration to design and develop new potentially useful therapeutic agents and to gain the first information about the structure-activity relationships.

In spite of the difficulties associated with the limited availability of the compounds under investigation, which is strictly related to the limited supply of the biological material correctly protected for environmental concerns, some interesting results have been obtained. Through the combined efforts of marine natural product chemists and pharmacologists, an astounding array of promising compounds have been identified. Some of these molecules are either at advanced stages of clinical trials or have been selected as promising candidates for extended pre-clinical evaluation. The majority of these products fall within the area of antimicrobial and cancer therapies. Just to cite an example, ecteinascidin 743 (ET-743), an anti-tumour compound especially effective against solid tumours, has entered the drug market in Europe.

1.2. STRUCTURAL DETERMINATION METHODS

Recently, natural products chemistry has undergone explosive growth due to advances in isolation techniques, synthetic and biosynthetic approaches as well as spectroscopic and chromatographic methods. Structural determination described in this thesis is largely based on spectroscopic techniques, mostly mass spectrometry (MS) and nuclear magnetic resonance (NMR), even if in some cases degradation methods were used. In addition, computational calculations are becoming increasingly important for the determination the stereostructure of target compound and, therefore, a short paragraph on the prediction of configuration with computational methods has been added.

1.2.1. Mass Spectrometry

Mass Spectrometry is an analytical technique, particularly used in organic chemistry, which allows to measure molecular masses of unknown compounds and thus to determine their elementary formula. Unlike other spectroscopic techniques, mass spectrometry is a destructive analytical technique, that is not based on the interaction between radiations and matter. Any molecule has first to be ionized and transferred to gas phase in the ion source and then it is transmitted to the mass analyzer where its mass properties are measured. These three fundamental step of the process occur in three different parts of the mass spectrometer, namely the *ionisation source*, the *analyser*, and the *detector*. In order to obtain a mass spectrum, in the ion source, must be produced ions in a gas-phase. they are subsequently accelerated, by an electric field, until they get to a specific speed and they are transferred to the mass analyzer, which separate different ions on the base of their mass/charge (m/z) ratio. The separated ions are then measured on the detector and the results displayed.

Most of compounds described in the following chapters have been analyzed by *Electrospray Ionisation* (ESI) mass spectrometry through an *Orbitrap* system.

ESI mass spectrometry allows the determination of non-volatile molecules to be analyzed directly from the liquid phase (**Fig.1.1**). The electrospray process is governed by a large number of chemical and physical parameters that together determine the quality of the process. Its start and end can be defined by an electrical circuit that drives the spray of liquid-charged droplets.

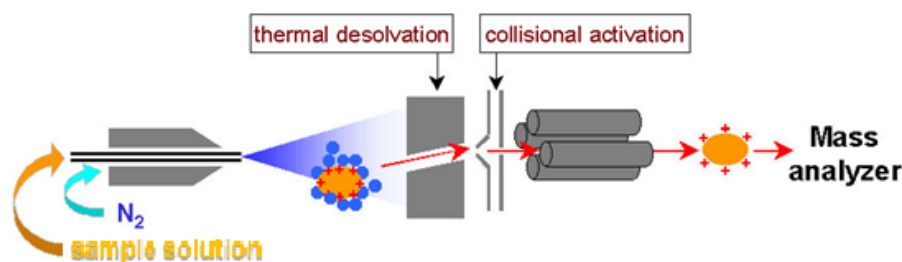


Figure 1.1. ESI mass spectrometry

In this process the biomolecule starts out as an entity or complex, usually charged and dissolved in a water-rich environment. At the end of the process the same biomolecule is represented and harvested through the orifice of a mass analyser as a series of ‘naked’ multicharged ions. In a vacuum, the biomolecular ions then are

selectively analysed according to their mass/charge ratio. Because of the electric potential of the capillary, each droplet of the spray carries an excess positive or negative charge, and this causes extensive protonation or deprotonation of the molecules of the sample, which become ions. An uncharged carrier gas such as nitrogen is used to help the liquid to nebulize and the neutral solvent in the droplets to evaporate.

Orbitrap is a new type of mass analyzer introduced by Makarov.⁹ The LTQ-Orbitrap combines the most advanced Ion Trap and Fourier Transform technologies into a single instrument with unprecedented analytical power and versatility. The instrument provides a high mass resolution, accurate mass determinations, and MSⁿ for routine high-throughput analysis.

In an orbitrap, ions are injected tangentially into the electric field between the electrodes and trapped because their electrostatic attraction to the inner electrode is balanced by centrifugal forces. Thus, ions cycle around the central electrode in rings. In addition, the ions also move back and forth along the axis of the central electrode. Therefore, ions of a specific mass-to-charge ratio move in rings which oscillate along the central spindle (**Fig.1.2**). The frequency of these harmonic oscillations is independent of the ion velocity and is inversely proportional to the square root of the mass-to-charge ratio (m/z).

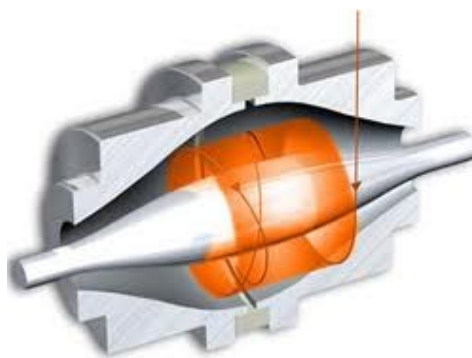


Figure 1.2. Ion trajectories in an Orbitrap mass spectrometer.

By sensing the ion oscillation similar as in the FT-MS (Fourier transform mass spectrometry), the trap can be used as a mass analyzer. Orbitraps have a high mass accuracy (1-2 ppm), a high resolving power (up to 200,000). Currently, there are two commercial LTQ-Orbitrap instruments, the Discovery and XL models. One of the primary differences is that the XL has a linear octopole collision cell (absent in the Discovery model), in which collisional activation and fragmentation can be

performed. Although this feature provides additional versatility to MS/MS experiments, the analytical performance and fundamental principles of operation of the Orbitrap analyzers in both instruments are identical.¹⁰

1.2.2 Nuclear Magnetic Resonance¹¹⁻¹³

Nuclear Magnetic Resonance spectroscopy is a powerful and theoretically complex analytical tool used for structure elucidation of the isolated secondary metabolites. It involves reorientations of nuclear spins with respect to an applied static magnetic field. In addition to standard ^1H and ^{13}C NMR spectra, a large use of 2D NMR experiments has been made in the course of my research activity. They are superior to their 1D NMR counterparts both for the information on the connection of nuclei and for the easier assignment of nuclei resonating in crowded regions of the spectra (signal overlapping is much less likely in two dimensions than in one).

The COSY (COrrrelation SpectroscopY) experiments allow you to determine the connectivity of a molecule by determining which protons are spin-spin coupled. In spite of the many modifications which have been proposed along the years, the very basic sequence composed of two $\pi/2$ pulses separated by the evolution period t_1 is still the best choice if one is simply dealing with the presence or the absence of a given coupling, but not with the value of the relevant coupling constant.

The HSQC (Heteronuclear Single Quantum Correlation) experiment is 2D NMR heteronuclear correlation experiment, in which only one-bond proton-carbon couplings ($^1J_{\text{CH}}$) are observed. The HSQC experiment correlates the chemical shift of proton with the chemical shift of the directly bonded carbon.

The HMBC (Heteronuclear Multiple Bond Correlation) experiment is a heteronuclear two- and three-bond ^1H - ^{13}C correlation experiment; its sequence is less efficient than HSQC because the involved $^{2,3}J_{\text{CH}}$ couplings are smaller (3-10Hz). Moreover, while $^1J_{\text{CH}}$ are all quite close to each other, $^{2,3}J_{\text{CH}}$ can be very different, making necessary the optimization of the experiment for each type of coupling. As a consequence, in many HMBC spectra not all of the correlation peaks which could be expected from the structure of the molecule are present. Cross peaks are between protons and carbons that are two or three bonds away while direct one-bond cross-peaks are suppressed. This experiment, finally, allow

the connection of the fragments and the assembling of the structure of the molecules.

1.3. METHODS FOR CONFIGURATION DETERMINATION

The determination of relative and absolute configuration of a natural substance is a key step in the process of its structural characterization. Only by knowing the stereochemistry of a molecule can be traced back to its three dimensional structure and approach to biological studies, e.g. studies of drug-receptor interaction, or chemical, such as the studies related to the total synthesis of complex molecules with a good activity pharmacological. Most of the natural compounds has one or more chiral centers. Usually, in the configuration determination, we start by establishing the relative configuration of chiral centers. NMR can be very useful through the values of chemical shifts (δ), coupling constants (J) and NOE effects.

The chemical shifts of protons are influenced by their chemical around, so the protons of two diastereomers have different values.

The Karplus's equation¹⁴ describes the influence of relative arrangements of protons in a molecules on the values of coupling constants (J_{H-H}).

$${}^3J = A\cos\theta^2 + B\cos\theta + C$$

This equation evidences that the values of homonuclear (${}^3J_{H-H}$) and heteronuclear (${}^3J_{C-H}$) coupling constants are related to the value of the dihedral angle θ between atoms. The superscript "3" indicates that a ${}^1\text{H}$ atom is coupled to another ${}^1\text{H}$ atom three bonds away, via H-C-C-H bonds. The magnitude of these couplings are generally smallest (0-1,5 Hz) when the torsion angle is close to 90° and largest at angles of 0 and 180° . In some cases the axial-axial coupling constant for an antiperiplanar 180° H-C-C-H configuration may be more than 9.5 Hz. Indeed for rigid cyclohexanes it is around 9-13 Hz, because the dihedral angle is close to 180° , where the orbitals overlap most efficiently.

Additional information about relative configuration of stereogenic centers can be obtained from the so-called NOE effect¹⁵ (N.O.E.: "Nuclear Overhauser Enhancement"). This effect can be observed upon irradiation, during the acquisition of the spectra, on a specific signal. In this way, the relaxation times of all the protons surrounding the irradiated proton (distance $\leq 2.5 \text{ \AA}$), even though

not belonging to the same spin system, are influenced and thus, their height changes. The NOE effect establishes a spatial relationship between substituents of fixed molecules, but this effect is dependent from the dimensions of the molecule. The ROESY (Rotating-frame Overhauser Spectroscopy) experiment is a chemical shift homonuclear correlation which can detect ROEs (Rotating-frame Overhauser Effect). ROE is similar to NOE, being related to dipolar coupling between nuclei, and depending on the geometric distance between the nuclei. While NOE is positive for small molecules and negative for macromolecules, ROE is always positive. Therefore, the ROESY experiment is particularly useful for mid-size molecules, which would show a NOE close to zero.

1.3.1 Circular Dichroism

First-principles calculations of electronic circular dichroism (ECD) are widely used to determine absolute configurations of chiral molecules. Circular Dichroism (CD) is observed when a molecule is optically active, it absorbs right- and left-handed circularly polarized light to different extents. The CD spectroscopy takes advantage of the different absorption shown by chiral compounds of left and right circularly polarized UV/Vis light. Plane polarized light can be viewed as being made up of 2 circularly polarized components of equal magnitude, one rotating counter-clockwise (left handed, L) and the other clockwise (right handed, R). Circular dichroism (CD) refers to the differential absorption of these 2 components (**Fig. 1.3**).

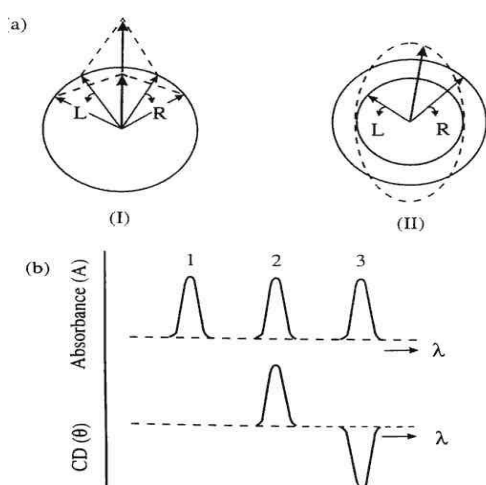


Figure 1.3. Origin of the CD effect. (a) The left (L) and right (R) circularly polarized components of plane polarized radiation: (I) the two components have the same amplitude and when combined generate plane polarized radiation; (II) the components are of different magnitude and the resultant (dashed line) is elliptically polarized. (b) The relationship between absorbance and CD spectra. Band 1 is not chiral; band 2 has a positive CD spectrum with L absorbed more than R; band 3 has a negative CD spectrum.

If, after passage through the sample being examined, the L and R components are not absorbed or are absorbed to equal extents, the recombination of L and R would regenerate radiation polarised in the original plane (**Fig. 1.3**). However, if L and R are absorbed to different extents, the resulting radiation would be said to possess elliptical polarization (**Fig. 1.3**).¹⁶

In practice, the CD instrument (spectropolarimeter) does not recombine the components but detects the two components separately; it will then display the dichroism at a given wavelength of radiation expressed as either the difference in absorbance of the two components: $\Delta\varepsilon = \varepsilon_L - \varepsilon_R$. $\Delta\varepsilon$ as a function of the incident light frequency ω is called CD spectrum.

The CD of pure enantiomers differs in sign, but not in magnitude. There is no simple relation between the absolute configuration of an enantiomer and the sign of its ECD spectrum: CD depends on details of the electronic and geometric molecular structure. However, *ab initio* electronic structure calculations are nowadays able to predict ECD accurately and thus allow an assignment of the absolute configuration by comparison of experimental and computed ECD spectra.

1.3.2. Computational methods for configuration determination

The increasing improvement of computer performances and the development of methods and algorithms ever more advanced and efficient, has led to the emergence of computational chemistry, a branch of chemistry that uses quantum mechanical principles to get the realistic representation of the three-dimensional structure of a molecule. To determine the conformation of a molecule, using a computer and a process called "minimization", the atoms must be moved from their positions evaluating the resulting changes of the total energy of the system. The geometry corresponding to the minimum energy is the most favored and, therefore, the most representative of the structure in solution. It is thus possible to compare the distances between protons in different stereoisomers and verify which of these corresponds to the spectroscopic data previously obtained. The molecular mechanics provides the force field for every molecule that describe the conformation and behavior of molecules. Force field allows to calculate the energy of each rearrangement of atoms in a system and allows you to evaluate how it changes with the position of the atoms. In this way, it is possible

to find the minimum point of this function, determining both conformation and minimum energy. This process, known as minimization, leads to a relative minimum, while the absolute minimum, in simple cases, can be found with processes known as conformational search (systematic search, random search, simulated annealing). The experimental information on the conformation of the molecule, mainly derived from NMR experiments (NOE effects) may be included in the force field to "help" to determine the actual conformation at low energy. In simulated annealing method, the molecule is subjected to a molecular dynamics simulation, starting at high temperature and gradually lowering the until get to absolute zero. At low temperatures the molecule is locked the energetically lowest conformer.

An alternative and complementary method to molecular dynamics for configuration determination of compounds structurally complex for flexibility or number of stereoisomers, is *ab initio* method that allow the prediction of chemical shifts of protons and carbons by values of coupling constants. Good matching between the calculated chemical shifts for one of the potential structures with the experimental values constitutes an excellent tool to support structural analysis of organic compounds. Density functional theory (DFT) has emerged in recent years as a promising alternative to conventional *ab initio* methods in quantum chemistry.

All calculations reported in my thesis have been performed using Gaussian 03.33¹⁷ while the preliminary conformational search was performed by Simulated Annealing in the INSIGHT II package.

References

1. V., Bankova; *Chemistry Central Journal*, **2007**, 1, 1.
2. Nakanishi, K.; A historical perspective of natural products chemistry in Barton D and Nakanishi K (eds.), *Comprehensive Natural Products Chemistry*, Vol. 2, XXI–XXXVIII, Elsevier Publishers, **1995**.
3. Ikan, R.; The origin and the nature of natural products in *Selected topics in the chemistry of natural products*, edited by Raphael Ikan, **2007**.
4. Dewick, P. M.; Medicinal Natural products, book, second edition, John Wiley & son,LTD.
5. Mechoulam, R.; Gaoni, Y.; *J Amer Chem Soc*, **1967**, 89, 4532–4552.
6. Pomponi, SA.; *J Biotechnol*, **1999**, 70, 5–13.
7. Newman, D.J.; Cragg, G. M.; *J. Nat. Prod.*, **2004**, 67 (8), 1216–1238.
8. Jimeno, JM.; *Anticancer Drugs*, **2002**, 13 (suppl 1), S15–19.
9. Hu, Q.; Noll, R. J.; Li, H.; Makarov, A.; Hardmanand, M.; Cooks, R. G.; *J. Mass Spectrom.*, **2005**, 40, 430–443.
10. Perry, R. H.; Cooks, R. G.; Noll, R. J.; *Mass Spectrometry Reviews*, **2008**, 27, 661– 69.
11. Bax, A.; Two Dimensional Nuclear Magnetic Resonance in Liquids, Delft University Press, Dordrecht, **1982**.
12. Palmer III, A. G.; Cavanagh, J.; Wright, P. E.; Rance, M.; *J. Magn. Reson*, **1991**, 151-170.
13. Bax, A.; Summers, M. F.; *J. Am. Chem. Soc*, **1986**, 2093.
14. Karplus, M.; *J. Chem. Phys.*, **1959**, 11.
15. Sanders, J. K. M.; Mersh, J. D.; *Prog. NMR Spectrosc.*, **1982**, 353.
16. Kelly, S. M.; Price, N.C.; *Current Protein and Peptide Science*, **2000**, 1, 349-384.

17. Gaussian 03-Revision B05: Frisch, M. J.; Trucks, G. W.; Schlegel, H. B.; Scuseria, G. E.; Robb, M. A.; Cheeseman, J. A.; Montgomery, Jr., J. A.; Vreven, T.; Kudin, K. N.; Burant, J. C.; Millam, J. M.; Iyengar, S. S.; Tomasi, J.; Barone, V.; Mennucci, B.; Cossi, M.; Scalmani, G.; Rega, N.; Petersson, G. A.; Nakatsuji, H.; Hada, M.; Ehara, M.; Toyota, K.; Fukuda, R.; Hasegawa, J.; Ishida, M.; Nakajima, T.; Honda, Y.; Kitao, O.; Nakai, H.; Klene, M.; Li, X.; Knox, J. E.; Hratchian, H. P.; Cross, J. B.; Bakken, V.; Adamo, C.; Jaramillo, J.; Gomperts, R.; Stratmann, R. E.; Yazyev, O.; Austin, A. J.; Cammi, R.; Pomelli, C.; Ochterski, J. W.; Ayala, P. Y.; Morokuma, K.; Voth, G. A.; Salvador, P.; Dannenberg, J. J.; Zakrzewski, V. G.; Dapprich, S.; Daniels, A. D.; Strain, M. C.; Farkas, O.; Malick, D. K.; Rabuck, A. D.; Raghavachari, K.; Foresman, J. B.; Ortiz, J. V.; Cui, Q.; Baboul, A. G.; Clifford, S.; Cioslowski, J.; Stefanov, B. B.; Liu, G.; Liashenko, A.; Piskorz, P.; Komaromi, I.; Martin, R. L.; Fox, D. J.; Keith, T.; Al-Laham, M. A.; Peng, C. Y.; Nanayakkara, A.; Challacombe, M.; Gill, P. M. W.; Johnson, B.; Chen, W.; Wong, M. W.; Gonzalez, C.; Pople, J. A. *Gaussian03W, Revision B05*, Inc., Wallingford CT, **2004**

Publications of the candidate during the Ph.D. period

1. Chianese, G.; Yerbanga, S.R.; Lucantoni, L.; Habluetzel, A.; Basilico, N.; Taramelli, D.; Fattorusso, E.; Tagliatela-Scafati, O. Antiplasmodial Triterpenoids from the Fruits of Neem, *Azadirachta indica*. *J. Nat. Prod.*, **2010**, *73*, 1448–1452.
2. Shokoohinia, Y.; Sajjadi, S.; Zolfaghari, B.; Chianese, G.; Appendino, G.; Tagliatela-Scafati, O. Diterpenoid (poly)esters and a ring A-secophorboid from the aerial parts of *Euphorbia macroclada* Boiss. *Fitoterapia*, **2010**, *81*, 884–890.
3. Shokoohinia, Y.; Chianese, G.; Zolfaghari, B.; Sajjadi, S.; Appendino, G.; Tagliatela-Scafati, O.; Macrocyclic diterpenoids from the Iranian Plant *Euphorbia bungei* Boiss. *Fitoterapia*, **2011**, *82*, 317-322.
4. Chianese, G.; Fattorusso, E.; Tagliatela-Scafati, O.; Bavestrello, G.; Calcinai, B.; Dien, H. A.; Di Marzo, V. Desulfohaplosamate, a new phosphate-containing steroid from *Dasychalina* sp., is a selective cannabinoid CB₂ receptor ligand. *Steroids*, **2011**, *76*, 998-1002.
5. Pagani, A.; Scala, F.; Chianese, G.; Grassi, G.; Appendino, G.; Tagliatela-Scafati, O. Cannabioxepane, a novel tetracyclic cannabinoid from hemp, *Cannabis sativa* L. *Tetrahedron*, **2011**, *67*, 3369-3373.
6. Appendino, G.; Chianese, G.; Tagliatela-Scafati, O. Cannabinoids: Occurrence and Medicinal Chemistry. *Curr Med Chem*, **2011**, *18*, 1085-1099.
7. Chianese, G.; Fattorusso, E.; Olapeju O. Aiyelaagbe, Luciano, P., Schroder, H. C., Muller, W. E. G.; Tagliatela-Scafati, O. Spirocurcasone, a Diterpenoid with a Novel Carbon Skeleton from *Jatropha curcas*. *Organic Letters*, **2011**, *13*, 316-319.
8. Persico, M.; Quintavalla, A.; Rondinelli, F.; Trombini, C.; Lombardo, M.; Fattorusso, C.; Azzarito, V.; Taramelli, D.; Parapini, S.; Corbett, Y.; Chianese, G.; Fattorusso, E.; Tagliatela-Scafati, O. A New Class of Antimalarial Dioxanes Obtained Through a Simple Two-Step Synthetic Approach: Rational Design and Structure-Activity Relationship Studies. *Journal of Medicinal*

Chemistry, ASAP. Publication date on web: November 4, **2011**, DOI: 10.1021/jm201056j.

9. Angawi, RF.; Bavestrello, G.; Calcinai, B.; Dien, H.; Donnarumma, G.; Tufano, M.A.; Paoletti, I.; Grimaldi, E.; Chianese, G.; Fattorusso, E.; Taglialatela Scafati, O.; Aurantoside J: a New Tetramic Acid Glycoside from *Theonella swinhoei*. Insights into the antifungal potential of Aurantosides. *Mar. Drugs*, **2011**, submitted.
10. Taglialatela-Scafati, O.; Pollastro, F.; Cicione, L.; Chianese, G.; Bellido, M. L.; Munoz, E.; Özen, H. Ç.; Toker , Z.; Appendino, G. STAT-3 Inhibiting Bisabolanes from *Carthamus glaucus* M. Bieb. *J. Nat. Prod.*, **2011**, submitted.

CHAPTER II

CANNABINOIDS: ISOLATION AND SYNTHESIS OF NEW COMPOUNDS

2.1. PHYTOCHEMISTRY AND MEDICINAL CHEMISTRY OF CANNABINOIDS

A combination of history, chemistry, pharmacology, toxicology, and deep social impact makes *Cannabis sativa* L. (hemp) a unique plant. *C. sativa* is relatively unique in taxonomic terms, since the genus *Cannabis* has only one species, and belongs to a family (*Cannabaceae*) including only two genera (*Cannabis* and *Humulus*). Various subspecies of *C. sativa* have been identified¹ but they reflect, however, mainly geographical and/or chemotypic variants of a single taxonomic entity rather than distinct species. From the medicinal point of view, two *Cannabis* phenotypes can be identified: 1) a fiber type *Cannabis*, rich of cannabidiol (CBD, **4**) and almost devoid of Δ^9 -tetrahydrocannabinol (Δ^9 -THC, **6**) (generally < 0.2% dry weight), also called hemp and used for textile or seed oil purposes, and 2) the drug type *Cannabis*, the well-known Δ^9 -THC-rich psychotropic cannabis, whose flowering tops are known as marijuana and are used to obtain hashish. The recreational use of the Δ^9 -THC-rich chemotype of *C. sativa* dates back to about 5000 years ago and constitutes now the most widely utilized illicit narcotic plant in the world. The psychotropic variety of *Cannabis* was, however, totally unknown to the ancient Mediterranean civilizations and became known in Europe only at the times of the Crusades in the XII-XIII centuries. The wealth of pharmacological activities discovered for *C. sativa* secondary metabolites make this plant one of the most thoroughly investigated from both the phytochemical and the pharmacological point of views, and, at the same time, one of the hottest topics in current medicinal chemistry research.

The chemistry of *C. sativa* is extremely complex and includes constituents belonging to the classes of polyketides, terpenoids (a mixture of about 120 mono- and sesquiterpenoids is responsible for the characteristic odour of the plant),

modified sugars, alkaloids, flavonoids, stilbenoids, and quinones. The sheer observation that more than 500 compounds have been characterized from *C. sativa* can give an idea of the phytochemical diversity of this plant. The concentration of these compounds depends on several factors including variety, age, growth conditions, harvesting time and storage conditions. Cannabinoids include about 100 (to date) meroterpenoids (prenylated polyketides) accumulated in tiny epidermal resinous glands and characterized by very specific and potent pharmacological activities. Cannabinoids exemplify the impact that natural products can have on modern medicinal chemistry and pharmacology. Investigation of cannabinoid chemistry has been an important part of the research activity during my Ph. D. and in this area I have been co-author of a review published on the journal *Current Medicinal Chemistry*.² In particular, this review aimed at giving a survey of the more recent advances in both phytochemistry of *C. sativa*, the medicinal chemistry of cannabinoids, and their distribution in plants, highlighting the impact that research in these hot fields could have for modern medicinal chemistry and pharmacology.

Cannabinoids, a class of mono- to tetracyclic C₂₁ (or C₂₂) meroterpenoids, are the most important secondary metabolites of *C. sativa*. The plant elaborates these molecules through the assemblage and subsequent modification of two building blocks coming from different biogenetic pathways, namely a C₁₂ polyketide unit and a monoterpene unit (geranyl pyrophosphate, GPP), originating from the deoxyxylulose phosphate/methylerythritol phosphate pathway. The first product of the attachment of these two units is cannabigerolic acid, which has been identified as the direct precursor (through subsequent cyclizations and rearrangements) of the most important phytocannabinoid subclasses.³ The parent compounds of these classes are cannabichromene (CBC, **2**), cannabicyclol (CBL, **3**), cannabidiol (CBD, **4**), cannabielsoin (CBE, **5**), Δ⁹-THC (**6**), and cannabicumaronone (CBCON, **7**), with the most recent additions to the cannabinoid inventory falling into the CBCON,⁴ CBC and CBG families.⁵ Despite all these studies, structural diversity within cannabinoids is far from having been exhaustively unravelled, as shown by the recent discovery of cannabimovone (CBM, **8**, Fig. 2.1).⁶

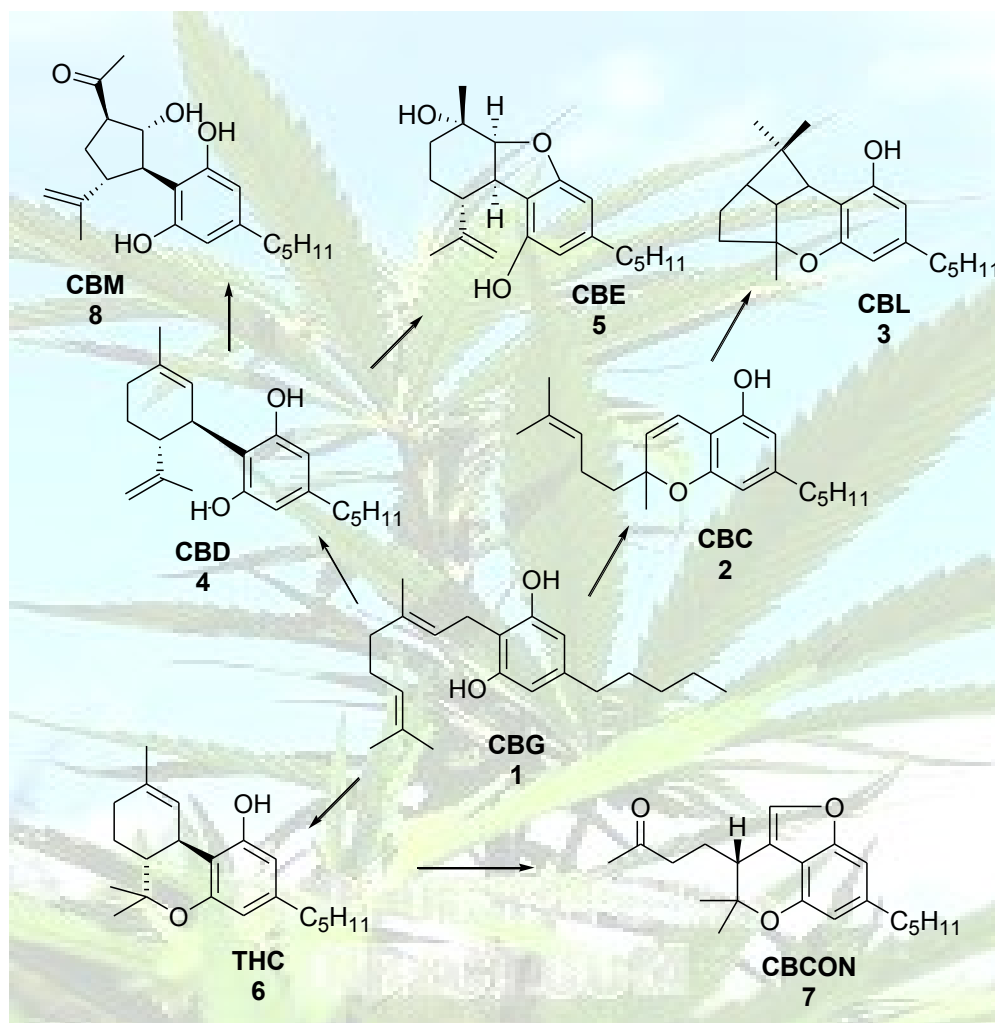


Figure 2.1. The parent compounds of the cannabinoid structural classes and their demonstrated or postulated biogenetic relationships.

The building blocks of cannabinoids, GPP and alkyl resorcinol derivatives, are very common in Nature. For example, olivetol is a common lichen constituent, while limonene, the terpenoid moiety of CBD (4), is widespread in plants. So far, only two cannabinoids (CBG, 1 and its corresponding acid) have been obtained from a non-*Cannabis* source. These compounds are accumulated by a South African *Helichrysum* (*H. umbraculigerum*)⁷ and plants from this asteraceous genus (used in traditional medicine for a host of inflammatory and anti-infective conditions) as well as liverworts have also provided compounds related to cannabinoids⁷. *Helichrysum* cannabinoids are prenylated dibenzyls bearing a close relationship with cannabinoids, from which they differ for the replacement of the *n*-pentyl (or *n*-propyl) C-3 side chain with a β -phenylethyl group (e.g. H-CBG, 9). The two classes of compounds are biogenetically related, differing only for the type of ketide starter, which is aliphatic in cannabinoids from hemp, and

aromatic in those from *Helichrysum*. Surprisingly, the bioactivity of *Helychrysum* cannabinoids has not yet been investigated, presumably due to their limited availability by isolation or by synthesis.

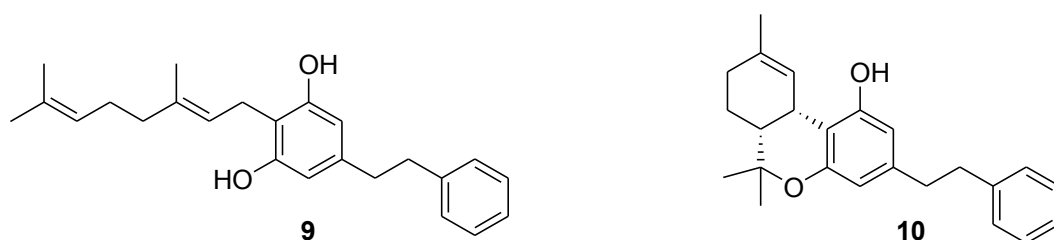
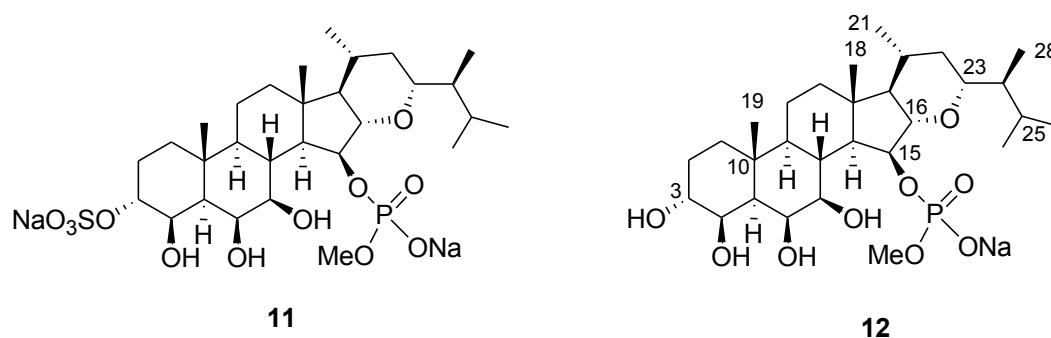


Figure 2.2. H-CBG (**9**) from *Helichrysum* and **10** from *Radula*

These prenylated bibenzyl compounds have been found also in tropical liverworts from the genus *Radula*, where they occur with their *ortho*-derivatives (abnormal cannabinoids).⁸ For example, compound **10** strictly resembles Δ^9 -THC (**6**) but no data on its binding to CB receptors are available so far.

Natural products with cannabinomimetic activity, whose structures are not related to the meroterpenoids of hemp nor to the endocannabinoids (polyunsaturated fatty acid amides or esters), are extremely rare. During my research activity, reported in this Ph.D. thesis, I have isolated haplosamate A (**11**) with its new desulfo analogue⁹ (**12**), which, to our knowledge, represents the first CB ligands belonging to the class of steroids.



The selectivity of desulfohaplosamate (**12**) for CB₂ receptor is particularly important and worthy of further investigation, given the involvement of this receptor in the immune response and inflammation¹⁰ and the lack of abuse potential and strong central effects related to the use of CB₂ ligands.

In the following paragraphs, I have reported the five most important structural classes of cannabinoids from *C. sativa*, briefly reporting and commenting on their biogenetic relationships.

2.1.1. Cannabigerol-type

As shown in **Figure 2.3**, the polyketide moiety of cannabinoids originates from *n*-hexanoylCoA through the tri-fold addition of malonyl-derived acetate units, unit, followed by cyclization and aromatization to give olivetolic acid. Condensation between olivetolic acid and GPP is catalyzed by a specific prenyltransferase identified in the expanding leaves of *C. sativa*.¹¹ The product of this reaction is cannabigerolic acid (CBGA), whose decarboxylated analogue is named cannabigerol (**1**, CBG). It is generally accepted that the decarboxylation step for CBGA and all the other cannabinoids is non-enzymatic and occurs spontaneously during either storage or extraction/purification of the compounds.

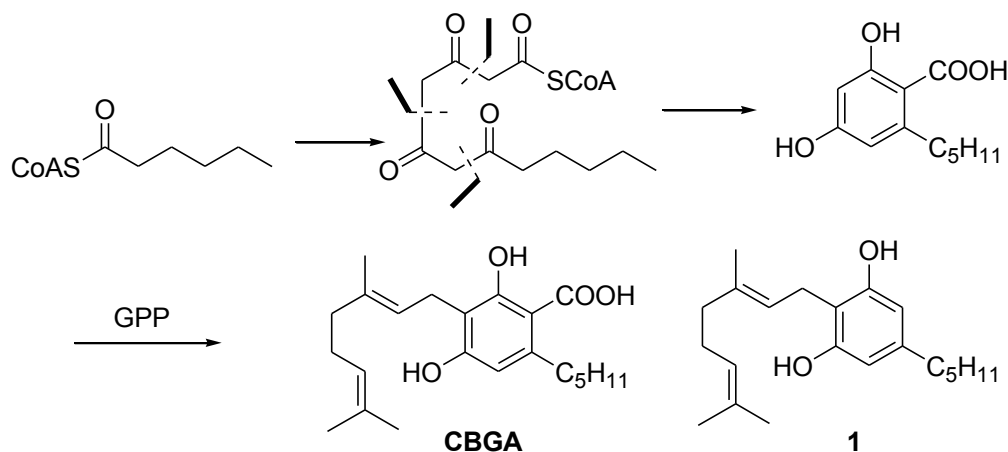


Figure 2.3. Biogenesis of cannabigerolic acid (CBGA) and cannabigerol (**1**)

A series of minor analogues of cannabigerol (**1**) showing a shorter alkyl chain attached to the phenyl ring have been found, e.g. cannabigerovarin¹² showing a linear C₃H₇ chain. These compounds (cannabivarins) could derive from either enzymatic shortening of the CBG pentyl chain or, more likely, from a shorter starter unit (butanoylCoA) for the ketide homologation. Similar shortened-side chain compounds (also with C₄ or C₁ side chains) have been found in all the other classes of cannabinoids but, for simplicity, they will not be reported here.

A CBGA analogue showing a *Z*-double bond in the prenyl unit has been isolated and named cannabinerolic acid.¹³ Carmagerol, *rac*-6',7'-dihydro,6',7'-dihydroxycannabigerol, has been obtained from the Carma variety of *C. sativa* and also identified as a possible mammalian metabolite of cannabigerol.¹⁴ Finally, a number of hydroxylated and oxidized quinone derivatives of cannabigerol have been recently reported from a high-potency Δ⁹-THC-rich variety of *C. sativa*.⁵

2.1.2. Cannabichromene- and cannabicyclol-type

The oxidative intramolecular cyclization of CBGA affords cannabichromenic acid (CBCA) and, by decarboxylation, cannabichromene (CBC, **2**, Fig.2.4). CBC is well represented in psychotropic and fiber-type varieties of *C. sativa* and has been isolated as a racemate.¹⁵ A [2 + 2] intramolecular cycloaddition of CBCA triggers the simultaneous formation of two additional rings (four- and five-membered, respectively) affording the tetracyclic system of cannabicyclolic acid (CBLA), next turned by decarboxylation into cannabicyclol¹⁶ (CBL, **3**, Fig. 2.4). It is not clear if the formation of cannabicyclol is the result of natural irradiation on the plant or it is an artifact formed in the crude extract. The photocycloaddition takes place with exquisite diastereoselectivity, and the adduct results from the approach of the terminal double bond from the face *anti* to that of the angular pyrane oxygen. Also cannabicyclol was isolated as a racemate.

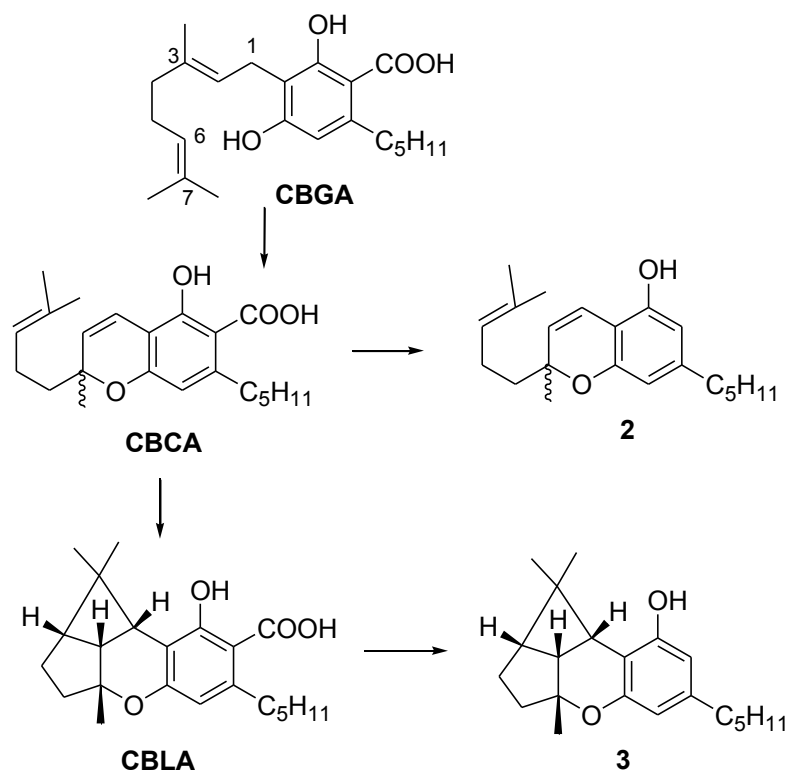


Figure 2.4. Biogenesis of cannabichromene- and cannabicyclol-type compounds

2.1.3. Cannabidiol- cannabielsoin- and cannabimovone-type

Cannabidiolic acid (CBDA) and cannabidiol (CBD, **4**) are the main constituent of the non-psychotropic (fiber-type) varieties of *C. sativa* (Fig. 2.5).

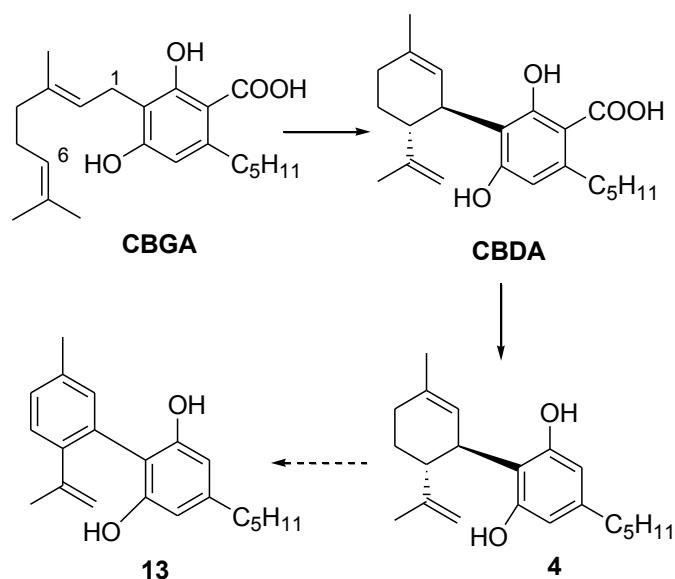


Fig. 2.5. Biogenesis of cannabidiol (**4**) and cannabinodiol (**13**)

These compounds are the result of an oxidative cyclization of CBGA, resulting in the formation of a link between C-1 and C-6 of the prenyl unit. The enzyme catalyzing this stereospecific reaction (cannabidiolic acid synthase) has been isolated and characterized.¹⁷ The aromatized analogue of CBD (**4**) is named cannabinodiol¹⁸ (**13**), and it is likely an artefact, since its concentration increases with the age of the stored plant.

Both compounds of the cannabielsoin-cannabifuran type and of the cannabimovone type likely derive from CBD (**4**, **Fig. 2.6**). Although not proven at the biochemical level, and uncharacterized in terms of enzyme(s) involved, these relationships are supported by model reactions that involve intermediates where the trisubstituted double bond of CBD has been epoxidized or dihydroxylated.

Attachment of one of the two phenolic oxygen atoms at the endocyclic double bond of the monoterpene unit generates the dihydrofuran ring of the cannabielsoin (CBE)-type compounds shown in **figure 2.6** (CBEA and **5**). These molecules have been both isolated from *C. sativa*¹⁹ but they have also been detected during studies of the mammalian metabolism of CBD.²⁰ It seems to be present a curious overlapping of cannabinoid oxygenating enzymes between *C. sativa* and mammals, as already suggested by the isolation of carmagerol, another mammalian metabolite of cannabinoids. The aromatized analogue of cannabielsoin, dihydrocannabifuran (**14**) and cannabifuran²¹ (CBF, **15**), whose presence has been demonstrated also in the smoke condensate of hashish, show a

dibenzofurane structure. Cannabielsoin is the only eponimic cannabinoid, and its name is a tribute to the technician Elsa Boyanova, who isolated it and shortly thereafter passed away.

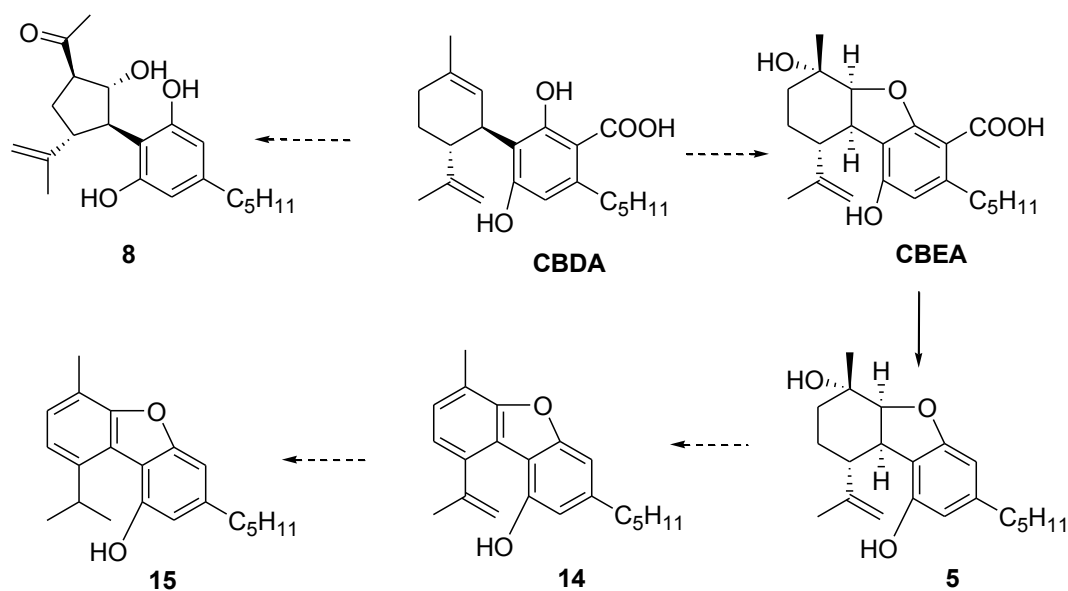


Fig. 2.6. Cannabielsoin- and cannabimovone-type compounds

The chemical investigation of a non-psychoactive variety of *C. sativa* (Carma) carried out during my Ph.D., and described in this thesis, led to isolation of cannabioxepane²² (CBX, **29**) (see below). Its new skeleton bears some relationships with some cannabinoids from the CBE family, and particularly with the aromatized analogue named cannabifuran, however, noteworthy, no member of the CBE family shows a fourth ring.

Cannabimovone (CBM, **8**), also was isolated from a non-psychoactive variety of *C. sativa* (Carma).⁶ CBM shows an unprecedented *abeo*-menthane terpenoid structure, seemingly derived from CBD (**4**) by stereoselective dihydroxylation of the endocyclic double bond, followed by oxidative cleavage of the glycol system and then aldolization of the resulting dicarbonyl intermediate. Attempts to reproduce this biogenetic scheme afforded only the cronotized analogue of CBM (**8**). Interestingly, this synthetic compound showed a biological profile similar, although less potent, to that of Δ^9 -THC (**6**), while CBM (**8**) acted as an analogue of CBD⁶ (**4**).

2.1.4. Tetrahydrocannabinol-type

Tetrahydrocannabinolic acid (THCA) and Δ^9 -tetrahydrocannabinol (Δ^9 -THC, **6**) are the main constituents of the psychotropic varieties of *C. sativa*. Although a rearrangement of CBD (**4**) precursors could seem a reasonable biogenesis for these molecules, the isolation and characterization of the specific FAD-dependent enzyme THCA synthase unambiguously demonstrated that these compounds actually derive from cyclization of CBGA through a cationic intermediate with positive charge at C-3.²³ Attachment of the phenolic oxygen at C-7 of the monoterpene unit and the linkage C-6/C-2 give rise to the tricyclic system of THCA and of its decarboxylated analogue Δ^9 -THC, **6** (for which the widely employed dibenzopyrane numbering system is indicated in **figure 2.7**).

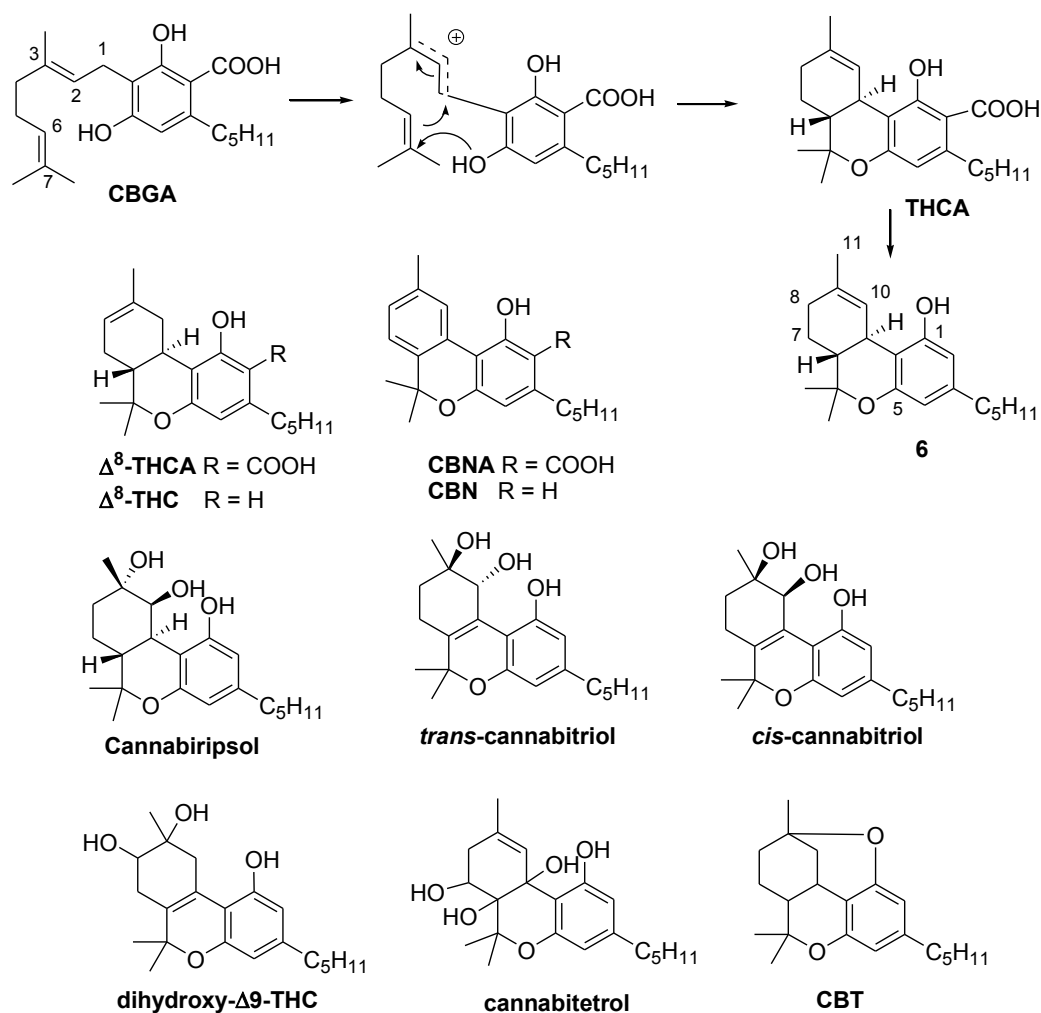


Figure 2.7. Tetrahydrocannabinol-type compounds

A number of analogues sharing this structural framework have been found. Δ^8 -THCA and the decarboxylated (Δ^8 -THC) show isomerization of the double bond, while the completely aromatized analogues are called cannabinolic acid (CBNA) and cannabinol (CBN). These molecules are thought to be artifacts since their concentration in extracts increases during storage, while simultaneously, the concentration of Δ^9 -THC decreases. The Δ^9 -THC/CBN ratio is used as indication of the age of stored marijuana samples. Hydroxylated CBNA and CBN derivatives have been recently reported.²⁴ Cannabiripsol is the dihydroxylated analogue of Δ^9 -THC,²⁵ and it differs from the *trans*- and *cis*-cannabitrinol²⁶ for a double bond at the junction with the oxygenated ring. Finally dihydroxy- Δ^9 -THC²⁷ and cannabitetrol²⁸ differ for the position and /or for the number of hydroxyl groups. Cannabicitran (CBT) is a cyclized and demethylated analogue of Δ^9 -THC.²⁹ Surprisingly, the configurational aspects of some of these oxygenated analogues of Δ^9 -THC, are still undefined and it is not clear if they were obtained in diastereomerically pure form or as mixtures. Isotetrahydrocannabinol (**16**)³⁰ is a minor cannabinoid deriving from a different cyclization mode of the cationic intermediate produced from CBGA (**Fig. 2.8**). The main difference between the two pathways is that, in this case, the phenolic oxygen atom quenches directly the carbocation.

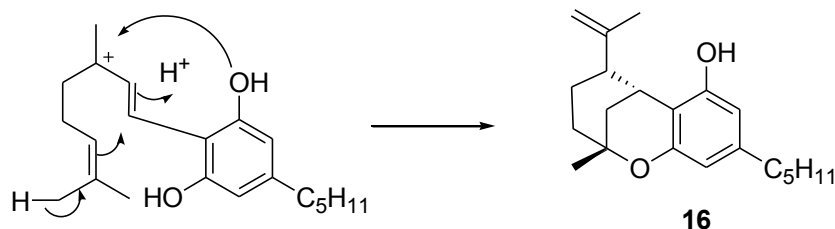


Figure 2.8. Biogenetic formation of isotetrahydrocannabinol (**16**)

2.1.5. *Cannabicumaronone- and cannabichromanone-type*

The carbon skeleton of cannabicumaronone (**7**) is, in principle, related to that of Δ^9 -THC (**6**) via the oxidative cleavage of its trisubstituted double bond (interestingly, a similar cleavage, on CBD (**4**), has been hypothesized for the formation of cannabimovone, CBM,**8**) followed by hemiacetalization/dehydration

yielding to the furan ring. A cell suspension culture of *C. sativa* has been demonstrated to be able to convert Δ^9 -THC (**6**) in cannabicumaronone (**7**).³¹

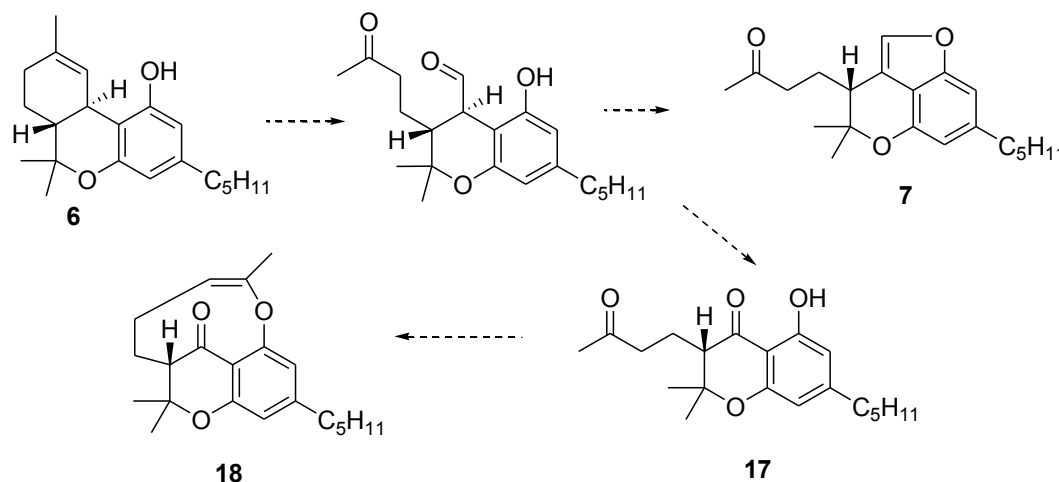


Fig. 2.9. Cannabicumaronone- and cannabichromanone-type compounds

Oxidative cleavage of the aldehyde is the likely biogenetic origin of cannabichromanone (**17**), for which a series of derivatives, including the cyclized derivative **18**, have been recently reported (**Fig. 2.9**).⁴

2.2. CANNABINOID RECEPTORS

Many of the potential therapeutic uses of cannabinoids are related to the interaction with (at least) two cannabinoid G-protein coupled receptors (CB₁ and CB₂). Cannabinoid receptors are the primary targets of endogenous cannabinoids (endocannabinoids). These G protein-coupled receptors are activated also, by two major group of ligands, plant and synthetic cannabinoids. Cannabinoid receptors play an important role in many processes, including metabolic regulation, craving, pain, anxiety, bone growth, and immune function.

Both the structure determination of Δ^9 -THC (**6**) and the discovery of a specific receptor for opioids, two scientific events of the 1960s-1970s, gave a strong impulse to the research on the cannabinoid receptors. The idea that, similarly to opioids, also the psychoactive constituents from *Cannabis* could act by interaction with a specific receptor located in the CNS, had been long dismissed, also basing

on the false assumption that Δ^9 -THC (**6**) and its enantiomer had similar mind-altering activity. Some technical difficulties (e.g. working with highly hydrophobic compounds as cannabinoids) and the lower social and health impact of cannabinoids compared to opioid-derived compounds, also contributed to slow down the research of a cannabinoid receptor. However, one of the most decisive impulse was given by the discovery, in the Pfizer labs, of CP 55,940 (**19**, **Fig. 2.10**), a synthetic molecule about 20 times more potent than Δ^9 -THC.³² The labelled version of CP 55,940 (**19**) was used to develop a binding assay for cannabinoid receptors, allowing the analysis of their distribution by quantitative autoradiography. High levels of cannabinoid receptors were found in cortex, hippocampus, amygdala, basal ganglia, and in the cerebellum.

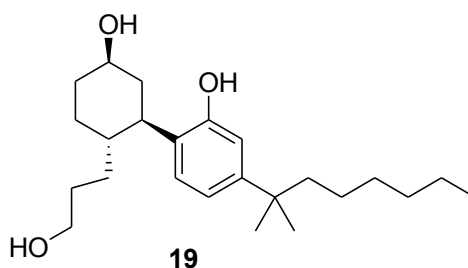


Figure 2.10. The chemical structure of CP 55,940 (**19**)

Two cannabinoid (CB) receptors have been identified and cloned to date: CB₁ and CB₂. They have a 40% of homology (CB₂ being the smallest one) and both share the heptahelical structure of G-protein coupled receptors.³³ The effect of interaction with cannabinoid receptors is mediated by a cascade of signal transduction pathways including interaction with potassium and calcium channels (for CB₁) and several kinases (e.g. MAP kinase). **Table 2.1** summarizes some selected properties of these receptors. The existence of other cannabinoid receptors different from CB₁ and CB₂ has long been pursued, since a number of cannabinoid-like effects persist in CB₁/CB₂ knockout mice. A proposed third cannabinoid receptor is the recently identified GPR55,³⁴ but its role in the pharmacological actions of Δ^9 -THC and in the physiological effects of endogenous cannabinoids are still controversial. GPR55 is activated by lysophosphatidylinositol and is expressed in human and mouse osteoclasts and

osteoblasts; it suppresses osteoclast formation but stimulates osteoclast function, exerting a pivotal role in bone physiology and turnover.

Table 2.1. Some selected features of CB₁ and CB₂ receptors.

	CB ₁	CB ₂
Type of receptor	G (G _i -G _o)-protein coupled	G (G _i -G _o)-protein coupled
Localization	Mostly CNS; Adipocytes; Kidney; Lung; Liver	Immune system cells; Spleen; CNS; Osteo-cells; Adipose tissue
Inducibility	Low inducibility	Highly inducible

The presence of cannabinoid receptors implies the existence of endogenous ligands. Mechoulam and Devane identified the first ligand molecule in 1992³⁵ and called it anandamide (**20**), from *ananda*, the Sanskrit word to describe “delight, bliss”. A number of endogenous CB₁ agonist fatty acid amides were then added to the list, while the ester derivative 2-arachidonoyl glycerol (2-AG)³⁶ (**21**) proved to be more potent than anandamide. Interestingly, virodhamine, an arachidonoyl ethanolamine where the two units are joined by an ester linkage in place of the amide linkage, is an antagonist of CB₁ receptor³⁷ and agonist of CB₂ receptor. It is highly produced in peripheral tissues express CB₂. Noladin (**22**) and other endocannabinoids have an ether-linkage in place of the ester linkage between the polar head and the apolar tail. Remarkably, all endocannabinoids (**Fig. 2.11**) described to date are either chemical unstable (virodhamine) or rapidly degraded by hydrolytic enzymes in vivo. The endocannabinoids are accompanied by saturated, and mono- or diunsaturated congeners which are CB₁ and CB₂ receptor-inactive. This CB₁ or CB₂ inactive molecules appear to potentiate the effect of anandamide or arachinoyl glycerol (“entourage effect”).³⁸ In this regard, my research group has recently shown³⁹ that introduction of a methylene lock on the ethanolamide head, thus generating a cyclopropane ring, as in **23**, is able to trigger strong CB₁ affinity in oleolyethanolamide.

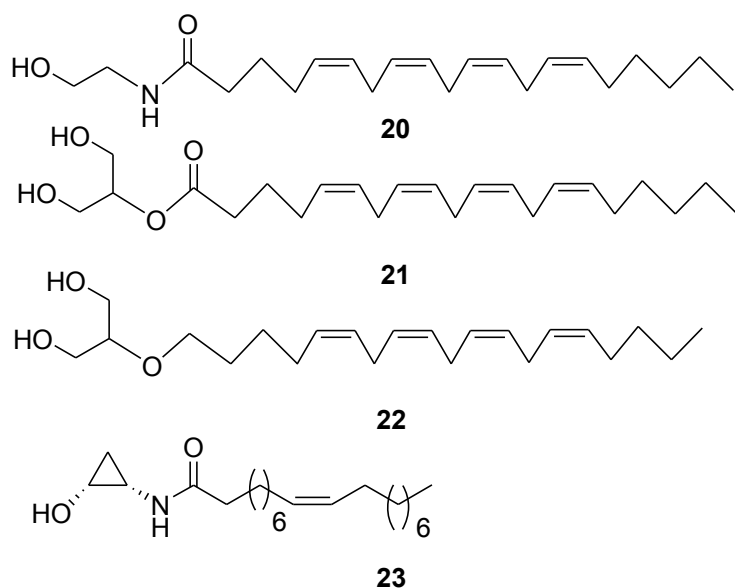


Figure 2.11. The chemical structures of endocannabinoids **20-22** and the synthetic analogue **23**

Apart from the metabotropic cannabinoid receptors CB₁, CB₂ and (possibly) GPR55, cannabinoids also bind to PPAR-gamma and to some thermo-TRPs, a series of ion-channels characterized by an intracellular ligand-binding domain and involved in pain and inflammation.⁴⁰ The regulation of ionotropic- and metabotropic proteins targeted by cannabinoids is, undoubtedly, one of the hottest field in cannabinoid research.

Interaction with CB receptors has been unambiguously associated to a number of pharmacological effects, but the most important are: 1) *psychotropic effects* (euphoria) 2) *antiemetic effect*, 3) *analgesic effect*, 4) *immunomodulation* 5) *motor effects* (hypokinesia, ataxia, antispasticity).

Many of the psychoactive effects of Δ^9 -THC (**6**) appear to be mediated by CB₁ receptors, while non-psychoactive cannabinoids (as CBD, **4**) have very low affinity both for CB₁ and CB₂. Δ^9 -THC (**6**) is the phytocannabinoid showing the highest affinity to CB receptors, with a K_i around 40 nM for both CB₁ and CB₂ (CBD K_i = 3000-4000 nM). Δ^8 -THC (see structure in **figure 2.7**) is almost equipotent to Δ^9 -THC⁴¹ (**6**). Interaction of Δ^9 -THC (**6**) with CB₁ receptors on presynaptic nerve terminals in the brain is responsible of the euphoric feelings associated with *Cannabis* use. Some data suggest that this effect could be beneficial in the treatment of depression, but further studies are needed to clarify the role of the cannabinoid system in the neurobiology of this pathology. Since

CB₁ receptors are not present in the brain region responsible for respiratory and cardiovascular functions, cannabinoid consumption cannot be associated to an increased risk of respiratory or cardiovascular failures, as happens for opiates.

Inhibition of gastrointestinal activity has been observed after administration of Δ^9 -THC (**6**), or of anandamide (**20**). This effect has been assumed to be CB₁-mediated: the location of CB₁ receptors in cholinergic nerve terminals of the gastrointestinal tract accounts for the THC-induced inhibition of digestive-tract motility, whereas the presence of CB₁ receptors in the brainstem is responsible of the THC-induced inhibition of emesis. The antiemetic effect of Δ^9 -THC (**6**) has been well established and proposed for treatment of chemotherapy-induced emesis⁴², in combination with new generation antiemetic drugs.

Many studies have reported that Δ^9 -THC (**6**) has a stimulatory effect on appetite and food intake, which can be co-adjuvant in cancer anorexia.⁴³ In 1992, FDA approved the use of Δ^9 -THC (**6**) to stimulate appetite in AIDS patients suffering from wasting syndrome. This effect could be mediated both by CB₁ receptors present in CNS or in nerve terminals and adipocytes.

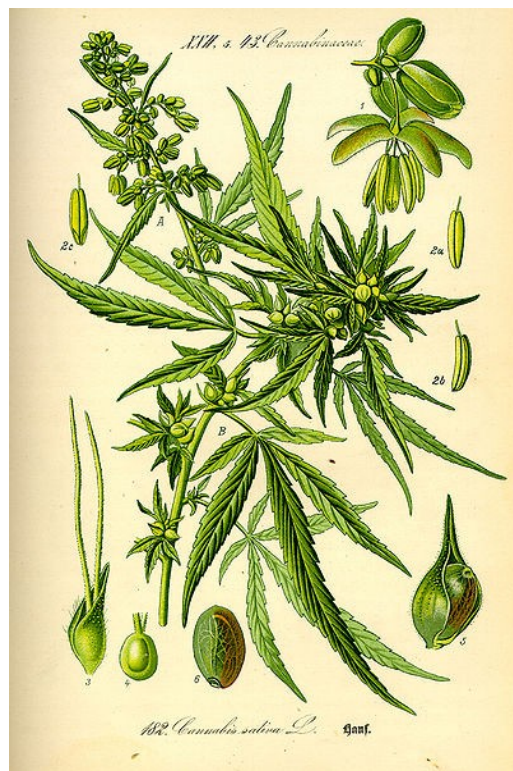
Noteworthy, CB₂ receptors are highly expressed in some cells of the immune system and they are believed to play a role in the immune cell function, thus providing a rationale to the immunomodulatory properties of Δ^9 -THC⁴⁴ (**6**). In addition, CB₂ receptor is suspected to mediate neuroinflammation, atherosclerosis, and bone remodelling.⁴⁵ The localization of both CB₁ and CB₂ on adipocytes, where their activation appears to stimulate lipogenesis, is particularly interesting and may have a clinical utility.⁴⁶

Most likely, the single most important potential therapeutic effect associated to the interaction with CB receptors is the analgesic effect, due to the role of CB₁ receptors in the transmission of nociceptive information in several key tissues. Δ^9 -THC (**6**) has been estimated to be as potent as morphine in blocking nociceptive stimuli in many animal models,⁴⁷ and, moreover, it can act synergistically with opioid-receptor agonists. Many studies are now aimed at establishing the beneficial effects of a concomitant administration of these drugs.

2.3. CANNABIOXEPANE, A NOVEL TETRACICLIC CANNABINOID FROM HEMP, *CANNABIS SATIVA* L.

2.3.1. *An ancient plant*

C. sativa L. is, arguably, the oldest plant domesticated by man, but its millenary history, crossing most of the human civilization, has always been accompanied by controversy and harsh contrasts. The geographical origin of *Cannabis* is probably Central Asia (Kazakhstan, Western China, and the Russian Far East), where also hop (*Humulus lupulus* L.), its only botanical relative, originated⁴⁸. The first known record of its use as a medicine was published in China 5000 years ago during the reign of the Emperor Chen Nung. Another important written description of *Cannabis* use dates back to 2350 B.C. on a stone of the Egyptian Old Kingdom in Memphis, at the end of the Fifth Dynasty.⁴⁹ A number of Egyptian papyri reporting *Cannabis* prescriptions (mainly as anti-inflammatory and antimicrobial agent) have been found and dated several centuries B.C. In Islamic countries the resin of *Cannabis* plants was better known as *hashish*, or *shadanaj* (literally, the royal grain) and widely used for its medical attributes, mainly in the treatment of pain. The name marijuana refers to the flowers and subtending leaves and stalks of mature pistillate of female plants.



As for the Western countries, the first detailed descriptions of the psychotropic variety of hemp dates to the Renaissance. Prosper Alpinus, a Venetian botanist, associated these properties to an Egyptian origin, a view long maintained in the botanical literature. The first impact in Europe occurred after the Napoleon invasion of Egypt. Important members of the French artistic community (Baudelaire, Honore' de Balzac, Alexandre Dumas, and Gustave Flaubert) under

the name “Club des Hashichins” (Hashish Club) met monthly in an old mansion in Paris.⁵⁰

Both the fiber and the psychoactive strains became used and investigated but, while opiate alkaloids were isolated early in the 19th century, the identification, isolation, and synthesis of Δ^9 -THC (**6**) was not achieved until 1964.⁵¹ Investigations on the mechanisms of the psychotropic action of Δ^9 -THC yielded to the discovery of the cannabinoid protein receptor family in 1988 and their cloning in early 1990s,²⁴ and the discovery of its endogenous ligand anandamide (the parent compound of the family of endocannabinoids) in 1992.³⁵ The last two decades of the twentieth century and the first decade of the present century can be indicated as the “cannabis Renaissance” due to the exceptional blooming of research on *Cannabis* and its metabolites. Although the clinical translation of this research activity is still limited, the recent approval (in Canada, UK and Spain, for symptomatic treatment of multiple sclerosis) of Sativex,TM a mixture of natural cannabinoids, constitutes a strong hope for the future. Cultivation and use of psychotropic *Cannabis*, even for medicinal purposes, is illegal in many countries due to the potentially harmful acute and short-lasting effects of this drug.

Cannabis is a genus of flowering plants that includes three putative species, *Cannabis sativa*, *Cannabis indica*, and *Cannabis ruderalis*. These three taxa are indigenous to Central Asia, and South Asia. *Cannabis* is an annual, dioecious, flowering herb. The leaves are palmately compound or digitate, with serrate leaflets. *Cannabis* normally has imperfect flowers, with staminate "male" and pistillate "female" flowers occurring on separate plants. The genus *Cannabis* was formerly placed in the Nettle (Urticaceae) or Mulberry (Moraceae) family, and later, along with hops (*Humulus* sp.), in a separate family, the hemp family (Cannabaceae sensu stricto). Recent phylogenetic studies based on cpDNA restriction site analysis and gene sequencing strongly suggest that the Cannabaceae sensu stricto arose from within the former Celtidaceae family, and that the two families should be merged to form a single monophyletic family, the Cannabaceae sensu lato.⁵² Basically, two types of *Cannabis* have been described, and classified as species, subspecies, or varieties:

- plants cultivated for fiber and seed production, described as low-intoxicant, non-drug, or fiber types.

- plants cultivated for drug production, described as high-intoxicant or drug types.

The phytochemistry of *C. sativa* has been thoroughly investigated, and several hundred compounds, often structurally unique, have been isolated from this plant, whose phytochemical profligacy is testified by the presence of alkaloids, fatty acids and esters, terpenoids, quinones, flavonoids, stilbenoids, and, above all, cannabinoids.⁵³ Despite all these studies, structural diversity within cannabinoids is far from having been exhaustively unravelled, as shown by the recent discovery of cannabimovone (CBM, **8**).⁶ This CBD analogue shows a unique resorcinyll *abeo*-menthane structure, and was isolated from an Italian fibre hemp derived from the historical cultivar *Carmagnola*.⁵⁴ During my Ph.D. studies, I have investigated the relatively apolar fractions from an extract of this plant and isolated five stilbenoids (**24-28**), including the new spirane isocannabispiradienone (**28**), and a novel bis-oxygen bridged diphenyl-type cannabinoid, which we have named cannabioxepane (**29**, CBX).

2.3.2. Extraction, isolation and structure elucidation

Dried female flowerheads of *C. sativa* were extracted with acetone at room temp. Removal of the solvent left a gummy residue that was partitioned between 1:1 aqueous methanol and petroleum ether. The defatted polar phase was then concentrated and extracted with CH₂Cl₂. The organic phase was dried (Na₂SO₄) and evaporated to afford a black gum, that was purified by flash chromatography on RP-18 silica gel (Biotage equipment). Repeated purification of the obtained fractions by gravity column chromatography on silica gel (petroleum ether-EtOAc mixtures) followed by HPLC yielded to the isolation of cannabispirane (**24**),⁵⁵ β-cannabispiranol (**25**),⁵⁶ α-cannabispiranol (**26**),⁵⁷ cannabispiradienone (**27**),⁵⁸ and two new compounds, isocannabispiradienone (**28**) and cannabioxepane (**29**) (Fig. 2.12).

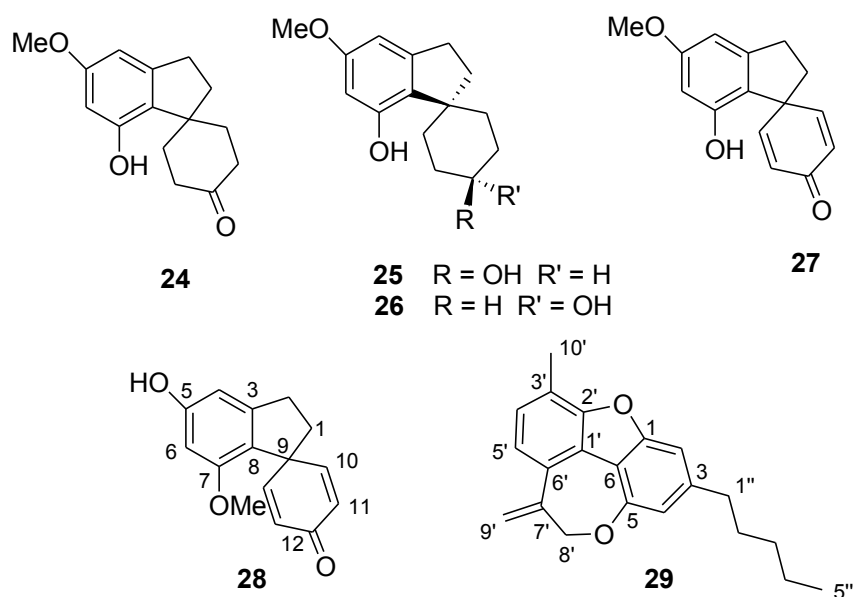
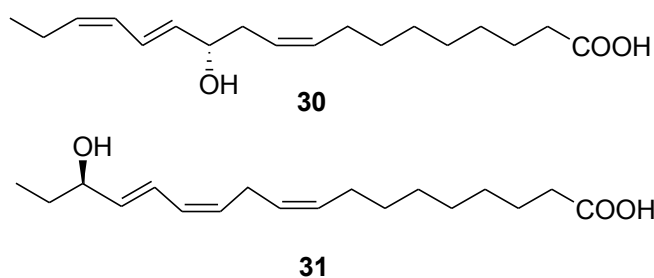


Figure 2.12. The six phenolic compounds isolated from *Cannabis sativa* L., including the new isocannabispiradienone (**28**) and cannabioxepane (**29**)

Two polyunsaturated fatty acids were also obtained, namely 12*S*-hydroxy-9*Z*,13*E*,15*Z*-octadecatrienoic acid (**30**) and 16*R*-hydroxy-9*Z*,12*Z*,14*E*-octadecatrienoic acid (**31**).



The known compounds **24-27** were identified by comparison of their spectral data with those reported in the literature.⁵⁵⁻⁵⁸ The fatty acids **30** and **31** have been recently obtained as methyl esters from *Swertia japonica* (Gentianaceae),⁵⁹ but had never been reported from *C. sativa*.

Isocannabispiradienone (28) has the molecular formula $C_{15}H_{14}O_3$ (by HR-ESIMS), indicative of nine unsaturation degrees. 1H NMR spectrum of **28** ($CDCl_3$) was reminiscent of that reported for **27**, being characterized by two coupled 2H doublets at δ_H 6.86 and 6.26 ($J = 10.0$ Hz), two coupled 2H triplets at δ_H 3.06 and 2.25 ($J = 7.8$ Hz), and two *m*-coupled aromatic protons at δ_H 6.19 and 6.36 ($J = 2.1$ Hz). A methyl singlet resonating at δ_H 3.61 and an exchangeable 1H singlet at δ_H 4.73 completed the signals of the 1H NMR spectrum of **28**. All the proton signals were associated with those of the directly attached carbon atoms with the help of the 2D NMR HSQC spectrum. The presence of a cross-

conjugated cyclohexadienone moiety was then deduced from the following experimental evidences: i) the ^{13}C NMR spectrum of **28** showed only 12 signals, as a result of the presence of symmetrical cyclohexadienone sub-structure (and the accidental isochronicity of two aromatic carbons, see *infra*); ii) the presence of a doubly conjugated ketone (C-12) was suggested by the ^{13}C NMR resonance at δ_{C} 186.9 and by the IR (KBr) peak at ν_{max} 1650 cm^{-1} ; iii) the HMBC cross-peaks of H-10 = H-14 with C-12, C-14 (= C-10) and with the unprotonated C-9 (δ_{C} 52.6). The latter carbon atom was subsequently identified as the spiro-carbon connecting the dienone ring with a five-membered ring, as indicated by the HMBC cross-peaks H-10/C-1, H-10/C-8 (δ_{C} 121.4), H-1/C-8, H-1/C-9, and H-1/C-3 (δ_{C} 147.2). The structural framework of isocannabispiradienone (**28**) is completed by a dioxygenated phenyl ring condensed with the five-membered ring. The signal at δ_{H} 6.36 showed HMBC cross-peaks with C-2, C-3, C-8, with the oxygenated C-5 (δ_{C} 157.6) and with the second aromatic methine carbon (C-6), and therefore it can be confidently assigned to H-4. Accordingly, the signal at δ_{H} 6.19, showing HMBC correlations with both the oxygenated carbons (C-5 and C-7) as well as with C-4 and C-8, can be assigned to H-6.

Unfortunately, the location of the methyl group could not be unambiguously achieved through the HMBC spectrum since the carbon resonances of C-5 and C-7 were incidentally coincident. However, inspection of the ROESY spectrum allowed a straightforward solution to this problem. Indeed, the OH signal at δ_{H} 4.73 showed cross-peaks with both H-4 and H-6, while the methoxy singlet at δ_{H} 3.61 showed cross-peak only with H-6, in agreement with its location at C-7, thus completely defining the chemical structure of **28**.

A derivation of isocannabispiradienone (**28**) from cannabispiradienone (**27**) by methyl swapping between the two phenolic hydroxyl seems unlikely. More plausibly, **27** and **28** might derive from the regiochemically divergent oxidative coupling of the same dihydrostilbene precursor (**Fig. 2.13**). Just like cannabispiradienone (**27**) is the alleged precursor of cannabispirane and cannabispiranol,⁵⁸ so isocannabispiradienone (**28**) might be the precursor of isocannabispirane.⁵¹ Therefore, the existence of isocannabispiranol in Cannabis extracts could be foreseen.

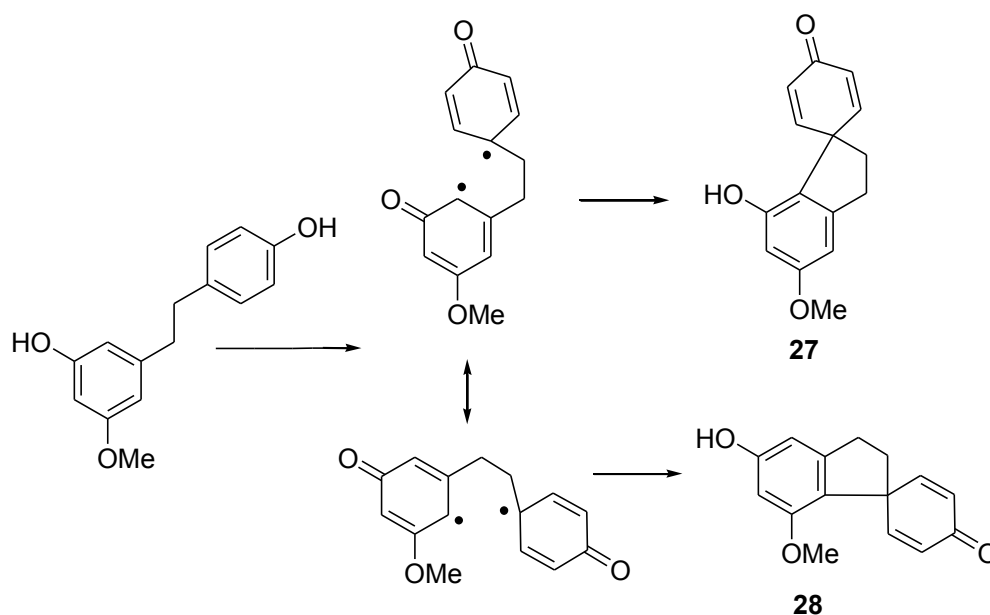


Figure 2.13. Postulated biogenetic origin of isocannabispiradienone (**28**).

HR-ESIMS established the molecular formula of **cannabioxepane** (CBX, **29**) as $C_{21}H_{22}O_2$, implying eleven degrees of unsaturation. The 1H NMR spectrum of **29** ($CDCl_3$, **Table 2.2**) showed a pair of coupled doublets at δ 7.34 and 7.16, four singlets between δ 7.10 and 5.40, a methylene broad singlet at δ 4.85, a deshielded methyl singlet at δ 2.56 and, finally, five well resolved multiplets between δ 2.70 and 0.80, which, on the basis of a 2D COSY spectrum, were combined into a linear pentyl chain (**Fig. 2.14**).

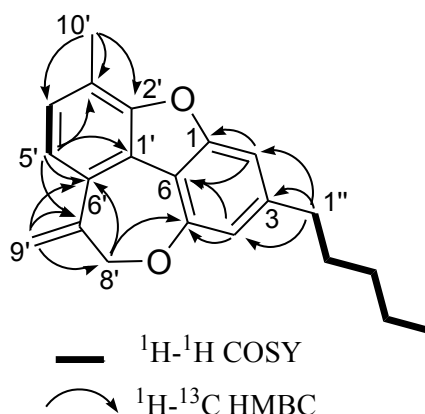


Figure 2.14. COSY and $^{2,3}J_{H \rightarrow C}$ HMBC correlations of cannabioxepane (**29**).

The 2D NMR HSQC spectrum of **29** made it possible to associate all the proton signals with those of the directly linked carbons, revealing that the singlets at δ_H 5.88 and 5.44 are actually linked at the same carbon at δ_C 118.6, and that the singlet at δ_H 4.85 must be an oxymethylene group (δ_C 75.1). The ^{13}C NMR

spectrum of **29** (CDCl_3 , **Table 2.2**) showed also the signals of nine unprotonated carbon atoms, all resonating in the sp^2 region of the spectrum, between δ_{C} 120 and 158. The above data were strongly suggestive of the presence of two phenyl rings and of an additional carbon-carbon double bond. Therefore, to account for the nine unsaturations implied by the molecular formula of CBX (**29**), two additional rings were required. A series of key $^{2,3}J_{\text{H,C}}$ correlations evidenced by the HMBC spectrum (**Fig. 2.14**) were critical to assemble the skeletal fragments and to draw the structure of CBX (**29**), allowing also the complete assignment of the proton and carbon resonances as reported in **Table 2.2**.

Table 2.2. ^1H (500 MHz) and ^{13}C (125 MHz) NMR Data of Cannabioxepane (**29**) in CDCl_3

Pos.	δ_{C} , mult.	δ_{H} , mult., J in Hz
1	157.5, C	
2	104.4, CH	7.01, s
3	144.3, C	
4	110.5, CH	6.72, s
5	155.2, C	
6	112.5, C	
1'	125.5, C	
2'	153.7, C	
3'	120.7, C	
4'	127.4, CH	7.16, d, 6.2
5'	118.4, CH	7.34, d, 6.2
6'	131.2, C	
7'	142.8, C	
8'	75.1, CH_2	4.85, bs
9'a	118.6, CH_2	5.88, bs
9'b		5.44, bs
10'	15.1, CH_3	2.56, s
1''	36.6, CH_2	2.70, t, 7.6
2''	31.4, CH_2	1.66, m
3''	31.2, CH_2	1.32, m
4''	22.7, CH_2	1.30, m
5''	14.3, CH_3	0.88, t, 7.0

In particular, the three correlations exhibited by $\text{H}_{3-10'}$ with the oxygenated C-2' (δ_{C} 153.7), with C-3' and with the methine carbon C-4' (δ_{C} 127.4), along with the correlations of H-5' with C-1', C-3' and C-6' allowed the identification of a tetrasubstituted phenyl ring bearing a methyl group and an oxygen atom on adjacent positions. The unprotonated sp^2 carbon C-7' was attached at C-6' on the

basis of the HMBC cross-peaks H-5'/C-7', H₂-9'/C-6', H₂-9'/C-7', H₂-8'/C-6', H₂-8'/C-7' and, these data, together with the HMBC cross peak H₂-9'/C-8' allowed also to establish the linkage of both the *sp*² methylene carbon (C-9') and the oxygenated *sp*³ methylene (C-8') at C-7'. The second phenyl ring was also tetrasubstituted, and its linkage with the pentyl chain at C-3 was indicated by the HMBC cross peaks of H₂-1'' with C-3 and with the methine carbons C-2 and C-4. The pattern of HMBC cross peaks shown by H-2 and H-4 suggested that both C-1 (δ_C 157.5) and C-5 (δ_C 155.2) are oxygenated carbons, and the key HMBC cross-peak H₂-8'/C-5 indicated the presence of an oxygen bridge to connect C-8' and C-5. Finally, the direct linkage of C-6 with C-1' (defining a seven-membered ring) and the presence of a second oxygen bridge to connect C-1 with C-2' (defining a furan ring), builded the dioxygenated tetracyclic structure of cannabioxepane (**29**), allowed the complete rationalization of NMR and MS data and was in perfect agreement with biogenetic arguments.

Cannabioxepane (**29**, CBX) is characterized by an unprecedented tetracyclic skeleton including, in addition to two phenyl rings, a furan and an oxygenated seven-membered ring. This skeleton bears some relationships with some cannabinoids from the CBE family (**Fig. 2.6**), and particularly with the aromatized analogue named cannabifuran (**15**),²⁴ however, noteworthy, no member of the CBE family shows a fourth ring. On the other hand, in the structure of Δ⁹-THC (**6**) and its derivatives (of their alleged CBG precursors) the oxygen atom at C-5 is involved in the formation of a six-membered ring with the unprotonated carbon of the isopropyl side chain (C-7'). CBX (**29**) is the first cannabinoid to show a linkage between the oxygen atom at C-5 and C-8', thus giving rise to the unprecedented seven-membered ring. From a biogenetical standpoint, CBX could be derived from the 7-*endo-tet* opening of the 7'-8' epoxide of a CBE-like precursor, followed by dehydration (**Fig. 2.15**).

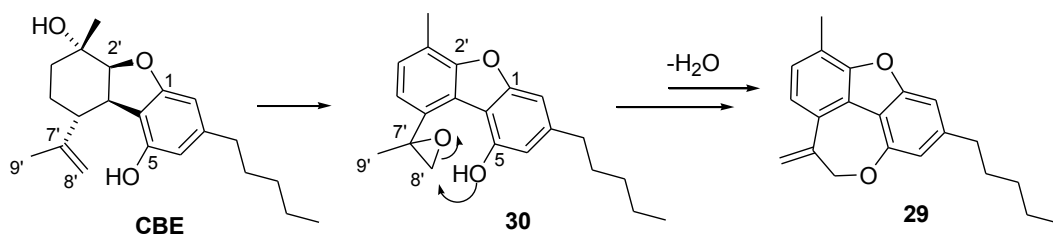


Figure 2.15. Possible biogenesis of CBX (**29**) from CBD via the epoxide **30**.

While cyclization of CBD-epoxides strongly favours the formation of pyrane derivatives via a 6-*exo-tet* process, it was noticed that closure of a furan ring between C-2' and the 1-hydroxyl could steer cyclization toward the formation of an alternative 7-*endo-tet* process, with formation of an oxepane rather than a pyran ring.³⁵ It seems therefore logic to assume that dehydrocannabifuran epoxide, a yet unreported cannabinoid, is the ultimate precursor of CBX.

2.3.3. Affinity of the cannabioxepane for cannabinoid receptors

Pharmacological evaluation of natural cannabinoids and of a number of synthetic molecules allowed the formulation of detailed structure-activity relationships for the interaction with the cannabinoid receptors (**Fig. 2.16**).

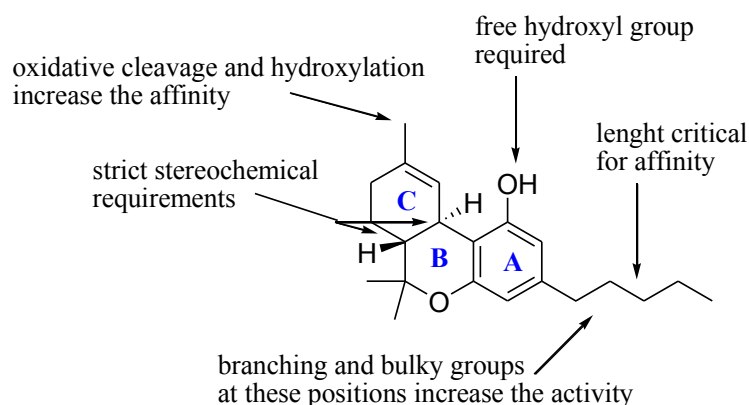


Figure 2.16. A schematic view of the structure-activity relationships for interaction with the cannabinoid CB₁ receptor.

A free hydroxyl group on ring A is required for activity on CB₁; presumably due to the formation of hydrogen bonding with the side-chain and the nitrogen atom of Lys12 in transmembrane helix 3 of the CB receptor.⁶⁰ The structure of synthetic cannabinoid CP-55,244 (see structure in **figure 2.17**) highlights the role exerted by the so-called northern aliphatic hydroxyl group (NAH) and the southern aliphatic hydroxyl group (SAH), both of them absent in the structure of classical cannabinoids (**Fig. 2.17**). Their presence is not crucial for receptor affinity but, most likely, they interact positively (and in a stereospecific way) with receptorial structures, thus potentiating the activity.

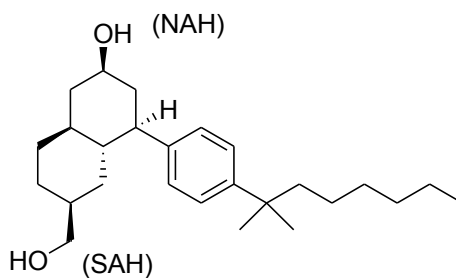


Figure 2.17. The chemical structure of CP-55,244

Another critical parameter for CB affinity is the length and the ramification of the pentyl side chain. A decrease in the length of this side chain results in a reduction of potency (THCV is about 75% less potent) and in the appearing of dose-dependent antagonist behaviour⁶¹, while an increase to C₇ or C₈ results in a systematic increase in affinity.

Modifications at ring C have been mostly concentrated on the allylic methyl group. A positive effect is shown by nabilone (**32**), where the methyl group is oxidatively cleaved to give a keto group. Nabilone has been introduced into the market as antiemetic agent for cancer supporting care and, recently, it has been approved in the USA also for the treatment of neuropathic pain.⁶¹

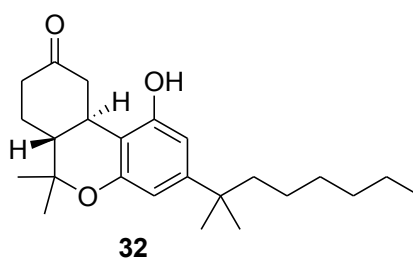


Figure 2.18. The chemical structure of nabilone (**32**)

CBX was evaluated for its affinity to CB₁ and CB₂ receptors but no significant activity was detected. Actually, this result was not surprising considering the negative effect reported for the etherification of the phenolic 1-hydroxyl, and for the aromatization of the terpene-derived six-membered ring.

2.3.4. Experimental

Collection, Extraction and Isolation

Cannabis sativa derived from a greenhouse cultivation at CRA-CIN, Rovigo (Italy), where a voucher specimen is kept, and was collected in November 2008. The isolation and manipulation of all cannabinoids was done in accordance with their legal status (Authorization SP/101 of the Ministero della Salute, Rome, Italy).

Dried flowerheads of *C. sativa* (500 g) were heated at 120°C for 2.5 h in a ventilated oven, to decarboxylate pre-cannabinoids. After cooling to room temp., the plant material was extracted with acetone (2 × 10 L). Removal of the solvent left a gummy residue that was partitioned between 1:1 aqueous methanol (1 L) and petroleum ether (1L). The defatted polar phase was concentrated and extracted with CH₂Cl₂. The organic phase was dried (Na₂SO₄) and evaporated to afford a black gum (10 g), that was purified by flash chromatography on RP-18 silica gel (Biotage equipment, 250 mL column, linear gradient, from MeOH/H₂O 55:45 to 90:10). Overall, five fractions (A1 to A5) were collected. Fraction A2 was further fractionated by gravity column chromatography on silica gel, using acidified (0.5% HOAc) petroleum ether-EtOAc mixtures to obtain 20 subfractions (B1 to B20) which were subsequently purified by HPLC. HPLC purification of fraction B2 (eluent *n*-hexane/EtOAc 85:15) yielded cannabispirane (**24**, 15.0 mg, 30 ppm on dried plant material). HPLC purification of fraction B3 (eluent *n*-hexane/EtOAc 8:2) yielded cannabispiradienone (**27**, 5.0 mg, 11 ppm on dried plant material). HPLC purification of fraction B4 (eluent *n*-hexane/EtOAc 75:25) yielded 12-hydroxy-3,9,15-octadecatrienoic acid (**30**, 6.0 mg, 12 ppm on dried plant material), isocannabispiradienone (**28**, 2.8 mg, 5 ppm on dried plant material), β-cannabispiranol (**25**, 22.0 mg, 48 ppm on dried plant material) and α-cannabispiranol (**26**, 15.0 mg, 30 ppm on dried plant material). HPLC purification of fraction B5 (eluent *n*-hexane/EtOAc 75:25) yielded 16-hydroxy-9Z,12Z,14E-octadecatrienoic acid (**31**, 4.0 mg, 9 ppm on dried plant material). The less polar fraction A4 was subjected to repeated column chromatographies on silica gel (petroleum ether-EtOAc mixtures) to obtain a crude fraction which was further purified by HPLC (eluent *n*-hexane/EtOAc 95:5) to yield cannabioxepane (**29**, 3.5 mg, 7 ppm on dried plant material).

Isocannabispiradienone (28). Colorless amorphous solid; IR (KBr): ν_{\max} 3100, 1650 cm^{-1} . UV (MeOH): λ_{\max} (ϵ) 215 (28000), 240 (23300), 277 (3000), 287 (3000) nm. ^1H NMR (CDCl_3 , 500 MHz): δ 6.86 (H-10 = H-14, 2H, d, $J = 10.0$ Hz), 6.36 (H-4, 1H, d, $J = 2.1$ Hz), 6.26 (H-11 = H-13, 2H, d, $J = 10.0$ Hz), 6.19 (H-6, 1H, d, $J = 2.1$ Hz), 4.73 (5-OH, 1H, s), 3.61 (7-OMe, 3H, s), 3.06 (H_2 -2, 2H, t, $J = 7.8$ Hz), 2.25 (H_2 -1, 2H, t, $J = 7.8$ Hz). ^{13}C NMR (CDCl_3 , 125 MHz): δ 186.9 (C-12), 158.9 (C-11 = C-13), 157.6 (C-5, C-7), 153.1 (C-10 = C-14), 147.2 (C-3), 121.4 (C-8), 103.8 (C-4), 97.5 (C-6), 55.9 (7-OMe), 52.6 (C-9), 38.1 (C-1), 31.6 (C-2). ESI-MS (positive ions) m/z 265 $[\text{M} + \text{Na}]^+$; HREIMS m/z 265.0844 $[\text{M} + \text{Na}]^+$ (calcd. for $\text{C}_{15}\text{H}_{14}\text{NaO}_3$ 265.0841).

Cannabioxepane (29). Colorless amorphous solid; ^1H and ^{13}C NMR (CDCl_3) see Table 2.2. ESI-MS (positive ions) m/z 329 $[\text{M} + \text{Na}]^+$; HREIMS m/z 329.1522 $[\text{M} + \text{Na}]^+$ (calcd. for $\text{C}_{21}\text{H}_{22}\text{NaO}_2$ 329.1517).

12S-hydroxy-9Z,13E,15Z-octadecatrienoic acid (30). Colorless amorphous solid; $[\alpha]_{\text{D}} = +2$ ($c = 0.05$); CD (MeOH): λ 243 nm ($\Delta\epsilon = +0.3$); ^1H NMR (CDCl_3): δ 6.52 (H-14, 1H, dd, $J = 15.5, 11.0$ Hz), 5.97 (H-15, 1H, t, $J = 11.0$ Hz), 5.69 (H-13, 1H, dd, $J = 15.5, 6.0$ Hz), 5.54 (H-9, 1H, dt, $J = 10.7, 7.2$ Hz), 5.42 (H-16, 1H, dt, $J = 11.0, 7.2$ Hz), 5.36 (H-10, 1H, dt, $J = 10.7, 7.2$ Hz), 4.21 (H-12, 1H, m), 2.33 (H_2 -11, 2H, t, $J = 7.2$ Hz), 2.30 (H_2 -2, 2H, t, $J = 7.2$ Hz), 2.18 (H_2 -17, 2H, q, $J = 7.2$ Hz), 2.09 (H_2 -8, 2H, q, $J = 7.2$ Hz), 1.35-1.30 (H_2 -7, H_2 -6, H_2 -5, H_2 -4, 8H, m), 1.60 (H_2 -3, 2H, q, $J = 7.2$ Hz), 1.01 (H_3 -18, 3H, t, $J = 7.2$ Hz). ESI-MS (positive ions) m/z 317 $[\text{M} + \text{Na}]^+$; HREIMS m/z 317.2100 $[\text{M} + \text{Na}]^+$ (calcd. for $\text{C}_{18}\text{H}_{30}\text{NaO}_3$ 317.2093).

16R-hydroxy-9Z,12Z,14E-octadecatrienoic acid (31). Colorless amorphous solid; CD (MeOH): λ 229 nm ($\Delta\epsilon = -0.8$); ^1H NMR (CDCl_3): δ 6.52 (H-14, 1H, dd, $J = 15.0, 11.0$ Hz), 6.00 (H-13, 1H, t, $J = 11.0$ Hz), 5.69 (H-15, 1H, dd, $J = 15.5, 7.0$ Hz), 5.45 (H-12, 1H, dd, $J = 11.0, 7.0$ Hz), 5.40 (H-9, 1H, dd, $J = 11.0, 7.0$ Hz), 5.35 (H-10, 1H, dt, $J = 11.0, 7.0$ Hz), 4.09 (H-16, 1H, m), 2.93 (H_2 -11, 2H, t, $J = 7.5$ Hz), 2.31 (H_2 -2, 2H, t, $J = 7.2$ Hz), 2.06 (H_2 -8, 2H, q, $J = 7.2$ Hz), 1.60 (H_2 -3, H_2 -17, 4H, m), 1.35-1.30 (H_2 -7, H_2 -6, H_2 -5, H_2 -4, 8H, m), 0.88 (H_3 -18, 3H, t, $J = 7.2$ Hz). ESI-MS (positive ions) m/z 317 $[\text{M} + \text{Na}]^+$; HREIMS m/z 317.2090 $[\text{M} + \text{Na}]^+$ (calcd. for $\text{C}_{18}\text{H}_{30}\text{NaO}_3$ 317.2093).

2.4. STEROIDAL CB RECEPTOR LIGANDS FROM THE INDONESIAN SPONGE *DASYCHALINA* sp.

2.4.1 Introduction

The research on CB receptors is a hot topic of modern pharmacology and medicinal chemistry. A few natural products, with the obvious exception of meroterpenoids from *C. sativa*, have been tested as CB receptor ligands⁶³. A recent example includes the polyine falcarinol (found in carrots, parsley and other plants) which exhibited micromolar binding affinity to both human CB receptors⁶⁴.

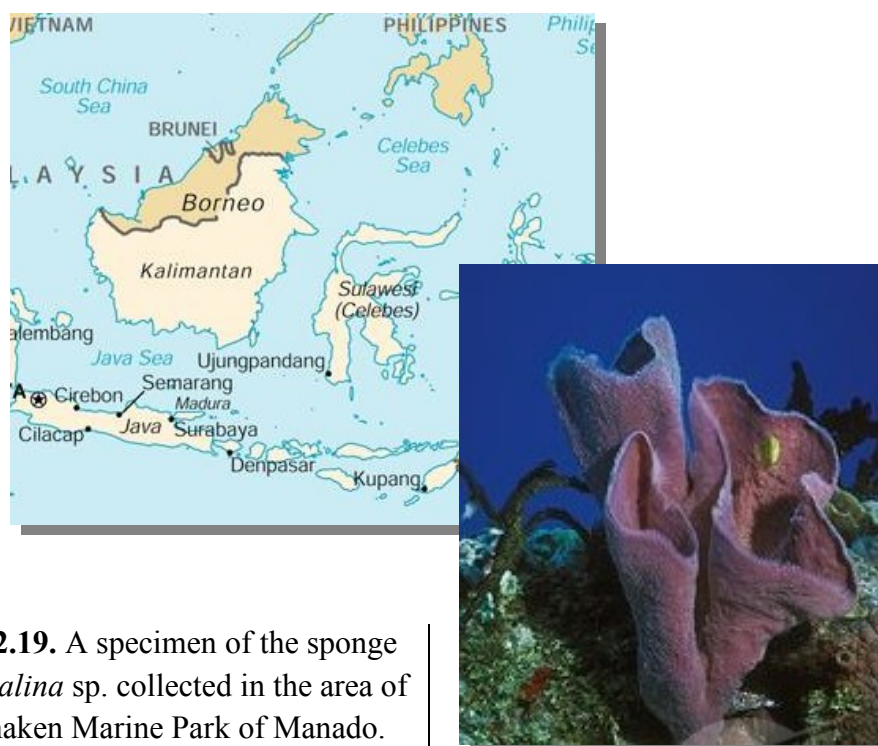
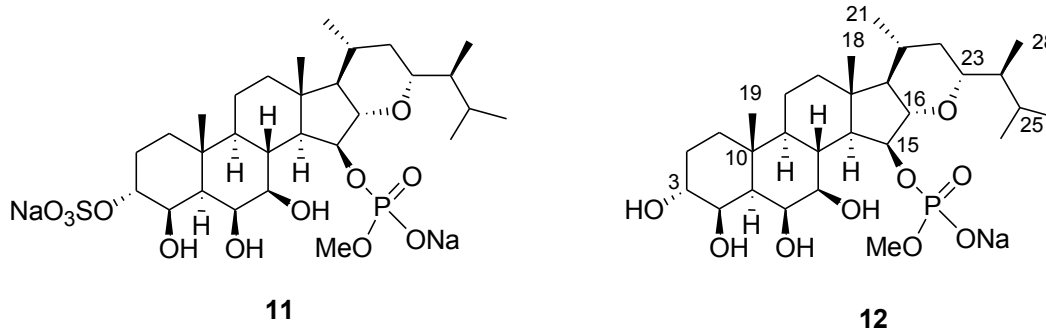


Figure 2.19. A specimen of the sponge *Dasychalina* sp. collected in the area of the Bunaken Marine Park of Manado.

As part of our ongoing screening for biologically active secondary metabolites from Indonesian marine invertebrates⁶⁵⁻⁶⁷, we had recently the opportunity to analyze a specimen of the sponge *Dasychalina* sp (order Haplosclerida, family Niphatidae, **Fig. 2.19**). From the polar organic extract we have isolated consistent amounts of two steroidal derivatives, haplosamate A (**11**) and its new desulfo analogue **12**. These two compounds, as well as their semi-synthetic analogues **33-35**, have been evaluated for interaction with CB₁ and CB₂ receptors.

2.4.2. Extraction, isolation and structure elucidation

A specimen of the sponge *Dasychalina* sp. was collected by hand in the area of the Bunaken Marine Park of Manado and kept frozen until sequentially extracted with methanol (MeOH) and dichloromethane by soaking the diced sponge tissue (210 g wet weight). The extracts were concentrated, combined, and then partitioned between ethyl acetate (EtOAc) and water. The polar material has been then partitioned between water and butanol to obtain a polar organic phase of 2.67 g. This was chromatographed on silica gel, using a gradient solvent system from EtOAc to MeOH. Fractions eluted with EtOAc/MeOH 7:3 to 1:1 were combined and further purified by reverse-phase HPLC (MeOH/H₂O mixtures) to obtain consistent amounts of haplosamate A (**11**, 480.5 mg, 0.2% based on wet weight) and the new desulfohaplosamate (**12**, 12.2 mg) in the pure form.



Haplosamate A (**11**) is a unique C₂₈ sterol containing seven oxygenated carbons and including a rare six-membered ether ring connecting C-16 and C-23, a sulfate group at C-3, and a methyl phosphate at C-15. Haplosamate A (**11**) was first isolated from the sponge *Xestospongia* sp.⁶⁸ and then re-isolated (and structurally revised) from another Haplosclerida sponge, *Cribrochalina* sp.⁶⁹ Although steroidal sulfates are well represented in marine sponges, the group of natural sterols including both sulphate and phosphate groups is restricted to a handful of members.⁷⁰

Compound **12** showed a prominent ion peak at *m/z* 573 in the ESI-MS spectrum (negative ion mode) and high resolution measurements indicated the molecular formula C₂₉H₅₀O₉P. ¹H and ¹³C NMR spectra of **12** (CD₃OD, **Table 2.3**) resembled parallel spectra of haplosamate A, but marked shifts were observed in several resonances.

Table 2.3. ^1H (500 MHz) and ^{13}C (125 MHz) NMR Data of Desulfohaplosamate (**12**) in CD_3OD

Pos.	δ_{C} , mult.	δ_{H} , mult., J in Hz
1a	30.3, CH_2	1.34 ^a
1b		1.29 ^a
2a	24.4, CH_2	2.04, m
2b		1.55 ^a
3	69.9, CH	3.74, d, 2.5
4	78.5, CH	3.85, bs
5	44.9, CH	1.52 ^a
6	78.2, CH	3.96, bs
7	80.0, CH	3.28, bd, 10.6
8	34.5, CH	2.29, ddd, 11.0, 10.6, 10.6
9	54.1, CH	0.86, m
10	36.8, C	
11a	20.0, CH_2	1.53 ^a
11b		1.44 ^a
12a	40.5, CH_2	1.84, m
12b		1.14, m
13	43.2, C	
14	58.2, CH	1.39, m
15	81.6, CH	4.72, m
16	91.8, CH	3.91, dd, 10.0, 3,5
17	62.5, CH	0.73, m
18	15.5, CH_3	0.99, s
19	17.5, CH_3	1.32, s
20	33.9, CH	1.82, m
21	20.5, CH_3	0.96, d, 7.0
22a	40.0, CH_2	1.65, m
22b		0.84, m
23	82.1, CH	3.45, ddd, 9.5, 8.5, 2.1
24	44.9, CH	1.41 ^a
25	27.8, CH	2.08, m
26	17.1, CH_3	0.81, d, 7.0
27	21.7, CH_3	0.89, d, 7.0
28	10.2, CH_3	0.76, d, 7.0
-OMe	52.8, CH_3	3.60, d, 11.0

^a Overlapped with other signals

In particular, the presence of the characteristic *O*-methyl doublet signal coupled to the phosphorous atom (δ_{H} 3.60, doublet, $J = 11.0$ Hz) clearly confirmed the presence of the methylphosphate functionality. All the proton resonances were associated to those of the directly attached carbon atoms through the 2D NMR HSQC experiment and then the proton multiplets were arranged in sequence through the COSY experiment, yielding to the single large spin system evidenced in bold in **figure 2.20**.

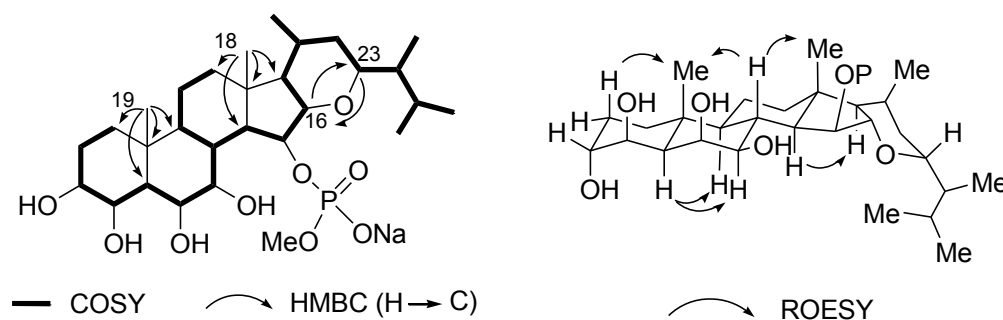


Figure 2.20. COSY and key HMBC cross-peaks (left) and ROESY correlations (right) of desulfohaplosamate (**12**)

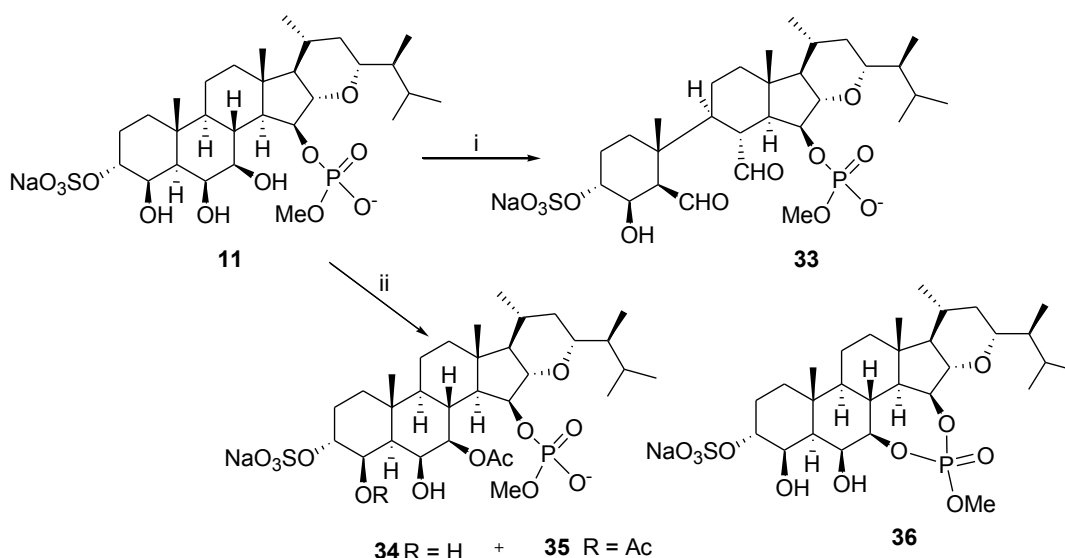
HMBC cross-peaks exhibited by Me-18 and Me-19 defined the tetracyclic steroidal skeleton, while the key HMBC correlations of H-16 (δ_{H} 3.91) with C-23 (δ_{C} 82.1) and H-23 with C-16 indicated the presence of a six-membered ether ring. Carbon-phosphorous couplings were observed in the ^{13}C NMR spectrum of **12** for C-14 ($^3J_{\text{C,P}} = 8.5$ Hz) and C-15 ($^2J_{\text{C,P}} = 7.0$ Hz), thus placing the methylphosphate group at C-15, and completely defining the planar structure of **12**. The comparison of the pattern of ^1H - ^1H coupling constants measured for **12** (Table 2.3) with those reported for haplosamate A, supported by the series of ROESY cross peaks shown in figure 2.20, indicated the relative configuration of **12**. Noteworthy, three of the four secondary hydroxyl groups are in axial orientation and they are all located on the “southern” part of rings A and B. The relatively low-field shifted resonance of Me-19 (δ_{H} 1.32) is in agreement with the β orientation of both the hydroxyl groups at C-4 and C-6. Desulfohaplosamate (**12**) is only the fourth member of the haplosamate group of steroids, in addition to haplosamate A, haplosamate B (showing a second phosphate group at C-7) and a minor analogue showing ring A contraction.⁶⁹

2.4.3. Preparation of semisynthetic derivatives of haplosamate A

Fusetani et al. reported that haplosamate A possessed a moderate inhibitory activity toward membrane type 1 matrix metalloproteinase, a key enzyme in tumor metastasis.⁶⁹ More recently, a seminal work by Andersen et al.⁷¹ identified haplosamate A as CB₁ and CB₂ receptor agonists, on the basis of a functional cell-based bioassay (*Spodoptera frugiperda* cells expressing one or the other of the human cannabinoid receptors) and saturation transfer double-difference NMR

experiments.⁷² In the same study, the Authors also suggested that phosphate and sulfate groups are not essential for binding to cannabinoid receptors, tentatively identifying the “northern” less polar region of the molecule as responsible for this interaction. Given our interest for the chemistry of both natural⁶ and synthetic³⁹ cannabinoids, the isolation of haplosamate compounds from *Dasychalina* sp. represented a unique opportunity to investigate the interaction of these steroidal derivatives with cannabinoid receptors through a binding test.

In order to increase the chemical diversity of the tested compounds, we took advantage of the relatively high amounts of haplosamate A obtained from the sponge to prepare a few simple semi-synthetic derivatives.



Scheme 2.1. Preparation of semisynthetic derivatives of haplosamate A (11).

i. NaIO₄; ii. Ac₂O/Pyr.

Treatment of haplosamate A (11) with NaIO₄ gave in good yields (65%) the dialdehyde 33 (Scheme 2.1) originating from the regioselective oxidative cleavage of the C-6/C-7 bond. The ¹H NMR spectrum of compound 33 (CD₃OD) showed the appearance of two broad singlets at δ_H 9.81 (H-6) and 10.22 (H-7) and a marked downfield shift of the other ring B proton signals (H-5: from δ 1.50 to 2.56; H-8 from δ 2.26 to 3.15; H-9 from δ 0.90 to 2.35). Inspection of 2D NMR COSY, HSQC and HMBC experiments allowed the assignment of all the proton and carbon resonances as reported in paragraph 2.4.3. Acetylation of haplosamate A (1) in standard conditions (Ac₂O/pyr) yielded to the formation of the 7-acetate

(**34**) and of the 4,7-diacetate (**35**) derivatives (**Scheme 2.1**). The acetylation positions in compounds **34** and **35** were unambiguously determined on the basis of the marked downfield shift of the relevant methine protons (e.g. H-7 is shifted from δ_{H} 3.34 to 4.64 in **34**) and of the $^3J_{\text{H,C}}$ HMBC cross peaks between each of these methines and the corresponding ester carbonyls. The easy esterification at C-7 can be rationalized on the basis of the equatorial position of the hydroxyl group; on the contrary, acetylation of the axial hydroxyl at C-4 was somewhat unexpected, due to the steric hindrance of Me-19. Noteworthy, Fusetani et al. reported that treatment of haplosmate A with benzoyl chloride not only failed to give esterification at C-4 but also at C-7, and the phosphotriester **36** (**Scheme 2.1**), formed by ester exchange, was the single reaction product.⁶⁹ This markedly different behaviour of the same compound upon treatment with benzoyl chloride and acetic anhydride appears intriguing.

The affinity of the natural haplosamates **11** and **12** and of the semisynthetic derivatives **33-35** for both human recombinant cannabinoid receptors CB₁ and CB₂ was evaluated (**Table 2.4**).

Table 2.4. Effects of haplosamate derivatives **1-5** on cannabinoid receptors

	K_i at hCB ₁ ^a (μM)	K_i at hCB ₂ ^a (μM)
Haplosamate A (11)	19.17	>50
Desulfohaplosamate (12)	19.47	2.82
Dialdehyde (33)	>50	>50
Haplosamate A-7-acetate (34)	9.74	8.89
Haplosamate A-4,7-diacetate (35)	19.98	11.85
Δ^9 -Tetrahydrocannabinol (6)	0.0016	0.0024

^a K_i values are calculated by applying the Cheng-Prusoff equation.

A comparison of affinity data obtained for haplosamate A (**11**) and desulfohaplosamate (**12**) appears quite interesting, since these two compounds showed an opposite behaviour. Compound **11** exhibited significant affinity only for CB₁ receptors, its potency in the binding assay being in the mid μM range, significantly higher than previously reported using a different type of assay.⁷¹ Instead, the desulfated analogue **12** showed a much higher affinity for CB₂ receptors, in the low μM range ($K_i = 2.8 \mu\text{M}$). The 7-monoacetylated derivative of

haplosamate A showed an increase in the affinity for both CB receptors, compared to its parent compound, but the further acetylation at C-4 proved to be deleterious for affinity on both CB₁ and CB₂. Finally, the dialdehyde derivative **33** showed a complete loss of affinity for both receptors, highlighting the importance of an intact steroid nucleus and, in particular, of intact rings A and B. Δ^9 -THC (**6**), used here as reference compound, was, as expected, about 1000-fold more potent than haplosamates in the same binding assays.

2.4.4. Experimental

Collection, Extraction and Isolation

A specimen of the sponge *Dasychalina* sp. (order Haplosclerida, family Niphatidae) was collected in January 2008 by hand in the area of the Bunaken Marine Park of Manado and kept frozen until extraction. A voucher sample (n° MAN08-07) has been deposited at the Dipartimento di Chimica delle Sostanze Naturali, Università di Napoli Federico II. The organism (210 g wet weight) was exhaustively extracted, in sequence, with methanol (MeOH) and dichloromethane (CH₂Cl₂) by soaking the diced sponge tissue. The extracts were combined and then partitioned between ethyl acetate (EtOAc) and H₂O. The polar material has been then partitioned between H₂O and butanol to obtain a polar organic phase (2.67 g), which was chromatographed on a silica gel column (230-400 mesh), using a gradient solvent system from EtOAc to MeOH. Fractions eluted with EtOAc/MeOH 7:3 to 1:1 were combined and further purified by reverse-phase HPLC (MeOH/H₂O 1:1) to obtain consistent amounts of haplosamate A (**11**, 480.5 mg) and the new desulfohaplosamate (**12**, 12.2 mg) in the pure state.

Desulfohaplosamate (12). Colorless powder. $[\alpha]_D = -3.8$ (c = 0.03 MeOH); ¹H and ¹³C NMR (CD₃OD): Table 2.3. ESI-MS (negative ions) *m/z* 573 [M - Na]⁻; HREIMS *m/z* 573.3200 [M - Na]⁻ (calcd. for C₂₉H₅₀O₉P 573.3198).

Oxidative cleavage of haplosamate A. To a solution of haplosamate A (43.4 mg, 0.062 mmol) in CH₂Cl₂ (1.2 mL) 50 μ L of NaHCO₃ sat. solution and 28 mg (0.13 mmol) of NaIO₄ were added. The mixture was left at room temp. for 3 hrs. under vigorous stirring. Then, the reaction mixture was treated with dry Na₂SO₄ and filtered. The obtained filtrate was purified by RP18 HPLC (H₂O/MeOH 1:1) to give 27.0 mg (65 % yield) of the dialdehyde **33**.

Dialdehyde (33). Colorless amorphous solid; $[\alpha]_D = -4.6$ ($c = 0.05$); $^1\text{H NMR}$ (CD_3OD , 500 MHz): δ 10.22 (H-7, bs), 9.81 (H-6, s), 4.60 (H-3, bs), 4.37 (H-15, m), 4.19 (H-4, bs), 3.68 (H-16, dd, $J = 10.5, 2.0$ Hz), 3.57 (OMe, d, $J = 10.5$ Hz), 3.36 (H-23, t, $J = 8.5$ Hz), 3.15 (H-8, t, $J = 11.0$ Hz), 2.56 (H-5, bs), 2.35 (H-9, m), 2.14 (H-2a, m), 2.09 (H-25, m), 1.84 (H-12a, overlapped), 1.80 (H-20, overlapped), 1.76 (H-2a, overlapped), 1.75 (H-14, overlapped), 1.73 (H-1a, overlapped), 1.63 (H-22a, overlapped), 1.60 (H-11a, overlapped), 1.55 (H-11b, overlapped), 1.41 (H-24, m), 1.30 (Me-19, s), 1.30 (H-1b, m), 1.27 (H-12b, overlapped), 0.96 (Me-18, s), 0.95 (Me-21, d, $J = 7.0$ Hz), 0.89 (Me-26, d, $J = 7.0$ Hz), 0.86 (H-22b, m), 0.81 (Me-27, d, $J = 7.0$ Hz), 0.80 (Me-28, d, $J = 7.0$ Hz), 0.80 (H-17, overlapped). $^{13}\text{C NMR}$ (CD_3OD , 125 MHz): δ 205.2 (C-7), 204.8 (C-6), 90.8 (C-16), 82.3 (C-3), 81.4 (C-23), 77.5 (C-15), 70.8 (C-4), 62.0 (C-17), 55.2 (C-5), 54.0 (OMe), 51.9 (C-14), 44.2 (C-24), 43.5 (C-9), 43.4 (C-13), 40.5 (C-22), 40.1 (C-8), 37.8 (C-12), 34.3 (C-1), 33.5 (C-20), 33.2 (C-10), 27.2 (C-25), 22.8 (C-2), 22.5 (C-11), 21.8 (C-27), 20.5 (C-21), 18.5 (C-19), 16.8 (C-26), 15.4 (C-18), 11.0 (C-28). ESI-MS (negative ions) m/z 651 $[\text{M} - 2\text{Na} + \text{H}]^-$, 673 $[\text{M} - \text{Na}]^-$; HR-ESI-MS m/z 673.2421 (calcd. for $\text{C}_{29}\text{H}_{47}\text{NaO}_{12}\text{PS}$ m/z 673.2429).

Acetylation of haplosamate A. Haplosamate A (33.5 mg, 0.048 mmol) was dissolved in dry pyridine (0.5 mL) and treated with Ac_2O (0.5 mL). After standing overnight under stirring at room temp, the reaction was worked up by addition of a few drops methanol to destroy the excess Ac_2O , water (*ca.* 1 mL) and EtOAc (*ca.* 3 mL). The organic phase was washed sequentially with 2N H_2SO_4 , sat. NaHCO_3 and brine. After drying (Na_2SO_4) and removal of the solvent, the residue was purified by HPLC ($\text{H}_2\text{O}/\text{MeOH}$ 6:4) to afford 25.5 mg (75% yield) of the 7-monoacetate **34** and 8.5 mg (22% yield) of the 4,7-diacetate **35**.

Haplosamate A 7-acetate (34). Colorless powder. $[\alpha]_D = -1.4$ ($c = 0.03$); $^1\text{H NMR}$ (CD_3OD , 500 MHz): δ 4.64 (H-7, bd, $J = 10.5$ Hz), 4.43 (H-3, bs), 4.36 (H-15, m), 4.14 (H-4, bs), 4.00 (H-16, dd, $J = 10.5, 2.0$ Hz), 3.89 (H-6, bs), 3.64 (OMe, d, $J = 10.5$ Hz), 3.52 (H-23, t, $J = 8.5$ Hz), 2.70 (H-8, t, $J = 11.0$ Hz), 2.32 (7-OAc, s), 2.03 (H-2a, m), 2.00 (H-25, m), 1.81 (H-20, overlapped), 1.77 (H-12a, overlapped), 1.68 (H-5, bs), 1.55 (H-11a, overlapped), 1.53 (H-22a, overlapped), 1.51 (H-1a, m), 1.42 (H-24, overlapped), 1.40 (H-11b, overlapped), 1.30 (H-14, overlapped), 1.38 (Me-19, s), 1.33 (H-2a, overlapped), 1.27 (H-1b, m), 1.05 (Me-

18, s), 1.01 (H-9, m), 0.99 (Me-21, d, $J = 7.0$ Hz), 0.89 (Me-26, d, $J = 7.0$ Hz), 0.88 (H-12b, overlapped), 0.86 (H-22b, m), 0.81 (Me-27, d, $J = 7.0$ Hz), 0.75 (Me-28, d, $J = 7.0$ Hz), 0.70 (H-17, overlapped). ESI-MS (negative ions) m/z 695 [$M - 2Na + H$]⁻, 717 [$M - Na$]⁻; HR-ESI-MS m/z 717.2702 (calcd. for $C_{31}H_{51}NaO_{13}PS$ m/z 717.2691).

Haplosamate A 4,7-diacetate (35). Colorless powder. $[\alpha]_D = -10.6$ ($c = 0.08$); 1H NMR (CD_3OD , 500 MHz): δ 5.42 (H-4, bs), 4.64 (H-7, bd, $J = 10.5$ Hz), 4.40 (H-15, m), 4.36 (H-3, bs), 3.99 (H-16, dd, $J = 10.5, 2.0$ Hz), 3.91 (H-6, bs), 3.67 (OMe, d, $J = 10.5$ Hz), 3.55 (H-23, t, $J = 8.5$ Hz), 2.70 (H-8, t, $J = 11.0$ Hz), 2.32 (7-OAc, s), 2.09 (4-OAc, s), 2.03 (H-2a, m), 2.00 (H-25, m), 1.81 (H-20, overlapped), 1.77 (H-12a, overlapped), 1.72 (H-5, bs), 1.55 (H-11a, overlapped), 1.53 (H-22a, overlapped), 1.51 (H-1a, m), 1.42 (H-24, overlapped), 1.40 (H-11b, overlapped), 1.35 (H-14, overlapped), 1.33 (H-2a, overlapped), 1.33 (Me-19, s), 1.27 (H-1b, m), 1.05 (Me-18, s), 1.01 (H-9, m), 0.99 (Me-21, d, $J = 7.0$ Hz), 0.89 (Me-26, d, $J = 7.0$ Hz), 0.88 (H-12b, overlapped), 0.86 (H-22b, m), 0.81 (Me-27, d, $J = 7.0$ Hz), 0.75 (Me-28, d, $J = 7.0$ Hz), 0.70 (H-17, overlapped). ESI-MS (negative ions) m/z 737 [$M - 2Na + H$]⁻, 759 [$M - Na$]⁻; HR-ESI-MS m/z 759.2802 (calcd. for $C_{33}H_{53}NaO_{14}PS$ m/z 759.2797).

Cannabinoid CB_1 and CB_2 receptor binding assays. Membranes from HEK-293 cells transfected with the human recombinant CB_1 receptor ($B_{max} = 2.5$ pmol/mg protein) and human recombinant CB_2 receptor ($B_{max} = 4.7$ pmol/mg protein) were incubated with the radiolabelled high affinity ligand [3H]-CP-55,940 (0.14 nM, $K_d = 0.18$ nM and 0.084 nM, $K_d = 0.31$ nM, for CB_1 and CB_2 receptors, respectively) and displaced with 10 μ M WIN 55212-2 as the heterologous competitor for non specific binding (K_i values 9.2 nM and 2.1 nM for CB_1 and CB_2 receptors, respectively). All compounds were tested following the procedure described by the manufacturer (Perkin Elmer, Italia). Displacement curves were generated by incubating drugs with [3H]-CP-55,940 for 90 minutes at 30°C. K_i values were calculated by applying the Cheng-Prusoff equation to the IC_{50} values (obtained by GraphPad) for the displacement of the bound radioligand by increasing concentrations of the test compound. Δ^9 -THC was used as the reference compound. Data are means of 3 experiments.

References

1. Hillig, K.W.; *Genet. Resour. Crop. Evol.*, **2005**, 52, 161–180.
2. **Appendino G, Chianese G, Tagliatela-Scafati O.; *Curr Med Chem*, 2011, 18, 1085-1099.**
3. ElSohly, M. A.; Slade, D. *Life Sci.*, **2005**, 78, 539-548.
4. Ahmed, S. A.; Ross, S. A.; Slade, D.; Radwan, M. M.; Khan, I. A.; ElSohly, M. A; *Tetrahedron Lett.*, **2008**, 49, 6050-6053.
5. Radwan, M. M.; ElSohly, M. A.; Slade, D.; Ahmed, S. A.; Khan, I. A.; Ross, S. A.; *J. Nat. Prod.*, **2009**, 72, 906-911.
6. Tagliatela-Scafati, O. Pagani, A; Scala, F; De Petrocellis, L; Di Marzo, V.; Grassi, G; Appendino, G. *Eur. J. Org. Chem.*, **2010**, 11, 2067-2072.
7. Bohlmann, F.; Hoffmann, E.; *Phytochemistry*, **1979**, 18, 1371-1374.
8. Toyota, M.; Shimamura, T.; Hishii, H.; Renner, M.; Braggings, J.; Asakawa, Y.; *Chem. Pharm. Bull.*, **2002**, 50, 1390-1392.
9. **Chianese, G.; Fattorusso, E.; Tagliatela-Scafati, O.; Bavestrello, G.; Calcinaï, B.; Dien, H. A.; Di Marzo, V.; *Steroids*, 2011, 76, 998-1002.**
10. Patel, KD; Davison, JS; Pittman, KJ; Sharkey, KA; *Curr Med Chem*, **2010**, 17, 1393-1410.
11. Fellermeier, M.; Zenk, M.H; *FEBS Lett.*, **1998**, 427, 283-285.
12. Shoyama, Y.; Hirano, H.; Oda, M.; Somehara, T.; Nishioka, I. *Chem. Pharm. Bull.*, **1975**, 23, 1894-5.
13. Taura, F.; Morimoto, S.; Shoyama, Y.; *Phytochemistry*, **1995**, 39, 457-8.
14. Appendino, G.; Giana, A.; Gibbons, S.; Maffei, M.; Gnavi, G.; Grassi, G.; Sterner, O. A.; *Nat. Prod. Commun.*, **2008**, 3, 1977-1980.
15. Gaoni, Y.; Mechoulam, R.; *Chem. Commun.*, **1966**, 20-21.
16. Claussen, U.; von Spulak, F.; Korte, F.; *Tetrahedron*, **1968**, 24, 1021-1050.

17. Taura, F.; Morimoto, S.; Shoyama, Y.; *J. Biol. Chem.*, **1996**, 271, 17411-17416.
18. Lousberg, R.J.J.C.; Bercht, C.A.L.; Van Ooyen, R.; Spronck, H.J.W.; *Phytochemistry*, **1977**, 16, 595-7.
19. Shani, A.; Mechoulam, R.; *Tetrahedron*, **1974**, 30, 2437-46.
20. Yamamoto, I.; Gohda, H.; Narimatsu, S.; Watanabe, K.; Yoshimura, H.; *Pharmacol. Biochem. Behav.*, **1991**, 40, 541-546.
21. Friedrich-Fiechtl, J.; Spittler, G.; *Tetrahedron*, **1975**, 31, 479-87.
- 22. Pagani, A.; Scala, F.; Chianese, G.; Grassi, G.; Appendino, G.; Tagliatela-Scafati, O.; *Tetrahedron*, 2011, 67, 3369-3373.**
23. Taura, F.; Morimoto, S.; Shoyama, Y.; Mechoulam, R.; *J. Am. Chem. Soc.*, **1995**, 117, 9766-9767.
24. Howlett, A.C.; Johnson, M.R.; Melvin, L.S.; Milne, G.M.; *Mol. Pharmacol.*, **1988**, 33, 297-302.
25. Boeren, E.G.; Elsohly, M.A.; Turner, C.E.; *Experientia*, **1979**, 35, 1278-1279.
26. Chan, W.R.; Magnus, K.E.; Watson, H.A.; *Experientia*, **1976**, 32, 283-284.
27. Elsohly, M.A.; Boeren, E.G.; Turner, C.E. *Experientia*, **1978**, 34, 1127-1128.
28. Ross, S.A.; ElSohly, M.A.; Sultana, G.N.N.; Mehmedic, Z.; Hossain, C.F.; Chandra, S.; *Phytochem. Anal.*, **2005**, 16, 45-48.
29. Bercht, C.A.L.; Lousberg, R.J.J.; Küppers, F.J.E.M.; Salemink, C.A.; *Phytochemistry*, **1974**, 13, 619-621.
30. Gaoni, Y.; Mechoulam, R.; *Isr. J. Chem.*, **1968**, 6, 679-690.
31. Braemer, R.; Paris, M.; *Plant. Cell. Rep.*, **1987**, 6, 150-152.
32. Rinaldi-Carmona, M.; Pialot, F.; Congy, C.; Redon, E.; Barth, F.; Bachy, A.; Brelière, J.C.; Soubrié, P.; Le Fur, G.; *Life Sci.*, **1996**, 58, 1239-1247.
33. Xie, X.-Q.; Chen, J.-Z.; Billings, E.M.; *Protein Struct. Funct. Genet.*, **2003**, 53, 307-319.

34. Sawzdargo, M.; Nguyen, T.; Lee, D.K.; Lynch, K.R.; Cheng, R.; Heng, H.H.; George, S. R.; Dowd, B.F.; *Brain Res. Mol. Brain Res.*, **1999**, 64, 193-198.
35. Devane, W.A.; Hanus, L.; Breuer, A.; Pertwee, R. G.; Stevenson, L.A.; Griffin, G.; Gibson, D.; Mandelbaum, A.; Etinger, A.; Mechoulam, R.; *Science*, **1992**, 258, 1946-1949.
36. Mechoulam, R.; Ben-Shabat, S.; Hanuš, L.; Ligumsky, M.; Kaminski, N.E.; Schatz, A.R.; Gopher, A.; Almog, S.; Martin, B.R.; Compton, D.R.; Pertwee, R.G.; Griffin, G.; Bayewitch, M.; Barg, J.; Vogel, Z.; *Biochem. Pharmacol.*, **1995**, 50, 83-90.
37. Porter, A.C.; Sauer, J.-M.; Knierman, M.D.; Becker, G.W.; Berna, M. J.; Bao, J.; Nomikos, G. G.; Carter, P.; Bymaster, F.P.; Leese, A.B.; Felder, C.C.; *J. Pharmacol. Exp. Ther.*, **2002**, 301, 1020-1024.
38. Garcia, M.C.; Adler-Graschinsky, E.; Celuch, S.M. *Eur. J. Pharmacol.*, **2009**, 610, 75-80.
39. Appendino, G.; Ligresti, A.; Minassi, A.; Cascio, M.G.; Allarà, M.; Tagliatalata-Scafati, O.; Pertwee, R.G.; De Petrocellis, L.; Di Marzo, V.; *J. Med. Chem.*, **2009**, 52, 3001-3009.
40. Akopian A.A.; Ruparel, N.B.; Jeske, N.A.; Patwardhan, A.; Hargreaves, K.M.; *Trend Pharmacol. Sci.*, **2009**, 30, 79-84.
41. Huffman, J.W.; *Mini Rev. Med. Chem.*, **2005**, 5, 641-649.
42. Garb, S.; *J. Clin. Pharmacol.*, **1981**, 21, 57S-59S.
43. Lewis, D.Y.; Brett, R.R.; *Eur. Neuropsychopharm.*, **2010**, 20, 622-631.
44. Galiegue, S.; Mary, S.; Marchand, J.; Dussossoy, D.; Carriere, D.; Carayon, P.; Bouaboula, M.; Shire, D.; Le Fur, G.; Casellas, P.; *Eur. J. Biochem.*, **1995**, 232, 54-61.
45. Bab, I.; Ofek, O.; Tam, J.; Rehnelt, J.; Zimmer, A.; *J. Neuroendocrinol.*, **2008**, 20, 69-74.
46. Matias, I.; Gonthier, M.P.; Orlando, P.; Martiadis, V.; De Petrocellis, L.; Cervino, C.; Petrosino, S.; Hoareau, L.; Festy, F.; Pasquali, R.; Roche, R.;

- Maj, M.; Pagotto, U.; Monteleone, P.; Di Marzo, V.; *J. Clin. Endocrinol. Metab.*, **2006**, 91, 3171–3180.
47. Mao, J.; Price, D.D.; Lu, J.; Keniston, L.; Mayer, D. J.; *Neurosci. Lett.*, **2000**, 280, 13-16.
48. Russo, E.B.; Jiang, H.-E.; Li, X.; Sutton, A.; Carboni, A.; del Bianco, F.; Mandolino, G.; Potter, D.J.; Zhao, Y.-X.; Bera, S.; Zhang, Y.-B.; Lu, E.G.; Ferguson, D.K.; Hueber, F.; Zhao, L.C.; Liu, C.-J., Wang, Y.-F.; Li, C.-S.; *J. Exp. Bot.*, **2008**, 59, 4171-4182.
49. Russo, E.B.; *Chem. Biodiv.*, **2007**, 4, 1614-1648.
50. Green J. *Cannabis* Thunder's Mouth Press: New York, **2001**.
51. Gaoni, Y.; Mechoulam, R.; *J. Am. Chem. Soc.*, **1964**, 86, 1646-1647.
52. Song, B.-H., Wang, X.-Q., Li, F.-Z., Hong, D.-Y.; *Plant Systematics and Evolution*, **2001**, 228, 107-115.
53. Flores-Sanchez, I. J.; Verpoorte, R.; *Phytochem. Rev.*, **2008**, 7, 615-639.
54. The ancient variety *Carmagnola* is named after the town of Carmagnola (Piedmont), where its cultivation thrived until the second half of the XX Century.
55. El-Feraly, F. S.; ElSohly, M. A.; Boeren, E. G.; Turner, C. E.; Ottersen, T.; Aasen, A.; *Tetrahedron*, **1977**, 33, 2373-2378.
56. Boeren, E. G.; ElSohly, M. A.; Turner, C. E.; Salemink, C. A.; *Experientia*, **1977**, 33, 848.
57. a) Crombie, L.; Crombie, W. M. L.; *J. Chem. Soc. Perkin Trans I*, **1982**, 1455-1466. b) Radwan, M. M.; ElSohly, M. A.; Slade, D.; Ahmed, S. A.; Wilson, L.; El-Alfy, A. T.; Khan, I. A.; Ross, S. A.; *Phytochemistry*, **2008**, 69, 2627-2633.
58. Crombie, L.; Crombie, W. M. L.; Jamieson, S. V.; *Tetrahedron Lett.*, **1979**, 7, 661-664.
59. Kikuchi, M.; Yaoita, Y.; Kikuchi, M.; *Helv. Chim. Acta*, **2008**, 91, 1857-1862.

60. Shim, J.Y.; Welsh, W.J.; Howlett, A.C.; *Biopolymers*, **2003**, 71, 169-189.
61. Razdan, R.K.; *Pharmacol. Rev.*, **1986**, 38, 75-149.
62. Frank, B.; Serpell, M. G.; Hughes, J.; Matthews, J.N.S.; Kapur, D.; *Brit. Med. J.*, **2008**, 336, 199-201.
63. Gertsch, J.; Pertwee, R.G.; Di Marzo, V.; *Brit J Pharmacol.*, **2010**, 160, 523-529.
64. Leonti, M.; Casu, L.; Raduner, S.; Cottiglia, F.; Floris, C.; Altmann, K-H.; Gertsch, J.; *Biochem pharmacol*, **2010**, 79, 1815-1826.
65. Fattorusso, E.; Romano, A.; Tagliatela-Scafati, O.; Achmad, M.J.; Bavestrello, G.; Cerrano C.; *Tetrahedron*, **2008**, 64, 3141-3146.
66. Fattorusso, E.; Romano, A.; Tagliatela-Scafati, O.; Achmad, M.J.; Bavestrello, G.; Cerrano, C.; *Tetrahedron Lett*, **2008**, 49, 2189-2192.
67. Angawi, R.F.; Calcinai, B.; Cerrano, C.; Dien, H.A.; Fattorusso, E.; Scala, F.; Tagliatela-Scafati, O.; *J Nat Prod*, **2009**, 72, 2195-2198.
68. Qureshi, A.; Faulkner, D.J.; *Tetrahedron*, **1999**, 55, 8323-8330.
69. Fujita, M.; Nakao, Y.; Matsunaga, S.; Seiki, M.; Itoh, Y.; van Soest, R.W.M.; Heubes, M.; Faulkner, D.J.; Fusetani, N.; *Tetrahedron*, **2001**, 57, 3885-3890.
70. De Riccardis, F.; Iorizzi, M.; Minale, L.; Riccio, R.; Debitus, C.; *Tetrahedron Lett*, **1992**, 33, 1097-1100.
71. Pereira, A.; Pfeifer, T.A.; Grigliatti, T.A.; Andersen, R.J.; *ACS Chem Biol*, **2009**, 4, 139-144.
72. Mayer, M.; Meyer, B.; *Angew Chem Int*, **1999**, 38, 1784-1788.

CHAPTER III

ISOLATION AND SYNTHESIS OF NEW ANTIMALARIAL COMPOUNDS

3.1. MALARIA

It has been estimated that 300-500 million cases of malaria occur annually with 1.75 to 2.5 million deaths. Malaria is a particularly important disease in sub-Saharan Africa, where about 90% of cases and deaths occur, but is also a serious public health problem in certain regions of Southeast Asia and South America.¹ Human malaria is caused by four species of *Plasmodium*, namely *P. falciparum*, *P. vivax*, *P. ovale* and *P. malariae*, which are transmitted by female *Anopheles* mosquitoes. *P. falciparum* is the parasite that causes most severe diseases and most fatal cases. The life cycle, immunological defence mechanisms, and clinical development of malaria in humans is complex. The sporozoites that develop in the salivary glands of the female mosquito are inoculated into the human when then the insect bites to acquire a blood meal. The protozoans in the sporozoite form invade selectively the parenchymal cells of the human liver. In this stage, the patient remains asymptomatic and, after an average incubation period of 5-7 days (in the case of *P. falciparum*), protozoa reach the merozoite stage and are released from the liver. The merozoites invade the erythrocytes and start feeding on the haemoglobin. After proliferation, the rupture of the erythrocyte membrane and the consequent liberation of other merozoites, that invade other erythrocytes, cause the massive infection and the symptoms. A small portion of merozoites develops into the sexual stage of gametocytes, a form that is able to re-start the life cycle of the malaria parasite when a mosquito takes a blood meal from an infected person² (Fig. 3.1).

The clinical symptoms of malaria infections are exclusively attributable to parasites in the erythrocytic stage. The rupture of infected erythrocytes is associated with the release into the blood stream of cell debris responsible for the characteristic fever spike patterns. In the lethal cases, a specific protein produced

by the protozoan is embedded into the cell membrane of the infected erythrocyte and, as a consequence of this modification, the erythrocyte sticks to the walls of capillaries causing obstruction of vessels. When this mechanism operates at the level of brain vessels, the loss of consciousness is the first symptom, but, if this form of cerebral malaria is not treated immediately, it is soon followed by death.

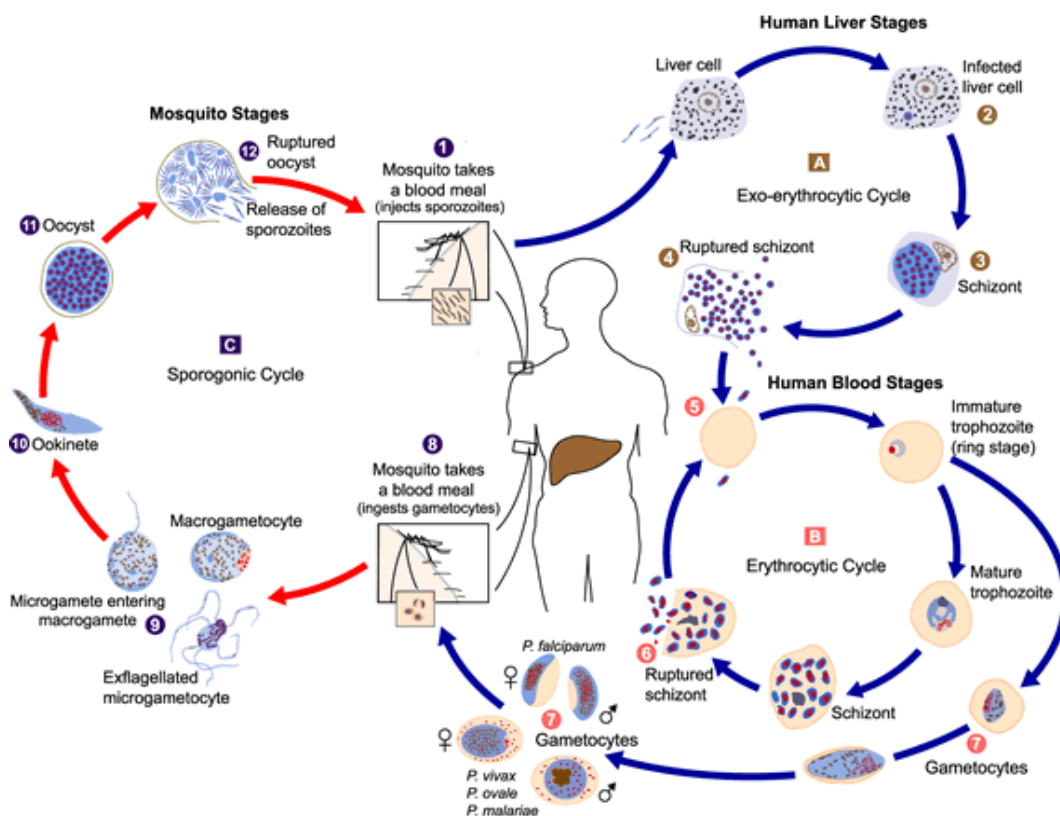


Figure 3.1 The malaria cell cycle

The treatment of malaria infections holds a venerable place in the history of medicinal chemistry and of natural product chemistry. As commonly well-known, the first specific treatment for malaria dates back to the 17th century when the bark of *Cinchona* trees was used as the best tool to face infections of malaria, that was endemic in Africa, Asia but also in several parts of Europe and North America. Later, malaria was the first disease to be treated with an active principle isolated from a natural source, quinine (37) isolated from the *Cinchona* bark in 1820, and, later again, the first human disease to be treated with a synthetic drug (methylene blue in 1891).

In the course of 20th century, especially during World War II, a series of effective synthetic antimalarial drugs have been developed. Among them, chloroquine (38), mefloquine (39), and pyrimethamine (40) (Fig. 3.2), became the drugs of choice

in several programs and contributed to the almost complete eradication of malaria from Europe and North America.

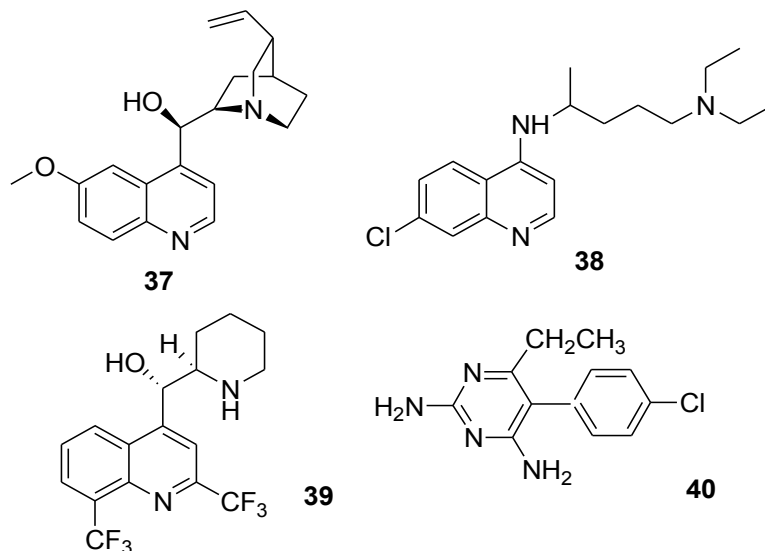


Figure 3.2. First-line antimalarial drugs: quinine (**37**), choloquine (**38**), mefloquine (**39**), pyrimetamine (**40**).

The chemotherapy and prophylaxis of malaria have been undermined by the development of worldwide resistance of *P. falciparum* to the 4-aminoquinoline chloroquine, first observed in the 1960s, as well as resistance to the antifolates pyrimethamine and cycloguanil. Two major breakthroughs of the past few decades have renewed the assault of scientists to this infective disease. The first is the complete sequencing of the genome of *Plasmodium falciparum* that is expected to provide useful information for the identification of new drug targets. The second is the discovery, by Chinese researchers, of artemisinin (**41**, qinghaosu), an endoperoxide sesquiterpene lactone which is the active principle of the sweet wormwood, *Artemisia annua*, an herbal remedy used in folk Chinese medicine for 2000 years. This molecule and its oil soluble (e.g. artemether, **42**, and arteether) and water soluble (e.g. artesunate, **43**, and artelinate) semi-synthetic derivatives (**Fig. 3.3**) have shown excellent efficacy against chloroquine-resistant *Plasmodium* strains and are becoming increasingly used, especially in combination with traditional antimalarials (e.g. mefloquine, **39**).

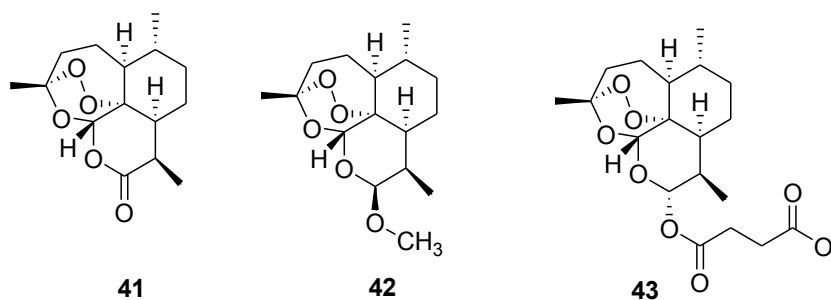


Figure 3.3. Chemical structures of artemisinin (**41**) and of its semisynthetic derivatives artemether (**42**) and artesunate (**43**).

Unfortunately, in our days malaria still continues to be an extremely important threat to the health and economic prosperity of the human race, constituting a major cause of morbidity and mortality in tropical countries of Asia, Africa and South America. Part of the reason for the failure to control malaria in these areas is the emergence and spread of resistance to first-line antimalarial drugs and recently to artemisinin (**41**) too, cross-resistance between the members of the limited number of drug families available, and in some areas, multi-drug resistance³. In addition, the prevalent spreading of the disease to poor countries has suggested to many pharmaceutical companies to categorize malaria as a low priority. In this context, funds provided by public agencies, as European Community, are the good news of recent years. Their specific aim is to encourage the antimalarial research in spite of the poor economic interest. The search for alternative antimalarials is one of the main topics of my Ph.D. activity discussed in this thesis.

3.2. ANTIMALARIAL ENDOPEROXIDES

In 1972, following an activity-guided fractionation, the sesquiterpene derivative artemisinin (in China named qinghaosu: “the active principle of qinghao”) was isolated from *Artemisia annua* (Compositae). Later its structure was elucidated and it was shown to possess a potent antimalarial activity. This molecule soon appeared to constitute a major breakthrough in the antimalarial therapy because of: 1) its nanomolar activity on chloroquine-resistant *P. falciparum* strains (higher than the activity on chloroquine-sensitive ones) even on cerebral malaria; 2) its fast action; 3) the absence of detectable toxicity at therapeutic doses.

Artemisinin (**41**) is a structurally complex cadinane sesquiterpene lactone bearing an endoperoxide group embedded in a 1,2,4-trioxane ring. Since the relatively efficient totally synthetic routes developed will very unlikely supplant the natural source, an intense scientific activity has been carried out entailed to the chemical derivatization of artemisinin. The aim was to obtain compounds with better solubility, higher stability, and possibly devoid of the neurotoxic side effects detected for the natural molecule. These efforts soon resulted in the recognition that the endoperoxide linkage is an essential feature for antimalarial activity, given that the acyclic diol and the ether (1,3-dioxolane) analogues of artemisinin were completely devoid of activity. Consequently, the lactone group became the main site for chemical variations that bore the preparation of the oil-soluble artemether (**42**) (**Fig. 3.3**), and the water-soluble artesunate (**43**). Although these molecules are now used for treatment of severe malaria with the support of the World Health Organization, unfortunately, they still possess neurotoxic activity⁴. An essential requirement to design optimized artemisinin derivatives would be a perfect knowledge of the mechanism of its antimalarial activity. Unfortunately, still today our knowledge appears incomplete. Artemisinin (or its analogues) should interact, within the parasite food vacuole, with the Fe(II) center of the heme unit released during the digestion of hemoglobin. The interaction of artemisinin with the heme ferrous iron would cause the cleavage of the peroxide bridge and the formation of alkoxy radicals that, after several rearrangements, would result in the formation of free C-centered radicals (**Figure 3.5**).

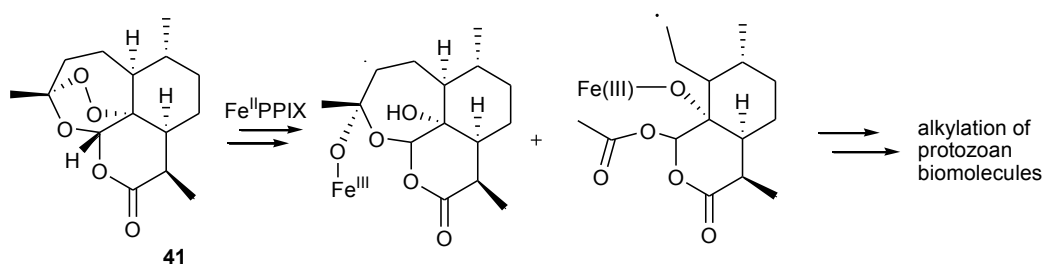


Figure 3.5. A schematic view of the postulated mechanism of action of artemisinin (**41**).

These should be toxic to the parasite because they should alkylate not better defined “sensitive” macromolecular targets. This hypothesis is based on the evidence that, in several experimental models, artemisinin (**41**) reacts with iron

ions and, in particular, it interacts strongly with hemin (ferriprotoporphyrin IX) and its ferrous form (ferroprotoporphyrin IX) to give covalent adducts.⁵

Further experiments would be required to gain more insights into the mechanism of action of the endoperoxide-containing antimalarial agents. The isolation of different antimalarial endoperoxides from natural sources can evidently help in this task. A large number of cyclic peroxides have been isolated from marine organisms and some of them have been tested for antimalarial activity.

Marine sponges belonging to the family Plakinidae contain a series of simple endoperoxide derivatives that have been identified as polyketide metabolites possessing six- or five-membered 1,2-dioxygenated rings (1,2-dioxane or 1,2-dioxolane, respectively). A further variation is represented, in some cases, by the presence of a 3-methoxy substitution, building a peroxyketal group. The parent compound of this group of secondary metabolites is plakortin (**44**) (Fig. 3.6), that was isolated more than 25 years ago from *Plakortis halichondroides*. This interesting secondary metabolite, whose polyketide skeleton suggests the involvement of butyrate units in the biogenesis, has been recently re-isolated in remarkable amounts from the Caribbean sponge *Plakortis simplex*,⁶ along with a related analogue, named dihydroplakortin (**45**), (Fig. 3.6).

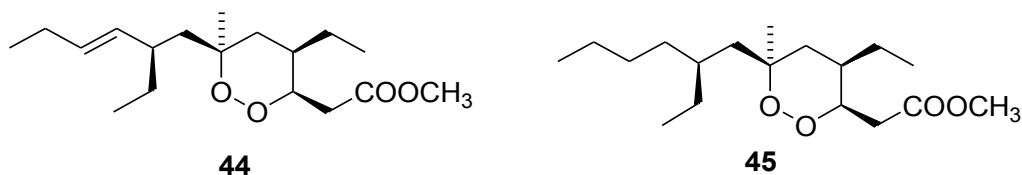


Figure 3.6. Chemical structures of plakortin (**44**) and dihydroplakortin (**45**)

At the time of its first isolation, plakortin was found to be a weak antibacterial agent, but a recent study has finally disclosed the antimalarial potential of this molecule.⁷ Using the pLDH assay, plakortin (**44**) and dihydroplakortin (**45**) were assayed against D10, chloroquine-sensitive strain, and W2, chloroquine-resistant strain of *P. falciparum*. The two compounds showed a good activity, that was more potent on the W2 strain (IC₅₀ = ab. 250 ng/mL on D10; ab. 180 ng/mL on W2). In addition, the two compounds proved to be non-cytotoxic in vitro.

Interestingly, in the same investigation⁷ the structurally related, even more sterically hindered, five-membered endoperoxide plakortide E (**46**) (**Fig. 3.7**) was found to be inactive.

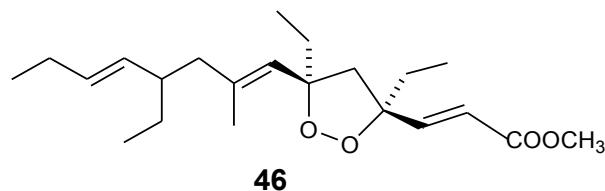
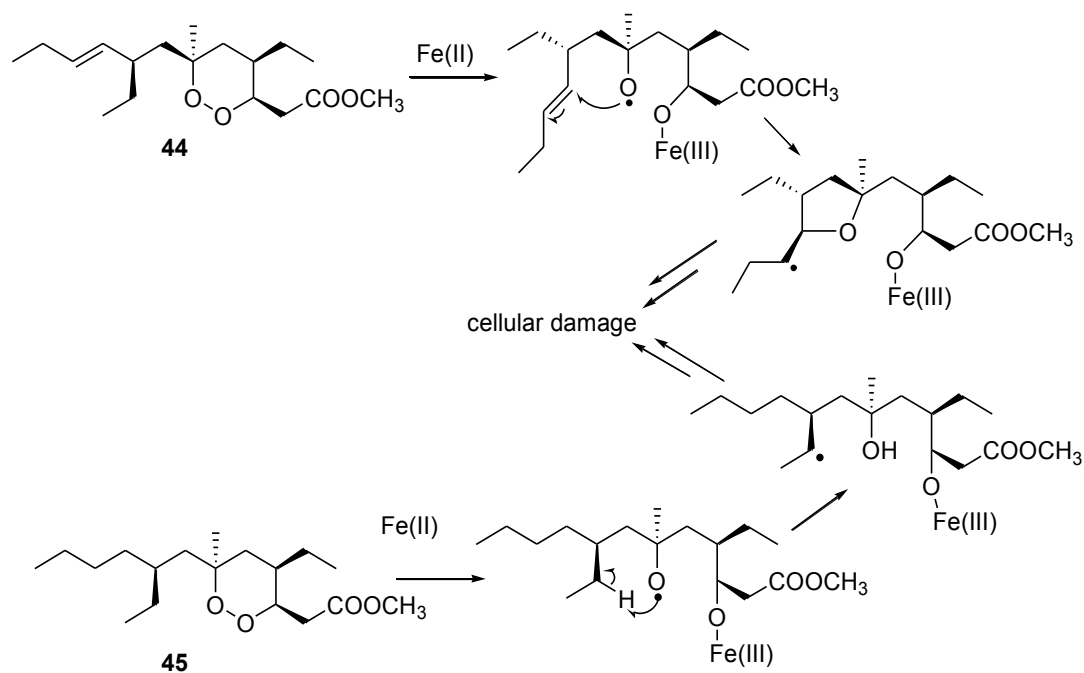


Figure 3.7. Chemical structure of the inactive plakortide E (**46**)

The chemical structure of these antimalarial leads is remarkably simple and thus they could constitute a good probe to establish structure-activity relationships, to check the currently postulated mechanisms of action for antimalarial peroxides and to prepare semi-synthetic or totally synthetic derivatives. In this area, my research group has launched a multidisciplinary investigation (including computational and experimental studies) on natural analogues^{8,9} and semi-synthetic derivatives¹⁰ that provided some valuable insights about the SARs needed for the antimalarial activity of these simple 1,2-dioxanes. These results unambiguously indicated the crucial role of the endoperoxide functionality, suggested the importance of the “western” alkyl side chain and revealed conformation-dependent features critical for antimalarial activity.¹⁰

In addition, in a recently reported investigation based on a combined chemical and computational approach,¹¹ my research group proposed that molecules belonging to the plakortin family, upon interaction with Fe(II) undergo a dissociative electron transfer (DET) of the endoperoxide bond giving rise to an oxygen-centered radical. This latter is simultaneously transferred by a “through space” 1,4- (**1**) or 1,5- (**2**) intramolecular radical shift to a western side chain carbon atom which, through a radical cascade, leads to the putative toxic species for the Plasmodium environment (**Scheme 3.1**).



Scheme 3.1. Proposed antimalarial mechanism of action of plakortin (**44**) and dihydroplakortin (**45**).

An indirect support to this mechanism comes from the inactivity of those plakortin analogues which experience steric problems to the accessibility of reactive iron species to the endoperoxide oxygens (as manadoperoxides), as well as from the very low activity of those plakortin analogues for which the orientation of reaction partners does not allow the intramolecular radical shift.

Further information on the structure-activity relationships come from data on synthetic and natural 3-alkoxy-1,2-dioxene and 3-alkoxy-1,2-dioxane (both peroxyketals) derivatives, which were shown to possess a very good antimalarial activity (peroxyplakoric B₃ ester, **Fig. 3.8**, IC₅₀ = 0.12 μM).

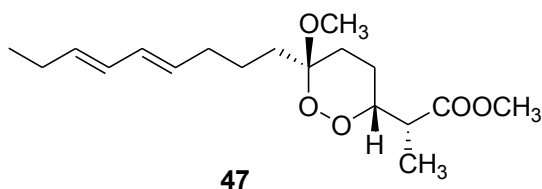


Figure 3.8. Chemical structures of peroxyplakoric acid B₃ (**47**) methyl ester.

Recently, four new peroxyketal polyketides, named manadoperoxides A-D¹² (**48-51**) (**Fig. 3.9**), were obtained from the organic extract of a specimen of *Plakortis* sp. collected in the Bunaken Marine Park of Manado (North Sulawesi, Indonesia).

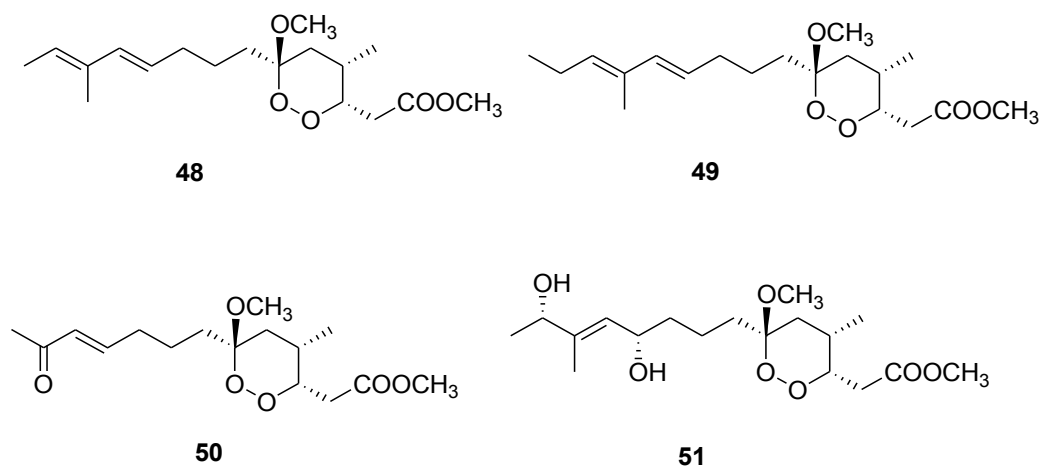


Figure 3.9. Chemical structures of manadoperoxides A (**48**), B (**49**), C (**50**) and D (**51**).

These endoperoxide derivatives **48-51** has a moderate antimalarial activity (low μM range) against both CQ-R and CQ-S *P. falciparum* clones (manadoperoxide B $\text{IC}_{50} = 6.76 \mu\text{M}$). The modest antimalarial activity of manadoperoxides is particularly surprising for example upon comparison of manadoperoxide B (**49**) with peroxyplakoric B₃ ester¹³ (**47**). In spite of the very small structural differences (a methyl group linked at C-2, in **47**, in place of C-4, in **49**), compound **47** exhibited a 56-times higher in vitro antimalarial activity compared to **49**. This unexpected difference should be caused by the presence of a methyl at C-4 on the dioxane ring of manadoperoxides, that induces a preferential chair B conformations where two groups are in axial positions. This implies that the approach of manadoperoxides to heme iron is complicated (if not prevented) by the orientation of groups on the dioxane ring (**Fig.3.10**).¹²

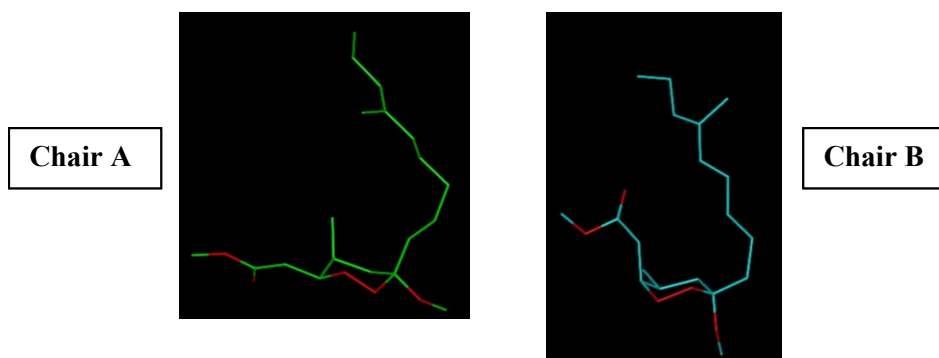


Figure 3.10. In manadoperoxides the endoperoxide bond in Chair B (85% pop.) is not accessible to heme iron or the evolution of the radical is not possible (Chair A, 5% population) .

The acquired information suggested that the essential pharmacophoric requirements for antimalarial activity should include: i) a 1,2 dioxane ring able to react with Fe(II) species through its endoperoxide group forming an oxygen radical, ii) a side-chain bearing possible partners for a “through-space” intramolecular radical shift to a carbon atom, iii) configurational and conformational features which allow accessibility of iron to 1,2-dioxane oxygens as well as the correct orientation of all the intramolecular reaction partners, iv) iron interacting with additional functionalities that favours the approach to heme without interfering with the redox reaction and v) the ability of the generated carbon radical to propagate via intermolecular reactions (**Fig. 3.11**).

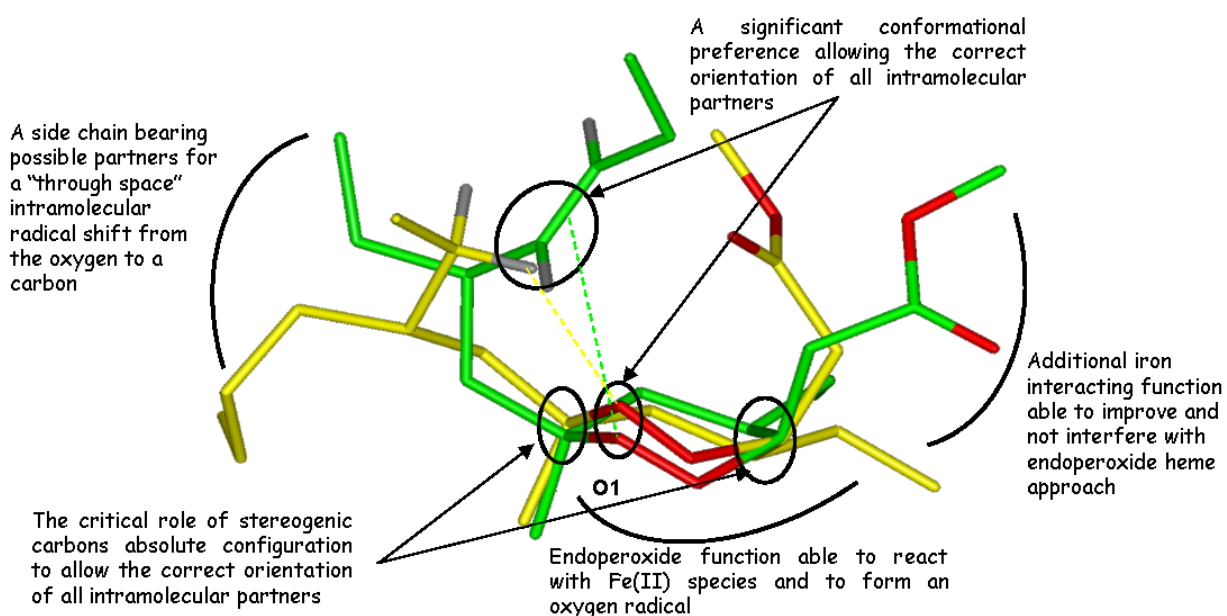


Figure 3.11. Plakortin (**44**, C atoms, green; O atoms, red) and Dihydroplakortin (**45**, C atoms, yellow; O atoms, red) pharmacophores.

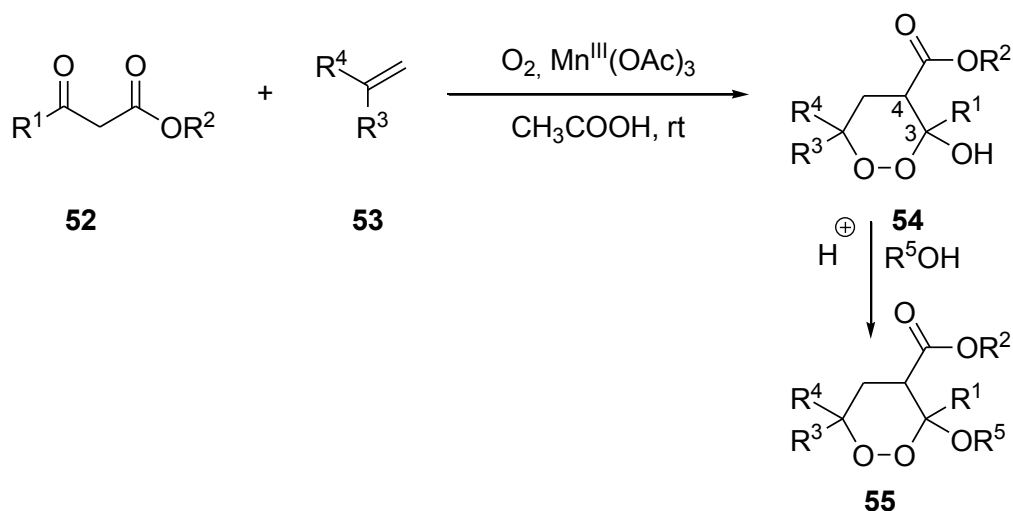
Basing on these information now available for plakortin antimalarials, in this thesis I report a synthesis of a new chemotype of antimalarial agents based on the simple, monocyclic 1,2-dioxane scaffold. Ideally, this simplified structure could allow an efficient chemical synthesis, amenable to large-scale preparation of new antimalarials at low costs. As suggested by the Target Product Profile (TPP) published by Medicine for Malaria Venture (MMV) in September 2010, cheapness is a crucial requirement for antimalarial drugs of the next generation. According to MMV, a likely clinical candidate should have oral activity with

SERC (single exposure radical cure) and a cost treatment of less than 1\$ for uncomplicated malaria.¹⁴ Taking into account the developed pharmacophore model (**Fig. 3.11**), in the following paragraph I report the design, the synthesis, the biological evaluation, and the 3D-SAR studies for a novel series of 1,2-dioxane antimalarials obtained by means of an efficient one-pot three-component Mn(III)-mediated synthesis which utilizes cheap starting materials. The obtained molecules are 3,6,6-trisubstituted 3-methoxy-1,2-dioxanes with simple alkyl chains and bearing an ester group at position 4, which were tested against *Pf*.

3.3. SYNTHESIS OF SIMPLIFIED ANTIMALARIAL ENDOPEROXIDES

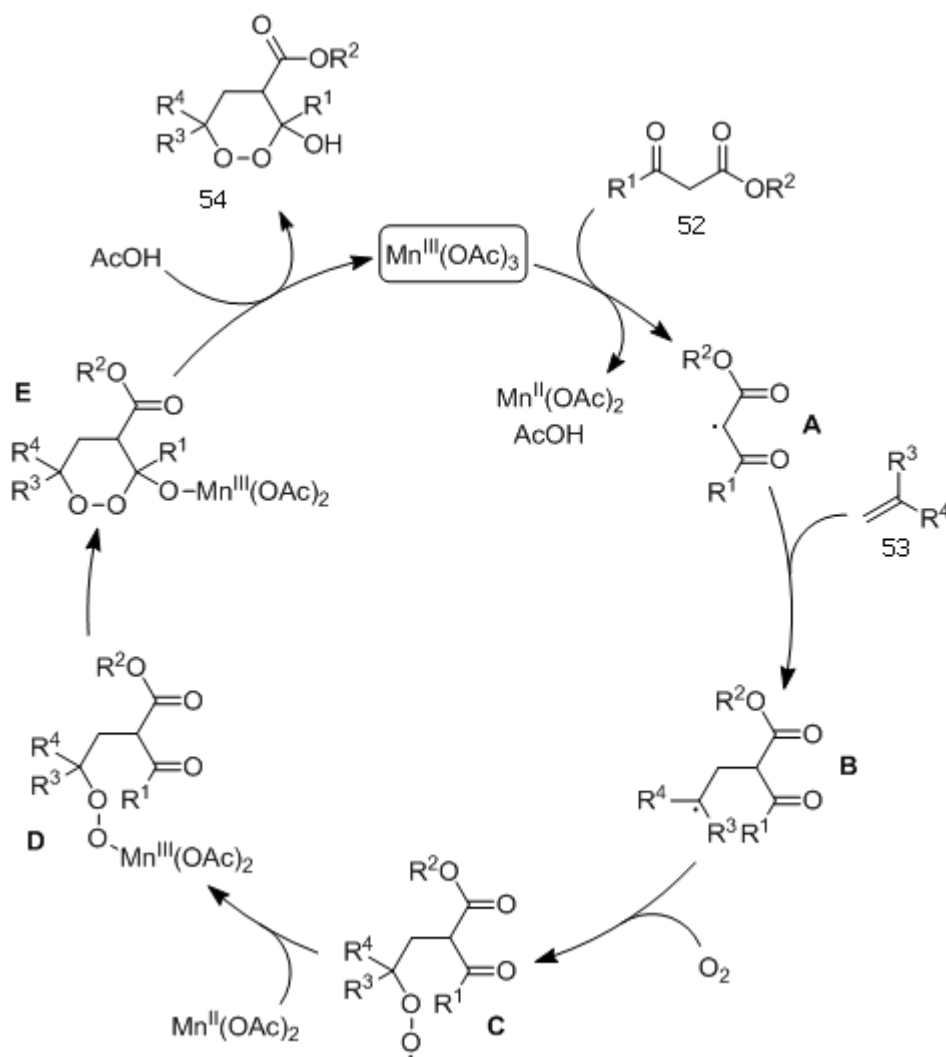
In the last few decades, a large number of synthetic endoperoxides (1,2-dioxolanes and 1,2-dioxanes),¹⁵ 1,2,4-trioxolanes,¹⁶ 1,2,4-trioxanes¹⁷ and 1,2,4,5-tetraoxanes²⁴⁻²⁵ have been synthesized and studied as potential antimalarial drugs for treatment of chloroquine (CQ) resistant *Pf* infections. The current status of synthetic peroxides inspired by artemisinin and other naturally occurring peroxides has been examined in recent review articles.¹⁸

In 1990, Nishino and co-workers reported a seminal research work on the synthesis of 1,2-dioxane-3-ol scaffolds (**54**) by the manganese(III) acetate-promoted formal [2+2+2] cycloaddition of activated methylene compounds (i.e. β -ketoesters **52**), olefins (**53**) and molecular oxygen¹⁹ a reaction first reported in 1989 to proceed under electrochemical oxidation conditions or by AIBN-promoted radical cascade.²⁰ In collaboration with the research group of prof. Trombini, at the University of Bologna, my research group has optimized the Nishino conditions to obtain the synthesis of 1,2-dioxane-3-ols as depicted in **Scheme 3.2**.



Scheme 3.2. Manganese(III) acetate-promoted synthesis of 1,2-dioxane-3-ols **54**

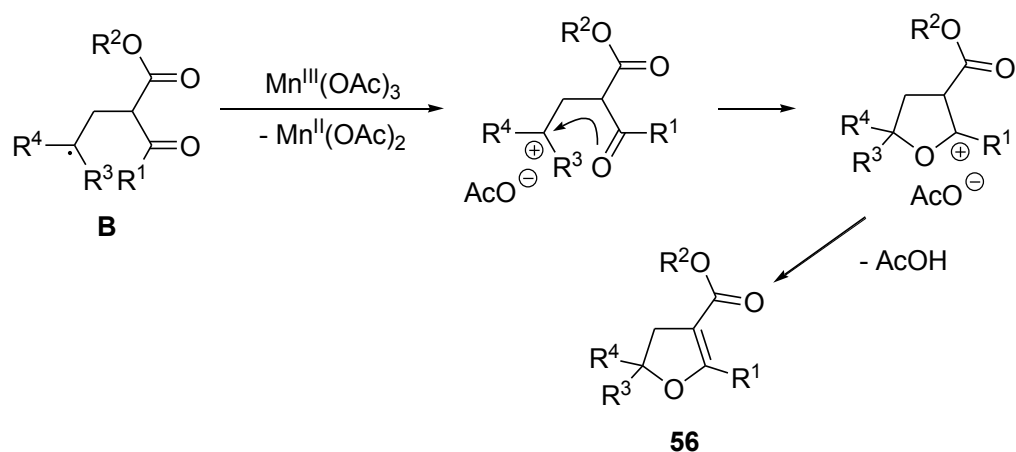
The formal catalytic cycle is based on the key generation of enol radicals **A** by oxidation of **52** using Mn(III) acetate, as depicted in **Scheme 3.3**.²¹



Scheme 3.3. Formal catalytic cycle for the Mn(III) acetate-promoted synthesis of 1,2-dioxane-3-ols **54**

In terms of structural versatility and flexibility, 1,2-dioxane **54** exhibits three interesting features: i) substituents R¹-R⁴ can be varied as a result of a rational choice of the β-ketoester **52** and the alkene component **53**; ii) the ester attached at C-4 offers manifold opportunities for chemical transformations (reductions, amide formation, *etc*), and finally, iii) the hemiketal group on C-3 can be converted into the corresponding ketal **55** upon incorporation of a suitable alcohol (R⁵OH, **Scheme 3.2**). Reactions are carried out in glacial acetic acid at room temperature. Manganese(III) acetate is insoluble in acetic acid at room temperature but, in the presence of an activated methylene compound, it gradually dissolves, suggesting the formation of a new Mn(III) complex by ligand exchange. The *in situ* generated Mn(III)-enolate rapidly collapses into the electrophilic carbon radicals **A** by single electron transfer from the electron-rich carbon-carbon double bond to Mn(III).

When the reaction is carried out at room temperature in the presence of an olefin (typically a *gem*-disubstituted alkene) and molecular oxygen, **A** adds first to the alkene providing the nucleophilic carbon centered radical **B**, which then takes up oxygen dissolved in acetic acid to produce **C**. A new one-electron transfer from Mn(II) to **C** restores Mn(III) and generates the hydroperoxy anion **D**, that rapidly collapses to **E** by ring-chain tautomerism. Acidic quenching by acetic acid affords the target 1,2-dioxane-3-ol **54**, restoring Mn(III) acetate in solution. The electronic properties of the intermediate free-radicals determine the order of the radical cascade, and reduce the side-reactions such as the homocouplings of **A** and **C**, as well as the combination of molecular oxygen, an electrophilic bi-radical, with the electrophilic enol radical **A**. This catalytic process has been reported to work efficiently with 1,1-diarylethenes, affording remarkable yields of the expected cycloadducts. Considerably lower are the conversions reported with *gem*-disubstituted aliphatic alkenes. In principle, with this family of alkenes, off-cycle redox reactions can have a significant impact on the final yields in 1,2-dioxane-3-ol **54**. For example, free-radical **B** may be over-oxidized by Mn(III) to carbenium ion that stabilizes upon cyclisation to dihydrofuran **56** (Scheme 3.4). Finally, alkene itself may be oxidized by Mn(III) in acetic acid, thus contributing to the presence of side-products together with homo-coupling reactions.



Scheme 3.4. Manganese(III) acetate promoted over-oxidation of carbon-radical **B** to dihydrofuran **56**

After several optimization runs, the best experimental conditions in terms of yields and purity of the products were reached by using: i) a catalytic amount of Mn(III) acetate (10 mol %), ii) a stoichiometric amount of Mn(II) acetate, iii) a

3:1 molar ratio between the β -ketoester **52** and the alkene **53**, and iv) oxygen at atmospheric pressure in acetic acid as solvent at room temperature. In all cases, the examined products were obtained in fair to good isolated chemical yields (39-89%). In the case of symmetrically di-substituted ($R^3 = R^4$) alkenes **53**, a single diastereoisomer of the product **54** was identified in the crude reaction mixture and isolated by flash-chromatography, possessing the hydroxyl group at C-3 and the carbomethoxy at C-4 in the *cis* stereo-relationship and adopting a preferred conformation with the hydroxyl group in the axial position. This was determined through complete assignment of ^1H NMR resonances followed by interpretation of cross-peaks in the 2D NMR ROESY spectrum (correlations H-4/alkyl group at C-6; H-4/alkyl group at C-3) (**Fig. 3.12**). On the other hand, when non-symmetrically disubstituted alkenes were used, only two of the four possible diastereoisomers were obtained and isolated, again possessing a fixed 3,4-*cis* stereo-relationship, but differing for the configuration at C-6 (**Fig. 3.12**). The preferential formation of 3,4-*cis* stereoisomers was already noticed by Nishino¹⁹⁻²¹ and it is likely the consequence of the stereospecific attack of the hydroperoxy oxygen at the ketone group, determined by the configuration at C-4.

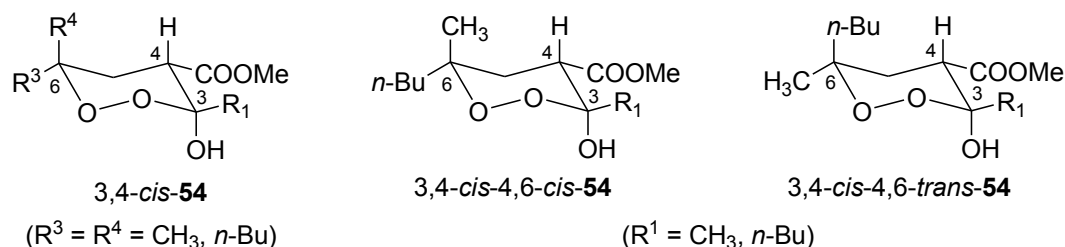


Figure 3.12. Most stable conformers of the products isolated from Mn(III) acetate-promoted cycloaddition

All the intermediate 1,2-dioxane-3-ols were tested for their *in vitro* antimalarial activity against both chloroquine-sensitive (D10) and chloroquine-resistant (W2) *Pf* strains, and all resulted completely inactive ($\text{IC}_{50} > 30 \mu\text{M}$). This result was not surprising since a very low antimalarial activity has already been reported for other hemiketal endoperoxides.²² Thus, the 1,2-dioxane-3-ols were transformed into the corresponding methyl ketal derivatives **57-63**. The ketalization reaction proved to be less easy than hoped and, after screening several different reaction conditions, we found the best results in terms of yields by using camphorsulfonic

acid (CSA) as the promoter in the presence of methyl-orthoformate at room temperature for 72 hrs.

According to this procedure, 1,2-dioxanes **57-63** were prepared (**Fig. 3.13**) which show different permutations of R¹, R³ and R⁴ substituents, corresponding mainly, but not exclusively, to methyl- or *n*-butyl groups.

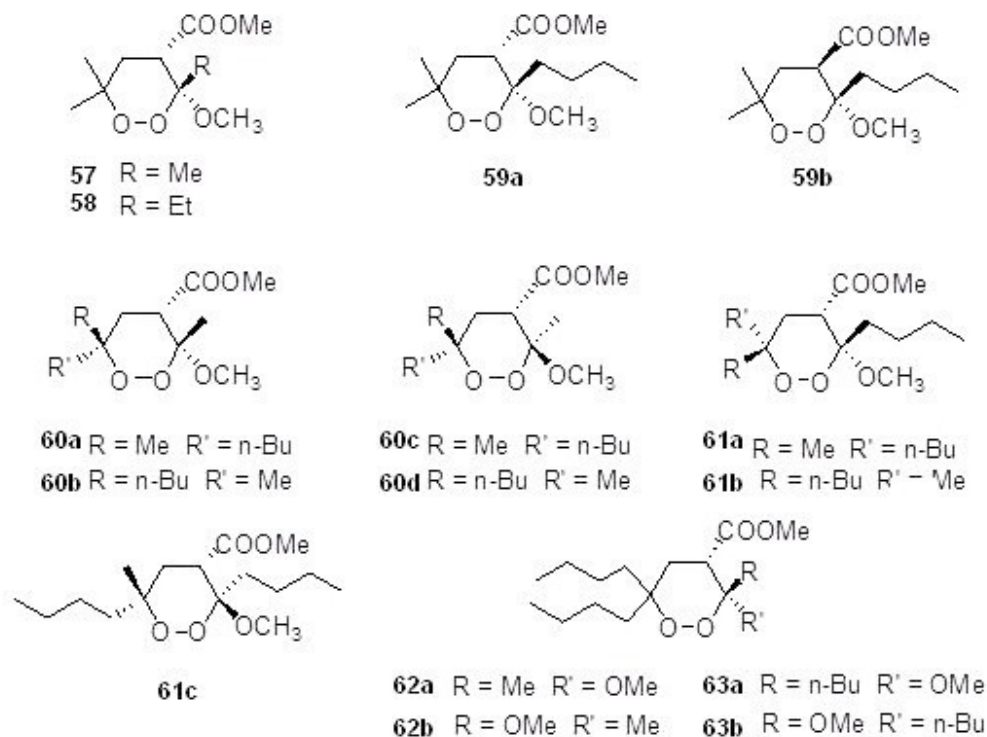


Figure 3.13. (±) 1,2-Dioxanes **57-63**.

When the reagent mixture consisted of a single diastereomer (see **Table 3.1**), two diastereomeric products were isolated, deriving from a partial epimerization at C-3 during the ketalization process, with diastereoselectivities in the 50:50 – 70:30 range, in favor of the 3,4-*cis* adduct. When a mixture of two diastereomeric 1,2-dioxane-3-ols **54** was used (see **Table 3.1**) a more complex mixture of diastereomers was isolated, but the same stereochemical trend was observed. **Table 3.1** summarizes conditions and results of the synthesis of methyl ketals **57-63**. Of course, all the compounds shown in **figure 3.13** and reported in **Table 3.1** have been obtained as racemic mixtures.

Table 3.1. Synthesis of methyl ketals **57-63**^a

Substituents	Comp. 54 , Yield (%)	Diastereomeric ratio of 54	Methyl ketals 57-63 , Yield (%)	Diastereomeric ratio of 57-63 (<i>3,4 cis / trans</i>)
R ¹ = R ³ = R ⁴ = CH ₃	89	3,4- <i>cis</i> (100%)	57 (81%)	70:30
R ¹ = Et R ³ = R ⁴ = CH ₃	39	3,4- <i>cis</i> (100%)	58 (48%)	70:30
R ¹ = Bu R ³ = R ⁴ = CH ₃	65	3,4- <i>cis</i> (100%)	59a-59b (69%)	70:30
R ¹ = R ³ = CH ₃ R ⁴ = Bu	54	3,4- <i>cis</i> -4,6- <i>cis</i> (50%)	60a-60c (40%)	60:40
		3,4- <i>cis</i> -4,6- <i>trans</i> (50%)	60b-60d (40%)	60:40
R ¹ = R ³ = Bu R ⁴ = CH ₃	64	3,4- <i>cis</i> -4,6- <i>cis</i> (50%)	61a-61c (30%)	60:40
		3,4- <i>cis</i> -4,6- <i>trans</i> (50%)	61b (30%)	>95:5 ^b
R ¹ = CH ₃ R ³ = R ⁴ = Bu	71	3,4- <i>cis</i> (100%)	62a-62b (73%)	60:40
R ¹ = R ³ = R ⁴ = Bu	53	3,4- <i>cis</i> (100%)	63a-63b (44%)	50:50

^a Conditions: CSA (5.0 equiv.), methylorthoformate (2 equiv.), MeOH (0.14 M), RT for 72 h. ^b The minor 3,4-*trans*-4,6-*trans* stereoisomer was not detected nor isolated.

All the diastereomeric mixtures were separated by gravity column chromatography followed by direct phase HPLC; then complete NMR assignments were obtained on the isolated diastereomers through 2D NMR spectroscopy (COSY, HSQC, HMBC experiments). Finally, the relative configuration around the six-membered ring was determined for each compound through inspection of the 2D NMR ROESY experiments. For example, the ROESY cross-peaks of H-4 (δ 3.07) with H₂-1'' (δ 1.83 and 1.70) and of H-5ax (δ 2.23) with Me-6 (δ 1.16) and with OMe-3 (δ 3.31) were used to infer the relative configuration of compound **60b** (Fig. 3.14).

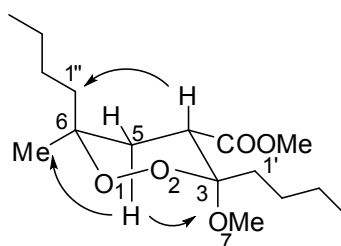


Figure 3.14 Determination of relative configuration for compound **60b** through ROESY correlations.

To overcome the partial isomerization at C3 in the acid-catalyzed ketalization step, we attempted a different approach to **55** treating **54** with a strong base in THF, in the presence of an excess of CH₃I. Surprisingly, under these conditions no trace of methylketals was detected, on the contrary methylation at C4 did occur, only.

3.3.1. *In vitro* antimalarial activity

The 1,2-dioxane-3-O-methyl derivatives **57-63** have been tested for their *in vitro* antimalarial activity against both CQ-S (D10) and CQ-R (W2) *Pf* strains by prof. Taramelli at the University of Milan. Results summarized in **Table 3.2** show that most of these compounds have antimalarial activity in the low μM range. In addition, all the compounds showed activity against the CQ-R strain higher than against CQ-S strain.

Table 3.2. Antimalarial activity of methyl-ketals **57-63** against chloroquine-sensitive (D10) and chloroquine-resistant (W2) *P. falciparum* strains.

Compound	D10 IC ₅₀	W2 IC ₅₀
57	> 30	> 30
58	> 30	> 30
59a	3.7 ± 0.2	1.5 ± 0.5
59b	> 30	> 30
60a	8.5 ± 3.8	4.9 ± 1.7
60b	12.6 ± 6.0	11.8 ± 2.2
60c	17.7 ± 4.0	8.4 ± 2.9
60d	17.7 ± 2.9	6.4 ± 1.4
61a	4.2 ± 1.0	1.5 ± 0.4
61b	2.6 ± 0.2	1.3 ± 0.2
61c	12.3 ± 1.7	5.0 ± 1.1
62a	7.4 ± 1.1	2.5 ± 0.7
62b	2.6 ± 0.7	0.8 ± 0.3
63a	2.9 ± 0.6	1.2 ± 0.2
63b	2.3 ± 0.6	1.2 ± 0.3
Chloroquine	0.029 ± 0.012	0.52 ± 0.02
44^b	0.9 ± 0.4	0.4 ± 0.1

^a Data are means ± SD of three different experiments in duplicate.

^b Data from Ref. 11.

When tested for cellular cytotoxicity against a human endothelial cell line, HMEC-1, compounds **59a**, **61b**, **62b** and **63a** were not toxic (**Table 3.3**) with a therapeutic index ranging from 90 to 250 (calculated on CQ-R strains). These results, although incomplete, suggest that this class of compounds is suitable for further development.

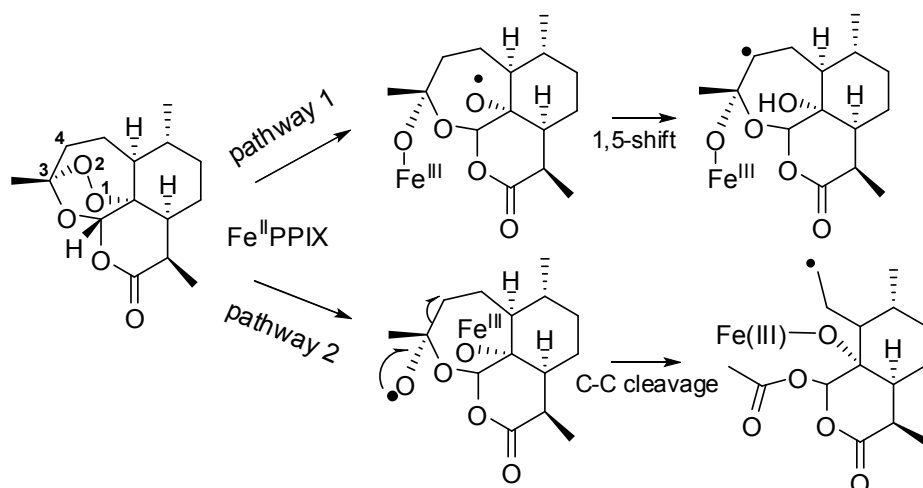
Table 3.3 Citotoxicity on human microvascular endothelial cell line HMEC-1.

Compound	IC₅₀ (μM)^a
59a	> 384
61b	167.3 ± 24.7
62b	98.3 ± 4.1
63a	107.9 ± 10.8

^a Data are means ± SD of three different experiments in duplicate.

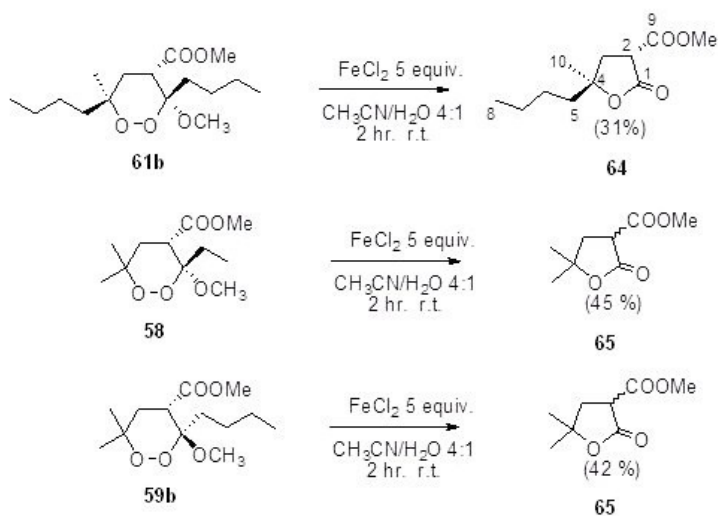
3.3.2. Reaction with Fe(II) chloride

The exact molecular mechanism underlying the biological activity of artemisinin and that of related antimalarial endoperoxides is still a matter of debate. The interaction with Fe(II)-heme, and the consequent oxidative stress in the plasmodium are believed to play a major role in this bioactivity. It has been proposed that the reaction of endoperoxides with Fe(II) involves a one-electron reduction leading to the cleavage of the oxygen-oxygen bond with the consequent formation of an oxygen anion bound to iron and of an oxygen free radical. Two possible evolutions of the generated oxygen radical have been postulated for artemisinin (**Scheme 3.5**), principally on the basis of theoretical studies²³ and of model reactions in vitro with heme or with Fe(II) inorganic salts,²⁴ which were used to mimic the antimalarial mechanism of action. In pathway 1, the oxygen O1 radical evolves through an intramolecular 1,5-H shift leading to a secondary carbon radical, while, alternatively, in pathway 2, the oxygen O2 radical evolves through a homolytic carbon-carbon cleavage of the C3-C4 bond.



Scheme 3.5. Schematic representation of the artemisinin (**41**) postulated mechanism of action.

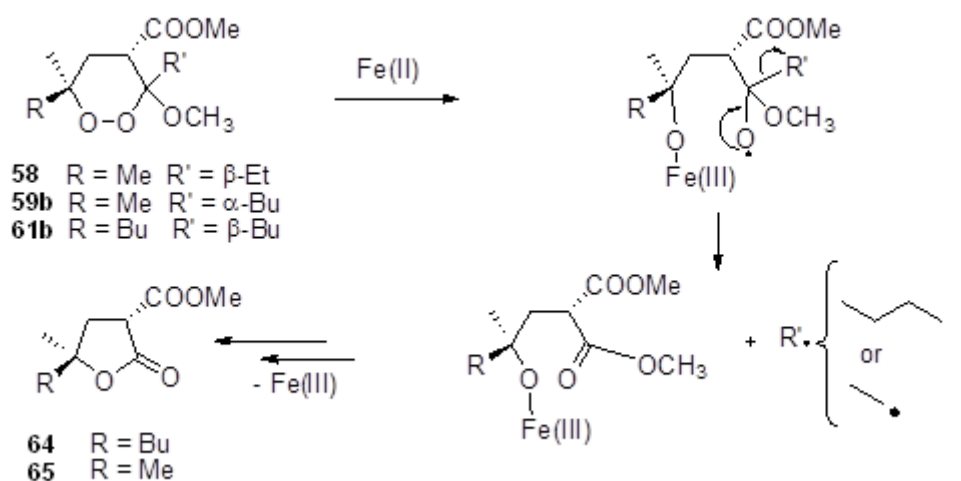
Assuming that reaction with Fe(II)-inorganic salts could give interesting information also in the case of the methyl ketal endoperoxides **57-63**, we selected three of them (**58**, **59b** and **61b**), on the basis of the diversity of their structural and bioactivity features, as test compounds to carry out the reaction. Thus, compound **61b** was allowed to react with FeCl₂ (5 equiv.) in CH₃CN/H₂O 4:1 at r.t. for 2 hours, and chromatographic purification of the reaction mixture, afforded as major products unreacted **61b** and the lactone **64** (Scheme 3.6), whose stereostructure has been identified by detailed spectroscopic investigation. When compounds **58** and **59b** were allowed to react with FeCl₂ in the same conditions both of them efficiently produced the same lactone **65** (Scheme 3.6).



Scheme 3.6. Reaction of compounds **61b**, **58** and, **59b** with FeCl₂.

The formation of compounds **64** and **65** can be rationalized through the mechanism shown in **Scheme 3.7**. Upon interaction with Fe(II) ion, the endoperoxide bond would be cleaved with regioselective formation of the oxygen radical at O2. Through the expulsion of a butyl (or ethyl) radical, this unstable intermediate would give rise to the methyl ester, which would then collapse into the final lactone.

The results of *in vitro* reaction of **58**, **59b**, and **61b** with FeCl₂ would indicate carbon-carbon cleavage pathway as responsible for bioactivity. This is in perfect agreement with results described by Kobayashi and co-workers²⁵ for peroxyplakortc derivatives, natural methyl ketal endoperoxides bearing some structural relationships with compounds **57-63**. Following **Scheme 3.7**, the *in vitro* activity of these compounds should be ascribed to the toxic action on parasite environment exhibited by the alkyl radicals released by means of the homolytic carbon-carbon cleavage. However, this mechanistic hypothesis does not agree with results obtained for compounds **58**, **59b** and **61b**. Indeed, the fact that the active (e.g. **61b**, **Table 3.2**) and inactive (e.g. **58** and **59b**, **Table 3.2**) compounds gave, with similar efficiency, the same primary carbon (**59b** and **61b**) or strictly related (**58**) one, is an unambiguous evidence of the lack of any direct correlation between the observed carbon-carbon cleavage reactions and the antimalarial activity.



Scheme 3.7. Mechanism postulated for the formation of compounds **64** and **65**.

These conclusions are in agreement with structure-activity relationship (SAR) studies reported for artemisinins (**41**) as well as for other endoperoxide derivatives, failing to relate the favoured *in vitro* carbon-carbon cleavage pathway with antimalarial activity, which is, instead, related to the intramolecular H-shift mechanism. Thus, in the 3-methoxy-1,2-dioxanes **57-63**, where both mechanisms (H-shift and carbon-carbon cleavage) can operate, the model reaction with FeCl₂ does not meet with the *in vivo* outcome of the reaction. In this scenario, a separate case is represented by non-ketal monocyclic endoperoxides, as plakortins, where the carbon-carbon cleavage mechanism does not occur¹¹ (see **Scheme 3.1**), likely due to the lack of the driving force conferred by the formation of the stable ester group (see **Scheme 3.7**). Indeed, the reaction of plakortins with FeCl₂ evidenced exclusively the “through space” intramolecular shift of the oxygen radical,¹¹ accounting for the observed SARs of plakortins and related non-ketal monocyclic endoperoxides.

As we will discuss in the next paragraph, also in the case of **57-63**, an intramolecular radical shift mechanism can well explain the marked difference of activity exhibited by very similar compounds (e.g. **58** and **59a**) or even by diastereoisomers (e.g. **59a** and **59b**), giving an overall rationale for all the SARs of this series of compounds.

3.3.3. Structure-Activity Relationship Studies

An extensive molecular modelling study, including molecular mechanic (MM), dynamics (MD), and density functional theory (DFT) calculations, has been undertaken by the group of prof. C. Fattorusso to analyze **57-63** structure-activity relationships (SARs) (see the Experimental Section for details). Since this part of the project has not been carried out in our laboratories, I will report only the most significant results.

As discussed in the previous paragraph, results obtained for compounds **58**, **59b**, and **61b** indicated that the antimalarial activity does not relate with the carbon-carbon cleavage observed *in vitro* upon their reaction with FeCl₂ (**Schemes 3.6** and **3.7**). Therefore, the newly designed compounds were subjected to an in-depth computational analysis taking into account the “through space” radical shift mechanism already reported for plakortins (**Scheme 3.1**). A simulated annealing

procedure followed by molecular mechanics (MM) energy minimization and semi-empirical PM6 full geometry optimization was applied. Low energy conformers (within 5 kcal/mol from the global minimum) were then classified and filtered on the basis of their: i) 1,2-dioxane ring conformation, ii) distance of endoperoxide oxygens from a putative partner for an 1,5- or 1,4-intra-molecular radical shift, and iii) endoperoxide oxygens lone pairs steric accessibility (see **Tables 5.1** and **5.2** in the Chapter V). The lowest energy conformers of each compound respecting the assumed pharmacophoric requirements were subjected to dynamic docking studies in complex with heme. Resulting structures, again checked for their pharmacophoric features, represented putative bioactive conformations and were then subjected to DFT calculations.

First, a structural analysis revealed that the electronic repulsion between the ester carbonyl oxygen and the endoperoxide oxygen O2 (for atom numbering see **Figure 3.14**), along with the steric repulsion between C-3 and C-4 substituents, drive the conformational preference of the 1,2-dioxane ring. Consequently, in agreement with NMR data, all compounds showed a definite conformational preference for one ring chair conformation, named Chair A, characterized by the equatorial position of the ester substituent at C-4 (**Table 5.1**). On the other hand, the steric repulsion between C-3 and C-6 substituents (**Figure 3.15a**) strongly reduced the rate of low energy conformers presenting intramolecular distances suitable for the 1,5-H shift (**Table 5.2**).

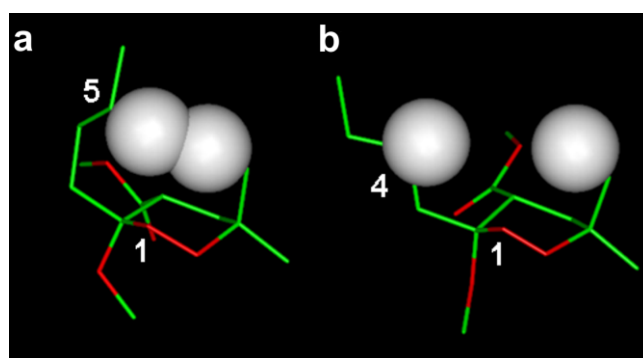


Figure 3.15. PM6 conformers of **10a** presenting intramolecular distances suitable for the 1,5-H shift (**a**) and 1,4-H shift (**b**). Atoms numbering is referred to the distance between H-shift possible partners. van der Waals volumes of the hydrogens responsible for steric hindrance between C-3 and C-6 substituents (**a**) are shown. Atoms are colored by atom type.

All the analyzed compounds presented a significant rate of low energy conformers able to undergo a 1,4-H shift from C3 and/or C6 alkyl chains to the oxygen radical (**Table 5.2** and **Figure 3.15b**). The only exception is, of course, represented by compound **57** which possesses only methyl substituents at C3 and C6, while compound **58** could undergo a 1,4-H shift but only forming a primary carbon radical.

All the computational investigations concur to suggest that the ability to form a carbon centred radical on the alkyl chain installed on C3 and/or C6 of compounds **57-63**, is related to their antimalarial activity. Computational and SAR studies suggest that, as in the case of plakortins, the putative toxic carbon radical species is formed through an intramolecular hydrogen shift. The presence of the methoxy group at C3 drives radical formation resulting in stricter stereochemical requirements for antimalarial activity compared to plakortins. Nevertheless, our study demonstrated that, according to the hypothesized mechanism of action, the antimalarial activity can be improved through rational structural modifications, thus disclosing the antimalarial potential of the new 3-methoxy-1,2-dioxane scaffold, obtained by means of an efficient and cheap two-pot Mn(III)-mediated synthesis. As an example, compound **62b**, bearing two *n*-butyl substituents at C6, showed antimalarial activity against CQ-R strains comparable to plakortin and no significant toxicity against HMEC-1 cells.

3.3.4. Experimental

Synthesis of 3-hydroxy-1,2-dioxanes 54. General procedure. The appropriate alkene (1 mmol) is added at room temperature to a mixture of the desired β -ketoester (3 mmol), $\text{Mn}^{\text{III}}(\text{OAc})_3 \cdot 2\text{H}_2\text{O}$ (0.1 mmol, 0.027 g) and $\text{Mn}^{\text{II}}(\text{OAc})_2 \cdot 4\text{H}_2\text{O}$ (1 mmol, 0.245 g) in acetic acid (5 mL). In the case of gaseous isobutylene (2-methylpropene), an excess of alkene was bubbled at $-10\text{ }^\circ\text{C}$ to a mixture of the desired β -ketoester (3 mmol), $\text{Mn}^{\text{III}}(\text{OAc})_3 \cdot 2\text{H}_2\text{O}$ (0.1 mmol, 0.027 g) and $\text{Mn}^{\text{II}}(\text{OAc})_2 \cdot 4\text{H}_2\text{O}$ (1 mmol, 0.245 g) in acetic acid (5 mL). The resulting heterogeneous solution was stirred at room temperature for 18-24 h under oxygen at atmospheric pressure (O_2 filled balloon) and the conversion was monitored by TLC. The reaction mixture was neutralized with stoichiometric NaOH (3 M aqueous solution) and then made slightly basic with a saturated NaHCO_3 solution. The aqueous phase is extracted with CH_2Cl_2 (3 x 10 mL) and the combined

organic phases are dried (Na_2SO_4) and evaporated to dryness. The intermediate 3-hydroxy-1,2-dioxanes **54** are purified by flash-chromatography on silica gel eluting with cyclohexane:ethyl acetate mixtures.

Synthesis of 3-methoxy-1,2-dioxanes 57-63. General procedure. (1*S*)-(+)-Camphorsulfonic acid (5 mmol, 1.16 g) was added at room temperature to a solution of the desired 1-hydroxy-1,2-dioxane **54** (1 mmol) and trimethylorthoformate (2 mmol, 0.22 mL) in anhydrous methanol (7 mL), and the solution was stirred at room temperature for 72 h. The reaction was quenched at 0 °C with saturated NaHCO_3 solution and the aqueous phase is extracted with CH_2Cl_2 (3 x 10 mL). The combined organic phases are dried (Na_2SO_4) and evaporated to dryness. 3-Hydroxy-1,2-dioxanes **57-63** are isolated after flash-chromatography on silica gel by elution with cyclohexane:ethyl acetate mixtures.

Compound 57. ESI-MS: m/z 241 $[\text{M} + \text{Na}]^+$; HR-ESIMS: m/z 241.1059 (calcd for $\text{C}_{10}\text{H}_{18}\text{NaO}_5$ 241.1052). ^1H NMR (500 MHz): δ 3.72 (s, COOMe), 3.32 (s, OMe-3), 2.86 (dd, $J = 12.9, 4.9$ Hz, H-4), 2.26 (t, $J = 12.9$ Hz, H-5a), 1.59 (dd, $J = 12.9, 4.9$ Hz, H-5b), 1.47 (s, Me-3), 1.36 (s, Me-6ax), 1.21 (s, Me-6eq). ^{13}C NMR (125 MHz): δ 171.3 (COOMe), 100.4 (C-3), 77.1 (C-6), 51.9 (COOMe), 49.1 (OMe-3), 45.7 (C-4), 32.7 (C-5), 27.2 (6-Me), 22.3 (6-Me), 19.6 (3-Me).

Compound 58. ESI-MS: m/z 255 $[\text{M} + \text{Na}]^+$; HR-ESIMS: m/z 255.1212 (calcd for $\text{C}_{11}\text{H}_{20}\text{NaO}_5$ 255.1218). ^1H NMR (500 MHz): δ 3.80 (s, COOMe), 3.31 (s, OMe-3), 3.10 (dd, $J = 12.9, 4.9$ Hz, H-4), 2.30 (t, $J = 12.9$ Hz, H-5a), 1.90 (q, $J = 7.2$ Hz, $\text{H}_2\text{-1}'$), 1.59 (dd, $J = 12.9, 4.9$ Hz, H-5b), 1.36 (s, Me-6ax), 1.21 (s, Me-6eq), 1.03 (t, $J = 7.2$ Hz, $\text{H}_2\text{-2}'$). ^{13}C NMR (125 MHz): δ 171.4 (COOMe), 102.3 (C-3), 77.1 (C-6), 52.0 (COOMe), 51.9 (OMe-3), 48.6 (C-4), 40.4 (C-1'), 32.6 (C-5), 26.8 (6-Me), 22.6 (6-Me), 8.5 (C-2').

Compound 59a. ESI-MS: m/z 283 $[\text{M} + \text{Na}]^+$; HR-ESIMS: m/z 283.1517 (calcd for $\text{C}_{13}\text{H}_{24}\text{NaO}_5$ 283.1521). ^1H NMR (500 MHz): δ 3.71 (s, COOMe), 3.31 (s, OMe-3), 3.08 (dd, $J = 12.9, 4.9$ Hz, H-4), 2.29 (t, $J = 12.9$ Hz, H-5a), 1.86 (m, H-1'a), 1.58 (dd, $J = 12.9, 4.9$ Hz, H-5b), 1.34 (s, Me-6ax), 1.54 (m, $\text{H}_2\text{-2}'$), 1.34 (m, $\text{H}_2\text{-3}'$), 1.20 (s, Me-6eq), 0.92 (t, $J = 6.9$ Hz, $\text{H}_3\text{-4}'$). ^{13}C NMR (125 MHz): δ 171.4 (COOMe), 102.3 (C-3), 65.8 (C-6), 52.0 (COOMe), 52.0 (OMe-3), 48.6 (C-

4), 40.4 (C-1'), 32.6 (C-5), 32.2 (C-2'), 26.8 (6-Me), 22.6 (6-Me), 21.0 (C-3'), 13.5 (C-4').

Compound 59b. ESI-MS: m/z 283 $[M + Na]^+$; HR-ESIMS: m/z 283.1522 (calcd for $C_{13}H_{24}NaO_5$ 283.1521). 1H NMR (500 MHz): δ 3.73 (s, COOMe), 3.41 (s, OMe-3), 3.06 (dd, $J = 13.0, 5.5$ Hz, H-4), 1.89 (m, H-1'a), 1.85 (dd, $J = 13.0, 5.5$ Hz, H-5a), 1.72 (t, $J = 13.0$ Hz, H-5b), 1.54 (m, H₂-2'), 1.37 (s, Me-6ax), 1.34 (m, H₂-3'), 1.19 (s, Me-6eq), 0.92 (t, $J = 6.9$ Hz, H₃-4'). ^{13}C NMR (125 MHz): δ 173.4 (COOMe), 104.2 (C-3), 73.8 (C-6), 52.5 (COOMe), 52.0 (OMe-3), 49.3 (C-4), 40.4 (C-1'), 35.6 (C-5), 32.2 (C-2'), 27.1 (6-Me), 21.6 (6-Me), 21.0 (C-3'), 13.5 (C-4').

Compound 60a. ESI-MS: m/z 283 $[M + Na]^+$; HR-ESIMS: m/z 283.1519 (calcd for $C_{13}H_{24}NaO_5$ 283.1521). 1H NMR (500 MHz): δ 3.70 (s, COOMe), 3.30 (s, OMe-3), 2.85 (dd, $J = 12.5, 6.4$ Hz, H-4), 2.22 (dd, $J = 12.0, 12.0$ Hz, H-5a), 1.53 (dd, $J = 12.0, 6.4$ Hz, H-5b), 1.50 (m, H₂-1'), 1.35 (m, H₂-2'), 1.30 (m, H₂-3'), 1.47 (s, Me-3), 1.32 (s, Me-6), 0.93 (t, $J = 6.9$ Hz, H₃-4').

Compound 60b. ESI-MS: m/z 283 $[M + Na]^+$; HR-ESIMS: m/z 283.1529 (calcd for $C_{13}H_{24}NaO_5$ 283.1521). 1H NMR (500 MHz): δ 3.70 (s, COOMe), 3.30 (s, OMe-3), 2.84 (dd, $J = 12.5, 6.4$ Hz, H-4), 2.22 (dd, $J = 12.0, 12.0$ Hz, H-5a), 1.80 (m, H₂-1'), 1.64 (dd, $J = 12.0, 6.4$ Hz, H-5b), 1.55 (m, H₂-2'), 1.30 (m, H₂-3'), 1.45 (s, Me-3), 1.13 (s, Me-6), 0.93 (t, $J = 6.9$ Hz, H₃-4'). ^{13}C NMR (125 MHz): δ 171.5 (COOMe), 100.1 (C-3), 79.9 (C-6), 52.5 (COOMe), 49.1 (OMe-3), 45.5 (C-4), 33.9 (C-1'), 31.2 (C-5), 26.1 (C-2'), 23.9 (Me-6), 23.1 (C-3'), 19.5 (Me-3), 14.7 (C-4').

Compound 60c. ESI-MS: m/z 283 $[M + Na]^+$; HR-ESIMS: m/z 283.1530 (calcd for $C_{13}H_{24}NaO_5$ 283.1521). 1H NMR (500 MHz): δ 3.73 (s, COOMe), 3.38 (s, OMe-3), 2.98 (dd, $J = 11.1, 6.4$ Hz, H-4), 1.77 (m, H₂-5), 1.59 (m, H₂-1'), 1.34 (m, H₂-2' and H₂-3'), 1.25 (s, Me-3), 1.12 (s, Me-6), 0.93 (t, $J = 6.9$ Hz, H₃-4'). ^{13}C NMR (125 MHz): δ 173.2 (COOMe), 105.7 (C-3), 82.1 (C-6), 52.5 (COOMe), 50.3 (OMe-3), 47.3 (C-4), 39.9 (C-5), 34.4 (C-1'), 26.1 (C-2'), 23.6 (C-3'), 20.6 (Me-6), 17.8 (Me-3), 14.7 (C-4').

Compound 60d. ESI-MS: m/z 283 $[M + Na]^+$; HR-ESIMS: m/z 283.1512 (calcd for $C_{13}H_{24}NaO_5$ 283.1521). 1H NMR (500 MHz): δ 3.73 (s, COOMe), 3.38 (s,

OMe-3), 2.98 (dd, $J = 13.8, 3.8$ Hz, H-4), 1.89 (dd, $J = 14.0, 3.4$ Hz, H-5a), 1.69 (dd, $J = 14.0, 12.5$ Hz, H-5b), 1.45 (m, H₂-1'), 1.32 (s, Me-6), 1.29 (m, H₂-2' and H₂-3'), 1.26 (s, Me-3), 0.89 (t, $J = 6.9$ Hz, H₃-4'). ¹³C NMR (125 MHz): δ 172.8 (COOMe), 105.7 (C-3), 82.1 (C-6), 52.0 (COOMe), 50.3 (OMe-3), 46.9 (C-4), 36.3 (C-5), 33.4 (C-1'), 26.0 (C-2'), 23.4 (C-3'), 20.6 (Me-6), 17.1 (Me-3), 14.3 (C-4').

Compound 61a. ESI-MS: m/z 325 [M + Na]⁺; HR-ESIMS: m/z 325.2000 (calcd for C₁₆H₃₀NaO₅ 325.1991). ¹H NMR (500 MHz): δ 3.71 (s, COOMe), 3.31 (s, OMe-3), 3.07 (dd, $J = 12.9, 4.5$ Hz, H-4), 2.23 (t, $J = 12.9$ Hz, H-5a), 1.85 (m, H-1'a), 1.80 (m, H-1''a), 1.79 (m, H-1'a), 1.70 (m, H-1''b), 1.62 (overlapped, H-5b), 1.59 (m, H₂-2' and H₂-2''), 1.34 (m, H₂-3' and H₂-3''), 1.30 (s, Me-6), 0.93 (t, $J = 6.9$ Hz, H₃-4' and H₃-4'').

Compound 61b. ESI-MS: m/z 325 [M + Na]⁺; HR-ESIMS: m/z 325.1987 (calcd for C₁₆H₃₀NaO₅ 325.1991). ¹H NMR (500 MHz): δ 3.71 (s, COOMe), 3.31 (s, OMe-3), 3.07 (dd, $J = 12.9, 4.5$ Hz, H-4), 2.23 (t, $J = 12.9$ Hz, H-5a), 1.92 (m, H-1'a), 1.83 (m, H-1''a), 1.82 (m, H-1'b), 1.70 (m, H-1''b), 1.64 (dd, $J = 12.9, 4.5$ Hz, H-5b), 1.54 (m, H₂-2' and H₂-2''), 1.34 (m, H₂-3' and H₂-3''), 1.13 (s, Me-6), 0.93 (t, $J = 6.9$ Hz, H₃-4' and H₃-4''). ¹³C NMR (125 MHz): δ 171.5 (COOMe), 102.0 (C-3), 79.1 (C-6), 51.8 (COOMe), 48.6 (OMe-3), 40.6 (C-4), 34.0 (C-5), 33.9 (C-1'), 32.5 (C-1''), 31.4 (C-2'), 29.7 (C-2''), 26.1 (C-3'), 25.8 (C-3''), 23.0 (Me-6), 14.0 (C-4'), 13.8 (C-4'').

Compound 61c. ESI-MS: m/z 325 [M + Na]⁺; HR-ESIMS: m/z 325.1993 (calcd for C₁₆H₃₀NaO₅ 325.1991). ¹H NMR (500 MHz): δ 3.73 (s, COOMe), 3.41 (s, OMe-3), 3.07 (dd, $J = 12.9, 4.5$ Hz, H-4), 1.92 (m, H-1'a), 1.83 (m, H-1''a, H-1'b), 1.77 (m, H₂-5), 1.70 (m, H-1''b), 1.54 (m, H₂-2' and H₂-2''), 1.34 (m, H₂-3' and H₂-3''), 1.11 (s, Me-6), 0.93 (t, $J = 6.9$ Hz, H₃-4' and H₃-4'').

Compound 62a. ESI-MS: m/z 325 [M + Na]⁺; HR-ESIMS: m/z 325.1988 (calcd for C₁₆H₃₀NaO₅ 325.1991). ¹H NMR (500 MHz): δ 3.71 (s, COOMe), 3.31 (s, OMe-3), 2.83 (dd, $J = 12.9, 4.5$ Hz, H-4), 2.21 (t, $J = 12.9$ Hz, H-5a), 1.82 (m, H-1''a), 1.81 (m, H-1'a), 1.60 (dd, $J = 12.9, 4.5$ Hz, H-5b), 1.60 (m, H-1''b, H-1'b), 1.54 (m, H₂-2' and H₂-2''), 1.45 (s, Me-3), 1.34 (m, H₂-3' and H₂-3''), 0.91 (t, $J = 6.9$ Hz, H₃-4' and H₃-4''). ¹³C NMR (125 MHz): δ 171.5 (COOMe), 100.5

(C-3), 81.0 (C-6), 51.8 (COOMe), 49.0 (OMe-3), 45.1 (C-4), 36.1 (C-5), 31.3 (C-1'), 29.6 (C-1''), 25.4 (C-2'), 24.8 (C-2''), 23.2 (Me-3), 19.6 (C-3', C-3''), 14.0 (C-4'), 13.9 (C-4'').

Compound 62b. ESI-MS: m/z 325 $[M + Na]^+$; HR-ESIMS: m/z 325.1995 (calcd for $C_{16}H_{30}NaO_5$ 325.1991). 1H NMR (500 MHz): δ 3.74 (s, COOMe), 3.40 (s, OMe-3), 3.00 (dd, $J = 13.5, 3.5$ Hz, H-4), 1.84 (dd, $J = 13.5, 3.5$ Hz, H-5a), 1.72 (t, $J = 13.5$, H-5b), 1.65 (m, H-1''a), 1.60 (m, H-1'a), 1.57 (s, Me-3), 1.45 (m, H-1''b, H-1'b), 1.39 (m, H₂-2' and H₂-2''), 1.34 (m, H₂-3' and H₂-3''), 0.93 (t, $J = 6.9$ Hz, H₃-4'), 0.90 (t, $J = 6.9$ Hz, H₃-4''). ^{13}C NMR (125 MHz): δ 172.6 (COOMe), 105.5 (C-3), 83.8 (C-6), 52.0 (COOMe), 49.6 (OMe-3), 46.4 (C-4), 36.7 (C-5), 32.6 (C-1'), 32.4 (C-1''), 26.2 (Me-3), 25.4 (C-2'), 25.2 (C-2''), 23.2 (C-3') 23.1 (C-3''), 14.0 (C-4'), 13.9 (C-4'').

Compound 63a. ESI-MS: m/z 367 $[M + Na]^+$; HR-ESIMS: m/z 367.2467 (calcd for $C_{19}H_{36}NaO_5$ 367.2460). 1H NMR (500 MHz): δ 3.71 (s, COOMe), 3.30 (s, OMe-3), 3.10 (dd, $J = 12.9, 4.5$ Hz, H-4), 2.21 (t, $J = 12.9$ Hz, H-5a), 1.87 (m, H₂-1'), 1.78 (m, H₂-1'', H₂-1'''), 1.60 (dd, $J = 12.9, 4.5$ Hz, H-5b), 1.49 (m, H₂-2' and H₂-2''), 1.25-1.35 (m, H₂-2''', H₂-3' H₂-3'', H₂-3'''), 0.91 (t, $J = 6.9$ Hz, H₃-4' H₃-4'', H₃-4'''). ^{13}C NMR (125 MHz): δ 171.6 (COOMe), 102.1 (C-3), 81.0 (C-6), 51.8 (COOMe), 48.6 (OMe-3), 44.2 (C-4), 32.9 (C-1'), 32.6 (C-1''), 31.3 (C-5), 26.1 (C-2' and C-2''), 23.2 (Me-3), 23.1 (C-3' and C-3''), 13.9 (C-4' and C-4'').

Compound 63b. ESI-MS: m/z 367 $[M + Na]^+$; HR-ESIMS: m/z 367.2452 (calcd for $C_{19}H_{36}NaO_5$ 367.2460). 1H NMR (500 MHz): δ 3.71 (s, COOMe), 3.30 (s, OMe-3), 3.07 (dd, $J = 12.9, 3.5$ Hz, H-4), 1.85 (dd, $J = 12.9, 3.5$ Hz, H-5a), 1.72 (t, $J = 12.9$ Hz, H-5b), 1.65 (m, H₂-1'), 1.60-1.63 (m, H₂-1'', H₂-1'''), 1.40-1.20 (m, H₂-2', H₂-2'', H₂-2''', H₂-3' H₂-3'', H₂-3'''), 0.89 (t, $J = 6.9$ Hz, H₃-4' H₃-4'', H₃-4'''). ^{13}C NMR (125 MHz): δ 172.8 (COOMe), 106.1 (C-3), 83.5 (C-6), 52.0 (COOMe), 50.0 (OMe-3), 44.2 (C-4), 36.6 (C-1'), 36.1 (C-1''), 30.5 (C-5), 29.6 (C-2' and C-2''), 25.3 (Me-3), 24.5 (C-3' and C-3''), 13.8 (C-4' and C-4'').

Reaction of methylketals with $FeCl_2$. Compound **61b**, (12.0 mg, 0.040 mmol) was dissolved in CH_3CN/H_2O 4:1 (5 mL) and freshly purchased $FeCl_2 \cdot 4H_2O$ (39 mg, 0.20 mmol) were added. The reaction mixture was left under stirring at room

temperature for 2 hours. Light was excluded from the reaction. Then the obtained mixture was partitioned between water and EtOAc. The organic phase, dried over Na₂SO₄, was purified by HPLC (SI60 *n*-hexane/EtOAc 85:15) affording compound **64** (2.7 mg, 0.0124 mmol, 31%) in the pure state. When the reaction was repeated with compounds **58** and **59b**, in the same conditions, compound **64** (45% and 42% yield, respectively) was obtained.

Compound 64. ESI-MS: m/z 237 [M + Na]⁺; HR-ESIMS: m/z 237.1100 (calcd for C₁₁H₁₈NaO₄ 237.1103). ¹H NMR (500 MHz): δ 4.12 (m, H-2), 3.90 (s, 9-OMe), 2.60 (dd, $J = 11.5, 4.5$ Hz, H-3a), 2.40 (dd, $J = 11.5, 6.0$ Hz, H-3b), 1.85 (m, H-5a), 1.70 (m, H-5b), 1.60 (s, Me-10), 1.50 (m, H₂-6), 1.30 (m, H₂-7), 0.93 (t, $J = 7.2$ Hz, Me-8). ¹³C NMR (125 MHz): δ 171.0 (C-1), 169.5 (COO-), 83.9 (C-4), 51.0 (OMe), 48.5 (C-2), 38.3 (C-5), 36.6 (C-3), 23.8 (C-6), 23.5 (C-10), 23.0 (C-7), 14.0 (C-8).

Compound 65. ESI-MS: m/z 195 [M + Na]⁺; HR-ESIMS: m/z 195.0639 (calcd for C₈H₁₂NaO₄ 195.0633). ¹H NMR (500 MHz): δ 3.90 (s, COOMe), 3.73 (t, $J = 6.0$ Hz, H-2), 2.55 (dd, $J = 11.5, 4.5$ Hz, H-3a), 2.32 (dd, $J = 11.5, 8.0$ Hz, H-3b), 1.53 (s, H₃-5), 1.42 (s, H₃-6). ¹³C NMR (125 MHz): δ 171.0 (C-1), 168.5 (COO-), 83.7 (C-4), 51.0 (OMe), 47.7 (C-2), 38.2 (C-3), 28.3 (C-5), 27.8 (C-6).

Molecular modeling.

Molecular modeling calculations were performed on SGI Origin 200 8XR12000 and E4 Server Twin 2 x Dual Xeon—5520, equipped with two nodes. Each node: 2 x Intel® Xeon® QuadCore E5520—2,26Ghz, 36 GB RAM. The molecular modeling graphics were carried out on SGI Octane 2 workstations.

Estimation of apparent pK_a values of the newly designed compounds **57-63** were calculated by using the ACD/pK_a DB version 12.00 software (Advanced Chemistry Development Inc., Toronto, Canada). All compounds were considered neutral in all calculations performed as a consequence of the estimation of percentage of neutral/ionized forms computed at the pH of 7.4 (physiological value), 7.2 (cytoplasmic pH value) and 5.5 (parasite vacuole pH) using the Handerson–Hasselbalch equation.

Conformational analysis.

Compounds **57-63** were built using the Insight 2005 Builder module (Accelrys Software Inc., San Diego). Atomic potentials and charges were assigned using the CFF91 force field. The conformational space of the compounds was sampled through 200 cycles of Simulated Annealing ($\epsilon=1$). In simulated annealing, the temperature is altered in time increments from an initial temperature to a final temperature by adjusting the kinetic energy of the structure (by rescaling the velocities of the atoms). The following protocol was applied: the system was heated up to 1000 K over 2000 fs (time step = 3.0 fs); the temperature of 1000 K was applied to the system for 2000 fs (time step = 3.0 fs) with the aim of surmounting torsional barriers; successively, temperature was linearly reduced to 300 K in 1000 fs (time step = 1.0 fs). Resulting conformations were then subjected to molecular mechanics (MM) energy minimization within Insight 2005 Discover module (CFF91 force field; $\epsilon=1$) until the maximum RMS derivative was less than 0.001 kcal/Å, using Conjugate Gradient as minimization algorithm. All MM conformers were then subjected to a full geometry optimization by semiempirical calculations, using the quantum mechanical method PM6 in the Mopac2009 package and EF (Eigenvector Following routine) as geometry optimization algorithm. GNORM value was set to 0.01. To reach a full geometry optimization the criteria for terminating all optimizations was increased by a factor of 100, using the keyword PRECISE.

Resulting conformers were grouped into families on the basis of their 1,2-dioxane ring conformation and ranked by their potential energy values (i.e., ΔE from the global energy minimum). Occurrence rates, together with the distance between endoperoxide oxygens (O1 and O2) and possible partners for a 'through space' (1,4 and 1,5) intramolecular radical shift, were calculated for all conformers within 5 kcal/mol from the global minimum. The accessible surface area of endoperoxide oxygens lone pairs has been evaluated by calculating Connolly surfaces (Insight 2005, Accelrys Software Inc., San Diego).

In vitro drug susceptibility assay on P. falciparum.

Plasmodium falciparum cultures were carried out according to Trager and Jensen with slight modifications. The CQ-sensitive, strain D10 and the CQ-resistant, strain W2 were maintained at 5% hematocrit (human type A-positive red blood

cells) in RPMI 1640 (EuroClone, Celbio) medium with the addition of 1% AlbuMax (Invitrogen, Milan, Italy), 0.01% hypoxanthine, 20 mM HEPES, and 2 mM glutamine. All the cultures were maintained at 37 °C in a standard gas mixture consisting of 1% O₂, 5% CO₂, and 94% N₂. Compounds were dissolved in either water or DMSO and then diluted with medium to achieve the required concentrations (final DMSO concentration <1%, which is non-toxic to the parasite). Drugs were placed in 96-well flat-bottomed microplates (COSTAR) and serial dilutions made. Asynchronous cultures with parasitaemia of 1–1.5% and 1% final hematocrit were aliquoted into the plates and incubated for 72 h at 37°C. Parasite growth was determined spectrophotometrically (OD₆₅₀) by measuring the activity of the parasite lactate dehydrogenase (pLDH), according to a modified version of the method of Makler in control and drug-treated cultures. The antimalarial activity is expressed as 50% inhibitory concentrations (IC₅₀); each IC₅₀ value is the mean and standard deviation of at least three separate experiments performed in duplicate.

Cell cytotoxicity assays

The long-term human microvascular endothelial cell line (HMEC-1) immortalized by SV 40 large T antigen was maintained in MCDB 131 medium (Invitrogen, Milan, Italy) supplemented with 10% fetal calf serum (HyClone, Celbio, Milan, Italy), 10 ng/ml of epidermal growth factor (Chemicon), 1 µg/ml of hydrocortisone, 2 mM glutamine, 100 U/ml of penicillin, 100 µg/ml of streptomycin, and 20 mM HEPES buffer (EuroClone). Unless stated otherwise, all reagents were from Sigma Italia, Milan, Italy. For the cytotoxicity assays, cells were treated with serial dilutions of test compounds and cell proliferation evaluated using the MTT assay already described. Plates were incubated for 72 h at 37°C in 5% CO₂, then 20 µL of a 5 mg/ml solution of 3-(4,5-dimethylthiazol-2-yl)-2,5-diphenyltetrazolium bromide (MTT) (M-2128 Sigma) in PBS was added for an additional 3 h at 37°C. The plates were then centrifuged, the supernatants discarded and the dark blue formazan crystals dissolved using 100 µL of lysing buffer consisting of 20% (w/v) of a solution of SDS (Sigma), 40% of N,N-dimethylformamide (Merck) in H₂O, at pH 4.7 adjusted with 80% acetic acid. The plates were then read on a microplate reader (Molecular Devices Co., Menlo Park, CA, USA) at a test wavelength of 550 nm and a reference wavelength of 650 nm.

The results are expressed as IC_{50} , which is the dose of compound necessary to inhibit cell growth by 50%. All the tests were performed in triplicate at least three times.

3.4. ANTIMALARIAL LIMONOIDS FROM THE NEEM PLANT (*AZADIRACHTA INDICA*)



A. indica, a plant of the Meliaceae family, has been used for centuries by the Ayurvedic medicine system as a source for the treatment of a wide variety of ailments. Since the beginning of the 20th century it has become part of several African pharmacopeias and,

nowadays, the populations of many tropical and sub-tropical countries use home made neem preparations against various illnesses including malaria.²⁶ The parts of the plant used, the dosage and the method of preparation (more frequently aqueous decoctions, but also infusions and macerations) are not well established, since they vary from region to region. However, either fruits, seeds, barks or, more frequently, leaves are utilized to this aim. Extracts of *A. indica* seeds and leaves are also widely applied as pesticides and insect repellents. The efficacy of such products has been unambiguously associated to their content of the highly functionalized and rearranged limonoid (C₂₆ tetranortriterpenoid) azadirachtin-A (**Fig.3.18**) and analogues.²⁷ Various biological effects have been evidenced also in mosquitoes, illustrating the potential of limonoid-rich products for the control of insect disease vectors.^{28,29}

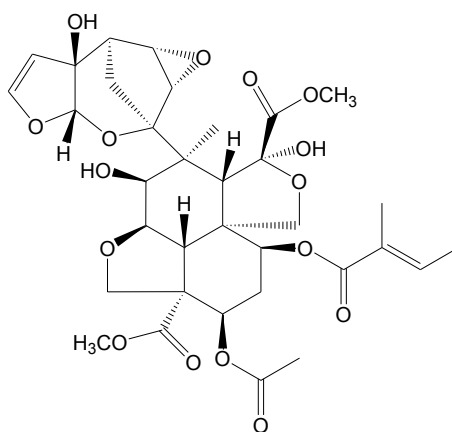


Figure 3.18. Azadirachtin-A structure.

Extensive chemical investigations carried out in the last decades have led to the identification of a large number of secondary metabolites from *A. indica*, including at least fifty bioactive limonoids with either insecticidal, antibacterial, anti-tumor or antiviral properties.³⁰ Studies aimed at isolating metabolites responsible for the *in vitro* antimalarial activity of neem extracts seemed to indicate that the limonoids nimbolide³¹ and gedunin (**66**)^{32,33} as the most potent components and likely responsible of the activity (**Fig. 3.19**).

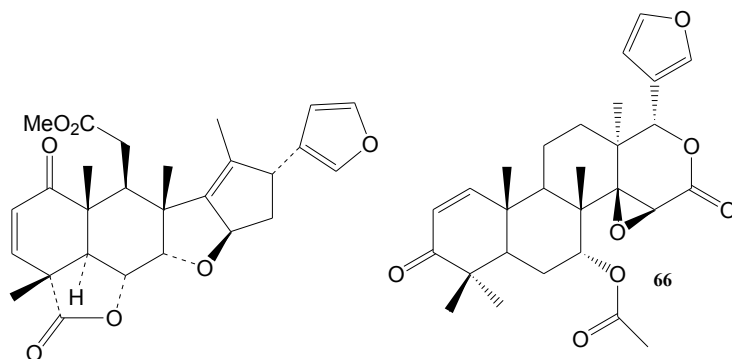


Figure 3.19. Two antimalarial limonoids: nimbolide and gedunin (**66**)

The mode of action of this natural product group is still unclear. The cytotoxic activity of gedunin (**66**) was moderate ($EC_{50} = 275 \mu\text{g/mL}$). Remarkably, gedunin (**66**) has also been recently shown to be a potent Hsp90 inhibitor with potential anticancer activity.³⁴ On the other hand, although azadirachtin showed a very poor antimalarial activity on the erythrocytic stages, a transmission blocking activity of azadirachtin-enriched neem seed extracts has been recently demonstrated *in vivo* using a murine malaria model.³⁵

As part of the ongoing research program established by my group and aimed at finding new antimalarial leads from natural sources, I have carried out a detailed phytochemical investigation of the fruit of an African sample of *Azadirachta indica*, collected in Burkina Faso. This analysis led to the isolation of ten pure triterpenoid derivatives (**66-75**), two of which were new molecules, named neemfruitins A (**67**) and B (**68**). The following paragraphs describes the structural characterization of these new metabolites and reports on the *in vitro* antimalarial activity of all the isolated triterpenoids.

3.4.1. Isolation and structure elucidation of new secondary metabolites

Preceding the detailed phytochemical investigation on the neem fruit, it was ascertained that this plant part actually contains antimalarial compounds by testing a crude fruit extract in a murine malaria model (*Plasmodium berghei*). In mice treated with the extract at a daily dosage of 200 mg/kg over 9 days and exposed to infectious mosquito bites on day 3 of treatment, parasitaemia levels reduced by 45% (CI95 40%-50%; $p < 0.001$) compared to control animals were observed, confirming the choice of this plant part as study object.

Dried fruits (25 g) of *A. indica* were exhaustively extracted with MeOH and the obtained material was then partitioned between H₂O and EtOAc to yield a brown organic extract (2.75 g). The water layer was further partitioned against *n*-BuOH yielding a polar organic extract (2.50 g) and a water extract (8.1 g). These three phases were subjected to a preliminary screening on *P. falciparum* blood stage cultures to assess the in vitro antimalarial activity. The results clearly indicated the EtOAc phase was the most promising for further investigation (Table 3.5). It was therefore subjected to MPLC chromatography over silica gel followed by repeated HPLC purifications to yield in the pure state the new limonoid neemfruitin A (67) and the new apotirucallane neemfruitin B (68), in addition to the known metabolites azadirone (69),³⁶ azadiradione (70),³⁷ epoxyazadiradione (also called nimbinin) (71),³⁸ gedunin (66),³⁹ deacetylgedunin (72),⁴⁰ desmethyllimocin B (73),⁴¹ protoxylocarpin G (74),⁴² and spicatin (75).⁴³ Protoxylocarpin G (74) has been very recently isolated from seed kernels of *Xylocarpus granatus*⁴² and this is the first report of its presence in *A. indica*. As already noticed in other studies, the neem fruit extract did not contain any azadirachtin.⁴⁴

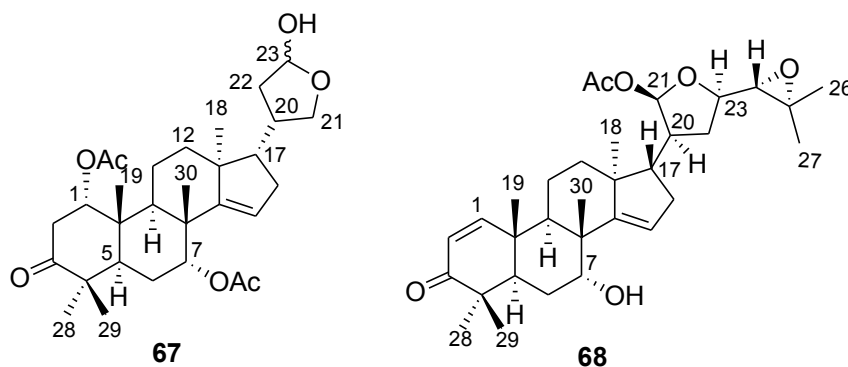


Figure 3.20. The new limonoids neemfruitin A (67) and B (68)

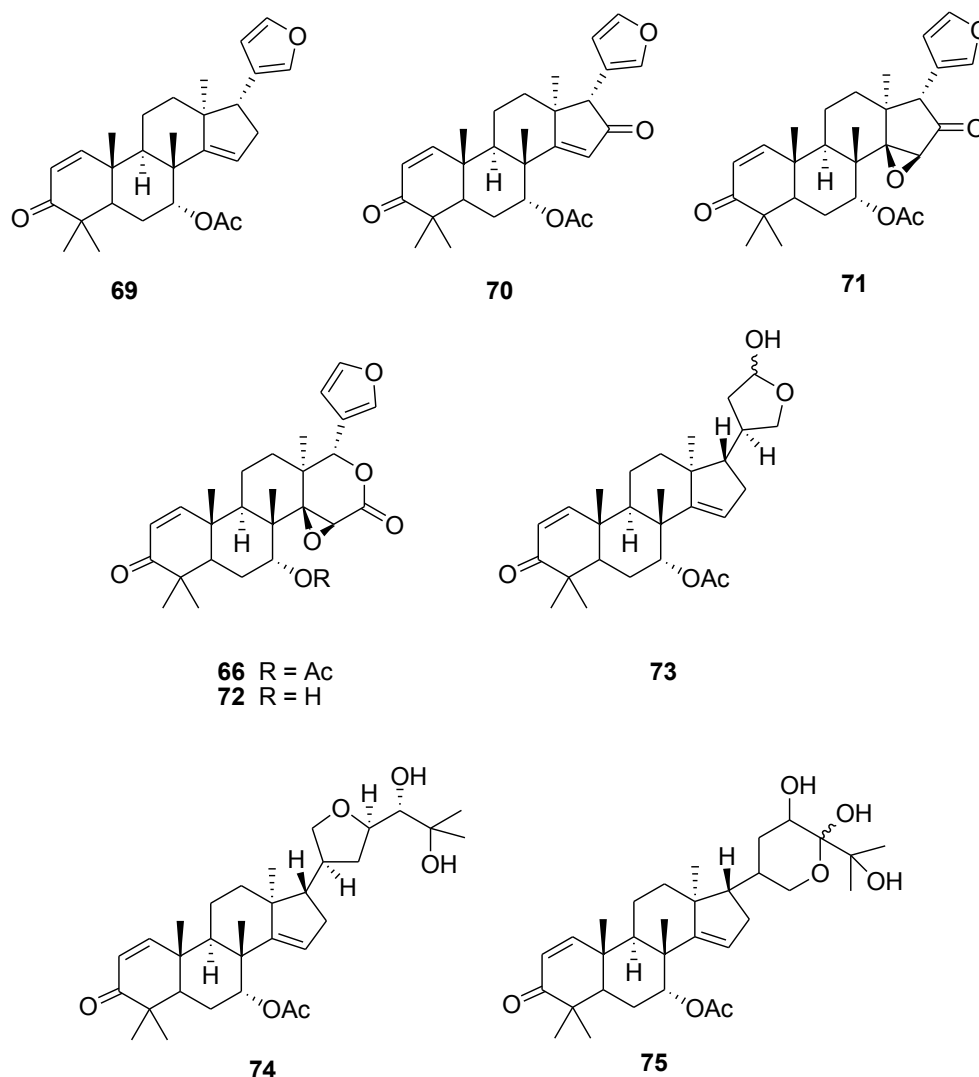


Figure 3.21. The known limonoids (**66**, **69-73**) and apotirucallanes (**74-75**) isolated from fruits of *A. indica*

HR-ESIMS data established the molecular formula of **neemfruitin A (67)** as $C_{30}H_{44}O_7$. The 1H NMR spectrum of **67** (Table 3.4, $CDCl_3$) showed seven methyl singlets, two of which (δ_H 2.09 and 1.98) belonging to acetyl groups, four broad singlets between δ_H 5.00 and 5.50 and a number of multiplets between δ_H 3.00 and 4.20. A combined analysis of ^{13}C NMR (Table 3.4) and HSQC data revealed the presence of three carbonyl resonances (two ester carbonyls at δ_C 170.5 and 170.1 and a ketone carbonyl at δ_C 213.8) and of a trisubstituted double bond (δ_C 159.2; δ_H 5.30, δ_C 119.1), accounting for four of the nine unsaturation degrees implied by the molecular formula. Neemfruitin A (**67**) must be, therefore, pentacyclic. The ^{13}C NMR spectrum of **67** contained also the resonances of two oxygenated methine carbons (δ_H 5.05, δ_C 76.7; δ_H 5.22, δ_C 74.6), of one oxymethylene (δ_H 4.20 and 3.44, δ_C 72.2) and of an hemiacetal group (δ_H 5.48, δ_C 97.8).

Table 3.4 ^1H (500 MHz) and ^{13}C (125 MHz) NMR data of neemfruitins A (**67**) and B (**68**)*

Pos.	67		68	
	δ_{H} , mult., J in Hz	δ_{C} , mult.	δ_{H} , mult., J in Hz	δ_{C} , mult.
1	5.05, bs	76.7, d	7.12, d, 10.2	161.8, d
2a	3.04, dd, 17.1, 3.6		5.84, d, 10.2	127.2, d
2b	2.48, dd, 17.1, 1.5			
3		213.8, s		205.8, s
4		42.4, s		44.3, s
5	2.31 ^a	47.8, d	2.07 ^a	44.7, d
6a	1.98 ^a	25.1, t	1.85 ^a	24.0, t
6b	1.80, m		1.80 ^a	
7	5.22, bs	74.6, d	3.98, bs	72.0, t
8		42.5, s		44.8, s
9	2.50 ^a	35.3, d	2.08 ^a	36.8, d
10		41.9, s		40.5, s
11a	1.80 ^a	16.5, t	1.75 ^a	16.8, t
11b	1.70 ^a		1.73 ^a	
12a	1.90 ^a	34.0, t	1.84 ^a	33.4, t
12b	1.50 ^a		1.51 ^a	
13		47.2, s		53.1, s
14		159.2, s		161.9, s
15	5.30, bs	119.1, d	5.52, bd, 6.5	119.9, d
16a	2.20 ^a	35.3, t	2.25 ^a	35.4, t
16b	2.10 ^a		2.20 ^a	
17	1.54, m	59.2, d	1.93 ^a	46.7, d
18	1.00, s	21.3, q	1.03, s	19.5, q
19	1.18, s	19.1, q	1.10, s	18.9, q
20	2.63, m	38.4, d	2.37, m	44.7, d
21a	4.20, t, 8.0	72.2, t	6.26, d, 6.6	96.8, d
21b	3.44, t, 8.0			
22a	2.49 ^a	35.5, t	2.09 ^a	32.3, t
22b	1.58 ^a		1.73 ^a	
23	5.48, bs	97.8, d	3.95 ^a	80.3, d
24			2.67, d, 7.2	67.0, d
25				57.8, s
26			1.33, s	23.2, q
27			1.29, s	25.9, q
28	1.08, s	22.0, q	1.08, s	21.3, q
29	1.18, s	25.2, q	1.16, s	27.1, q
30	1.19, s	27.3, q	1.12, s	27.4, q
21-OAc				170.7, s
			2.07, s	21.2, q
1-OAc		170.1, s		
	1.98, s	21.0, q		
7-OAc		170.5, s		
	2.09, s	21.2, q		

* Data taken in CDCl_3 . For neemfruitin A (**67**) data of the major epimer have been listed. ^1H NMR data of the minor epimer are reported in the Experimental Section.

^a Overlapped with other signals.

The 2D NMR COSY spectrum of **67** allowed the arrangement of the proton multiplets into four spin systems (indicated in bold in **Fig. 3.22**), one of which is a C_7 moiety spanning from the sp^2 methine at C-15 to the hemiacetal proton and including an oxymethylene branching at C-20. The HMBC data (shown in **Fig. 3.22**) allowed the connection of the above described moieties and the assembly of the protolimonoid-type neemfruitin A planar structure.

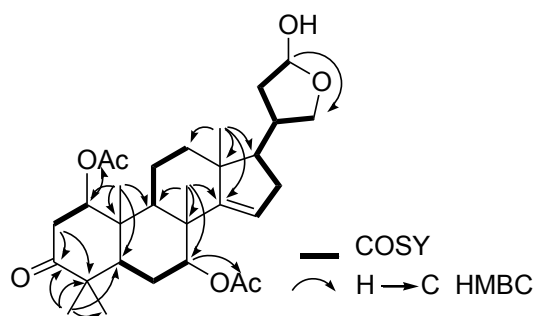


Figure 3.22. COSY and key H→C HMBC correlations detected for neemfruitin A (**67**)

In particular, cross-peaks of Me-19, Me-28 and Me-29 indicated the structure of ring A, including the placement of an oxymethine at C-1 and of the ketone carbonyl at C-3. Analogously, cross-peaks of Me-18, Me-19 and Me-30 disclosed the structure of rings B, C, and D, placing the second oxymethine at C-7. Both H-1 and H-7 showed 3J HMBC cross-peaks with an ester carbonyl, thus inferring the attachment of the two acetyl groups. Finally, the key cross-peak of H-23 with C-21 indicated the presence of a γ -lactol ring with an oxygen atom connecting C-21 and the hemiacetal C-23.

Actually, a series of signals attributable to a minor compound appeared to be present in both 1H and ^{13}C NMR spectra of **67** and all our initial attempts to further purify compound **67** failed. However, once the structure of compound **67** was disclosed, these signals were easily rationalized with the presence of an equilibrating mixture (ca. 3:1 ratio) of the two epimers at C-23. 1H and ^{13}C NMR resonances of the minor epimer have been reported in the Experimental Section.

The relative configuration of neemfruitin A (**67**) was assigned on the basis of ROESY cross-peaks aided by analysis of proton-proton coupling constants. The correlation of Me-19 with both Me-29 and Me-30 was indicative of the *cis* orientation of these groups (which is β in all the *Azadirachta* limonoids), while correlations of H-5 with both Me-28 and H-9, and of H-9 with Me-18 indicated

their α -orientation. Both H-1 and H-7 must be in equatorial (β) orientation on the basis of their very small coupling constants with protons on the adjacent carbons. ROESY cross-peaks H-1/Me-19 and H-7/Me-30 further supported this assignment. The cross-peak of Me-18 with H-20 indicated the β -orientation of H-17, but it cannot be used to gain information on the relative orientation at C-20. Given the free-rotating nature of the C-17/C-20 bond and the lack of unambiguous information, we prefer to leave undetermined the configuration at C-20.

Neemfruitin B (68) was isolated as a colorless amorphous solid with the molecular formula $C_{32}H_{46}O_6$ (established by HR-ESIMS), implying ten unsaturation degrees. The stereostructure of **68** (**Fig. 3.20**) was established on the basis of full 1D and 2D (COSY, HSQC, HMBC) NMR analysis, following the same approach above reported in detail for compound **67** (complete NMR assignment is reported **Table 3.4**). In particular, combined analysis of COSY and HSQC spectra allowed the elucidation of the four spin systems depicted in bold in **Fig. 3.23**, with a large moiety connecting the sp^2 methine at δ_H 5.52 (C-15) with the oxymethine at δ_H 2.67 (δ_C 67.0; C-24) and including a deshielded methine (δ_H 6.26 C-21) branching. Analysis of the HMBC cross-peaks (see **Fig. 3.23**) allowed the assembly of the tetracyclic system of rings A-D, whose structure is almost identical to that of compounds **69** and **73-75**, with the single exception of functionalization at C-7, which should be a non-acetylated hydroxyl group (H-7 resonates at δ_H 3.98 in **68** and at δ_H 5.20 in **74**).

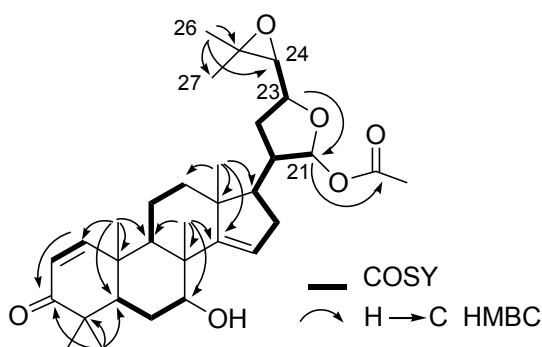


Figure 3.23. COSY and key H→C HMBC correlations detected for neemfruitin B (**68**)

Since this tetracyclic system included seven unsaturation degrees and two oxygen atoms, the side chain moiety should account for the three remaining unsaturation

degrees and should include four oxygen atoms. The HMBC cross-peak H-23/C-21 implied the presence of an oxygen bridge between C-23 and C-21, giving rise to a tetrahydrofuran ring. In addition, H-21 showed HMBC cross-peak with an acetyl carbonyl (δ_C 170.7), thus identifying C-21 as an acetylated hemiacetal carbon, in agreement with its downfield resonance (δ_C 96.8). Finally, since both Me-26 and Me-27 showed HMBC cross peak with two oxygenated carbons (the unprotonated C-25 and the oxymethine C-24), the last unsaturation degree and the last oxygen atom can be both accounted by the presence of an epoxide ring connecting C-24 and C-25. This is also in agreement with resonance of H-24 (δ_H 2.67), a typical value of oxirane methines. So, the gross structure of neemfruitin B (**68**) was defined as a new monoacetylated apotirucallane triterpenoid.

Relative configuration of the tetracyclic core of **68** was assigned by inspection of its ROESY spectrum and resulted to exactly parallel that detected for compound **67**. Cross-peaks H-23 with H-20 and H-21 implied the *cis* relationship of these protons. The relative arrangement of H-17 and H-24 with the stereogenic centers belonging to the tetrahydrofuran ring was deduced through the high similarity of $^1\text{H}/^{13}\text{C}$ NMR data of **68** with those of acetyltoosendantriol,⁴⁵ a triterpenoid derivative isolated from *Melia toosendan* possessing the same structure of **68** as for ring D and the entire side chain (from C-20 to C-27) and whose stereochemical details had been secured by X-ray analysis.⁴⁵ The whole of the above evidence is in agreement with the stereochemistry of **68** reported in **figure 3.20**.

3.4.2. Pharmacological activity

All the triterpenoids isolated from fruits of *A. indica* (**66-75**) were assayed *in vitro* against D10 (chloroquine sensitive, CQ-S) and W2 (chloroquine resistant, CQ-R) strains of *Plasmodium falciparum* using the pLDH assay by the group of prof. Taramelli at the University of Milan. Results are compiled in **Table 3.5**.

Interestingly, the tested compounds were found to be more active on the chloroquine-resistant clone (W2), a behavior already observed with antimalarials of the endoperoxide class. The most active compounds were the three limonoids (C₂₆) azadirone (**69**), gedunin (**66**) and neemfruitin A (**67**), while, on the contrary, the apotirucallane (C₃₀) derivative **68** emerged to be the less active compound. In addition, comparison of the structures of **74** and **75** with that **69** indicates that

their different activities should be attributed to the differences in the side chain. Also interesting is the comparison between the activities of **69** and **70**, clearly indicating that the presence of a second conjugated ketone group at C-16 is deleterious for the antimalarial activity.

Table 3.5. *In vitro* antimalarial activity of the extracts and of the triterpenoids isolated from the fruits of *A. indica* (**66-75**) tested against D10 (CQ-S) and W2 (CQ-R) strains of *P. falciparum*.

	D10	W2
	IC ₅₀ µg/mL	IC ₅₀ µg/mL
Fruit (EtOAc phase)	1.31 ± 0.48	1.92 ± 0.84
Fruit (BuOH phase)	3.18 ± 0.38	3.35 ± 0.35
Fruit (H ₂ O phase)	> 50	> 50
Azadirone (69)	0.71 ± 0.10	0.53 ± 0.13
Azadiradione (70)	2.68 ± 0.34	1.53 ± 0.37
Epoxyazadiradione (71)	1.54 ± 0.35	1.01 ± 0.34
Gedunin (66)	0.80 ± 0.18	0.63 ± 0.20
Deacetylgedunin (72)	2.26 ± 0.54	1.45 ± 0.26
Desmethyllumocin B (73)	2.19 ± 0.24	1.18 ± 0.32
Protoxylocarpin G (74)	2.64 ± 0.35	1.27 ± 0.48
Spicatin (75)	2.94 ± 0.41	1.49 ± 0.43
Neemfruitin A (67)	1.46 ± 0.36	0.90 ± 0.13
Neemfruitin B (68)	4.99 ± 0.57	5.28 ± 1.41
Chloroquine (38)	0.011 ± 0.004	0.11 ± 0.03

Data are means ± SD of three different experiments in duplicate

It is important to notice that gedunin (**66**) was identified as the most potent antimalarial limonoid of both barks³² and leaves³³ of *A. indica*. We have now found that the fruits of the same plant contain two limonoids which are as active as gedunin (**66**), namely azadirone (**69**) and the new neemfruitin A (**67**). A previous study³⁵ identified the conjugated enone system, the furan ring and the acetoxy group at C-7 as critical for the antimalarial activity of gedunin (**66**). The comparable activity of neemfruitin A (**67**), lacking the double bond at C-1/C-2 and showing a lactol ring in place of the furan ring, indicate that the above relationships, found for the D-*seco*-limonoid gedunin, do not apply to tetracyclic limonoids. The pharmacophoric portions for limonoid antimalarials are evidently still far from being identified. Only a more detailed investigation on the mechanisms of their antimalarial action, which remain still elusive, could

allow a better understanding of the structural requirements needed by an active molecule.

In conclusion, the present analysis on the fruits of *A. indica* revealed the presence of two new triterpenoid derivatives, one which, neemfruitin A (**67**), represents, together with gedunin (**66**) and azadirone (**69**) (a major component of the organic extract), the most active antimalarial limonoid of this part of the tree. Due to the importance placed on the traditional use of neem remedies for the treatment of malaria patients, this investigation could be potentially useful in the view of developing improved standardized herbal formulations that can be produced locally in African and Asian countries.

3.4.3. Experimental

Plant Material. Fresh, uncrushed, ripe neem fruits were collected from the region of Oubritenga (Ziniaré), Burkina Faso in June 2008. The tree was identified by Prof. Jeanne Millogo, full professor of Botanic of the Life Science Unit, and a voucher specimen (N°2 NFE) has been deposited in the Laboratory of Ecology at the University of Ouagadougou.

Extraction and isolation. After elimination of seeds, fruits of *A. indica* were dried (25 g, dry weight) and repeatedly extracted with MeOH (4 x 500 mL) and the obtained material was then partitioned between H₂O and EtOAc to yield a brown organic extract (2.75 g). The water extract was then partitioned against *n*-BuOH, yielding a polar organic (2.50 g) and a water (8.1 g) phase. The EtOAc extracts was subjected to chromatography over silica column (230-400 mesh) eluting with a solvent gradient of increasing polarity from hexane to EtOAc. Fractions eluted with *n*-hexane/EtOAc 9:1 were subjected to repeated HPLC chromatographies (*n*-hexane/EtOAc 95:5) affording azadirone (**69**, 112.1 mg) and epoxyazadiradione (**71**, 135.4 mg). Fractions eluted with *n*-hexane/EtOAc 8:2 were re-chromatographed by HPLC (*n*-hexane/EtOAc 85:15) to give gedunin (**66**, 11.3 mg) and deacetylgedunin (**72**, 7.3 mg). Fractions eluted with *n*-hexane/EtOAc 7:3 contained pure azadiradione (**70**, 118.5 mg). Fractions eluted with *n*-hexane/EtOAc 6:4 were subjected to repeated HPLC purifications to yield neemfruitin B (**68**, 4.5 mg), protoxylocarpin G (**74**, 2.2 mg), and

desmethyllimocin B (**73**, 14.6 mg). Fractions eluted with *n*-hexane/EtOAc 1:1 were re-chromatographed by HPLC (*n*-hexane/EtOAc 55:45) affording pure neemfruitin A (**67**, 3.5 mg) and spicatin (**75**, 2.8 mg).

Neemfruitin A (**67**): Colorless amorphous solid; $[\alpha]_D -17.2$ (*c* 0.2 in CHCl₃); ¹H NMR (CDCl₃, 500 MHz) Table 3.4; ¹H NMR data for the minor epimer (only resonances differing from those of the major epimer are reported): δ_H 5.54 (1H, H-23, bs), 3.98 (1H, H-21a, t, *J* = 8.0 Hz) 3.60 (1H; H-21b, t, *J* = 8.0 Hz), 2.81 (1H, H-20, m), 2.25 (1H, H-22a, overlapped), 1.63 (1H, H-22a, overlapped), 0.96 (3H, Me-18, s); ¹³C NMR (CDCl₃, 125 MHz) Table 3.4; (+) ESI-MS *m/z* 539 [M + Na]⁺. HR-ESIMS *m/z* 539.2979; (calcd for C₃₀H₄₄O₇Na 539.2985).

Neemfruitin B (**68**): Colorless amorphous solid; $[\alpha]_D + 5.3$ (*c* 0.4 in CHCl₃); ¹H NMR (CDCl₃, 500 MHz) Table 3.4; ¹³C NMR (CDCl₃, 125 MHz) Table 3.4; (+) ESI-MS *m/z* 549 [M + Na]⁺. HR-ESIMS *m/z* 549.3200 (calcd for C₃₂H₄₆O₆Na 549.3192).

In vitro drug susceptibility assay on P. falciparum: see paragraph 3.3.4

In vivo antimalarial activity: The *in vivo* antimalarial activity was assessed with the rodent malaria model *Plasmodium berghei* - *Anopheles stephensi* - BALB/c mice. Groups of six mice (5 weeks old females) were treated for nine days with an ethanol extract of neem fruits, administered orally twice a day at a dose of 100 mg/kg (200 mg/kg/d), or with control solution. On treatment day 3, mice were exposed to ~20 bites of infectious mosquitoes, i.e. *Anopheles* females harboring *P.berghei* sporozoites in their salivary glands. The day following the last treatment (day 10), percent parasitaemia was assessed by the examination of Giemsa-stained thin blood smears at the light microscope (1000 x magnification). Reduction in parasite proliferation as a result of treatment was estimated by comparing the mean parasitaemia values of treated and control group mice from 2 experimentations using the Student's *t* test.

References

1. Kayser, O.; Kiderlen, A. F.; Croft, S. L.; *Parasitology research*, Vol. 90, Supplement 2, S55-S62.
2. Casteel, D.A.; In *Burger's Medicinal Chemistry and Drug Discovery 5*; Wolff, M. E., Ed.; John Wiley and Sons, New York, **1997**, 3-91.
3. Arav-Boger, R.; Shapiro, T. A.; *Annu Rev Pharmacol Toxicol.*, **2005**, 45, 565-585.
4. Schmuck, G.; Roehrdanz, E.; Haynes, R. K.; Kahl, R.; *Antimicrob. Agent Chemother.*, **2002**, 46, 821-827.
5. Robert, A.; Benoit-Vical, F.; Meunier B.; *Coord Chem Rev*, **2005**, 249, 1927-1936.
6. Cafieri, F.; Fattorusso, E.; Tagliatela-Scafati, O.; Ianaro, A.; *Tetrahedron*, **1999**, 55, 7045-7056.
7. Fattorusso, E.; Parapini, S.; Campagnuolo, C.; Basilico, N.; Tagliatela-Scafati, O.; Taramelli, D. *J. Antimicrob. Chemother.*, **2002**, 50, 883-888.
8. Campagnuolo, C.; Fattorusso, E.; Romano, A.; Tagliatela-Scafati, O.; Basilico, N.; Parapini, S.; Taramelli, D.; *Eur. J. Org. Chem.*, **2005**, 5077-5083.
9. Fattorusso, E.; Tagliatela-Scafati, O.; Ianaro, A.; Di Rosa, M.; *Tetrahedron*, **2000**, 56, 7959-7967.
10. Fattorusso, C.; Campiani, G.; Catalanotti, B.; Persico, M.; Basilico, N.; Parapini, S.; Taramelli, D.; Campagnuolo, C.; Fattorusso, E.; Romano, A.; Tagliatela-Scafati, O.; *J. Med. Chem.*, **2006**, 49, 7088-7094.
11. Tagliatela-Scafati, O.; Fattorusso, E.; Romano, A.; Scala, F.; Barone, V.; Cimino, P.; Stendardo, E.; Catalanotti, B.; Persico, M.; Fattorusso, C.; *Org. Biomol. Chem.*, **2010**, 8, 846-856.
12. Fattorusso, C.; Persico, M.; Calcinai, B.; Cerrano, C.; Parapini, S.; Taramelli, D.; Novellino, E.; Romano, A.; Scala, F.; Fattorusso, E.; Tagliatela-Scafati, O.; *J. Nat. Prod.*, **2010**, 73, 1138-1145.

13. Kobayashi M., Kondo K., Kitagawa I.; *Chem. Pharm. Bull.*, **1993**, 41, 1324-1326.
14. <http://www.mmv.org>
15. Fattorusso, C.; Persico, M.; Basilico, N.; Taramelli, D.; Fattorusso, E.; Scala, F.; Taglialatela-Scafati O.; *Bioorg. Med. Chem.*, **2011**, 19, 312-320.
16. Vennerstrom, J. L.; Arbe-Barnes, S.; Brun, R.; Charman, S. A.; Chiu, F. C. K.; Chollet, J.; Dong, Y.; Dorn, A.; Hunziker, D.; Matile, H.; McIntosh, K.; Padmanilayam, M.; Santo Tomas, J.; Scheurer, C.; Scoreneaux, B.; Tang, Y.; Urwyler, H.; Wittlin, S.; Charman, W. N.; *Nature*, **2004**, 430, 900-904.
17. Singh, C.; Hassam, M.; Naikade, N. K.; Verma, V. P.; Singh, A. S.; Puri, S. K.; *J. Med. Chem.*, **2010**, 53, 7587-7598.
18. Fattorusso, E.; Taglialatela-Scafati O.; *Mar. Drugs*, **2009**, 7, 130-152.
19. Tategami, S.; Yamada, T.; Nishino, H.; Korp, J. D.; Kurosawa, K.; *Tetrahedron Lett.*, **1990**, 31, 6371-6374.
20. Yoshida, J.; Nakatani, S.; Sakaguchi K.; Isoe, S.; *J. Org. Chem.*, **1989**, 54, 3383-3389.
21. Nishino, H.; *Top. Heterocycl. Chem.*, **2006**, 6, 39-76.
22. Posner, G. H.; O'Dowd, H.; Ploypradith, P.; Cumming, J. N.; Xie, S.; Shapiro, T. A.; *J. Med. Chem.*, **1998**, 41, 2164-2167.
23. a) Arantes, C.; de Araujo, M. T.; Taranto, A. G.; Carneiro, J. W. D.; *Int. J. Quantum Chem.*, **2005**, 103, 749-762; b) Drew, M. G. B.; Metcalfe, J.; Dascombe, M. J.; Ismail, F. M. D.; *J. Mol. Struct. (Theochem)*, **2007**, 823, 34-46.
24. a) Posner, G. H.; Wang, D.; Cumming, J. N.; Oh, C. H.; French, A. N.; Bodley, A.L.; Shapiro, T. A.; *J. Med. Chem.*, **1995**, 38, 2273-2275. b) Robert, A.; Benoit-Vical, F.; Dechy-Cabaret, O.; Meunier, B.; *Pure Appl. Chem.*, **2001**, 73, 1173-1188.
25. Kawanishi, M.; Kotoku, N.; Itagaki, S.; Horii, T.; Kobayashi, M.; *Bioorg. Med. Chem.*, **2004**, 12, 5297-5307.

26. Sofowora, A. *Medicinal Plants and Traditional Medicine in Africa*, Wiley: New York; **1982**.
27. (a) Veicht, G. E.; Boyer, A.; Ley, S. V. *Angew. Chem. Intl. Ed.*, **2008**, 47, 9402-9429. (b) Morgan E. D. *Bioorg Med Chem*, **2009**, 17, 4096-4105.
28. Lucantoni, L.; Giusti, F.; Cristofaro, M.; Pasqualini, L.; Esposito, F.; Lupetti, P.; Habluetzel, A.; *Tissue Cell.*, **2006**, 38, 361-71
29. Habluetzel, A.; Lucantoni, L.; Esposito, F.; *Indian J Med Res.*, **2009**, 130, 112-114
30. Brahmachari G.; *Chembiochem*, **2004**, 5, 408-421.
31. Rochanakij, S.; Thebtaranonth, Y.; Yenjai, C.; Yuthavong, Y.; *Southeast Asian J. Trop. Med. Public Health*, **1985**, 15, 201-209.
32. Khalid, S. A.; Duddeck, H.; Gonzalez-Sierra, M.; *J. Nat. Prod.*, **1989**, 52, 922-927.
33. MacKinnon, S.; Durst, T.; Arnason, J. T.; Angerhofer, C.; Pezzuto, J.; Sanchez-Vindas, P. E.; Poveda, L. J.; Gbeassor, M.; *J. Nat. Prod.*, **1997**, 60, 336-341.
34. Brandt, G. E. L.; Schmidt, M. D.; Prisinzano, T. E.; Blagg, B. S. J.; *J. Med. Chem.*, **2008**, 51, 6495-6502.
35. Lucantoni, L.; Yerbanga, R. S.; Lupidi, G.; Pasqualini, L.; Esposito, F.; Habluetzel, A.; *Malar. J.*, **2010**, 9, 66.
36. Lavie, D.; Levy, E. C.; Jain, M. K.; *Tetrahedron*, **1971**, 27, 3927-3939.
37. Saewan, N.; Sutherland, J. D.; Chantrapromma, K.; *Phytochemistry*, **2006**, 67, 2288-2293.
38. Singh, S.; Garg, H. S.; Khanna, N. M. *Phytochemistry*, **1976**, 15, 2001-2002.
39. Akisanya, A.; Bevan, C. W. L.; Hirst, J.; Halsall, T. G.; Taylor, D. A. H. *J. Chem. Soc.*, **1960**, 3827-3829.
40. Akisanya, A.; Bevan, C. W. L.; Halsall, T. G.; Powell, J. W.; Taylor, D. A. H.; *J. Chem. Soc.*, **1961**, 3705-3708.

41. Kumar, S. S. R.; Srinivas, M.; Yakkundi, S.; *Phytochemistry*, **1996**, 43, 451-455.
42. Pudhom, K.; Sommit, D.; Nuclear, P.; Ngamrojanavanich, N.; Petsom, A.; *J. Nat. Prod.*, **2009**, 72, 2188-2191.
43. Connolly, J. D.; Phillips, W. R.; Mulholland, D. A.; Taylor, D. A. H.; *Phytochemistry*, **1981**, 20, 2596-2597.
44. Siddiqui, B. S.; Rasheed, M.; Ghiasuddin; Faizi, S.; Naqvi, S. N. H.; Tariq R. M.; *Tetrahedron*, **2000**, 56, 3547-3551.
45. Nakanishi, T.; Inada, A.; Nishi, M.; Miki, T.; Ino, R.; Fujiwara, T.; *Chem. Lett.*, **1986**, 15, 69-72.

CHAPTER IV

DITERPENOIDS FROM PLANTS OF THE FAMILY EUPHORBIACEAE

Plant secondary metabolites can be divided into three broad categories, (a) terpenes or terpenoids, (b) alkaloids and (c) phenolic compounds. The compounds classified as terpenes contribute arguably the largest and most diverse class of natural products.¹

The family Euphorbiaceae includes 300 genera and about 7,500 species. Despite the common knowledge that many species of Euphorbiaceae are toxic, many species have also found commercial importance (example: Hevea for rubber, Ricinus for castor oil and Manihot for cassava) also as ornamental plants and. Euphorbiaceae plants are a recognized source of structurally diverse diterpenoids and triterpenoids which have been shown to possess various biological activities (example: cytotoxic, anti-proliferative and wound healing), including also controversial biological activities such as tumor promoting and antitumor activity.² Diterpenoid polyesters are the most peculiar group of secondary metabolites obtained from plants of the Euphorbiaceae family.³ The first member of this class was serendipitously discovered over a century ago while manipulating lamp oil from the caper spurge (*Euphorbia lathyris* L.), and few other members were obtained in the course of studies on tumor promoting phorboids, mainly by Hecker.⁴

Terpenes are classified based on the number and structural organization of carbons formed by the linear arrangement of isoprene units followed by cyclization and rearrangements of the carbon skeleton with an empirical feature known as the isoprene rule. The term terpene refers to a hydrocarbon molecule, while terpenoid refers to a terpene that has been modified, for example by the addition of oxygen.⁵

Diterpenoids are, by definition, C₂₀ compounds based on four isoprene (C₅H₈) units which arise from two molecules of acetyl-coenzyme A derived by carbohydrate, fat, or protein catabolism yielding acetoacetyl-coenzyme A (**Fig. 4.1**). Further condensation with another molecule of acetyl-coenzyme A, now in

aldol-type reaction, results in β -hydroxy- β -methylglutaryl-coenzyme A (HMG-CoA), which is irreversibly reduced through intervention of NADPH to *R*-mevalonic acid (MVA), the building block of almost all isoprenoids. Phosphorylation of mevalonic acid by ATP, in two steps, leads to mevalonic acid 5-pyrophosphate. The latter reacts on the enzyme with ATP generating isopentenyl pyrophosphate (IPP), the long-sought biological isoprene unit. This elimination reaction, which had no previous analogy in biochemistry, proceeds by a concerted *trans*-elimination. Next, isopentenyl pyrophosphate is converted by an isomerase into an equilibrium mixture with dimethylallyl pyrophosphate (DMAPP), in which the latter predominates. The two intermediates react as shown (Fig. 4.1) with the aid of a ‘prenyl transferase’ generating geranyl pyrophosphate (GPP) in a stereospecific condensation. Further condensation of GPP and IPP will lead to farnesyl pyrophosphate (FPP) and, so on. Specifically, by this sequence of reactions geranylgeranyl pyrophosphate (GGPP) (Fig. 4.1) is generated and represents the acyclic precursor for further elaboration into cyclic diterpenoids.

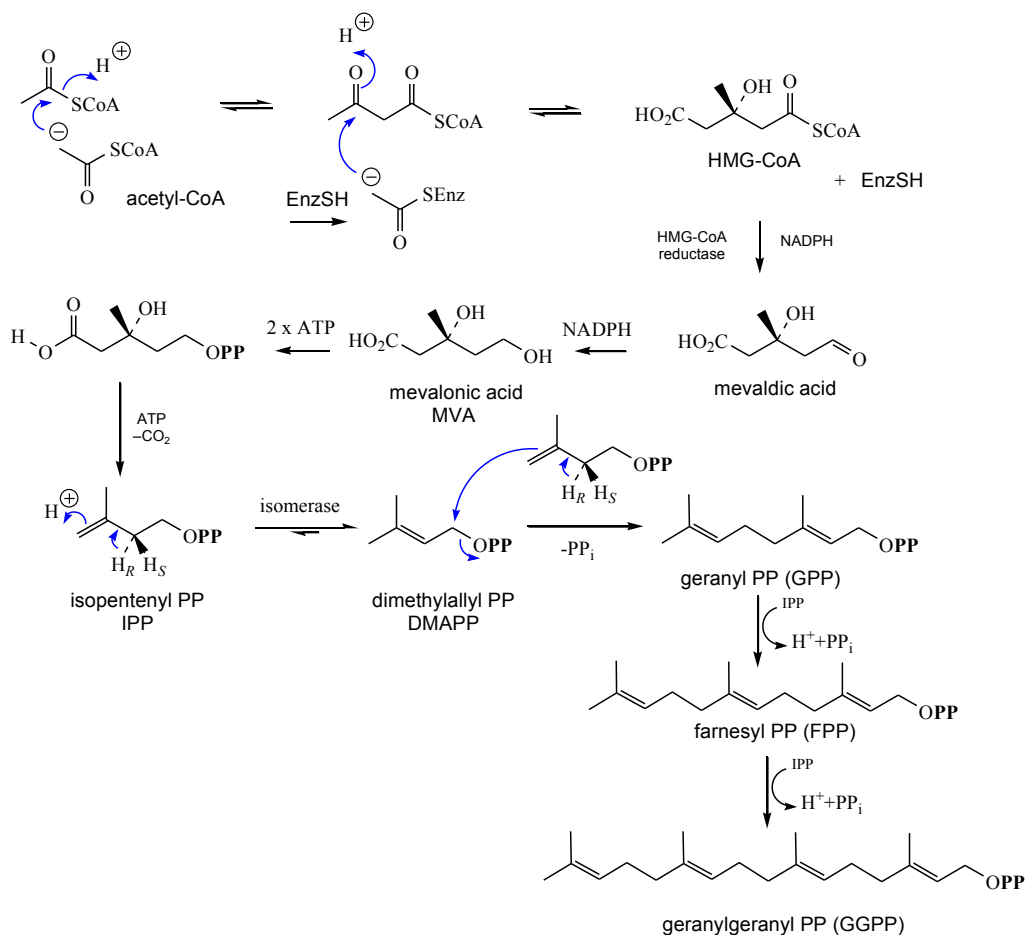


Figure 4.1. Biosynthesis of geranylgeranyl PP

Cyclization reactions of the acyclic precursor GGPP can occur from either side of the molecule: tail (alcohol end) or head (isopropylidene end). Cyclization generally involves carbocations and proceeds by a concerted addition mechanism generating different cyclic systems, dictated by the folding of the acyclic substrate chain on the enzyme template.⁶

In this way, many structural variants are produced. Indeed, diterpenoids constitute a so rich and diverse array of cyclic systems, that till now over 2000 diterpenes embracing more than 170 skeletal types have been recorded. The diterpene compounds are classified according to their biogenetic origin as acyclic (phytanes), bicyclic (labdanes, halimane, clerodanes), tricyclic (pimaranes, abietanes, cassanes, rosanes, vouacapanes, podocarpanes), (Fig. 4.2) tetracyclic (trachlobanes, kauranes, aphidicolanes, stemodanes, stemaranes, bayeranes, atisanes, gibberellanes), macrocyclic diterpenes (taxanes, cembranes, daphnanes, tiglianes, ingenanes) (Fig. 4.3) and mixed compounds, in accordance with the number and the cyclization patterns displayed by their skeletal structure.⁷⁻¹¹

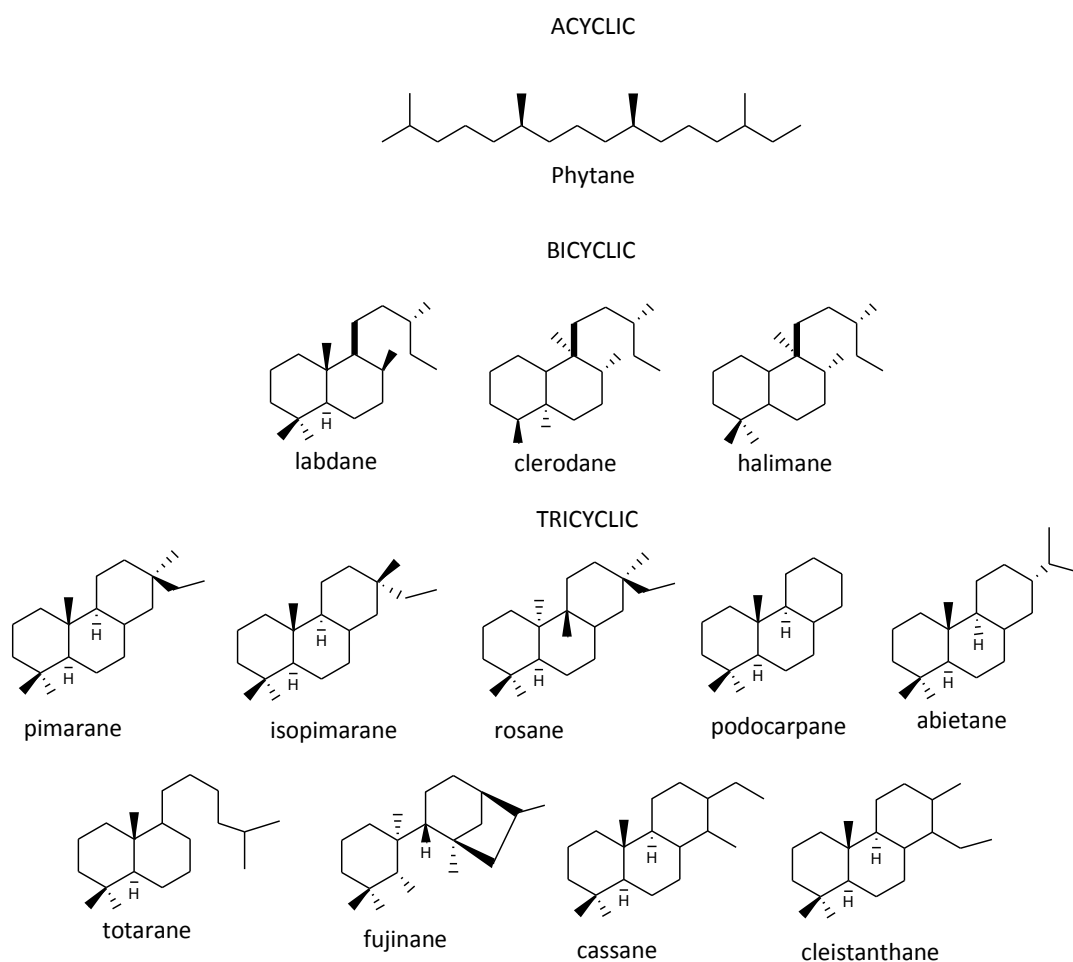


Figure 4.2. Important diterpene skeletal types

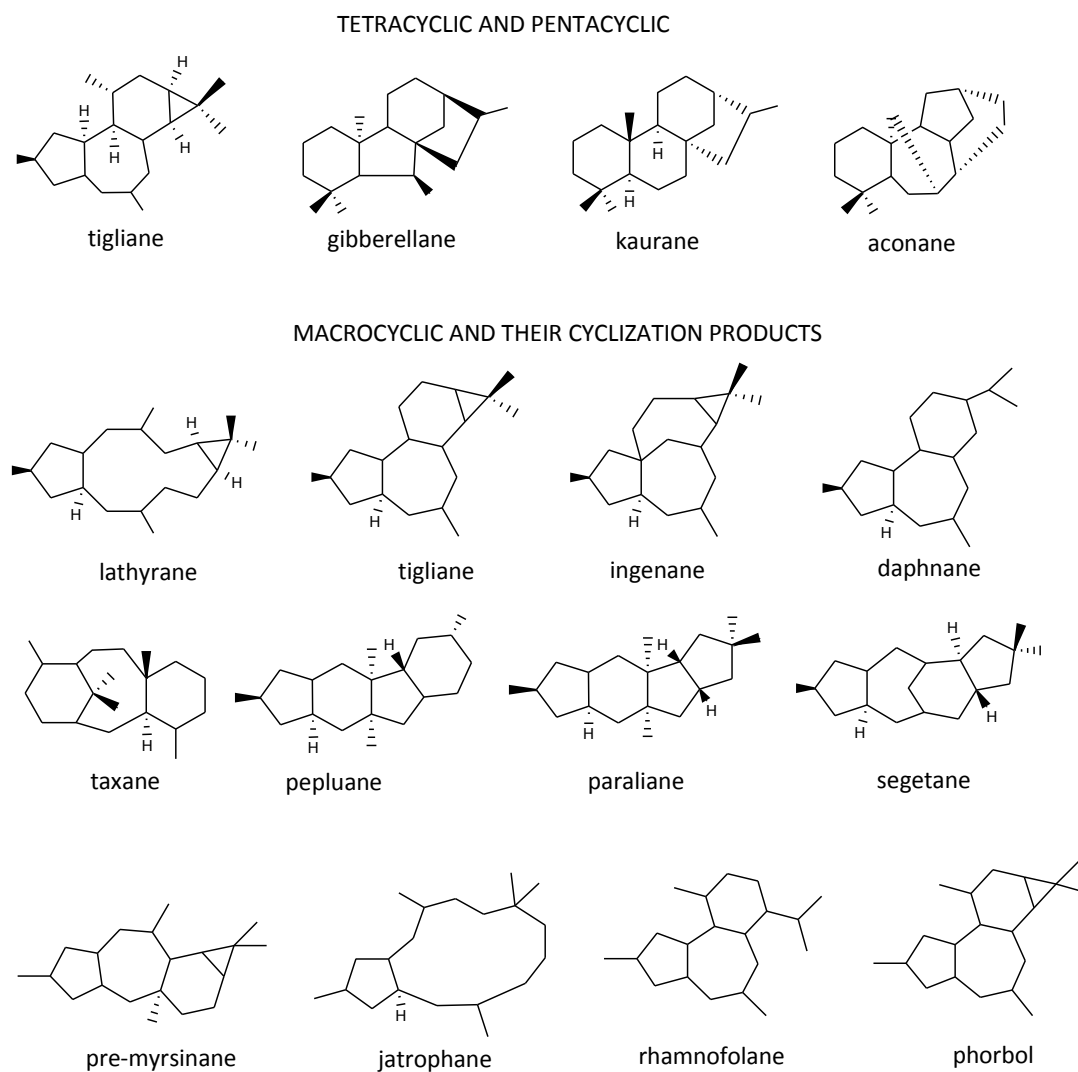
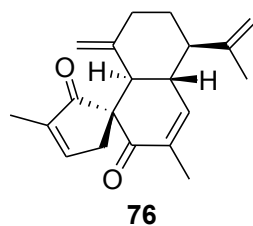
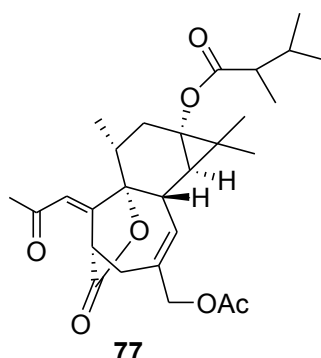


Figure 4.3. Important diterpene skeletal types

The chemical investigation of Euphorbiaceae plants carried out during my Ph.D., and described in this thesis, led to isolation (from *Jatropha curcas*) of a diterpenoid (spirocurcasone, **76**) characterized by a novel carbon skeleton, including an unprecedented spiro-connection between a decaline system and a five-membered ring, for which we propose the trivial name of spirorhamnfolane.¹²



In my research work I isolated, from *Euphorbia macroclada*, a diterpenoid with a naturally unprecedented ring A-secophorboid skeleton¹³(77).



The majority of diterpenes isolated from Euphorbiaceae plants are from casbane, labdane or clerodane skeletons and some of them (tiglane, daphnane and ingenane) have proven to be limited to Crotonideae and Euphorbioideae subfamilies. These diterpenes esters are toxic to livestock and humans¹⁴ and they exert tumor promoting and skin irritant activities. Many species of *Euphorbia* are regarded as potentially toxic, and latex can produce severe irritant effects, especially on mucous membranes and the eyes. Most of the biological effects are due to diterpene esters, e.g. esters of phorbol (**Fig. 4.4**), which activate protein kinase C, an important and widely distributed enzyme responsible for phosphorylating many biochemical entities. The permanent activation of protein kinase C is thought to lead to the uncontrolled cancerous growth. The most commonly encountered ester of phorbol is 12-O-myristoylphorbol 13-acetate. The origins of phorbol are not fully delineated, but may be rationalized as in **figure 4.4**. Casbene, via the ring closures shown in **figure 4.4** is then likely to be the precursor of the phorbol ring system.⁶

The diterpenoids of lathyrene and casbane skeleton obtained from different species of Euphorbiaceae have been found to exhibit anti-leukemic, cytotoxic, antitumor activities. The compounds in daphnane ester series also occur in complex mixtures. The most compounds in this class are intra molecular 9,13,14-ortho-(2-hexadecanoic acid) esters. Clerodane diterpenes have shown to act as vasorelaxants.¹⁵

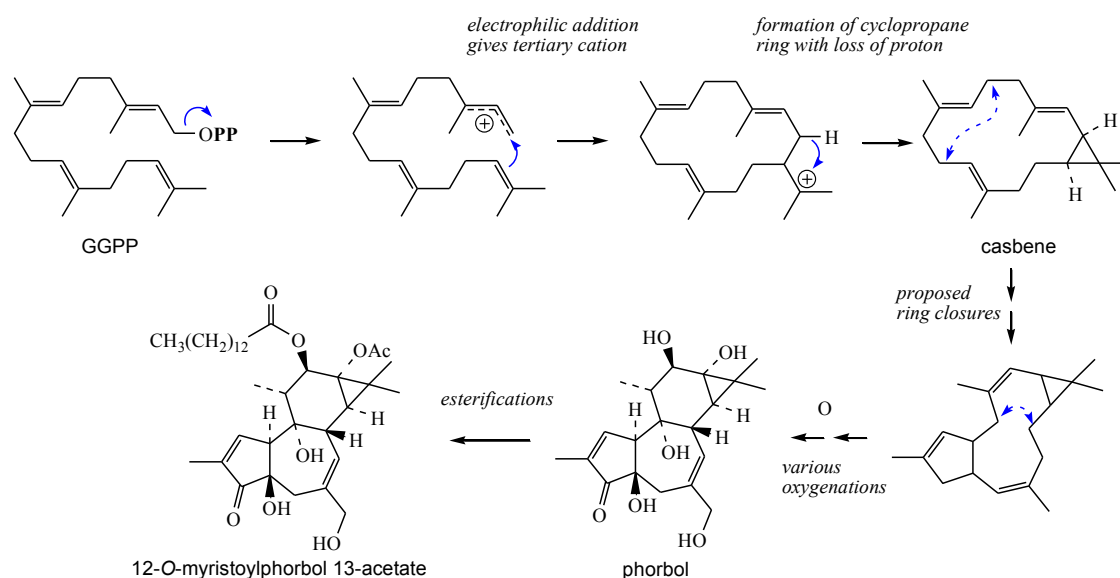
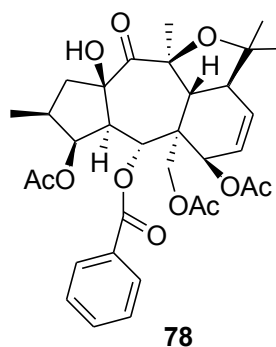


Figure 4.4 Biosynthetic pathway of phorbol.

Myrsinanes and cyclomyrsinanes are derived from lathyranes via premyrsinanes. In addition to the normal myrsinanes (6,12 cyclojatrophanes) with a 5/7/5-ring carbon framework, there are compounds with a hemiacetal ring, a 13,17-epoxy ring, or a 10,13-epoxy ring. The stereochemistry of all the frameworks and substituents are the same in myrsinanes.³ A recent report disclosed the identification of the myrsinane diterpenoid cheiradone (**78**) as a potent vascular endothelial growth factor receptor (VEGFR) antagonist with negligible affinity for epidermal growth factor receptor (EGFR).¹⁶



The structure of **78** is remarkable for a kinase inhibitor, since kinase ligands are generally unsophisticated flat molecules that act as ATP-mimics, while **78** is exuberant in terms of tridimensional chirality and structural complexity.

4.1. SECONDARY METABOLITES FROM ROOT BARKS OF *JATROPHA CURCAS*

4.1.1. Introduction



Jatropha curcas L. (Euphorbiaceae) is a deciduous and drought-resistant shrub, originated in Central and South America and now widely distributed in tropical and subtropical areas of Africa and Southeast Asia (Fig. 4.5).



Figure 4.5

J. curcas has long been used around the world as a source of lamp oil and soap, and also as a hedging plant, but in recent years the interest in this plant has experienced an inconceivable explosion (“the *Jatropha* fever”)¹⁷ due to the possible use of its seeds as a sustainable source for biodiesel production, outperforming biodiesels from rapeseed, sunflower and soya bean oil in terms of performance, efficiency and emissions, also in standard diesel engines. In many countries, extensive cultivation of *J. curcas* have been implanted in areas which do not compete with the food cultivation, as non-arable wastelands. For example, in 2007, China claimed to have 2 million hectares of *J. curcas* already under cultivation and announced plans to plant an additional 11 million hectares across its southern states by 2010.¹⁷

Extracts from *J. curcas* have also found a number of traditional medical uses and they have been intensively investigated for their secondary metabolites content.¹⁸⁻

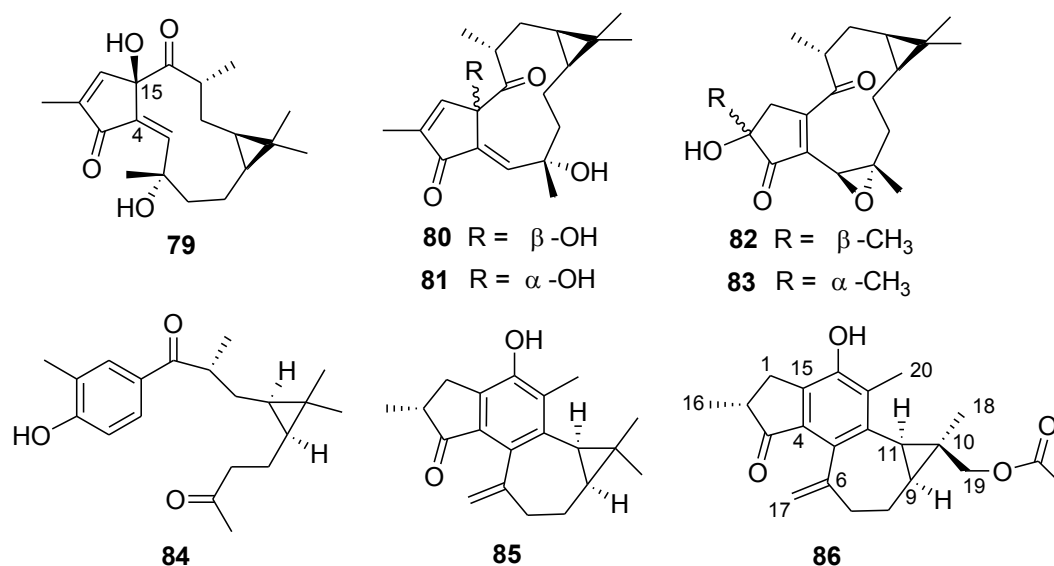
²¹ This plant continues to attract the interest of natural products chemists and the most recent report about its chemical composition has disclosed the presence of jatrophalactam, a diterpenoid lactam possessing a novel tricyclic skeleton.²²

As a result of a bioassay-guided purification of *J. curcas* root barks, I have isolated 11 known (79-85 and 87-90) and three new (86, 91, 76) diterpenoids,

including spirocurcasone (**76**), a novel diterpenoid possessing an unprecedented carbon framework which includes a spiro-[4,5]-decane junction.

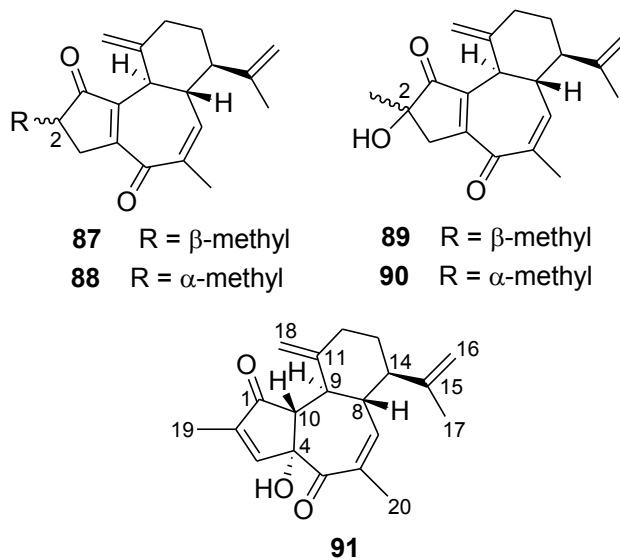
4.1.2. Isolation and structure elucidation of new secondary metabolites

The dried and powdered root barks of *J. curcas* were extracted at room temperature sequentially with hexane and EtOAc. Both the obtained crude extracts proved to be active in preliminary cytotoxicity tests and were subjected to column chromatography fractionation. Selected bioactive fractions were further purified over silica gel HPLC to yield five diterpenoids of the jatrogrossidentadione family (**79-83**),^{23,24} multidione (**84**),²⁵ jatropholone B (**85**),²⁶ curcusones A-D (**87-90**),²⁷ and three new diterpenoids which we have named acetoxyjatrophenolone (**86**), curcusone E (**91**), and spirocurcasone (**76**).



Acetoxyjatrophenolone (**86**), C₂₂H₂₆O₄ by HR-ESIMS, was isolated as a colorless amorphous solid. Its ¹H and ¹³C NMR data were fully assigned¹² with the help of 2D NMR experiments and appeared strongly suggestive of a molecular architecture of the jatropholone-type. Particularly, the network of the key HMBC cross-peaks (e.g. H₂-1 with C-4, C-14, and C-15; H-2 with the ketone carbonyl C-3, C-15 and C-4; the *sp*² methylene H₂-17 with C-5, C-6 and C-7; the cyclopropane methine H-11 with C-5, C-10, C-12 and the methyl-linking C-13) indicated the structure with a 5-6-7-3 membered condensed ring system. Accordingly, the ¹H NMR spectrum of **86** closely resembled that of jatropholone

B (**85**)²⁷ with the exception of the lack of one of the two high-field methyl singlets, and the appearance of an oxygenated diastereotopic methylene (δ 4.11 and 3.95) and an acetyl singlet (δ 2.12). The HMBC cross-peak of the above methylene protons with C-9, C-10, C-11, C-18 and with the acetyl ester carbonyl indicated the attachment of an acetoxymethyl group at the cyclopropane unprotonated carbon C-10. The β -orientation of this group was deduced on the basis of the ROESY cross-peaks H₃-18/H-11 and H₂-19/H-8a.



Curcusone E (**91**), C₂₀H₂₄O₃ by HR-ESIMS, is a new rhamnofolane diterpene of the curcusone-type.²⁷ It differs from curcusones C (**89**) and D (**90**) for the positional isomerization of both the hydroxyl group and one of the double bonds. Both these changes occurred at the five-membered ring and, accordingly, the ¹H and ¹³C NMR resonances of the seven- and six-membered ring nuclei (and those of the attached substituents), fully assigned through 2D NMR experiments (COSY, HSQC, HMBC) were suggestive of an unchanged arrangement compared to the other curcusones. On the other hand, Me-19 (δ_{H} 1.83) was now an allylic methyl showing HMBC cross-peaks with the conjugated ketone carbonyl at C-1 (δ_{C} 204.1) and with two *sp*² carbons, the unprotonated C-2 (δ_{C} 145.7) and the methine C-3 (δ_{C} 152.1). In turn, the methine proton H-3 showed HMBC cross-peaks with two ketone carbonyls, C-1 and C-5 (δ_{C} 206.3), with the oxygenated unprotonated carbon C-4 (δ_{C} 88.9, showing also HMBC correlation with the OH proton at δ_{H} 4.64), and with the methine at C-10 (δ_{C} 57.4), whose relevant proton (H-10, δ_{H} 3.32) was coupled with H-9 in the COSY spectrum. Once the planar structure of **91** was defined, its relative configuration could be established on the

basis of 2D NMR ROESY cross-peaks. In particular, coupling of H-14 with H-9 and of Me-17 with H-8 indicated the relative arrangement around the six-membered ring, supported by the high proton-proton coupling constants ($J = 8.5$ Hz) showed by H-8 with both H-9 and H-14, indicative of *pseudo* axial-axial relationships. Finally, the ROESY cross-peaks of OH-4 with H-9 and of H-10 with H-18a fully defined the relative configuration of the new curcusone E (**91**).

4.1.3. Spirocurcasone, a diterpenoid with a novel carbon skeleton

Spirocurcasone (**76**, Fig. 4.6) was obtained as a colorless amorphous solid. HR-ESIMS established the molecular formula $C_{20}H_{24}O_2$, which indicated nine degrees of unsaturation. The 1H NMR spectrum of **76** showed the presence of six broad singlets in the region between δ 4.10 and 7.30, a series of multiplets between δ 1.50 and 3.20 and three allylic methyl singlets (δ 1.72, 1.74 and 1.84). The ^{13}C NMR spectrum of **76** showed 20 carbon signals that, with the help of the 2D NMR HSQC experiment, were sorted into two ketone carbonyls, eight sp^2 carbons (including two methylenes, two methines and four unprotonated carbons) identifying four carbon-carbon double bonds, three methyls, three sp^3 methylenes, three sp^3 methines and one sp^3 unprotonated carbon (δ 60.7). This preliminary analysis pointed to a tricyclic skeleton for spirocurcasone (**76**).

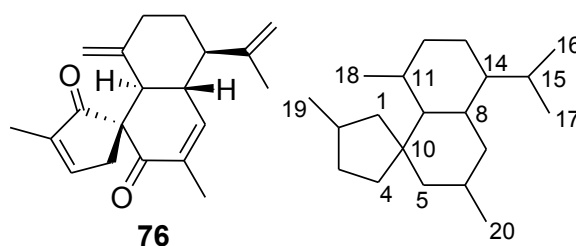


Figure 4.6. Spirocurcasone (**76**) and its new diterpene skeleton, named spirorhamnofolane

Analysis of the COSY spectrum allowed the definition of the two structural moieties drawn with bold lines in **figure 4.7**, namely a six-carbon fragment going from the sp^2 methine H-7 to H₂-12, with a methine branching, and a two-carbon fragment including only the downfield shifted sp^2 methine H-3 (δ 7.27) and the

diastereotopic methylene H₂-4 (δ 3.17 and 2.42). The HMBC cross-peaks (**Fig. 4.7**) of H₂-18 with C-9, C-11 and C-12 defined the structure of the six-membered ring, while the cross-peaks of H₃-17 with C-14, C-15 and C-16 indicated the attachment of an isopropenyl group at C-14. Both the allylic methyls H₃-19 and H₃-19 showed HMBC correlations with a ketone carbonyl and two *sp*² carbons, thus attaching two α -methyl- α,β -unsaturated ketone fragments to the spin systems above evidenced by the COSY spectrum. Finally, a series of HMBC cross-peaks of H₂-4 and H-9 proved to be of pivotal importance to disclose the tricyclic planar structure of compound **76** (**Fig. 4.7**). Indeed, both H₂-4 and H-9 were correlated with the two ketone carbonyls (C-1 and C-5) and with the unprotonated carbon at C-10, which must be the spiro-carbon connecting a five- and a six-membered ring. Hence, the planar structure of **76** was determined as a diterpenoid with a novel carbon skeleton, characterized by an unprecedented spiro-connection between a decaline system and a five-membered ring, for which we propose the trivial name of spirorhamnofolane (see **Fig. 4.6**).

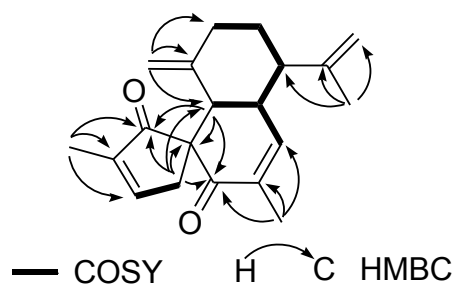


Figure 4.7. COSY and key HMBC correlation of spirorcurcasone (**76**)

The relative configuration of **76** has been assigned by a ROESY spectrum, in which the correlations H-14/H-9 and H-8/Me-17 defined the relative orientation of three adjacent stereogenic centers of the “upper” six-membered ring. The ROESY correlation of H-4a with H-18b and with H-8 defined the relative configuration at the spiro-carbon C-10.

Given the novelty of the tricyclic framework of spirorcurcasone (**76**), an unambiguous determination of its absolute configuration appeared mandatory. We decided to face this problem by measurement of the electronic circular dichroism (ECD) spectrum and comparison with the ECD spectrum predicted from quantum mechanical TDDFT calculations, a recent approach increasingly applied for the

determination of absolute configurations of natural products.²⁸ The conformational analysis of one of the two possible enantiomers of spirocurcasone (the one shown in **Fig. 4.6** as **76**) was performed by using the simulated annealing procedure (INSIGHT II package). This afforded a set of conformers which were ranked on the basis of their conformational energy values and grouped into two families, which were further optimized with the software package Gaussian 03²⁹ by using DFT at the RB3LYP/6-31G(d) level (**Fig. 4.8**). The excitation energies as well as the oscillator and rotatory strengths of the electronic excitation were calculated for both the conformational families using the TDDFT methodology and their ECD spectra were then simulated by the overlapping Gaussian function.³⁰

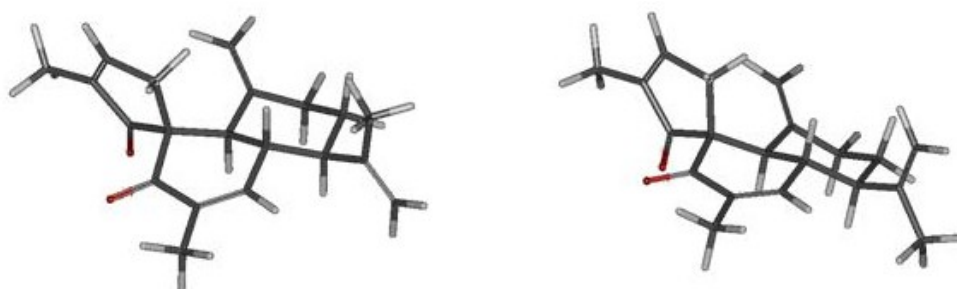


Figure 4.8. The two conformational families of **76**

In order to obtain the final ECD spectrum, the simulated spectra of the lowest energy conformers were averaged on the basis of their Boltzmann distribution and were UV corrected. **Figure 4.9** shows the close similarity between the obtained theoretical curve and the experimental spectrum, which allowed a confident assignment of the absolute configuration of spirocurcasone as shown in **76**.

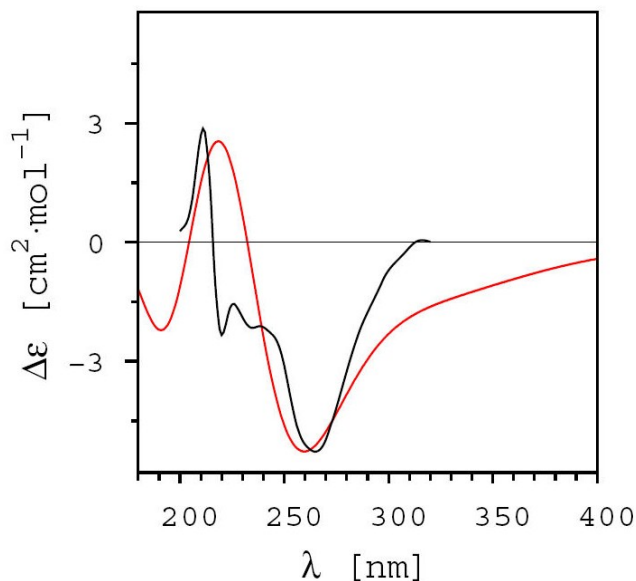


Figure 4.9. Theoretical CD curve (red) of **76** vs experimental curve (black)

The new spirorhamnofolane skeleton of **76** could biosynthetically derive from a rhamnofolane derivative related to curcusone E (**91**) following the mechanism shown in **figure 4.10**, which envisages, as key step, a [1,5] sigmatropic alkyl shift on a cyclopentadiene. Although the 5/7 bicyclic system of the rhamnofolane A/B rings is widely represented in the diterpene class (e.g. daphnanes, tiglianes, ingenanes), to our knowledge, this kind of rearrangement is unprecedented.

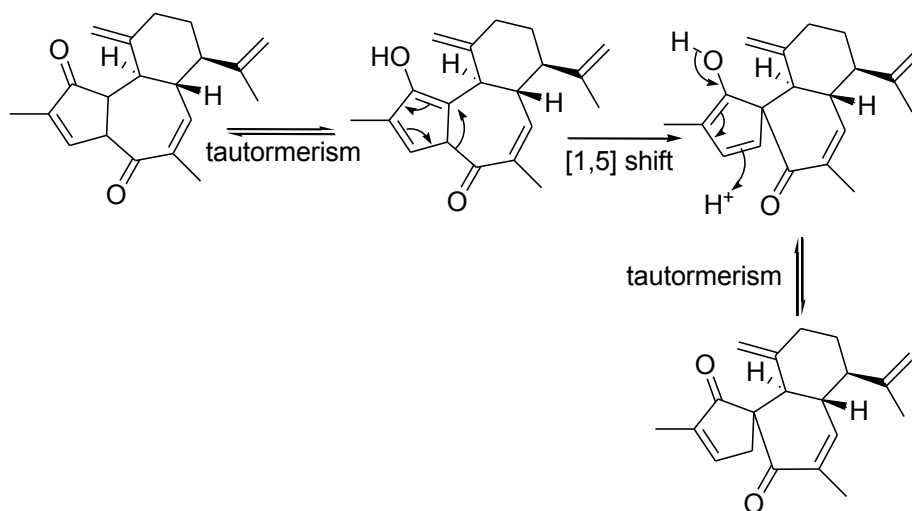


Figure 4.10. Proposed biogenesis for the spirorhamnofolane skeleton

4.1.4. Pharmacological activity

All the 14 diterpenes obtained in this study have been tested for their antiproliferative activity on L5178Y (mouse lymphoma) cell line. A very potent activity was exhibited by curcusones A (**87**, $IC_{50} = 0.21 \mu\text{g/mL}$), B (**88**, $IC_{50} = 0.27 \mu\text{g/mL}$), C (**89**, $IC_{50} = 0.09 \mu\text{g/mL}$), and D (**90**, $IC_{50} = 0.16 \mu\text{g/mL}$), and by compounds **79** ($IC_{50} = 0.60 \mu\text{g/mL}$), **81** ($IC_{50} = 0.85 \mu\text{g/mL}$), **82** ($IC_{50} = 0.20 \mu\text{g/mL}$), and **83** ($IC_{50} = 0.24 \mu\text{g/mL}$). On the other hand, multidione (**84**, $IC_{50} = 5.5 \mu\text{g/mL}$), jatropholone (**85**, $IC_{50} = 7.5 \mu\text{g/mL}$), acetoxyjatropholone (**86**, $IC_{50} = 2.5 \mu\text{g/mL}$), and compound **80** ($IC_{50} = 2.1 \mu\text{g/mL}$) showed a moderate activity, while the remaining compounds **91** and **76** were practically inactive ($IC_{50} > 10 \mu\text{g/mL}$). The mechanism of this antiproliferative activity has not been investigated, however, the presence of Michael acceptors should not fulfil the structural requirements of the pharmacophoric regions, since the inactive compounds **80**, **91**, and **76** all encompass more than one Michael acceptor sites in their structures.

4.1.5 Experimental

Collection, extraction and isolation.

A ground root bark of *J. curcas* (1.0 kg) was extracted with at room temp sequentially with hexane (2 x 3 L) and EtOAc (3 x 3 L), to give the respective crude extracts which were concentrated *in vacuo*. The hexane extract (10.5 g) was fractionated by gravity column chromatography on silica gel (60 g) using a *n*-hexane/EtOAc gradient. Fractions eluted with *n*-hexane/EtOAc 9:1 were further purified by HPLC (*n*-hexane/EtOAc 9:1, flow 0.8 mL/min) to yield curcusones A (**87**, 85.2 mg), B (**88**, 99.7 mg), E (**91**, 11.5 mg). Fractions eluted with *n*-hexane/EtOAc 8:2 were further purified by HPLC (*n*-hexane/EtOAc 8:2, flow 0.8 mL/min) to yield curcusones C (**89**, 13.2 mg), D (**90**, 5.7 mg), 15-epi-4E-jatrogrossidentadion (**81**, 15.5 mg), and 4Z-jatrogrossidentadion (**79**, 8.4 mg). Fractions eluted with *n*-hexane/EtOAc 7:3 were further purified by HPLC (*n*-hexane/EtOAc 85:15, flow 0.8 mL/min) to yield multidione (**84**, 14.2 mg), 4E-jatrogrossidentadion (**80**, 19.3 mg). Fractions eluted with *n*-hexane/EtOAc 6:4 were further purified by HPLC (*n*-hexane/EtOAc 7:3, flow 0.8 mL/min) to yield

hydroxyisojatrogrossidion (**82**, 12.2 mg) and 2-epi-hydroxyisojatrogrossidion (**83**, 7.1 mg). The EtOAc extract (11.2 g) of root barks was fractionated by gravity column chromatography on silica gel (60 g) using a *n*-hexane-EtOAc gradient. Fractions eluted with *n*-hexane/EtOAc 9:1 were further purified by HPLC (*n*-hexane/EtOAc 9:1, flow 0.8 mL/min) to yield spirocurcasone (**76**, 14.5 mg). Fractions eluted with *n*-hexane/EtOAc 8:2 were further purified by HPLC (*n*-hexane/EtOAc 8:2, flow 0.8 mL/min) to yield jatropholone B (**85**, 11.4 mg) and acetoxyjatropholone (**86**, 3.4 mg).

Acetoxyjatropholone (**86**): colorless amorphous solid; $[\alpha]_{26}^D + 18.1$ (*c* 0.01 CHCl₃); UV (MeOH) λ_{\max} (log ϵ) 275 (3.84), 220 (4.11) 204 (4.30) nm; ¹H NMR (500 MHz, CDCl₃) δ 5.26 (bs, H-17a), 4.69 (bs, H-17b), 4.11 (d, *J* = 11.6 Hz, H-19a), 3.95 (d, *J* = 11.6 Hz, H-19b), 3.19 (dd, *J* = 16.7, 8.3 Hz, H-1a), 2.70 (overlapped, H-7a), 2.67 (overlapped, H-7b), 2.63 (overlapped, H-2), 2.52 (dd, *J* = 16.7, 2.3 Hz, H-1b), 2.31 (bs, Me-20), 2.12 (s, OAc), 1.84 (m, H-8a), 1.34 (m, H-8b), 1.30 (d, *J* = 6.9 Hz, Me-16), 0.93 (overlapped, H-9), 0.92 (overlapped, H-10), 0.91 (s, Me-18); ¹³C NMR (125 MHz, CDCl₃) δ 208.0 (C-3), 170.5 (OAc), 150.6 (C-14), 145.5 (C-6), 137.5 (C-4), 136.0 (C-12), 134.0 (C-5), 131.8 (C-15), 131.0 (C-13), 115.6 (C-17), 74.1 (C-19), 42.7 (C-2), 33.5 (C-7), 30.4 (C-1), 26.2 (C-9), 23.3 (C-10), 23.1 (C-11), 20.9 (OAc), 17.3 (C-16), 13.2 (C-20), 12.5 (C-18); HR-ESIMS *m/z* 377.1734 ([M + Na]⁺ calcd for C₂₂H₂₆NaO₄ 377.1729).

Curcusone E (**91**): colorless amorphous solid; $[\alpha]_{26}^D - 155.5$ (*c* 0.03 CHCl₃); UV (MeOH) λ_{\max} (log ϵ) 239 (3.55) 207 (4.05) nm; ¹H NMR (500 MHz, CDCl₃) δ 6.68 (bs, H-3), 5.77 (bd, *J* = 2.1 Hz, H-7), 4.95 (bs, H-18a), 4.80 (bs, H-18b), 4.76 (bs, H-16a), 4.71 (bs, H-16b), 4.64 (s, 4-OH), 3.32 (bs, H-10), 2.65 (dt, *J* = 8.5, 8.5, 2.1 Hz, H-8), 2.42 (td, *J* = 11.6, 2.5, 2.5 Hz, H-12a), 2.37 (bd, *J* = 8.5 Hz, H-9), 2.05 (m, H-12b), 1.93 (dt, *J* = 8.5, 8.5, 2.5 Hz, H-14), 1.83 (s, Me-19), 1.75 (bs, Me-20), 1.74 (partially overlapped, H-13a), 1.65 (s, Me-17), 1.60 (ddd, *J* = 9.0, 8.5, 2.5 Hz, H-13b); ¹³C NMR (125 MHz, CDCl₃) δ 206.3 (C-5), 204.1 (C-1), 152.1 (C-3), 148.7 (C-11), 146.8 (C-15), 145.7 (C-2), 139.0 (C-7), 131.2 (C-6), 112.5 (C-16), 108.0 (C-18), 88.9 (C-4), 57.4 (C-10), 53.7 (C-14), 45.7 (C-8), 42.8 (C-9), 36.9 (C-12), 34.4 (C-13), 22.0 (C-20), 20.2 (C-17), 10.8 (C-19); HR-ESIMS *m/z* 335.1630 [M + Na]⁺ (calcd for C₂₀H₂₄NaO₃ 335.1623).

Spirocurcasone (76): C₂₀H₂₄O₂, colorless amorphous solid; $[\alpha]_{26}^D + 3.5$ (c 0.02 CHCl₃); UV (MeOH) λ_{\max} (log ϵ) 230 (3.32) nm; ECD (MeOH) λ_{\max} ($\Delta\epsilon$) 208.0 (+ 2.9) 266.5 (- 5.6); ¹H NMR (700 MHz, CDCl₃) δ 7.27 (bs, H-3), 6.60 (bs, H-7), 4.94 (bs, H-16a), 4.85 (bs, H-16b), 4.66 (bs, H-18b), 4.18 (bs, H-18b), 3.17 (bd, $J = 18.8$ Hz, H-4a), 3.07 (bd, $J = 10.8$ Hz, H-9), 2.42 (bd, $J = 18.8$ Hz, H-4b), 2.35 (bdd, $J = 11.9, 10.8$ Hz, H-8), 2.32 (ddd, $J = 13.2, 3.5, 3.5$ Hz, H-12a), 2.17 (ddd, $J = 13.2, 11.9, 3.5$ Hz, H-12b), 2.11 (ddd, $J = 11.9, 11.0, 2.8$ Hz, H-14), 1.89 (bs, H-19), 1.84 (dddd, $J = 13.2, 3.5, 3.5, 2.8$ Hz, H-13a), 1.74 (bs, H-20), 1.72 (bs, H-17), 1.53 (m, H13b); ¹³C NMR (175 MHz, CDCl₃) δ 208.8 (C-1), 199.7 (C-5), 153.4 (C-3), 146.6(C-7), 146.2 (C-15), 145.3 (C-11), 144.3 (C-2), 133.5 (C-6), 113.4 (C-16a), 106.7 (C-18a), 60.7 (C-10), 50.4 (C-14), 47.9 (C-9), 40.9 (C-8), 36.8 (C-12), 33.6 (C-13), 33.0 (C-4), 19.4 (C-17); ESI-MS m/z 297 [M + H]⁺ 319 [M + Na]⁺; HR-ESIMS m/z 319.1669 [M + Na]⁺ (calcd. for C₂₀H₂₄NaO₂ 319.1674).

Pharmacological tests.

The extracts were subjected to *in vitro* cytotoxicity assay applying the MTT [3-(4,5-dimethylthiazol-2-yl)-2,5-diphenyl tetrazolium bromide] (Sigma-Aldrich, Taufkirchen; Germany) method (Sarin PS, Sun D, Thornton A, Müller WEG J Natl. Cancer Inst., 1987, 78, 663-666). L5178y mouse lymphoma cells have been selected for *in vitro* toxicity testings (The cells were grown in RPMI 1640 medium (Gibco BRL, Eggenstein; Germany), supplemented with 10 mM HEPES [hydroxyethyl-piperazineethane-sulfonic acid], 10% fetal calf serum (FCS) (PAA, Cölbe, Germany) and 0.1 % gentamycin. The cells were routinely passaged twice weekly. The cells were kept in a humidified atmosphere of 95% air and 5% CO₂ at 37°C.

To estimate the EC₅₀ values, L5178Y, PC12 or HeLa cells were incubated for 72 hrs in the presence of different concentrations (0.1; 0.3; 1.0; 3.0, and 10.0 µg/ml) of the respective compounds. The final volumes in the assay were 200 µL. All compounds/extracts were dissolved in DMSO and stored at -20°C. The viability of the cells was determined using the MTT colorimetric assay system. The evaluation was performed in 96-well plates at 595 nm using an ELISA plate reader, after overnight incubation at 37°C as described (Schröder HC, Sarin PS, Rottmann M, Wenger R, Maidhof A, Renneisen K, Müller WEG. Biochem Pharmacol, 1988, 37, 3947-3952). The 50% effective concentration (IC₅₀),

representing that concentration at which the growth rate of the infected cells was reduced by 50%, was estimated by logit regression as described (Weiler BE, Schröder HC, Stefanovich V, Stewart D, Forrest JMS, Allen LB, Bowden BJ, Kreuter MH, Voth R, Müller WEG. *J Gen. Virol* 1990, 71, 1957-1963). The means (\pm SD) from 10 separate experiments are given.

Computational Details.

A preliminary conformational search on spirocurcasone (**76**) was performed by Simulated Annealing in the INSIGHT II package. The CHCl_3 solution phases were mimicked through the value of the corresponding dielectric constant. Using the steepest descent followed by quasi-Newton–Raphson method (VA09A) the conformational energy was minimized. Restrained simulations were carried out for 500 ps using the CVFF force field as implemented in Discover software (Accelrys, San Diego, USA). The simulation started at 1000 K, and then the temperature was decreased stepwise to 300 K. The final step was again the energy minimization, performed in order to refine the structures obtained, using the steepest descent and the quasi-Newton–Raphson (VA09A) algorithms successively. Both dynamic and mechanic calculations were carried out by using 1 (kcal/mol)/Å² flat well distance restraints. One hundred structures were generated. To simulate the solvent chosen for NMR analysis, a distance-dependent dielectric constant set to the value of CHCl_3 (ϵ 4.8) was used during the calculations. All optimizations were performed with the software package Gaussian 03,^a by using the DFT functional RB3LYP and the basis set 6-31G(d). The B3LYP/6-31G(d) harmonic vibrational frequencies were further calculated to confirm their stability. Rotatory strength values for the electronic transitions from the ground state to the singly excited states for all conformers of **76** were obtained by TDDFT calculations RB3LYP/6-31G(d,p) with Gaussian 03. The excitation energies as well as the oscillator and rotatory strengths of the electronic excitation were calculated for both the conformational families using the TDDFT methodology and their ECD spectra were then simulated by overlapping the Gaussian functions for each transition. The simulated spectra of the lowest energy conformers were averaged on the basis of their Boltzmann distribution. $\Delta\epsilon$ values were calculated by forming sums of Gaussian functions centred at the wavelengths of the respective electronic transitions and multiplied by the

corresponding rotatory strengths. The obtained ECD spectra were UV-corrected and compared with the experimental ones.

^aGaussian 03-Revision B05: Frisch, M. J.; Trucks, G. W.; Schlegel, H. B.; Scuseria, G. E.; Robb, M. A.; Cheeseman, J. A.; Montgomery, Jr., J. A.; Vreven, T.; Kudin, K. N.; Burant, J. C.; Millam, J. M.; Iyengar, S. S.; Tomasi, J.; Barone, V.; Mennucci, B.; Cossi, M.; Scalmani, G.; Rega, N.; Petersson, G. A.; Nakatsuji, H.; Hada, M.; Ehara, M.; Toyota, K.; Fukuda, R.; Hasegawa, J.; Ishida, M.; Nakajima, T.; Honda, Y.; Kitao, O.; Nakai, H.; Klene, M.; Li, X.; Knox, J. E.; Hratchian, H. P.; Cross, J. B.; Bakken, V.; Adamo, C.; Jaramillo, J.; Gomperts, R.; Stratmann, R. E.; Yazyev, O.; Austin, A. J.; Cammi, R.; Pomelli, C.; Ochterski, J. W.; Ayala, P. Y.; Morokuma, K.; Voth, G. A.; Salvador, P.; Dannenberg, J. J.; Zakrzewski, V. G.; Dapprich, S.; Daniels, A. D.; Strain, M. C.; Farkas, O.; Malick, D. K.; Rabuck, A. D.; Raghavachari, K.; Foresman, J. B.; Ortiz, J. V.; Cui, Q.; Baboul, A. G.; Clifford, S.; Cioslowski, J.; Stefanov, B. B.; Liu, G.; Liashenko, A.; Piskorz, P.; Komaromi, I.; Martin, R. L.; Fox, D. J.; Keith, T.; Al-Laham, M. A.; Peng, C. Y.; Nanayakkara, A.; Challacombe, M.; Gill, P. M. W.; Johnson, B.; Chen, W.; Wong, M. W.; Gonzalez, C.; Pople, J. A. *Gaussian03W, Revision B05*, Inc., Wallingford CT, **2004**

4.2. DITERPENOIDS FROM THE IRANIAN PLANT *Euphorbia macroclada* Boiss.

4.2.1. Introduction

Given the current great interest for selective VEGFR antagonists in the realm of cancer and eye diseases,³¹ a systematic investigation on the druggability of the myrsinane chemotype would therefore be of great medicinal relevance. However, compounds of this type are generally of limited availability from natural sources, and usually occur as complex mixtures of related analogues. With the aim of finding a source of myrsinane derivatives sufficient to sustain a medicinal chemistry effort, I have screened several spurges for the occurrence of myrsinane diterpenes, identifying *E. macroclada* Boiss. as a novel source of this type of compounds. This spurge is native to the Iranian Plateau, and also grows in Syria, Armenia and Turkey.³² Cytotoxicity has been reported for extracts of *E. macroclada*,³³ but no specific reference to this plant could be found in the rich Iranian ethnopharmacology of spurges (*Farphyun* in Farsi).³⁴

4.2.2. Pre-myrsinane derivatives

A diterpenoid-rich fraction was obtained by liquid-liquid partition of a crude EtOAc extract from the aerial parts of *E. macroclada* (Fig. 4.11).



Figure 4.11. *Euphorbia macroclada*

By a combination of gravity column chromatography and repeated HPLC purifications detailed in the Experimental paragraph, four new (**92-95**) diterpenoid polyesters were obtained in the pure state (**Fig. 4.12**).

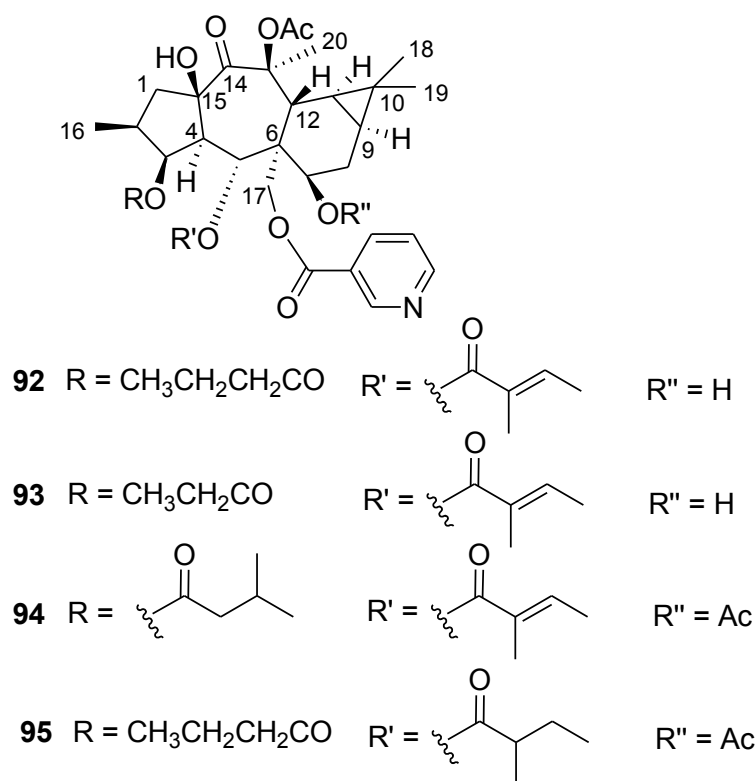


Figure 4.12. The four new pre-myrsinanes (**92-95**)

HR-ESIMS identified C₃₇H₄₉NO₁₁ as the molecular formula of compound **92**. Analysis of its ¹³C NMR spectrum (CDCl₃, **Table 4.1**) revealed the presence of four ester carbonyls (δ 164.9, 168.8, 170.2, 174.1), which were subsequently assigned to a nicotinate, a tiglate, an acetate and a butyrate unit, respectively, basing on diagnostic resonances in ¹H and ¹³C NMR spectra. The presence of these groups was further supported by 2D NMR COSY, HSQC and HMBC spectra, which allowed also complete assignment of their NMR resonances.

Table 4.1. ^1H (500 MHz) and ^{13}C (125 MHz) NMR data of compound **92** in CDCl_3 .

Pos.	δ_{H} , mult., <i>J</i> in Hz	δ_{C} , mult.	Pos.	δ_{H} , mult., <i>J</i> in Hz	δ_{C} , mult.
1a	3.14, dd, 13.7, 7.9	42.9, t	<i>3-O-Bu</i>		
1b	1.62, dd, 13.7, 9.4		1'		174.1, s
2	1.85, m	37.0, d	2'	2.21 ^a	36.3, t
3	5.30, t, 3.2	78.9, d	3'	1.53, m	18.1, t
4	2.38, dd, 11.4, 3.2	49.5, d	4'	0.88, t, 7.2	14.8, q
5	6.26, d, 11.4	70.7, d	<i>5-O-Tig</i>		
6		49.2, s	1''		168.8, s
7	3.89, d, 8.7	66.2, d	2''		127.8, s
8a	2.21 ^a	24.4, t	3''	6.64, q, 7.2	140.6, d
8b	1.92, d, 16.3		4''	1.36, d, 7.2	14.5, q
9	0.84, bd, 7.5	20.0, d	5''	1.49, s	11.8, q
10		18.9, s	<i>13-O-Ac</i>		
11	0.69, dd, 7.5, 6.6	24.2, d	1'''		170.2, s
12	3.39, d, 6.6	34.3, d	2'''	2.11, s	21.5, q
13		86.4, s	<i>17-O-Nic</i>		
14		204.4, s	CO		164.9, s
15		79.0, s	2''''	9.02, s	
15-OH	4.72, s		3''''		127.2, s
16	0.87, d, 7.2	14.3, q	4''''	8.13, d, 8.1	137.4, d
17a	4.93, d, 11.9	64.5, t	5''''	7.40, dd, 8.1, 5.1	123.8, d
17b	4.50, d, 11.9		6''''	8.78, d, 5.1	153.3, d
18	1.12, s	15.5, q			
19	1.06, s	29.8, q			
20	1.71, s	24.4, q			

The diterpenoid core of compound **92**, showing resonances of four methyls (three singlets and a doublet) bound to sp^3 carbons, three oxymethines and one uncoupled oxymethylene resonating as AB system, must be responsible for the remaining five unsaturation degrees requested by the molecular formula. Since one ketone carbonyl was present (δ 204.4), **92** must be tetracyclic. Analysis of the COSY spectrum allowed the identification of the two spin systems depicted in bold in **Fig. 4.13**: the first spans from a pair of diastereomeric protons H₂-1 (δ 3.14 and 1.62) to H-5 and includes a methyl branching (δ 0.87, d) and two oxymethines; the second spin system connects the third oxymethine (H-7) to H-12. All the proton resonances were then associated to those of the relevant carbon atoms by 2D HSQC data and this allowed the interpretation of the $^{2,3}J_{\text{H,C}}$ HMBC spectrum. This, allowing the connection of the different moieties was instrumental to the assembling of the diterpenoid skeleton of compound **92**. The most important HMBC cross-peaks are shown in **figure 4.13**. In particular correlations

of H₂-1 with C-4, with the oxygenated C-15 and with the ketone carbonyl (C-14) indicated the presence of the five-membered ring; correlations of the Me-20 with C-12, with the oxygenated C-13 and with C-14 provided the first connection between the two spin systems. The second connection was established on the basis of the HMBC cross-peaks exhibited by the oxymethylene H₂-17 with C-5, C-6, C-7 and C-12, indicating the presence of the condensed seven- and six-membered rings. Finally, the pre-myrsinane skeleton of **92** was deduced from the HMBC correlation of Me-18 and Me-19, which were in accordance with the presence of a dimethylcyclopropane ring, also suggested by the high field chemical shift of methines H-9 (δ 0.84) and H-11 (δ 0.69).

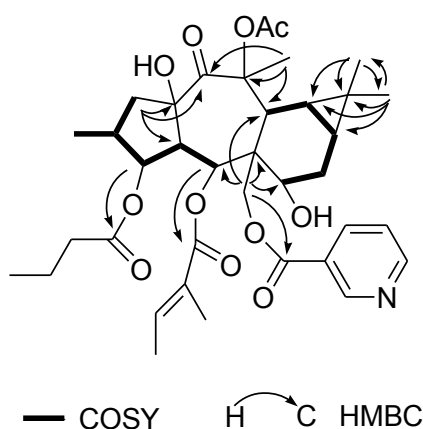


Figure 4.13. COSY (in bold) and key $^{2,3}J$ (H \rightarrow C) HMBC cross peaks detected for compound **92**.

The pre-myrsinane core of **92** includes six oxygenated sp^3 carbons which could potentially link the four previously identified acyl groups. HMBC cross-peaks of H-3, H-5, and H₂-17 with the relevant ester carbonyls allowed the location of the butyrate, the tiglate and the nicotinoate groups, respectively. The relatively high-field ^1H NMR resonance of H-7 and the absence of HMBC correlation with ester carbonyls indicated that C-7 should not be an acylating position and, consequently, the acetate group should be attached at one of the two oxygenated quaternary carbons flanking the ketone group. Since the exchangeable proton at δ 4.72 showed a 2J HMBC correlation with C-15, the acetate attachment site was identified as C-13, in agreement with its relatively low-field resonance (δ 86.4) in the ^{13}C NMR spectrum.

The relative configuration of the eleven stereogenic centers of **92** was deduced from the network of cross-peaks present in the ROESY spectrum (summarized in **Fig. 4.14**) and by comparison of ^1H - ^1H coupling constants with those reported in the literature for other pre-myrsinanes.³⁵ Finally, the ROE correlation of the two tiglate methyls disclosed also the *E* geometry of the tiglate double bond.

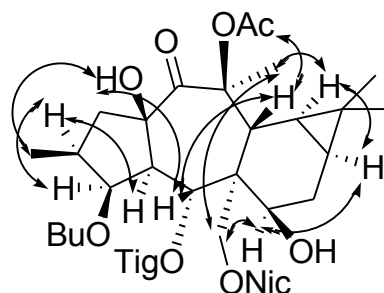


Figure 4.14. Key ROESY cross-peaks detected for compound **92**.

The myrsinane fraction proved to contain also three additional polyesters (**93-95**), sharing with **92** the same diterpenoid core and differing for the esterification pattern. Their stereostructures and, particularly the location of the acyl groups, were established on the basis of full MS and NMR analysis, following the same approach above reported in detail for compound **92** (complete NMR assignment is reported in the Experimental). Thus, compound **93**, $\text{C}_{36}\text{H}_{47}\text{NO}_{11}$, is a close analogue of **92**, differing only for the replacement of the butyrate with a propionate unit. On the other hand, both compounds **94** and **95** showed a fifth acyl group, which, in both cases, was identified as an acetate group linked at C-7; accordingly, a consistent low-field shift was observed for H-7. In addition, compound **94** differs from **92** also for the replacement of the butyrate unit with an isobutyrate, while compound **95** differs from **92** also for the replacement of the tiglate unit with a 2-methylbutyrate.

4.2.3. *Tigliane derivatives*

The aerial parts of *E. macroclada* afforded also five diterpenes belonging to the tigliane class (**77**, **96-99**, **Fig. 4.15**).

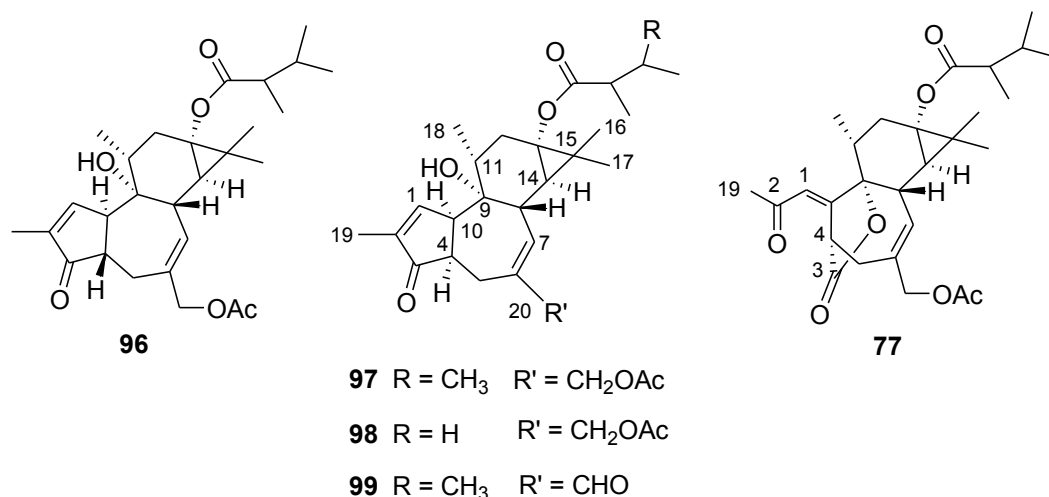


Figure 4.15. The known β -phorboid **96**, the three new α -phorboids (**97-99**) and the new A-secophorboid (**77**)

Compound **96** proved to be a known β -phorboid, previously isolated in trace amounts from a Sardinian collection of *Euphorbia pithyusa* subsp. *cupanii*,³⁵ as confirmed by comparison of available spectroscopic data. Detailed analysis of 1D and 2D NMR spectra of compound **97** allowed the full assignment of all its NMR resonances (**Table 4.2**), and the assembly of a planar structure identical to that of **96**. On the other hand, the strong NOE coupling H-4/H-10, together with the characteristic upfield shift of H-1 (δ 7.55 in **96** and 6.99 in **97**), and the consistent shifts of H-4 (δ 2.40 in **96** and 2.75 in **97**) and H₂-5 (δ 2.80 and 2.10 in **96** and 3.42 and 2.44 in **97**) in the ¹H NMR spectrum, unambiguously indicated that this compound was the 4- α analogue of **96**.

Compounds **98** and **99** are close analogues of the α -phorboid **97**. Compound **98**, C₂₇H₃₈O₆ by HR-ESIMS, showed a 2-methylbutyrate in place of the 2,3-dimethylbutyrate as C-13 acylating group. Compound **99**, C₂₆H₃₆O₅ by HR-ESIMS, proved to differ from **97** for the presence of an aldehyde group (δ_{H} 9.33, δ_{C} 193.0) in place of the acetoxymethyl at C-20. The ¹H NMR resonance of the conjugated double bond proton H-7 was accordingly downfield shifted at δ_{H} 6.07 (instead of δ_{H} 5.16).

Table 4.2. ^1H (500 MHz) and ^{13}C (125 MHz) NMR data of compounds **97** and **77** in CDCl_3 .

Pos.	97		77	
	δ_{H} , mult., <i>J</i> in Hz	δ_{C} , mult.	δ_{H} , mult., <i>J</i> in Hz	δ_{C} , mult.
1	6.99, bs,	156.1, d	6.07, bs	118.1, d
2		143.5, s		197.2, s
3		212.2, s		176.7, s
4	2.75, m	49.8, d	4.24, bt, 3.5	44.0, d
5a	3.43 ^a	26.7, t	2.98, dd, 15.5, 3.5	33.4, t
5b	2.44, dd, 16.5, 3.5		2.76 ^a	
6		136.5, s		141.8, s
7	5.16, bs	130.2, d	5.49, bs	130.0, d
8	1.79, bd, 5.0	41.9, d	1.98, bs	45.1, d
9		75.5, s		88.8, s
10	3.47 ^a	47.0, d		159.3, s
11	1.57, m	37.2, d	1.81, m	36.0, d
12a	2.13 ^a	31.1, t	2.75 ^a	31.5, t
12b	1.93 ^a		1.63, m	
13		62.9, s		64.5, s
14	0.52, d, 5.0	33.4, d	0.73, d, 5.0	30.3, d
15		22.4, s		24.8, s
16	1.07, s	14.9, q	1.14, s	16.2, q
17	1.16, s	23.9, q	1.14, s	23.9, q
18	1.05, d, 7.2	15.5, q	0.92, d, 7.2	21.3, q
19	1.75, bs	11.0, q	2.28, s	32.1, q
20a	4.46, d, 11.5	71.3, t	4.44, s	71.4, t
20b	4.35, d, 11.5		4.44, s	
<i>13-O-2',3'-diMeBu</i>				
1'		178.7, s		178.5, s
2'	2.17 ^a	46.5, d	2.20, m	46.6, d
3'	1.92 ^a	30.5, d	1.92, m	30.5, d
4'	0.94, d, 7.2	21.2, q	0.91, d, 7.2	19.5, q
5'	1.09, d, 7.2	14.0, q	1.10, d, 7.2	14.0, q
6'	0.91, d, 7.2	19.5, q	0.87, d, 7.2	19.2, q
<i>20-O-Ac</i>				
1'''		171.4, s		171.0, s
2'''	2.13, s	21.7, q	2.07, s	21.8, q

^a Overlapped with other signals.

Compound **77**, $\text{C}_{28}\text{H}_{38}\text{O}_7$, by HR-ESIMS, is a new phorbol derivative showing a *seco*-A structure. The presence of 2,3-dimethylbutyrate and acetate groups was easily determined by analysis of 1D (**Table 4.2**) and 2D NMR spectra, as well as by comparison with data of compounds **96** and **97**. Inspection of COSY, HSQC, and HMBC spectra of **77** revealed that the skeletal arrangements of rings B (seven-membered), C (six-membered) and D (three-membered) should be identical to those of compound **96**, including also the placement of the two acyl groups. Consequently, the additional oxygen atom and the additional unsaturation degree implied by the molecular formula of **77** should be accounted by

modification(s) at ring A. The downfield shifted Me-19³⁶ (δ_{H} 2.28 in place of 1.75; δ_{C} 32.1 in place of 11.0) showed HMBC cross-peaks with the ketone carbonyl at δ_{C} 197.2 and with the sp^2 methine at δ_{C} 118.1 (C-1). A signal at δ_{C} 159.3 (C-10) completed the enone system, attached at the seven-membered ring, as confirmed also by HMBC cross-peaks of the markedly downfield shifted H-4 (δ_{H} 4.24) with signals at δ_{C} 118.1 and 159.3. H-4 showed also 2J HMBC cross-peak with a novel carbonyl resonance at δ_{C} 176.7, implying the cleavage of ring A, and accounting for the additional oxygen atom. The downfield shift of C-9 (δ_{C} 88.8) and the further unsaturation degree were both accounted by the presence of an ester linkage connecting C-3 and C-9 to build a γ -lactone ring and completely define the structural arrangement of the *A-seco*-phorbol **77**. A ROESY experiment secured the relative configuration of ring C stereogenic centers and indicated the *E*-geometry of the exocyclic double bond (cross-peak H-1/H-11). While unprecedented in Nature, an *A-seco*-phorbol skeleton has been previously obtained by treatment of a phorbol derivative with 0.2 M NaOMe in MeOH under oxygen atmosphere for two weeks.³⁷ The mild conditions used for the extraction of *E. macroclada* and all the fractionation steps suggests a non-artifact origin for **77**. The formation of this compound could be rationalized through an intramolecular rearrangement of the C-2 hydroperoxide derivative obtained from β -phorbol **96**, as shown in **figure 4.16**. The *E*-geometry of the exocyclic double bond gives support to this hypothesis.

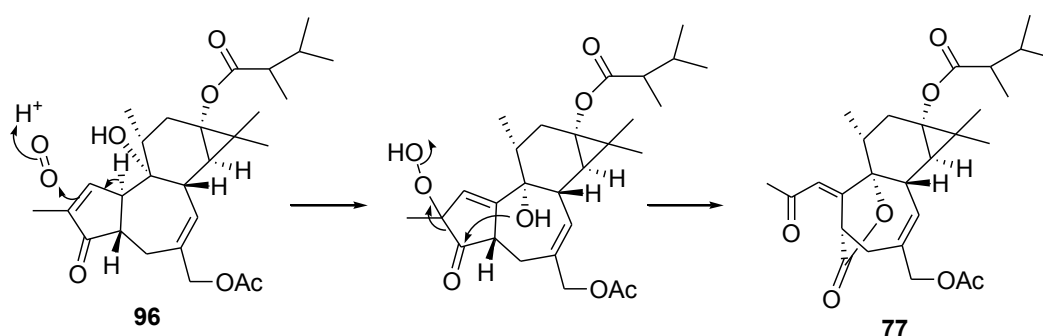


Figure 4.16. Postulated biogenesis for the *A-seco*phorboid **77**

In conclusion, a phytochemical investigation of the aerial parts of *E. macroclada* from Iran afforded eight new diterpene polyesters, four belonging to the premysinanone class, three to the α -phorbol class, and one to an unprecedented type

for natural diterpenoids. Both premyrsinanes- and α -phorbol esters have a valuable biological potential, binding to VEGFR¹⁶ and the transient receptor potential vanilloid channel³⁸ (TRPV4), and qualifying *E. macroclada* as an interesting source of chemical diversity to explore these important pharmacological targets.

4.2.4. Experimental

Plant material, extraction and isolation

Euphorbia macroclada Boiss. was collected in the surroundings of Naein (Isfahan, Iran) in April 2007. The plant material was identified by Prof. Mohammad Reza Rahimnejad, Department of Biology, University of Isfahan, Isfahan, and a voucher specimen (No. 1117) has been deposited at the Herbarium of Faculty of Pharmacy, Isfahan University of Medical Sciences, Isfahan, Iran. The air dried aerial parts of *E. macroclada* (2 kg) were exhaustively extracted with EtOAc at room temperature. After removal the solvent *in vacuo*, the residue (50g) was dissolved in methanol (1000 mL), water was added (500 mL), and the suspension was sequentially extracted with petroleum ether and dichloromethane, respectively. Evaporation of the petroleum ether left a residue (30 g) that was purified by vacuum chromatography using mixtures of heptanes and chloroform to afford 4 fractions (A-D). NMR analysis showed that fraction A contained fats and alkanes, fraction B triterpenoids, and fraction D a mixture of polar compounds, while fraction C was characterized by a mixture of diterpenoids. This was purified by MPLC on RP18 silica by using a MeOH: H₂O gradient (6:4 to 10:0) as eluant. Fraction C2 was further purified by normal phase column chromatography to afford 5 fractions (C2a-e). Final purification of fraction C2a by Biotage fractionator and prep. HPLC on normal phase (petroleum ether-EtOAc 7: 3 and 6:4) afforded the phorboids **98** (16 mg), **96** (35 mg, 0.00175% of dry wt), **97** (84 mg), **77** (18 mg), and **99** (55 mg). After repeated HPLC purification (on petroleum ether-EtOAc 6:4 and 5:5), fraction C2b, C2c and C2d afforded premyrsinanes **92** (352 mg), **94** (185 mg), **93** (19 mg) and **95** (2 mg).

Compound 92: 0.0176 % of dry wt. Colorless amorphous solid; $[\alpha]_D + 2.1$ (c 0.12, CHCl₃); ¹H NMR (CDCl₃, 500 MHz) Table 4.1; ¹³C NMR (CDCl₃, 125 MHz)

Table 4.1; (+) ESI-MS m/z 684 $[M + H]^+$, 706 $[M + Na]^+$. HR-ESIMS found 706.3212; $C_{37}H_{49}NNaO_{11}$ requires 706.3203.

Compound 93: \approx 0.00095 % of dry wt. Colorless amorphous solid; $[\alpha]_D$ -5.6 (c 0.18, $CHCl_3$); 1H NMR ($CDCl_3$, 500 MHz, J in Hz): δ 9.02 (1H, bs, Nic-2'''), 8.76 (1H, d, $J = 6.5$, H-5'''), 8.12 (1H, d, $J = 8.0$, Nic-4'''), 7.39 (1H, dd, $J = 8.0$, 6.5, Nic-5'''), 6.64 (1H, q, $J = 7.2$, Tig-3''), 6.26 (1H, d, $J = 11.5$, H-5), 5.30 (1H, t, $J = 3.2$, H-3), 4.93 (1H, d, $J = 12.0$, H-17a), 4.49 (1H, d, $J = 12.0$, H-17b), 3.88 (1H, bd, $J = 8.5$, H-7), 3.37 (1H, d, $J = 6.6$, H-12) 3.13 (1H, dd, $J = 13.7$, 8.0, H-1a), 2.38 (1H, dd, $J = 11.5$, 3.2, H-4), 2.25 (2H, overlapped, Prop-2'), 2.23 (1H, overlapped, H-8a), 2.12 (1H, overlapped, H-8b), 2.11 (3H, s, Ac), 1.86 (1H, m, H-2), 1.71 (3H, s, H-20), 1.61 (1H, dd, $J = 13.7$, 11.5, H-1b), 1.49 (3H, bs, Tig-5'''), 1.36 (3H, d, $J = 7.2$, Tig-4''), 1.11 (3H, s, H-18), 1.05 (3H, s, H-19), 1.01 (3H, t, $J = 7.2$, Prop-3'), 0.86 (3H, d, $J = 7.2$, H-16), 0.84 (1H, d, $J = 7.5$, H-9), 0.70 (1H, dd, $J = 7.5$, 6.6, H-11); ^{13}C NMR ($CDCl_3$, 125 MHz): δ 204.5 (s, C-14), 174.1 (s, Prop-C-1'), 172.0 (s, Ac), 168.8 (s, Tig-C-1'), 165.0 (s, Nic-CO), 153.5 (d, Nic-C-6''') 150.5 (d, Nic-C-2'''), 140.6 (d, Tig-C-3''), 137.3 (d, Nic-C-4'''), 127.8 (s, Tig-C-2''), 126.0 (s, Nic-C-3'''), 123.6 (d, Nic-C-5'''), 86.5 (s, C-13), 79.0 (s, C-15), 78.8 (d, C-3), 70.7 (d, C-5), 66.2 (d, C-7), 64.4 (t, C-17), 49.7 (d, C-4), 48.8 (s, C-6), 42.9 (t, C-1), 37.7 (d, C-2), 34.3 (d, C-12), 29.8 (q, C-19), 27.8 (t, Prop-C-2'), 25.3 (q, C-20), 24.6 (t, C-8), 24.1 (d, C-11), 21.9 (t, Ac), 20.0 (d, C-9), 18.9 (s, C-10), 15.4 (q, C-18), 14.6 (q, C-16), 14.5 (q, Tig-C-4''), 11.9 (q, Tig-C-5''), 9.0 (q, Prop-C-3'). (+) ESI-MS m/z 692 $[M + Na]^+$. HR-ESIMS found 692.3042; $C_{36}H_{47}NNaO_{11}$ requires 692.3047.

Compound 94: 0.00925% of dry wt. Colorless amorphous solid; $[\alpha]_D$ -2.7 (c 0.11, $CHCl_3$); 1H NMR ($CDCl_3$, 500 MHz, J in Hz): δ 9.12 (1H, bs, Nic-2'''), 8.78 (1H, d, $J = 6.5$, H-5'''), 8.10 (1H, d, $J = 8.0$, Nic-4'''), 7.40 (1H, dd, $J = 8.0$, 6.5, Nic-5'''), 6.52 (1H, q, $J = 7.2$, Tig-3''), 6.25 (1H, d, $J = 11.5$, H-5), 5.28 (1H, t, $J = 3.2$, H-3), 4.93 (1H, overlapped, H-17a), 4.92 (1H, overlapped, H-7), 4.56 (1H, d, $J = 12.0$, H-17b), 3.56 (1H, d, $J = 6.6$, H-12) 3.17 (1H, dd, $J = 13.7$, 8.0, H-1a), 2.33 (1H, dd, $J = 11.5$, 3.2, H-4), 2.14 (2H, overlapped, MeBu-2'), 2.15 (3H, s, Ac), 2.13 (3H, s, Ac), 2.00 (1H, m, MeBu-3'), 1.96 (1H, overlapped, H-8a), 1.92 (1H, overlapped, H-8b), 1.89 (1H, overlapped, H-2), 1.74 (3H, s, H-20), 1.66 (1H, m, H-1b), 1.47 (3H, bs, Tig-2''-Me), 1.29 (3H, d, $J = 7.2$, Tig-4''), 1.08 (3H, s, H-

18), 0.92 (6H, d, $J = 7.2$, MeBu-4',5'), 0.97 (3H, s, H-19), 0.89 (3H, d, $J = 7.2$, H-16), 0.80 (1H, d, $J = 7.5$, H-9), 0.70 (1H, dd, $J = 7.5, 6.6$, H-11); ^{13}C NMR (CDCl_3 , 125 MHz): δ 204.5 (s, C-14), 174.5 (s, MeBu-C-1'), 172.0 (s, Ac), 172.5 (s, Ac), 166.4 (s, Tig-C-1''), 164.9 (s, Nic-CO), 153.3 (d, Nic-C-6'''), 150.6 (d, Nic-C-2'''), 140.6 (d, Tig-C-2''), 137.6 (d, Nic-C-4'''), 128.4 (s, Tig-C-3''), 126.0 (s, Nic-C-3'''), 123.7 (d, Nic-C-5'''), 84.4 (s, C-13), 79.1 (s, C-15), 78.6 (d, C-3), 70.8 (d, C-7), 69.5 (d, C-5), 64.2 (t, C-17), 50.9 (d, C-4), 48.5 (s, C-6), 43.6 (t, MeBu-C-2'), 43.3 (t, C-1), 37.8 (d, C-2), 35.5 (d, C-12), 29.5 (q, C-19), 25.4 (d, MeBu-C-3'), 25.3 (q, C-20), 24.1 (d, C-11), 22.4 (t, C-8), 23.3, (q, MeBu-C-4',5'), 22.1 (t, Ac), 21.9 (t, Ac), 19.2 (d, C-9), 18.6 (s, C-10), 15.3 (q, C-18), 14.4 (q, C-16), 14.3 (q, Tig-C-4''), 11.9 (q, Tig-C-2''-Me); (+) ESI-MS m/z 762 [$\text{M} + \text{Na}$] $^+$. HR-ESIMS found 762.3470; $\text{C}_{40}\text{H}_{53}\text{NNaO}_{12}$ requires 762.3465.

Compound 95: ≈ 0.0001 % of dry wt. Colorless amorphous solid; $[\alpha]_{\text{D}} -2.4$ (c 0.04, CHCl_3); ^1H NMR (CDCl_3 , 500 MHz, J in Hz): δ 9.22 (1H, bs, Nic-2'''), 8.84 (1H, d, $J = 6.5$, H-5'''), 8.10 (1H, d, $J = 8.0$, Nic-4'''), 7.49 (1H, dd, $J = 8.0, 6.5$, Nic-5'''), 6.22 (1H, d, $J = 11.5$, H-5), 5.22 (1H, t, $J = 3.2$, H-3), 4.90 (1H, d, $J = 12.0$, H-17a), 4.70 (1H, bd, $J = 8.5$, H-7), 4.50 (1H, d, $J = 12.0$, H-17b), 3.48 (1H, d, $J = 6.6$, H-12), 3.17 (1H, dd, $J = 13.7, 8.0$, H-1a), 2.40 (1H, m, MeBu-2''), 2.31 (1H, dd, $J = 11.5, 3.2$, H-4), 2.29 (2H, overlapped, Bu-2'), 2.11 (6H, s, Ac), 1.96 (1H, overlapped, H-8a), 1.94 (1H, overlapped, H-8b), 1.88 (1H, m, H-2), 1.72 (3H, s, H-20), 1.63 (1H, overlapped, H-1b), 1.62 (2H, overlapped, Bu-3'), 1.56 (1H, m, MeBu-3''a), 1.15 (1H, m, MeBu-3''b), 1.06 (3H, s, H-18), 0.96 (3H, t, $J = 7.2$, Bu-4'), 0.95 (3H, s, H-19), 0.85 (3H, d, $J = 7.2$, H-16), 0.80 (3H, $J = 7.2$, MeBu-5''), 0.77 (1H, overlapped, H-9), 0.70 (1H, dd, $J = 7.5, 6.6$, H-11) 0.63 (3H, t, $J = 7.2$, MeBu-4''); ^{13}C NMR (CDCl_3 , 125 MHz): δ 204.6 (s, C-14), 175.3 (s, Bu-C-1'), 174.6 (s, MeBu-C-1''), 171.0 (s, Ac), 170.1 (s, Ac), 165.0 (s, Nic-CO), 153.5 (d, Nic-C-6'''), 150.5 (d, Nic-C-2'''), 137.6 (d, Nic-C-4'''), 126.0 (s, Nic-C-3'''), 123.6 (d, Nic-C-5'''), 86.5 (s, C-13), 79.0 (s, C-15), 78.6 (d, C-3), 71.0 (d, C-7), 70.7 (d, C-5), 64.4 (t, C-17), 49.5 (d, C-4), 48.8 (s, C-6), 43.8 (t, C-1), 41.0 (s, MeBu-C-2''), 38.0 (d, C-2), 36.8 (t, Bu-C-2'), 34.3 (d, C-12), 29.9 (q, C-19), 26.3 (t, MeBu-C-3''), 25.3 (q, C-20), 24.6 (t, C-8), 23.8 (d, C-11), 21.9 (t, Ac), 21.5 (t, Ac), 20.0 (d, C-9), 18.9 (s, C-10), 18.2 (t, Bu-C-3'), 16.6 (q, MeBu-C-4''), 15.2 (q, C-18), 14.6 (q, C-16), 14.0 (q, Bu-C-4'), 11.0 (q, MeBu-C-5'');

(+) ESI-MS m/z 750 $[M + Na]^+$. HR-ESIMS found 750.3469; $C_{39}H_{53}NNaO_{12}$ requires 750.3465.

Compound 97: $\approx 0.0042\%$ of dry wt. Colorless amorphous solid; $[\alpha]_D - 34.3$ (c 0.06, $CHCl_3$); 1H NMR ($CDCl_3$, 500 MHz) Table 4.2; ^{13}C NMR ($CDCl_3$, 125 MHz) Table 4.2; (+) ESI-MS m/z 472 $[M + Na]^+$. HR-ESIMS found 495.2722; $C_{28}H_{40}NaO_6$ requires 495.2723.

Compound 98: $\approx 0.0008\%$ of dry wt. Colorless amorphous solid; $[\alpha]_D - 39.5$ (c 0.08, $CHCl_3$); 1H NMR ($CDCl_3$, 500 MHz, J in Hz): δ 6.99 (1H, bs, H-1), 5.17 (1H, bs, H-7), 4.46 (1H, d, $J = 12.0$, H-20a), 4.35 (1H, d, $J = 12.0$, H-20b), 3.45 (1H, overlapped, H-10), 3.43 (1H, overlapped, H-5a), 2.76 (1H, m, H-4), 2.44 (1H, dd, $J = 16.5, 3.5$, H-5b), 2.32 (1H, hex, $J = 7.2$, MeBu-2'), 2.15 (1H, overlapped, H-12a), 2.08 (3H, s, Ac), 2.00 (1H, overlapped, H-12b), 1.80 (1H, m, H-8), 1.75 (3H, bs, H-19), 1.57 (1H, m, H-11), 1.48 (2H, m, MeBu-3'), 1.15 (3H, s, H-17), 1.11 (3H, d, $J = 7.2$, MeBu-5'), 1.07 (3H, s, H-16), 1.03 (3H, d, $J = 7.2$, H-18), 0.89 (3H, t, $J = 7.2$, MeBu-4'), 0.50 (1H, d, $J = 5.2$, H-14); ^{13}C NMR ($CDCl_3$, 125 MHz): δ 211.9 (s, C-3), 174.6 (s, MeBu-C-1'), 172.0 (s, Ac), 155.9 (d, C-1), 143.7 (s, C-2), 136.9 (s, C-6), 130.3 (d, C-7), 76.0 (s, C-9), 71.5 (t, C-20), 63.1 (s, C-13), 49.8 (d, C-4), 47.1 (d, C-10), 42.0 (d, C-8), 41.3 (d, MeBu-C-2'), 37.2 (d, C-11), 33.4 (d, C-14), 31.3 (t, C-12), 26.8 (t, C-5), 26.3 (t, MeBu-C-3'), 24.0 (q, C-17), 22.6 (s, C-15), 21.0 (q, Ac), 16.9 (q, MeBu-C-4'), 15.6 (q, C-18), 14.7 (q, C-16), 11.0 (q, C-19), 10.5 (q, MeBu-C-5'); (+)-ESI-MS m/z 481 $[M + Na]^+$. HR-ESIMS found 481.2569; $C_{27}H_{38}NaO_6$ requires 481.2566.

Compound 99: $\approx 0.0027\%$ of dry wt. Colorless amorphous solid; $[\alpha]_D - 2.7$ (c 0.02, $CHCl_3$); 1H NMR ($CDCl_3$, 500 MHz, J in Hz): δ 9.33 (1H, bs, H-20), 7.02 (1H, bs, H-1), 6.07 (1H, bs, H-7), 3.58 (1H, bs, H-10), 3.28 (1H, dd, $J = 15.5, 4.5$, H-5a), 3.21 (1H, dd, $J = 15.5, 1.5$, H-5b), 2.88 (1H, m, H-4), 2.19 (1H, overlapped, diMeBu-2'), 2.17 (1H, overlapped, H-8), 2.10 (1H, overlapped, H-12a), 1.95 (1H, overlapped, diMeBu-3'), 1.94 (1H, overlapped, H-12b), 1.75 (3H, bs, H-19), 1.60 (1H, m, H-11), 1.14 (3H, s, H-17), 1.10 (3H, d, $J = 7.2$, H-18), 1.09 (3H, d, $J = 7.2$, diMeBu-5'), 1.08 (3H, s, H-16), 0.94 (3H, d, $J = 7.2$, MeBu-4'), 0.92 (3H, d, $J = 7.2$, MeBu-6'), 0.61 (1H, d, $J = 5.2$, H-14); ^{13}C NMR ($CDCl_3$, 125 MHz): δ 208.9 (s, C-3), 193.0 (t, C-20), 174.0 (s, diMeBu-C-1'), 160.3 (d, C-7), 155.9 (d, C-1), 143.0 (s, C-2), 142.9 (s, C-6), 78.0 (s, C-9), 64.5 (s, C-13), 52.1

(d, C-10), 46.3 (d, diMeBu-C-2'), 44.8 (d, C-4), 42.0 (d, C-8), 37.2 (d, C-11), 33.4 (d, C-14), 31.3 (t, C-12), 29.6 (d, MeBu-C-3'), 24.5 (t, C-5), 24.0 (q, C-17), 22.6 (s, C-15), 21.2 (q, MeBu-C-4'), 19.5 (q, MeBu-C-6'), 15.6 (q, C-18), 14.7 (q, C-16), 14.5 (q, MeBu-C-5'), 11.0 (q, C-19); (+)-ESI-MS m/z 481 $[M + Na]^+$. HR-ESIMS found 451.2469; $C_{26}H_{36}NaO_5$ requires 451.2460.

Compound 77: 0.00035% of dry wt. Colorless amorphous solid; $[\alpha]_D -42.7$ (c 0.01, $CHCl_3$); 1H NMR ($CDCl_3$, 500 MHz) Table 4.2; ^{13}C NMR ($CDCl_3$, 125 MHz) Table 4.2; (+) ESI-MS m/z 509 $[M + Na]^+$. HR-ESIMS found 509.2521; $C_{28}H_{38}NaO_7$ requires 509.2515.

4.3. DITERPENOIDS FROM THE IRANIAN PLANT *Euphorbia bungei* Boiss

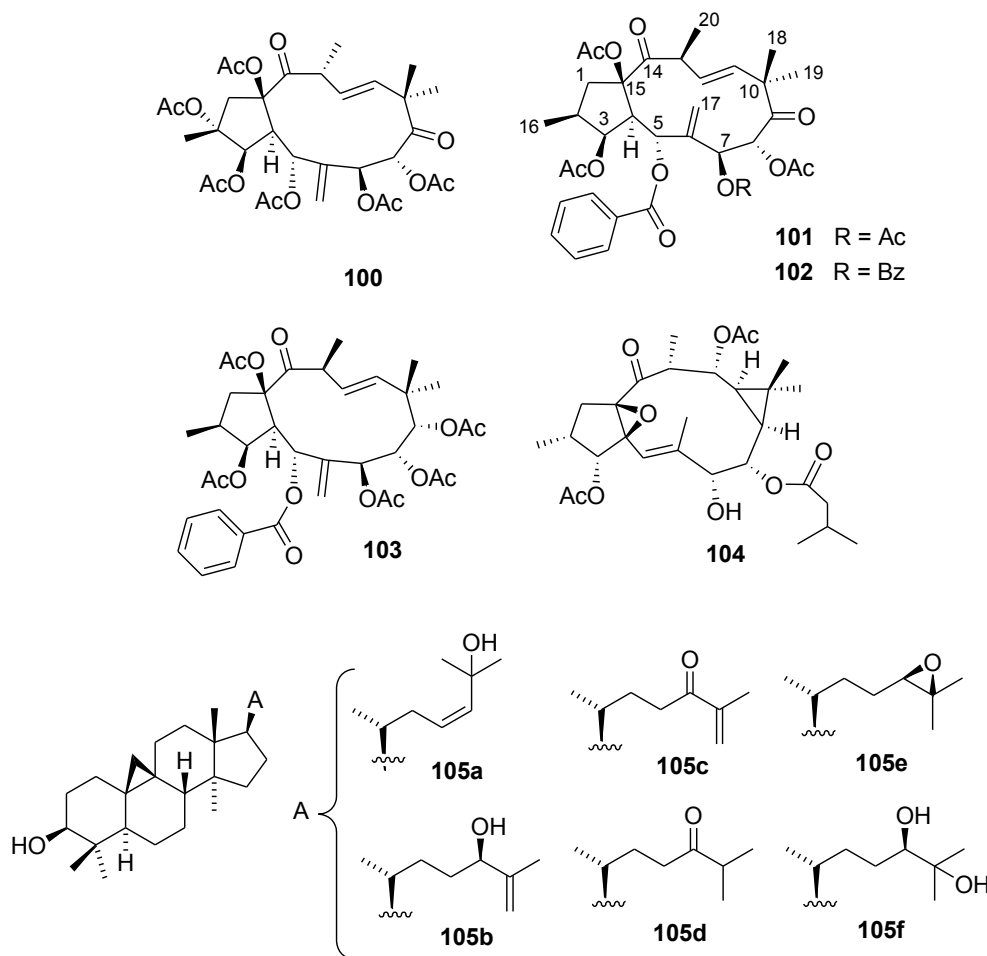
4.3.1. Introduction

About 70 species of *Euphorbia* grow in Iran, and 17 of them are endemic.³² Their ethnopharmacology is not basically different from that of hardy spurges from other parts of the world, with these plants being mainly used in folk medicine as cathartic and, topically, to remove warts.³⁹ I have undertaken the phytochemical analysis of *E. bungei* Boiss., a species endemic to Iran, and previously poorly characterized from the phytochemical point of view, since only its flavonoid profile has been described in a certain detail.⁴⁰ A leishmanicidal activity has been reported for preparations of *E. bungei*,⁴¹ a finding inspired by the ethnopharmacology of this plant, but the activity was not associated to a specific class of compounds.

From this plant I have isolated three novel diterpenoids, two of them belonging to the jatropane class (**101-102**) and one to the lathyrane class (**104**), along with the known jatropane **103**⁴² and several cycloartane triterpenoids, two of which (**105a** and **105b**) were assayed for antiviral activity.

4.3.2. Structure elucidation

Diterpenoid-rich fractions were obtained by liquid-liquid partition of a crude acetone extract of the aerial parts of *E. bungei*. By a combination of gravity column chromatography and repeated HPLC purifications, as detailed in the Experimental Section, one known (**103**) and three new (**101**, **102**, **104**), diterpenoid polyesters were obtained in the pure state, along with various known cycloartane triterpenoids (**105a-f**).



The HR-ESIMS data of compound **101**, a colorless amorphous solid, indicated the molecular formula $C_{35}H_{42}O_{12}$, in agreement with the presence of 15 unsaturation degrees. Analysis of the ^{13}C NMR spectrum of **101** ($CDCl_3$, **Table 4.3**) revealed the presence of five ester carbonyls (δ 164.8, 170.1, 170.3, 170.4, 170.8), which were easily assigned to one benzoate and four acetate groups, respectively, based on diagnostic resonances in 1H and ^{13}C NMR spectra. Analysis of 2D NMR COSY, HSQC and HMBC spectra confirmed the presence of these groups and allowed also the complete assignment of their NMR resonances, as reported in **Table 4.3**. Interestingly, while three acetyl methyls resonated at typical values for these groups (δ_H 2.14, 2.10, 2.08), the fourth acetyl methyl exhibited a severely shielded resonance (δ_H 1.40, singlet) in the 1H NMR spectrum of **101**.

All the remaining 1H and ^{13}C NMR signals were assigned to the diterpenoid core of **101** using 2D NMR experiments. In particular, the ^{13}C NMR spectrum of **101** showed resonances of two ketone carbonyls (δ_C 205.3 and 204.1), one *exo*-methylene group (δ_C 124.1, HSQC associated with the proton broad singlets at δ_H 5.60 and 5.70), and one *vic*-disubstituted double bond (δ_C 135.3 and 134.4, HSQC

associated with the proton signals at δ_{H} 5.96 and 5.92, respectively). The four unsaturations corresponding to the above moieties added up to the nine unsaturations of the acyl groups, implying a bicyclic nature of the C_{20} core of **101**. This penta-acylated diterpenoid included also four methyl groups (two singlets at δ_{H} 1.35 and 1.24, two doublets at δ_{H} 1.03 and 1.43), four oxymethines (δ_{H} 5.96, bs; 5.85, bs; 5.73, d; 5.35, bs) and one oxygenated unprotonated carbon atom (δ_{C} 91.9).

Table 4.3. ^1H (500 MHz) and ^{13}C (125 MHz) NMR data of compounds **101** and **104** in CDCl_3

Pos.	101		104	
	δ_{H} , mult., J in Hz	δ_{C} , mult.	δ_{H} , mult., J in Hz	δ_{C} , mult.
1a	2.13 ^a	45.2, t	2.28, dd, 13.0, 10.5	32.8, t
1b	2.93 ^a		2.01, dd, 13.0, 7.5	
2	2.41, m	39.1, d	2.12 ^a	32.7, d
3	5.73, bd, 4.5	77.1, d	5.34, d, 5.5	77.5, d
4	2.94, bd, 4.5	49.7, d		71.3, s
5	5.96, bs	73.4, d	5.87, s	115.7, d
6		137.1, s		141.9, s
7	5.85, bs	63.3, d	4.22, bs	76.8, d
8	5.35, bs	72.9, d	4.57, dd, 10.7, 1.5	73.8, d
9		205.3, s	1.39, t, 10.7	24.0, d
10		49.4, s		19.2, s
11	5.96, d, 16.0	135.3, d	1.14, t, 10.7	31.1, d
12	5.92, d, 16.0	134.5, d	4.86, dd, 10.7, 3.8	71.4, d
13	3.50, m	43.9, d	2.93, m	44.0, d
14		204.1, s		207.6, s
15		91.9, s		73.5, s
16	1.03, d, 7.0	14.1, q	0.96, d, 6.4	12.1, q
17a	5.60, bs	124.1, t	2.03, s	17.3, q
17b	5.70, bs			
18	1.35, s	26.2, q	1.09, s	29.5, q
19	1.24, s	24.1, q	0.86, s	16.9, q
20	1.43, d, 6.8	20.6, q	1.06, d, 7.0	13.3, q
<i>3-O-Ac</i>				
1'		170.4, s		170.4, s
2'	2.14, s	20.8, q	2.14, s	20.8, q

^a Overlapped with other signals.

Additional acyl groups of compound **101**: 5-*O*-Bz [δ_{H} 7.90 (2H), 7.53 (1H), 7.40 (2H); δ_{C} 164.8 (1C), 129.8 (1C), 129.2 (2C), 129.1 (2C), 133.4 (1C)]. 7-*O*-Ac [δ_{H} 1.40 (3H); δ_{C} 170.8 (1C), 20.4 (3C)]. 8-*O*-Ac [δ_{H} 2.10 (3H); δ_{C} 170.3 (1C), 20.1 (3C)]. 15-*O*-Ac [δ_{H} 1.98 (3H); δ_{C} 170.1 (1C), 20.9 (3C)].

Additional acyl groups of compound **104**: 8-*O*-Isoval [δ_{H} 2.26 (1H), 2.12 (2H), 0.96 (3H) 0.93 (3H); δ_{C} 173.1 (1C), 44.3 (1C), 25.2 (1C), 22.9 (2C)]. 12-*O*-Ac [δ_{H} 2.11 (3H); δ_{C} 170.8 (1C), 20.3 (3C)].

The COSY spectrum of **101** identified three spin systems, highlighted in bold in **figure 4.17**. Fragment A spans from a pair of diastereotopic protons H₂-1 (δ 2.93 and 2.13) to the oxymethine H-5 (δ 5.96) and includes a methyl branching at C-2 and another oxymethine at position 3 (δ_C 77.1, δ_H 5.73); the second spin system (fragment B) includes only the mutually coupled oxymethines H-7 and H-8, while the third spin system (fragment C) shows the connection of the *trans* ($J_{H-11/H-12} = 16.0$ Hz) disubstituted double bond Δ^{11} with H-13, in turn coupled to the methyl doublet Me-20 (δ 1.43). Having associated all the proton resonances to those of the relevant carbon atoms by 2D HSQC, interpretation of the $^{2,3}J_{H,C}$ HMBC spectrum was instrumental to link these moieties to quaternary carbons and tertiary methyls (key HMBC cross-peaks are shown in **Fig. 4.17**).

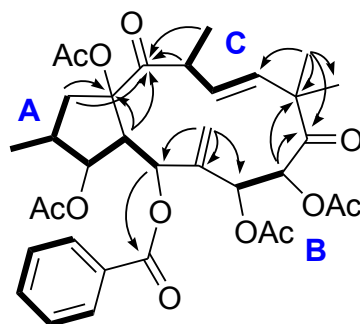


Figure 4.17. COSY (in bold) and key $^{2,3}J(H \rightarrow C)$ HMBC cross peaks detected for compound **101**.

Correlations of H₂-17 with C-4, C-5, and C-6 indicated that fragments A and B were connected through the sp^2 carbon C-6. The quaternary carbon C-10 and the ketone carbonyl at C-9 were long-range coupled with H-8 and with Me-18/Me-19, which also showed HMBC coupling with C-11, thus establishing the connection between fragments B and C. Finally, Me-20, H-13, H₂-1, and H-4 showed coupling with the ketone C-14, while both H₂-1 and H-4 were coupled also to the oxygenated quaternary carbon C-15. These correlations defined the connections between fragments A and C and the linkage between C-4 and C-15, showing the presence of condensed five- and twelve-membered rings. Therefore, compound **101** is a penta-acetylated jatrophone derivative with keto groups at C-9 and C-14. Since the jatrophone core of **101** includes five oxygenated sp^3 carbons (C-3, C-5, C-7, C-8, C-15), all these carbons must bear acyl groups. The HMBC cross-peak of H-5 with the ester carbonyl at δ_C 164.8 located the benzoyl group at C-5, and, therefore, all the remaining oxygenated carbons were acetylated.

The relative configuration of the eight stereogenic centers of **101** was deduced from the network of cross-peaks present in the ROESY spectrum (summarized in **Fig. 4.18**) and by comparison of ^1H - ^1H coupling constants with those reported in the literature for similar jatrophanes^{42,43}. In this context, especially diagnostic were the low values of $J_{\text{H-H}}$ displayed by H-5, H-7 and H-8, all resonating as broad singlets. The proton at the ring junction (H-4) displayed ROESY correlations with H-2, H-3, H-7 and H-13 indicating their *cis* (conventionally α -) orientation, while the ROESY cross-peak observed between Me-16 and the acetoxy methyl at C-15 revealed their β -orientation. Further diagnostic ROESY cross-peaks were those between H-12/Me-18, Me-18/H-8, H-4/H-11, OAc-3/H-5, which allowed the complete and unambiguous definition of the stereostructure of the new jatropane **101**.

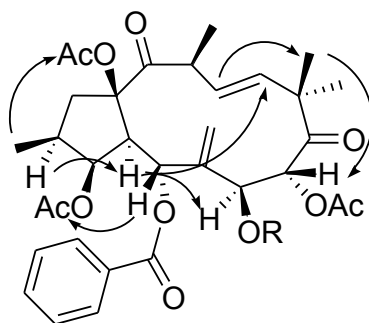


Figure 4.18. Key ROESY cross-peaks detected for compound **101**

The diterpene fraction of *E. bungei* contained also two additional jatrophanes (**102** and **103**), closely related to compound **101**. Compound **102**, $\text{C}_{40}\text{H}_{44}\text{NaO}_{12}$ by HR-ESIMS, is a new jatropane polyester sharing with **101** the same diterpenoid core but a slightly different esterification pattern, with a benzoate rather than an acetate at C-7. The stereostructure of **102** was established on the basis of full MS and NMR analysis, following the same approach detailed for compound **101**, and full NMR assignments are reported in the Experimental Section. Compound **103**, which differs from **101** for the replacement of the ketone at C-9 with a further acetoxy group, is a known compound previously reported from the aerial parts of *Euphorbia mongolica* as an inhibitor of the efflux pump in multidrug-resistant L5178 mouse lymphoma cells.⁴²

The aerial parts of *E. bungei* afforded also a new diterpene (**104**) belonging to the lathyrene class. The HR-ESIMS data of compound **104** indicated the molecular formula $\text{C}_{29}\text{H}_{42}\text{O}_9$, in agreement with of nine degrees of unsaturation. ^1H and ^{13}C

NMR data (**Table 4.3**) showed the presence of an isovalerate and two acetate groups (δ_{H} 2.11 and 2.14, s) linked to a diterpenoid core. The stereostructure of this moiety was deduced on the basis of a detailed analysis of 2D NMR spectra. Combined inspection of COSY and HSQC spectra of **104** disclosed the two structural moieties depicted in bold in **figure 4.19**, namely the methyl branched fragment from C-1 to C-3 and the seven-carbon moiety spanning C-7 to C-20. The sp^2 methine singlet at δ_{H} 5.87 (H-5) showed five diagnostic ${}^{2,3}J_{\text{H,C}}$ HMBC correlations with the oxygenated quaternary carbons C-4 and C-15 and with C-3, C-6, and C-7, and these two latter carbons were also HMBC-correlated to the methyl singlet at δ_{H} 2.03 (H-17). The above cross-peaks allowed the definition of a first connection between the two moieties through the oxygenated C-4 and the methylated double bond Δ^5 . The second connection point and the linkage of C-4 with C-15 were established on the basis of the HMBC correlations of both H₂-1 and H-13 with C-15 and with the ketone carbonyl resonating at δ_{C} 207.6 (C-14). Finally, the lathyranes carbon framework of **104** was defined on the basis of the HMBC cross-peaks of both Me-18 and Me-19 with C-9, C-11 and with the unprotonated C-10, in agreement with the presence of a cyclopropane ring.

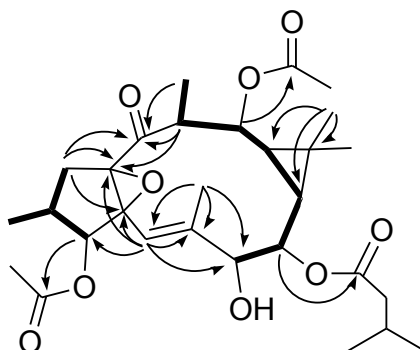


Figure 4.19. COSY (in bold) and key ${}^{2,3}J_{\text{H}\rightarrow\text{C}}$ HMBC cross peaks detected for compound **104**

At this stage, we reasoned that the structure of compound **104** should include four oxygenated sp^2 carbons (three esters and one ketone) and six oxygenated sp^3 carbons, three of which must be acylated, with therefore, ten oxygenated carbons. The presence of an ether linkage could rationalize the nine oxygen atoms and the additional unsaturation degree present in the molecular formula of **104**. The HMBC cross-peaks of H-3, H-8, and H-12 with the corresponding ester carbonyls allowed the placement of the acyl groups, leaving C-4, C-7, and C-15 as non-acylated positions. The lack of HMBC correlations of H-7 with C-4 or C-15, and

comparison with literature data⁴⁴ were both indicative that C-7 must bear a hydroxyl group, while C-4 and C-15 should be involved in an epoxide ring, thus defining an ingol-type structure for **104**.

The NOE correlation of H-5 with H-7 indicated the *E* configuration of the endocyclic double bond of **104**, while the pattern of chemical shifts and coupling constants for the fragment going from C-5 to C-13, strictly paralleling the values reported for other ingol esters,^{44,45} indicated that compound **104** shares with them the configurational and conformational arrangements of the 11-membered ring. Thus, substituents at C-7, C-8, C-12, and C-13 are α -oriented, while both the cyclopropane and the epoxide rings are β -oriented. As for the relative configuration at C-2 and C-3, we could assign a $2\alpha,3\alpha$ orientation on the basis of the coupling constant value $J_{H-2/H-3} = 5.5$ Hz. As reported by Marco et al.⁴⁴, all the other possible relative orientations would be associated with very different coupling constant values ($J_{H-2/H-3} = 9$ Hz for $2\beta,3\beta$ and $2\alpha,3\beta$ and 1.5 Hz for $2\beta,3\alpha$). Thus, compound **104** was identified as 2,3-diepiingol 7,12-diacetate 8-isovalerate, a relatively rare class of ingol derivatives.

A complex mixture of cycloartane triterpenoids was also characterized. Remarkably, its composition was similar to the one reported from the totally unrelated plant *Juncus effusus*.⁴⁶ The major constituents were the isomeric diols **105a** and **105b**,⁴⁶ that were the only compounds that could be obtained in pure form. In other subfractions, four related compounds (**105c-105f**) were identified. Since they are all known compounds and the biological evaluation of **105a** and **105b** was disappointing (see infra), no attempt was done to obtain them in pure form.

The evaluation of the biological profile of the macrocyclic diterpenoids from *E. bungei* will be reported independently as a part of a structure-activity study on this type of compounds. On the other hand, several *Euphorbia*-triterpenoids show potent anti-HIV activity,⁴⁷ providing a rationale to investigate the cycloartanes **105a** and **105b** in anti-HIV assays. However, neither of them showed significant activity in an assay of NF- κ B-dependent transcription of the HIV-LTR-luc.⁴⁸

In conclusion, a phytochemical investigation of the aerial parts of the Iranian spurge *E. bungei* afforded, in addition to known triterpenoids, three new macrocyclic diterpene polyesters, two belonging to the jatrophone class and one to the lathyrene class. While the two major triterpenoids did not show anti HIV

activity, the availability of the new macrocyclic polyesters will be useful for studies to evaluate the potential of *Euphorbia* diterpenoids as modulators of multidrug resistance in cancer chemotherapy⁴⁹ and as adjuvants in the anti-AIDS therapy.⁵⁰

4.3.3. Experimental

Plant material, extraction and isolation

Aerial parts of *Euphorbia bungei* Boiss. were collected in the surroundings of Fereydan (Isfahan, Iran) in April 2007. The plant material was identified by Mr. Bahram Zehzad, Department of Biology, University of Shahid Beheshti, Isfahan, and a voucher specimen (No. 2143) has been deposited at the Herbarium of School of Pharmacy, Isfahan University of Medical Sciences, Isfahan, Iran.

The air dried aerial parts of *E. bungei* (2440 g) were exhaustively extracted with acetone at room temperature. After removal of solvent *in vacuo*, the residue (210 g) was dissolved in EtOH (1.5 L) and treated with the same volume of 3% lead(II) acetate. After two hours, the black suspension was filtered on a bed of Celite, obtaining a light brown filtrate. After evaporation of ethanol, the filtrate was saturated with NaCl and extracted with dichloromethane (1,5 L × 3). The organic extract was dried over anhydrous Na₂SO₄ and evaporated, affording a brown residue (14 g) which was filtered on neutral alumina (140 g, petroleum ether (PE):EtOAc (50:50) as solvent) to remove fatty acids, eventually obtaining 3.0 g of a terpenoid-rich extract. The latter was purified by normal phase gravity column chromatography eluting with mixtures PE:EtOAc of increasing polarity, affording 8 fractions (F1 to F8), all containing complex mixtures. Inspection of the NMR spectrum of F3-F5 showed several signals typical of triterpenoids, and were purified by HPLC (PE:EtOAc 8:2, 75:25, and 6:4, respectively) to afford the cycloartane triterpenoids **105b**, **105c**, **105d**, **105e** and **105f** in different mixtures (totally 38 mg ≈ 0.0016%) from F3, as well as **105a** (50 mg ≈ 0.0020%) and **105b** (24 mg ≈ 0.00098%) from F5. This fraction also afforded the lathyrene diterpenoid **104** (2.5 mg ≈ 0.00010%). The more polar fraction F6 was further purified through reversed phase flash chromatography (MeOH:H₂O 70% to 100%) to afford the new jatrophone diterpenoids **101** (33 mg ≈ 0.00135%) and **102** (3.5 mg ≈ 0.00014%), finally purified by normal phase HPLC (PE:EtOAc 5:5). Fraction F7 was purified by reversed phase flash chromatography

(MeOH:H₂O 60% to 100%) to yield the jatrophone diterpenoid **103** (2.5 mg \approx 0.00010%).

Compound 101: 0.00135% of dry wt. Colorless amorphous solid; $[\alpha]_D + 6.3$ (c 0.07, CHCl₃); ¹H NMR (CDCl₃, 500 MHz) Table 4.3; ¹³C NMR (CDCl₃, 125 MHz) Table 4.3; (+) ESI-MS m/z 677 [M + Na]⁺. HR-ESIMS found 677.2570; C₃₅H₄₂NaO₁₂ requires 677.2574.

Compound 102: 0.00014% of dry wt. Colorless amorphous solid; $[\alpha]_D + 5.4$ (c 0.02, CHCl₃); ¹H NMR (CDCl₃, 500 MHz, J in Hz): δ 7.60 (2H, overlapped, 5-*O*-Bz), 7.60 (2H, overlapped, 7-*O*-Bz), 7.25 (1H, t, $J = 7.0$ Hz, 5-*O*-Bz), 7.19 (1H, t, $J = 7.0$ Hz, 7-*O*-Bz), 7.10 (2H, t, $J = 7.0$ Hz, 5-*O*-Bz), 6.99 (2H, t, $J = 7.0$ Hz, 7-*O*-Bz), 6.20 (1H, bs, H-7), 6.07 (1H, d, $J = 5.5$ Hz, H-5), 5.96 (1H, d, $J = 16.0$ Hz, H-11), 5.92 (1H, d, $J = 16.0$ Hz, H-12), 5.73 (1H, bd, $J = 3.0$ Hz, H-3), 5.70 (1H, bs, H-17a), 5.60 (1H, bs, H-8), 5.40 (1H, bs, H-17b), 3.52 (1H, m, H-13), 3.03 (1H, dd, $J = 5.5, 3.0$ Hz, H-4), 2.93 (1H, dd, $J = 15.7, 9.2$ Hz, H-1a), 2.41 (1H, m, H-2), 2.13 (1H, overlapped, H-1b), 2.08 (3-*O*-Ac, s), 2.07 (15-*O*-Ac), 1.92 (8-*O*-Ac, s), 1.32 (3H, s, H-18), 1.42 (3H, d, $J = 6.8$ Hz, H-20), 1.24 (3H, s, H-19), 1.01 (1H, d, $J = 7.0$ Hz, H-16); ¹³C NMR (CDCl₃, 125 MHz): δ 205.3 (s, C-9), 204.1 (s, C-14), 170.7 (s, 15-*O*-Ac), 170.3 (s, 3-*O*-Ac), 170.2 (s, 8-*O*-Ac), 163.9 (s, 5-*O*-Bz), 163.3 (s, 7-*O*-Bz), 137.7 (s, C-6), 135.3 (d, C-11), 134.5 (d, C-12), 133.1-128.5 (5-*O*-Bz and 7-*O*-Bz carbons), 126.1 (t, C-17), 92.0 (s, C-15), 77.4 (d, C-3), 73.5 (d, C-5), 72.9 (d, C-8), 71.6 (s, C-7), 49.5 (d, C-4), 49.1 (s, C-10), 45.2 (t, C-1), 43.9 (d, C-13), 39.1 (d, C-2), 26.2 (q, C-18), 24.1 (q, C-19), 20.6 (s, C-20), 20.7 (q, 15-*O*-Ac), 20.4 (q, 8-*O*-Ac), 20.1 (q, 3-*O*-Ac), 14.4 (q, C-16). ESI-MS m/z 739 [M + Na]⁺. HR-ESIMS found 739.2734; C₄₀H₄₄NaO₁₂ requires 739.2730.

Compound 104: 0.00010% of dry wt. Colorless amorphous solid; $[\alpha]_D + 2.9$ (c 0.01, CHCl₃); ¹H NMR (CDCl₃, 500 MHz) Table 4.3; ¹³C NMR (CDCl₃, 125 MHz) Table 4.3; (+) ESI-MS m/z 557 [M + Na]⁺. HR-ESIMS found 557.2733; C₂₉H₄₂NaO₉ requires 557.2727.

References

1. Croteau, R.; Kutchan, T.M.; Lewis, N.G.; Natural production (secondary metabolites). In: Buchanan B, Gruissem W, Jones R (eds) *Biochemistry and molecular biology of plants*. American, **2000**.
2. Evans, F.J.; Taylor, S.E.; *Prog Chem Org Nat Prod*, **1983**, 44, 1–99.
3. Shi, Q. W.; Su, X. H.; Kiyota, H.; *Chem. Rev.*, **2008**, 108, 4295-4327.
4. Adolf, W.; Hecker, E.; *Z Krebsforsch*, **1975**, 84, 325-344.
5. Zwenger, S.; Basu, C.; *Biotechnol Mol Biol Rev*, **2008**, 3, 1–7.
6. Paul M Dewick, *Medicinal Natural products*, book, second edition, John Wiley & sons, LTD.
7. Roberts, S.C.; *Nat Chem Biol*, **2007**, 3, 387–395.
8. Bruneton, J.; *Pharmacognosy, phytochemistry, medicinal plants; part 3*. Lavoisier, London, **1995**.
9. Hanson J.R.; Diterpenoids. In: Charlwood B.V., Banthorpe D.V. (eds) *Methods in plant biochemistry*. Academic Press, London, **1991**, pp 263–288.
10. Hanson J.R.; *Nat Prod Rep*, **2004**, 21, 785–793.
11. Hanson J.R.; *Nat Prod Rep*, **2009**, 26, 1156–1171.
12. Chianese, G.; Fattorusso, E.; Aiyelaagbe, Olapeju O.; Luciano, P.; Schroder, Heinz C.; Muller, Werner E. G.; Taglialatela-Scafati, O.; *Organic letters*, **2011**, 13, 316-319.
13. Shokoohinia, Y.; Sajjadi, S.; Zolfaghari, B.; Chianese, G.; Appendino, G.; Taglialatela-Scafati, O.; *Fitoterapia*, **2010**, 81, 884–890.
14. Kingsbury J.M.; *Poisonous plants of the United States and Canada*. Prentice-Hall, New Jersey, **1964**.
15. Guerrero, M.F.; Pueblab, P.; Carrón, R.; Martín, M.L.; Romána, L.S.; *J Ethnopharmacol*, **2004**, 94, 185–189
16. Hussain, S.; Slevin, M.; Mesaik, M. A.; Choudhary, M. I.; Elostá, A. H.; Matou, S.; Ahmed, N.; West, D.; Gaffney, J.; *BMC Cell Biol*, **2008**, 9,7.
17. Fairless, D.; *Nature*, **2007**, 449, 652-655.
18. Haas, W.; Sterk, H.; Mittelbach, M. *J. Nat. Prod.* **2002**, 65, 1434-1440.
19. Ravindranath, N.; Reddy, M. R.; Ramesh, C.; Ramu, R.; Prabhakar, A.; Jagadeesh, B.; Das, B. *Chem. Pharm. Bull.* **2004**, 52, 608-611.
20. Ravindranath, N.; Ravinder Reddy, M.; Mahender, G.; Ramu, R.; Ravi Kumar, K.; Das, Biswanath.; *Phytochemistry* **2004**, 65, 2387-2390.

21. Zhang, X.-P.; Zhang, M.-L.; Su, X.-H.; Huo, C.-H.; Gu, Y.-C.; Shi, Q.-W. *Chem. Biodiv.* **2009**, *6*, 2166-2183.
22. Wang, X.-C.; Zheng, Z.-P.; Gan, X.-W.; Hu, L.-H. *Org. Lett.* **2009**, *11*, 5522-5524.
23. Schmeda-Hirschmann, G.; Tschritzis, F.; Jakupovic, J. *Phytochemistry*, **1992**, *31*, 1731-1735.
24. Das, B.; Ravikanth, B.; Reddy, K. R.; Thirupathi, P.; Raju, T. V.; Sridhar, B. *Phytochemistry*, **2008**, *69*, 2639-2641.
25. Das, B.; Laxminarayana, K.; Krishnaiah, M.; Srinivas, Y.; Raju, T. V.; *Tetrahedron Lett.*, **2009**, *50*, 4885-4887.
26. Purushothaman, K. K.; Chandrasekharan, S.; Cameron, A. F.; Connolly, J. D.; Labbe, C.; Maltz, A.; Rycroft, D. S.; *Tetrahedron Lett.*, **1979**, *11*, 979-980.
27. Naengchomnong, W.; Thebtaranonth, Y.; Wiriyaichitra, P.; Okamoto, K. T.; Clardy, J.; *Tetrahedron Lett.*, **1986**, *27*, 2439-2442.
28. Stephens, P. J.; Pan, J. J.; Krohn, K.; *J. Org. Chem.*, **2007**, *72*, 7641-7649.
29. Details about Gaussian 03 are provided as Supporting Information.
30. Diedrich, C.; Grimme, S. J.; *Phys. Chem. A*, **2003**, *107*, 2524-2539.
31. Kiselyov, A.; Balakin, K.V.; Tkachenko, S. E.; *Expert Opin Investig Drugs*, **2007**, *16*, 83-107.
32. Mozaffarian, V.; A Dictionary of Iranian Plant Names. Farhang Mo'aser Publishers. Tehran, **1996**.
33. H. Sadeghi-Aliabadia, Sajjadi, S. E.; Khodamoradi, M. *Iranian J. Pharm. Sci*, **2009**, *5*, 103-108.
34. Zargari, A.; Medicinal plants. Vol2, Tehran: Tehran University Press. **1989**.
35. Appendino, G.; Belloro, E.; Tron, G. C.; Jakupovic, J.; Ballero, M.; *J. Nat. Prod.*, **1999**, *62*, 1399-1404.
36. For a better comparison of the spectroscopic data, the phorbol numbering has been maintained in **10**.
37. Appendino, G.; Carello, G. P.; Enriù, R.; Jakupovic, J.; *J. Nat. Prod.*, **1995**, *58*, 284-287.
38. Klausen, T. K.; Pagani, A.; Minassi, A.; Ech-Chahad, A.; Prenen, J.; Owsianik, G.; Hoffmann, E. K.; Pedersen, S. F.; Appendino, G.; Nilius, B.; *J. Med. Chem.*, **2009**, *52*, 2933-2999.

39. Mahvan, A.; Dictionary of Iranain Plants. Farhang Mo'aser Publishers, Tehran, **2002**.
40. Noori, M.; Chehreghani, A.; Kaveh, M.; *Toxicol. Environ. Chem.*, **2009**, 91, 631-641.
41. Jaafari, M. R.; Behravan, J.; Abde-Emami, J.; Saghafi-Khadem, F.; Ramezani, M.; *Int. J. Pharmacol.*; **2006**, 2, 571-575.
42. Hohmann, J.; Redei, D., Forgo, P., Molnar, J., Dombi, G., Zorig, T.; *J. Nat. Prod.*, **2003**, 66, 976-979.
43. Liu, L. G.; Tan, R.; *J. Nat. Prod.*, **2001**, 64, 1064-1068.
44. Marco, J. A.; Sanz-Cervera, J. F.; Yuste, A.; *Phytochemistry*, 1997, 45, 563-570.
45. Khan, A. Q.; Malik, A.; *J. Nat. Prod.*, **1990**, 53, 728-731.
46. Della Greca, M.; Fiorentino, A.; Monaco, P.; Previtera, L.; *Phytochemistry*, **1994**, 35, 1017- 1021.
47. Akihisa, T.; Wijeratne, E. M. K.; Tokuda, H.; Enjo, F.; Toriumi, M.; Kimura, Y.; Koike, K.; Nikaido, T.; Tezuka, Y.; Nishino, H.; *J. Nat. Prod.*, **2002**, 65, 158-162.
48. Appendino, G.; Ottino, M.; Marquez, N.; Bianchim, F.; Giana, A.; Ballero, M.; Sterner, O.; Fiebich, B. L.; Muñoz, E.; *J. Nat. Prod.*, **2007**, 70, 608-612.
49. Corea, G.; Di Pietro, A.; Dumontet, C.; Fattorusso, E.; Lanzotti,; *Phytochem. Rev.*, **2009**, 8, 431-447.
50. Bedoya, L. M.; Marquez, N.; Martinez, N.; Gutierrez-Eisman, S.; Alvarez, A.; Calzado, M. A.; Rojas, J. M.; Appendino, G.; Muñoz, E.; Alcami, J.; *Biochem. Pharmacol.*, **2009**, 77, 965-978.

CHAPTER V

SUPPORTING DATA

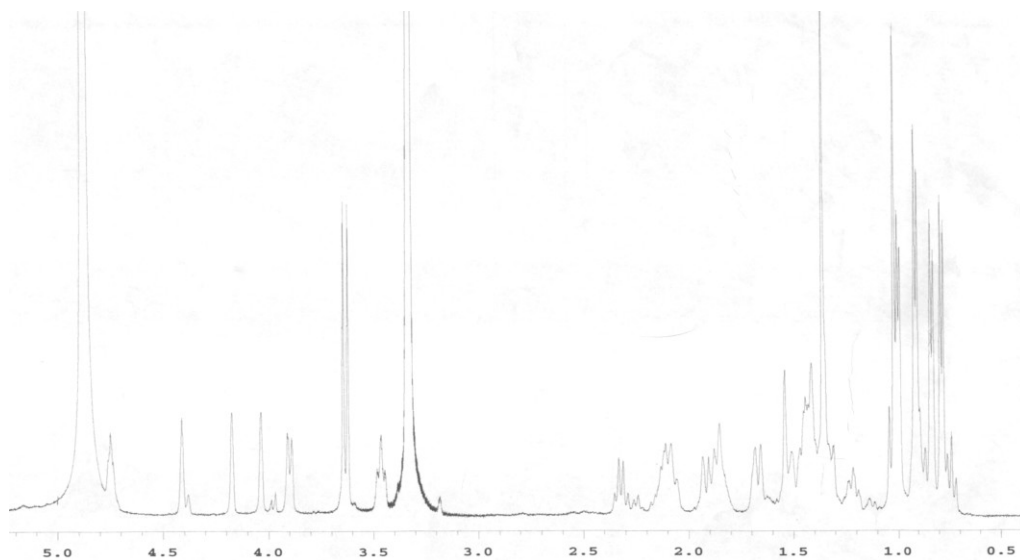
5.1. *General methods*

This paragraph describes the chromatographic and spectroscopic methods employed for the execution of the research. This techniques have been applied for all the projects.

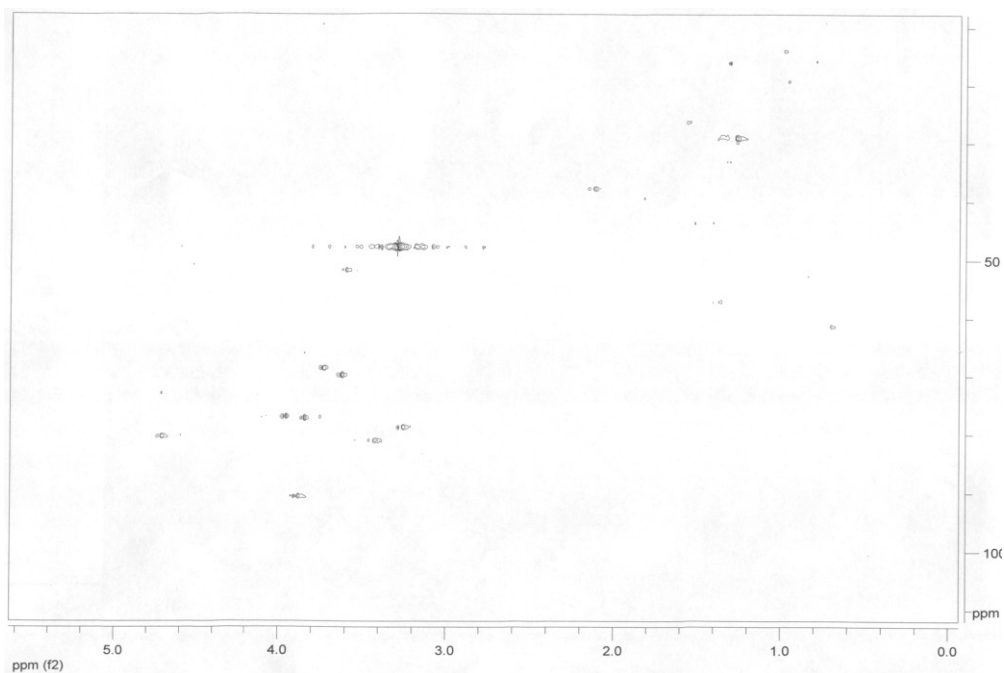
Low and high resolution ESI-MS spectra were performed on a LTQ OrbitrapXL (Thermo Scientific) mass spectrometer. Optical rotations (CHCl_3) were measured at 589 nm on a P2000 Jasco polarimeter using a 10 cm microcell. UV spectra were measured on a Thermo Scientific (mod. Nanodrop 2000c) instrument. CD spectra were registered on a Jasco J-710 instrument. ^1H (700 and 500 MHz) and ^{13}C (175 and 125 MHz) NMR spectra were measured on Varian INOVA spectrometers. Chemical shifts were referenced to the residual solvent signal (CDCl_3 : δ_{H} 7.26, δ_{C} 77.0). Homonuclear ^1H connectivities were determined by the COSY experiment. Through-space ^1H connectivities were evidenced using a ROESY experiment with a mixing time of 500 ms. One-bond heteronuclear ^1H - ^{13}C connectivities was determined by the HSQC experiment; two- and three-bond ^1H - ^{13}C connectivities by gradient-HMBC experiments optimized for a $^{2,3}J$ of 8 Hz. Medium pressure liquid chromatography was performed on a Büchi apparatus using a silica gel (230-400 mesh) column. HPLC were achieved on a Knauer apparatus equipped with a refractive index detector and LUNA (Phenomenex) SI60 or C18 (250 × 4 mm) columns.

5.2. NMR spectra

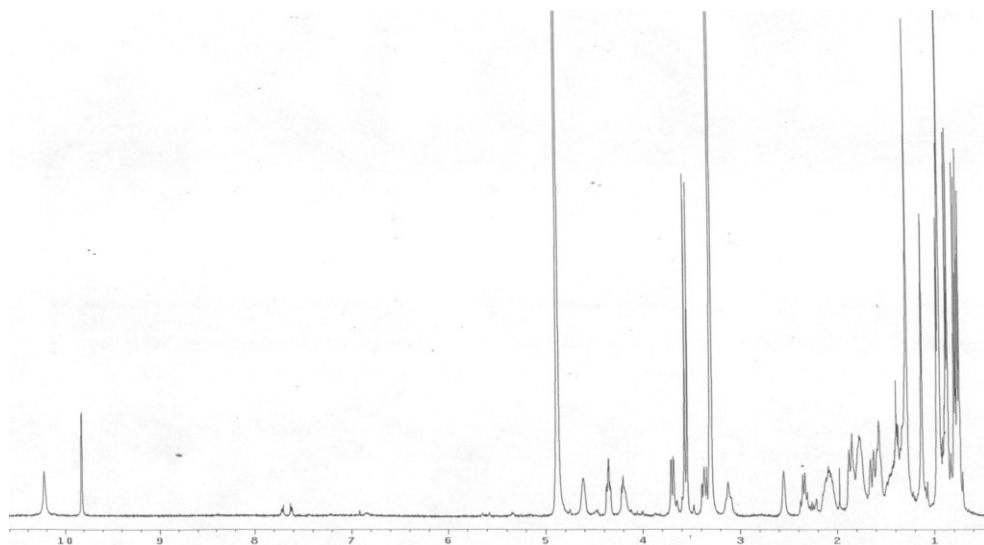
^1H NMR spectrum (500 MHz) of Haplosamate A (**11**) in CD_3OD .



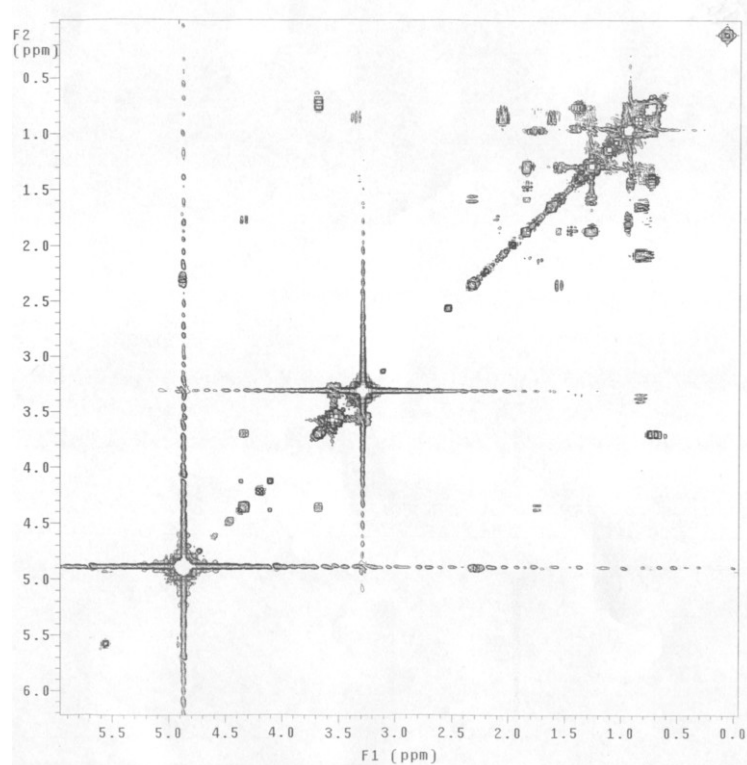
HSQC 2D NMR spectrum (700 MHz) of Desulfohaplosamate (**12**) in CD_3OD .



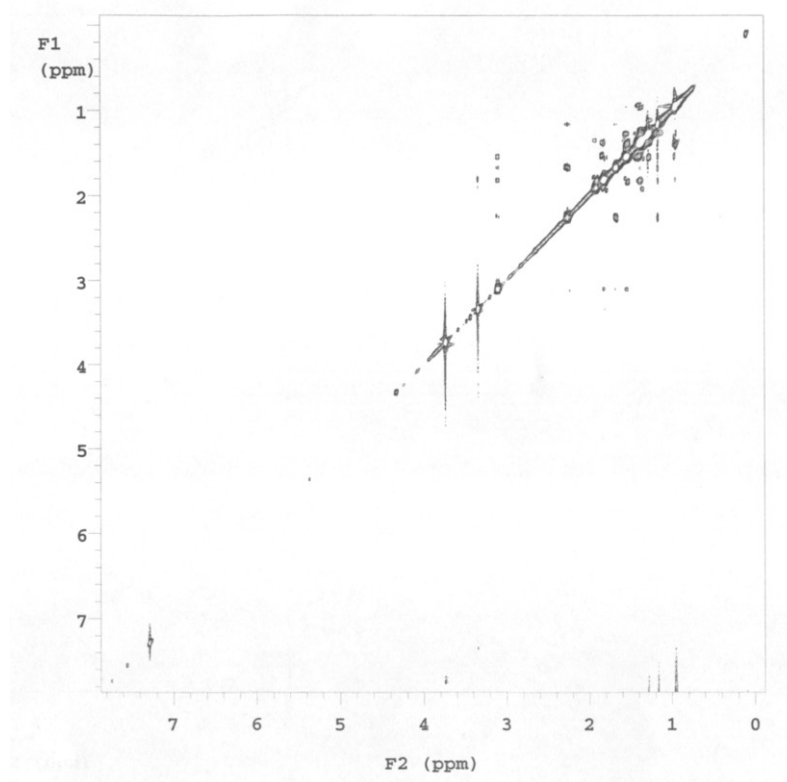
^1H NMR spectrum (500 MHz) of compound **33** in CD_3OD .



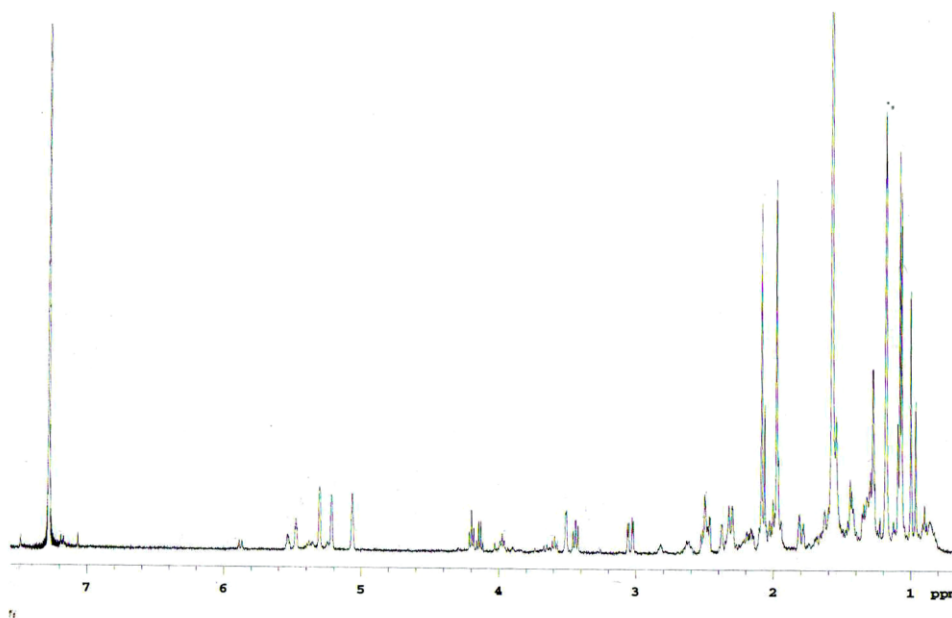
COSY 2D NMR spectrum (500 MHz) of compound **33** in CD_3OD .



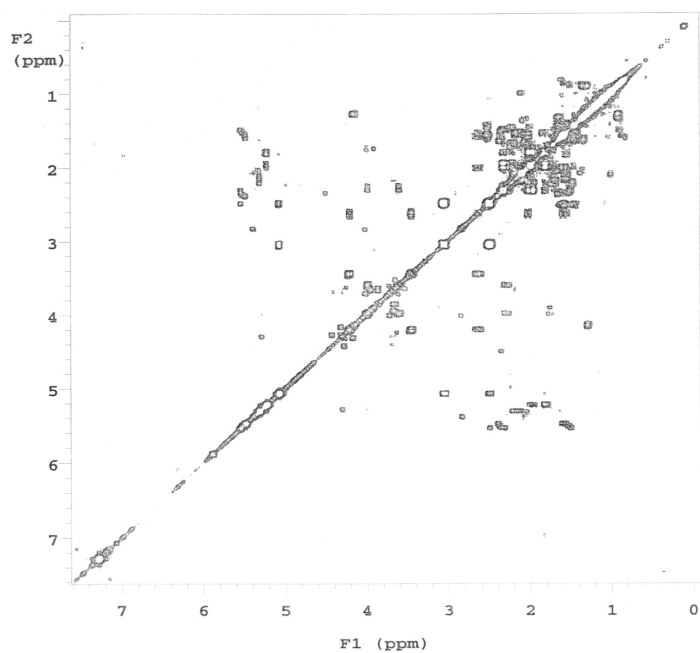
ROESY 2D NMR spectrum (500 MHz) of compound **60b** in CDCl₃.



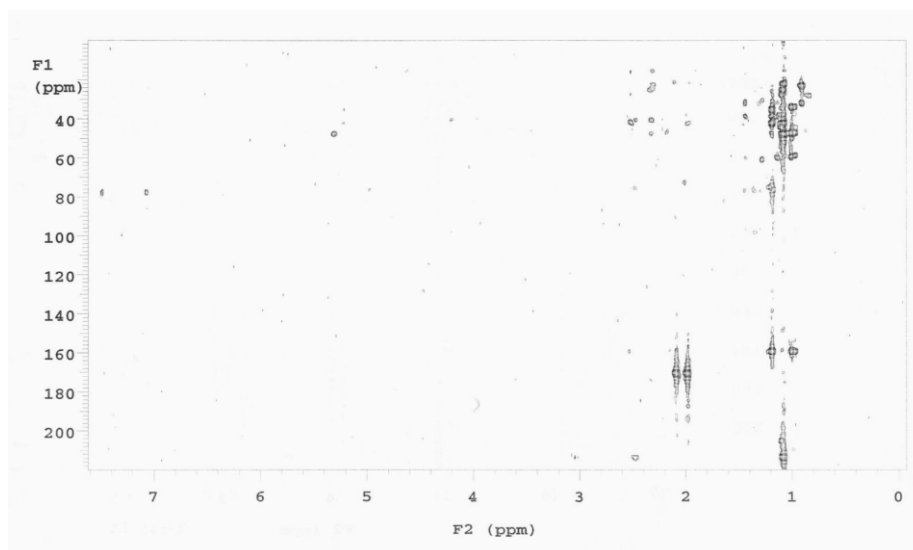
¹H NMR spectrum (500 MHz) of Neemfruitin A (**67**) in CDCl₃.



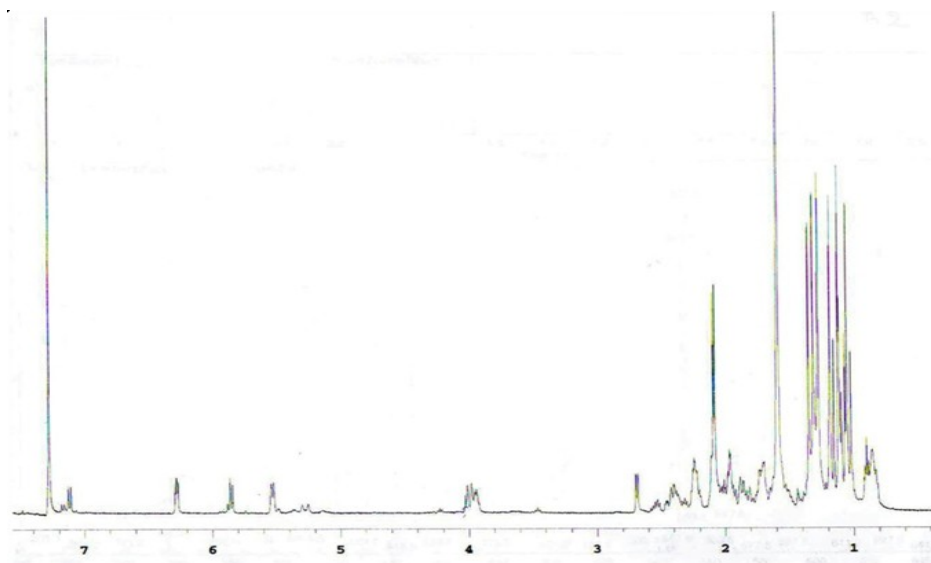
COSY 2D NMR spectrum (500 MHz) of Neemfruitin A (**67**) in CDCl₃.



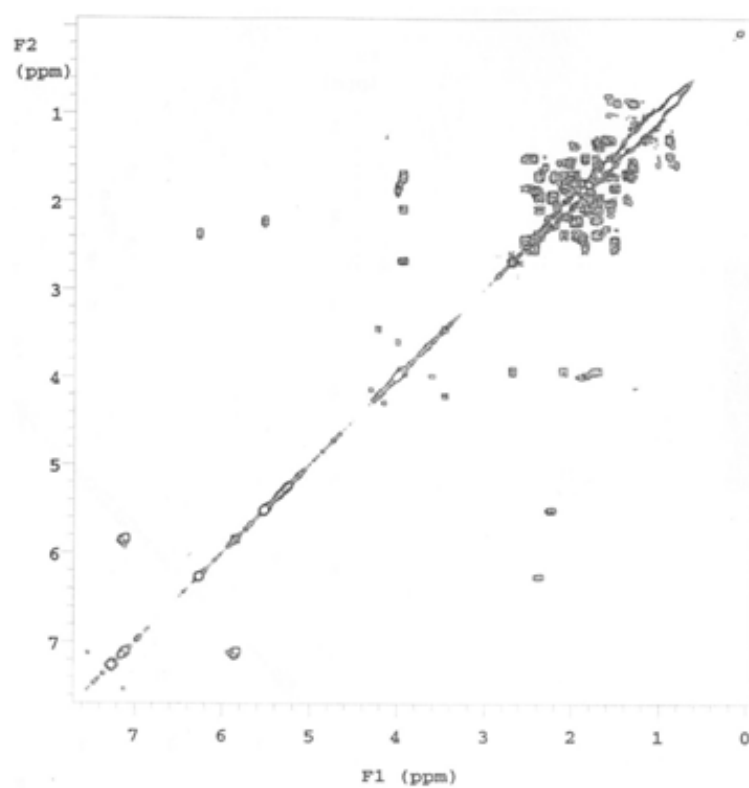
HMBC 2D NMR spectrum (500 MHz) of Neemfruitin A (**67**) in CDCl₃.



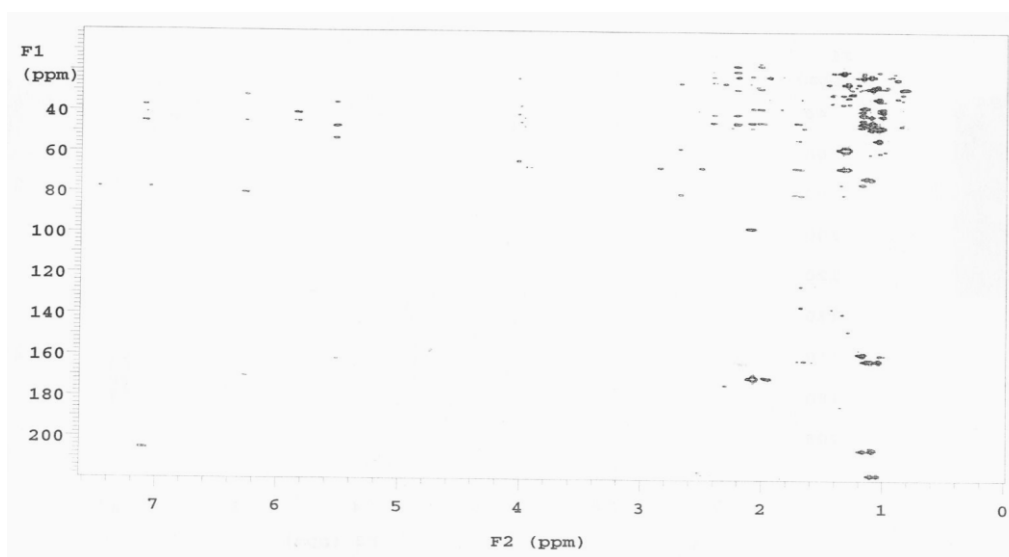
^1H NMR spectrum (500 MHz) of Neemfruitin B (**68**) in CDCl_3 .



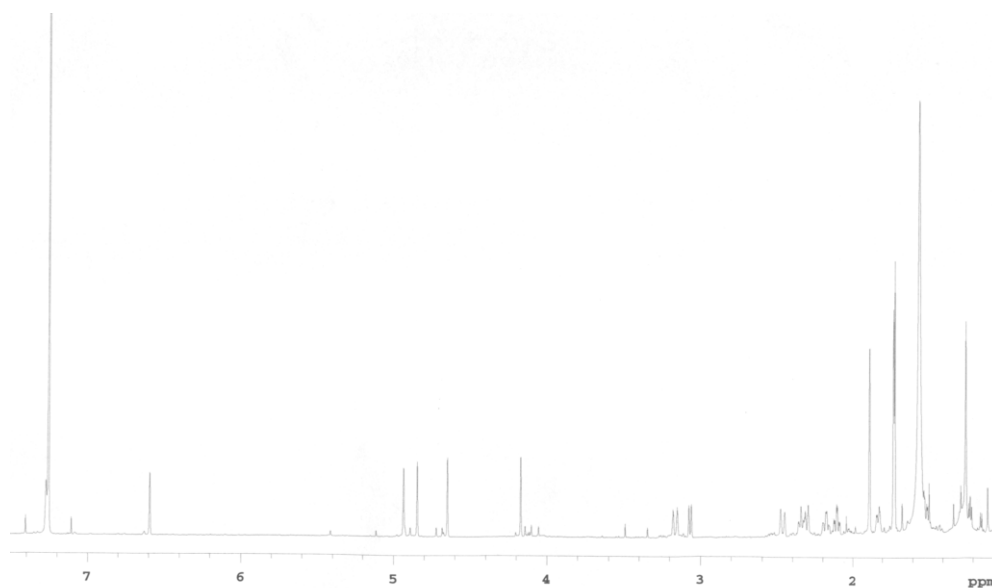
COSY NMR spectrum (500 MHz) of Neemfruitin B (**68**) in CDCl_3 .

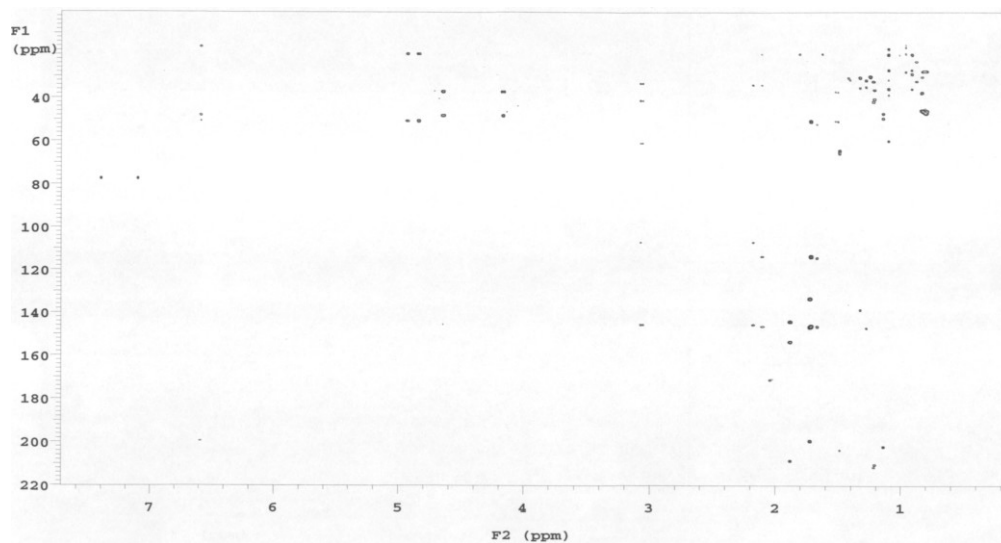
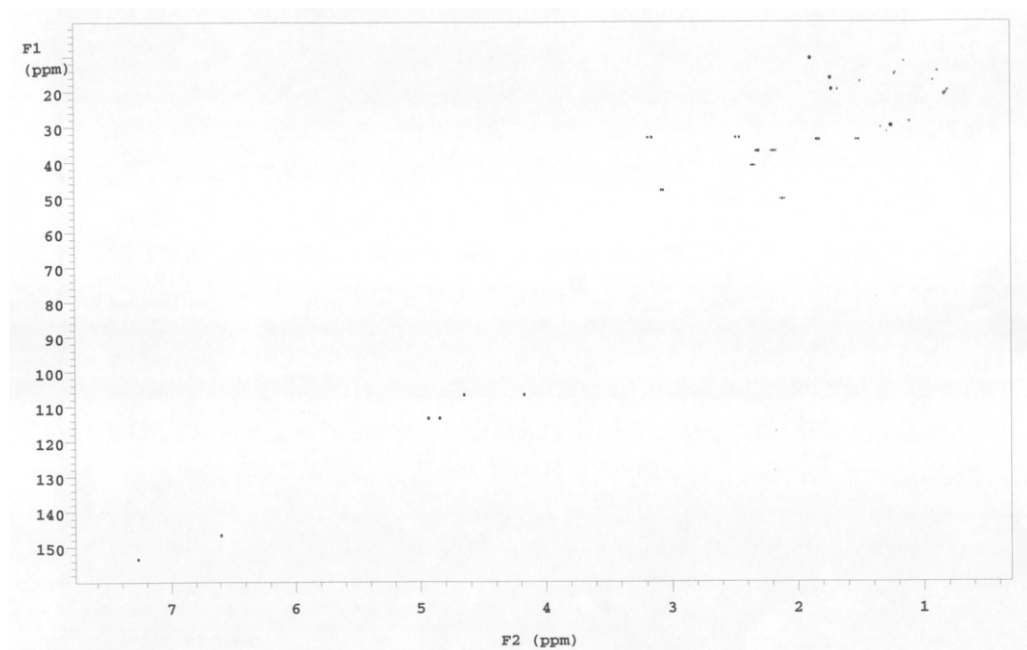


HMBC 2D NMR spectrum (500 MHz) of Neemfruitin B (**68**) in CDCl₃.

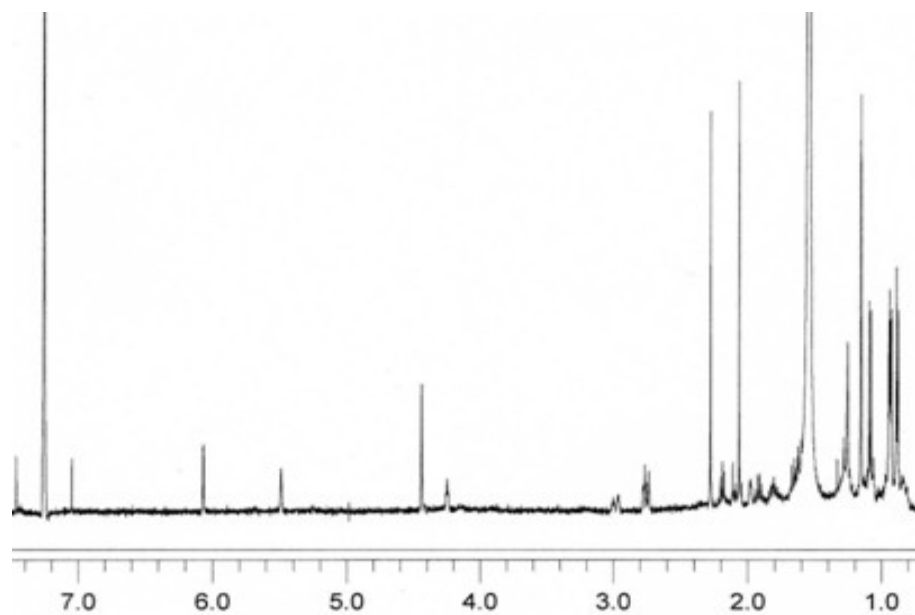


¹H NMR spectrum (700 MHz) of Spirocurcasone (**76**) in CDCl₃.

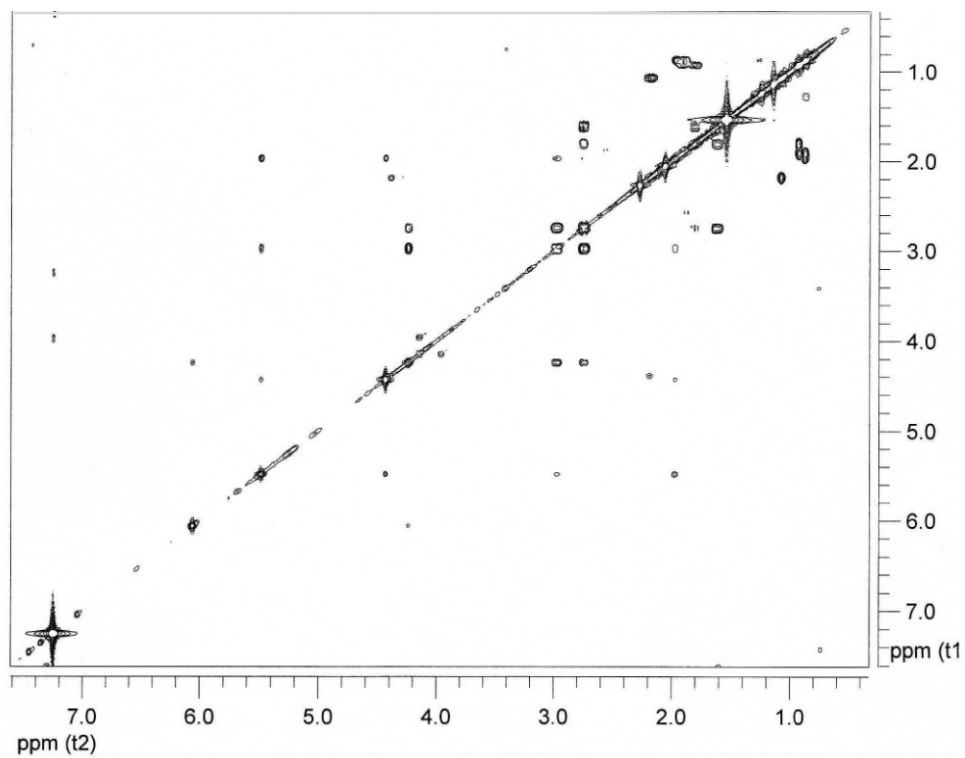


HMBC 2D NMR spectrum (700 MHz) of Spirocurcasone (**76**) in CDCl₃.HSQC 2D NMR spectrum (700 MHz) of Spirocurcasone (**76**) in CDCl₃.

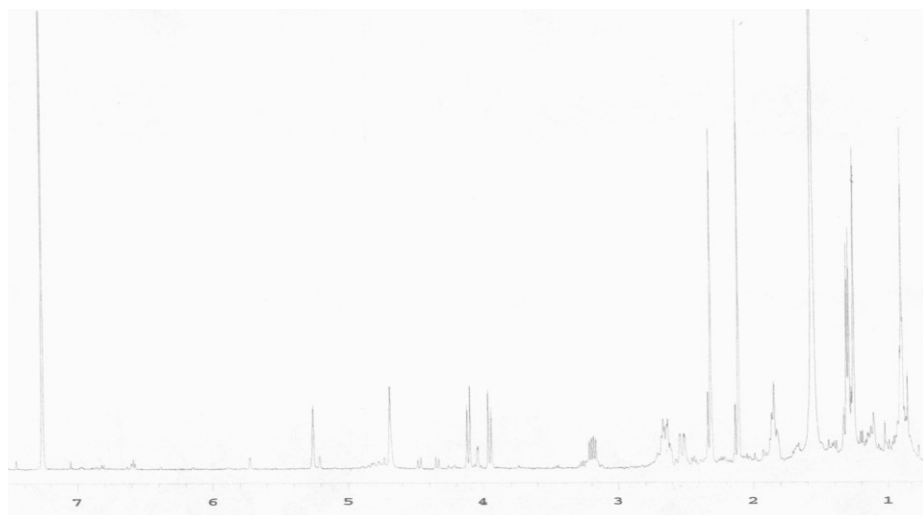
^1H NMR spectrum (500 MHz) of A-secophorboid **77** in CDCl_3 .



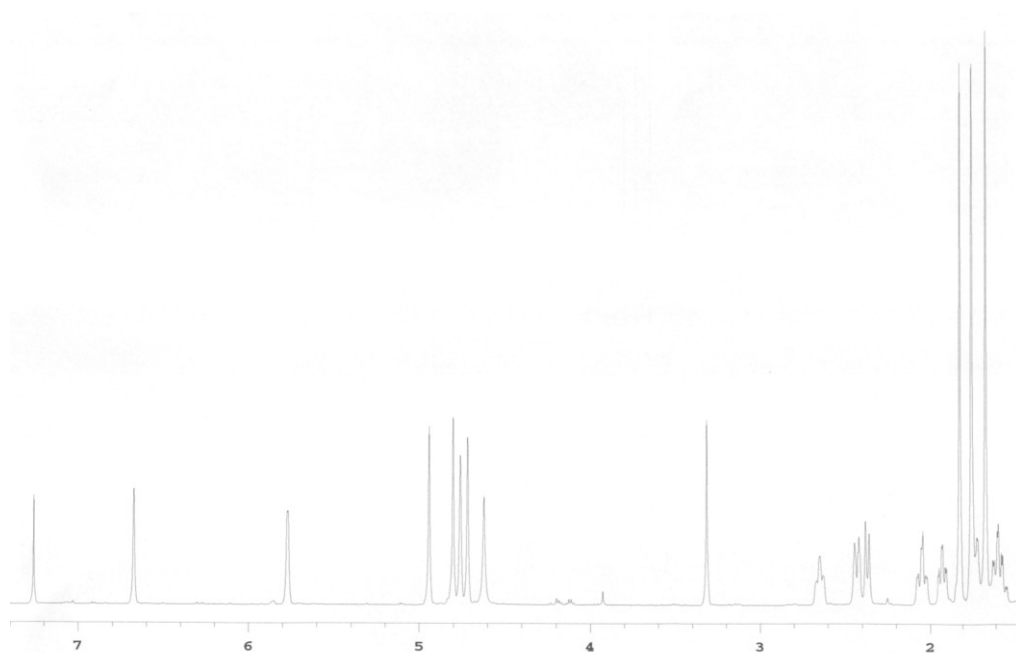
COSY 2D NMR spectrum (500 MHz) of A-secophorboid **77** in CDCl_3 .

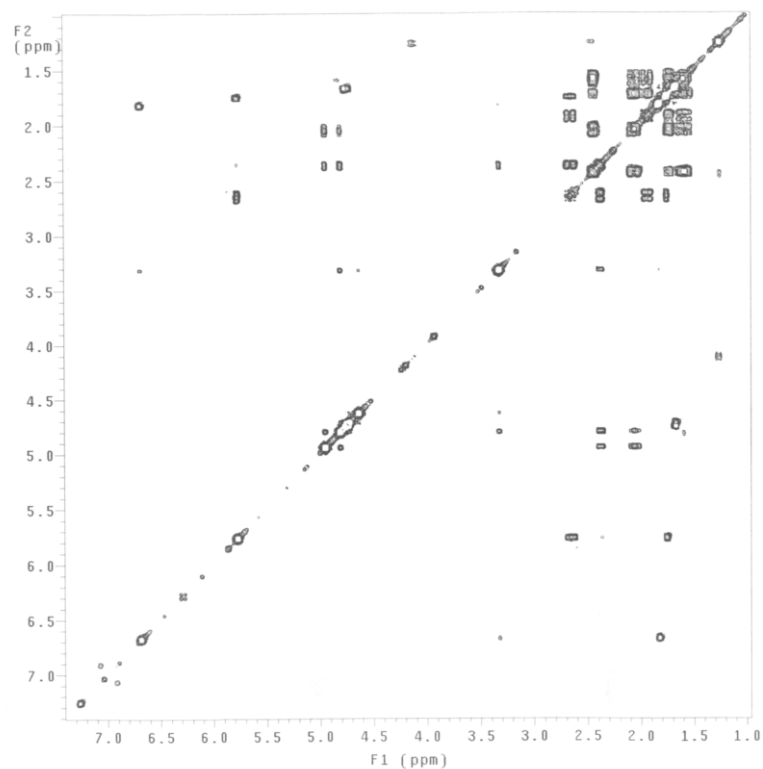
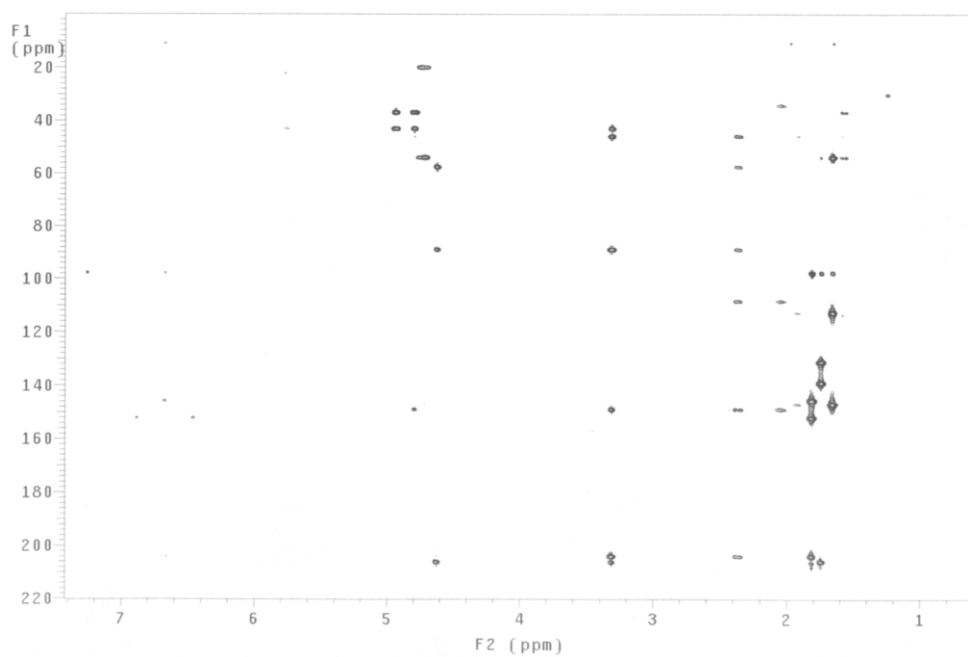


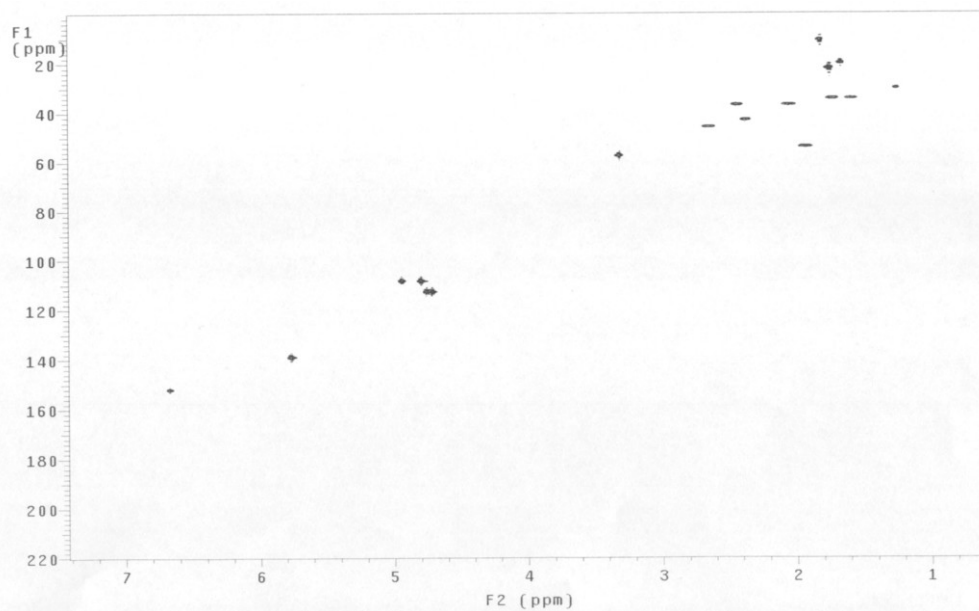
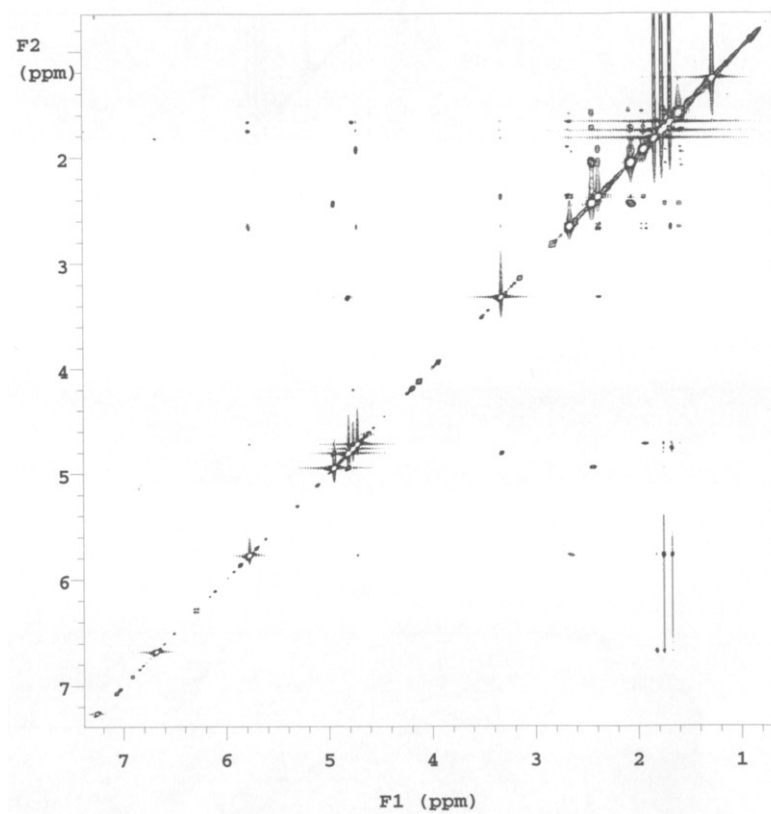
^1H NMR spectrum (500 MHz) of Acetoxyjatropholone (**86**) in CDCl_3 .



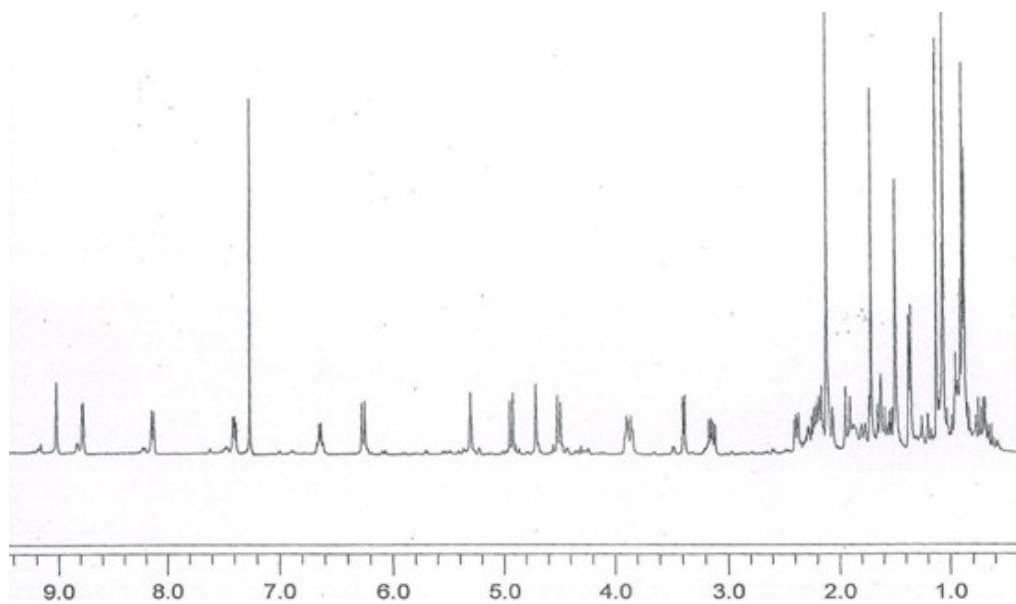
^1H NMR spectrum (500 MHz) of Curcusone E (**91**) in CDCl_3 .



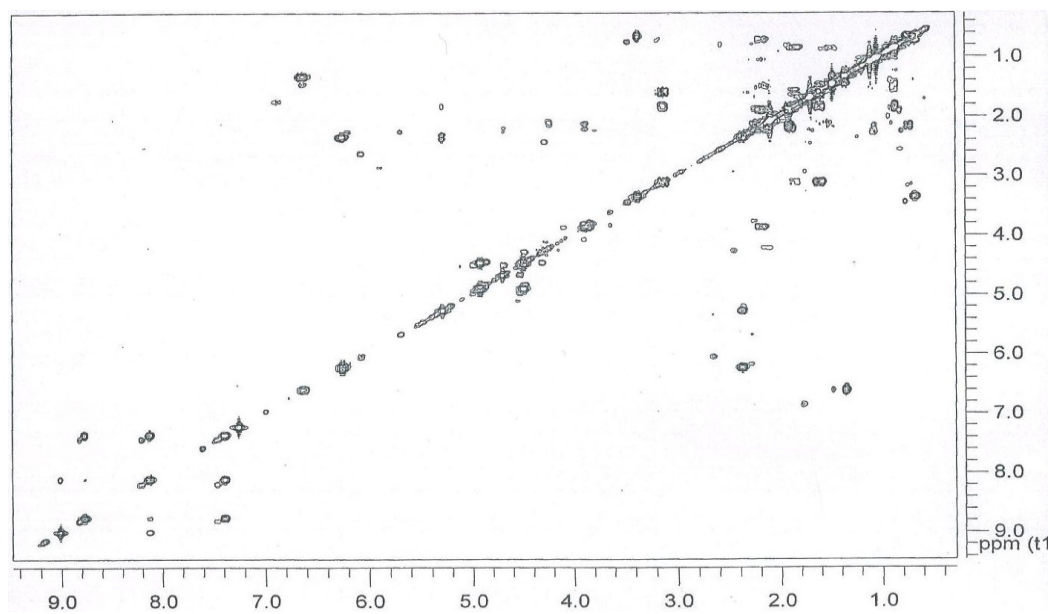
COSY 2D NMR spectrum (500 MHz) of Curcusone E (**91**) in CDCl₃.HMBC 2D NMR spectrum (500 MHz) of Curcusone E (**91**) in CDCl₃.

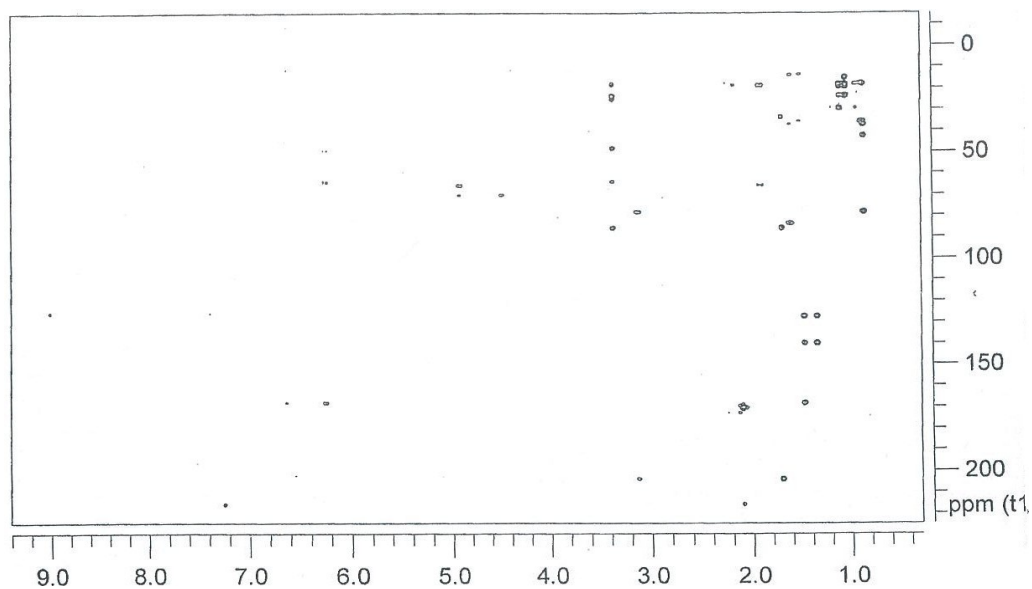
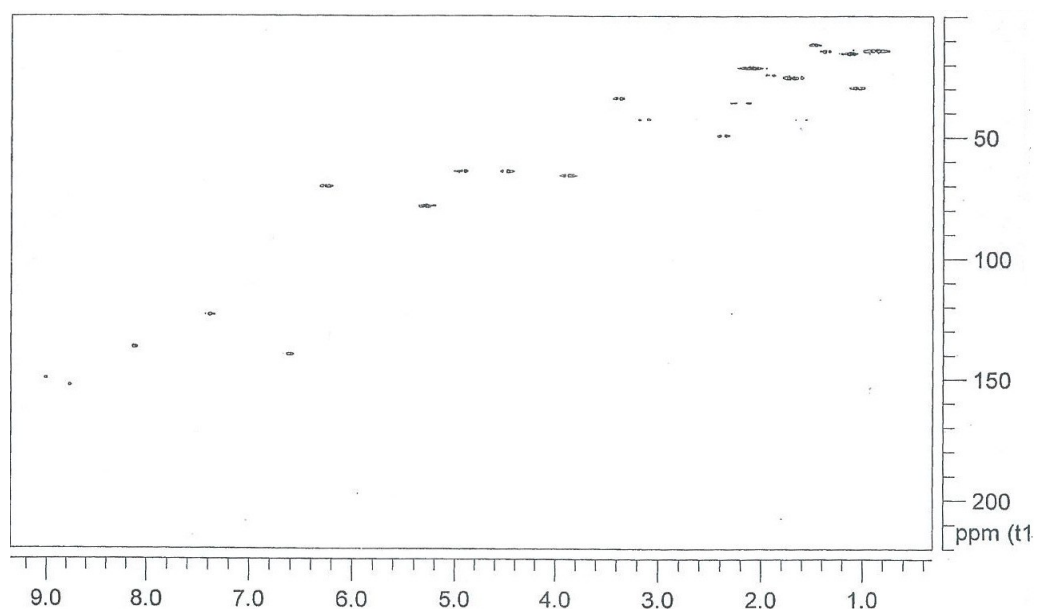
HSQC 2D NMR spectrum (500 MHz) of Curcusone E (**91**) in CDCl₃.ROESY 2D NMR spectrum (500 MHz) of Curcusone E (**91**) in CDCl₃.

^1H NMR spectrum (500 MHz) of compound **92** in CDCl_3 .

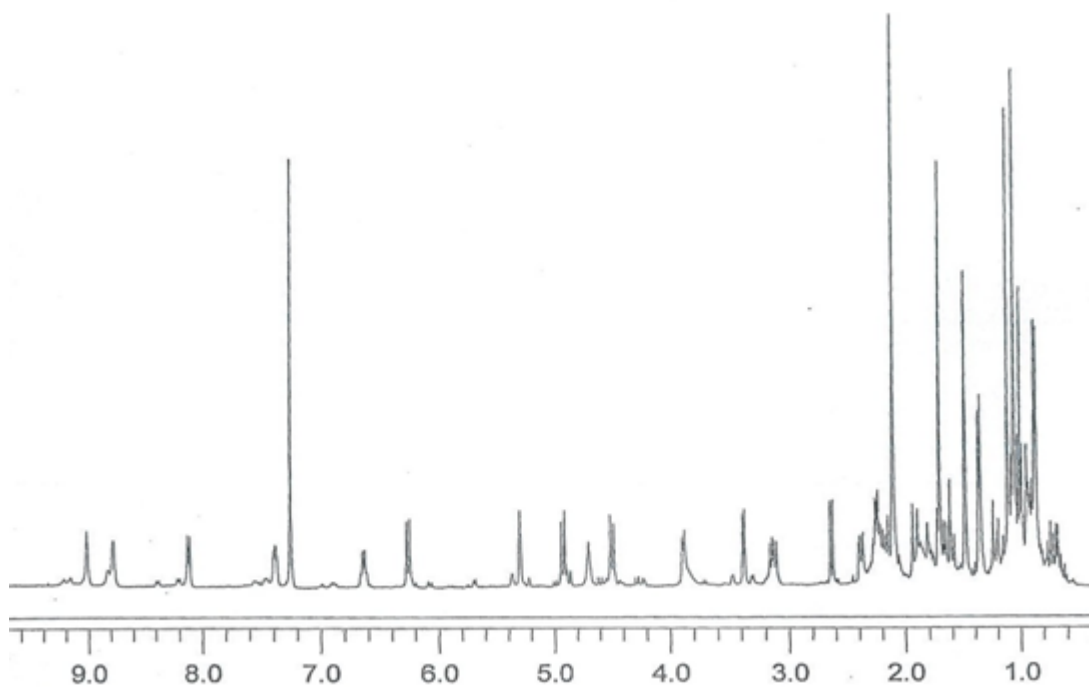


COSY 2D NMR spectrum (500 MHz) of compound **92** in CDCl_3 .

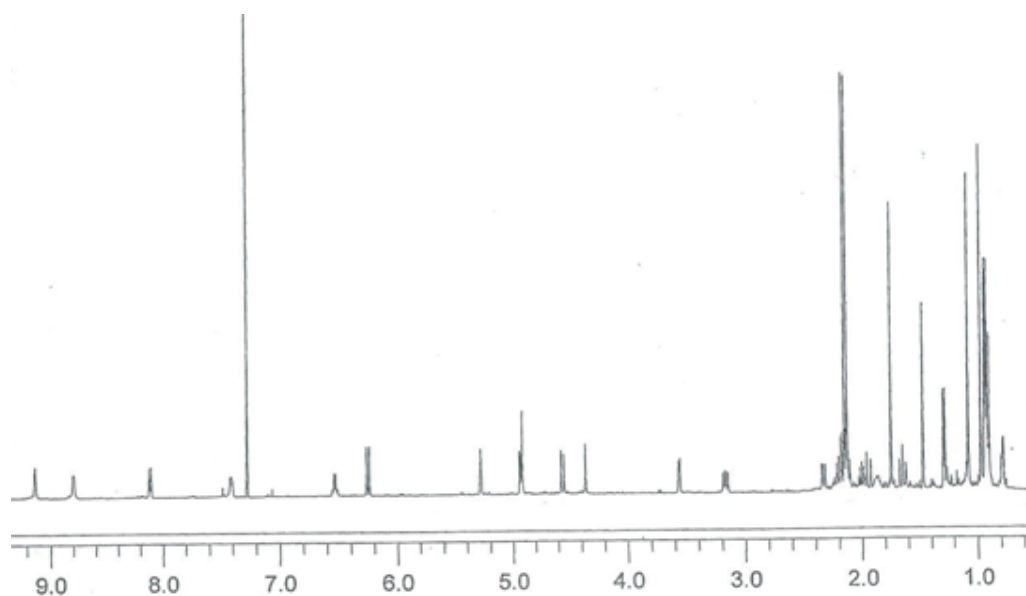


HMBC 2D NMR spectrum (500 MHz) of compound **92** in CDCl₃.HSQC 2D NMR spectrum (500 MHz) of compound **92** in CDCl₃.

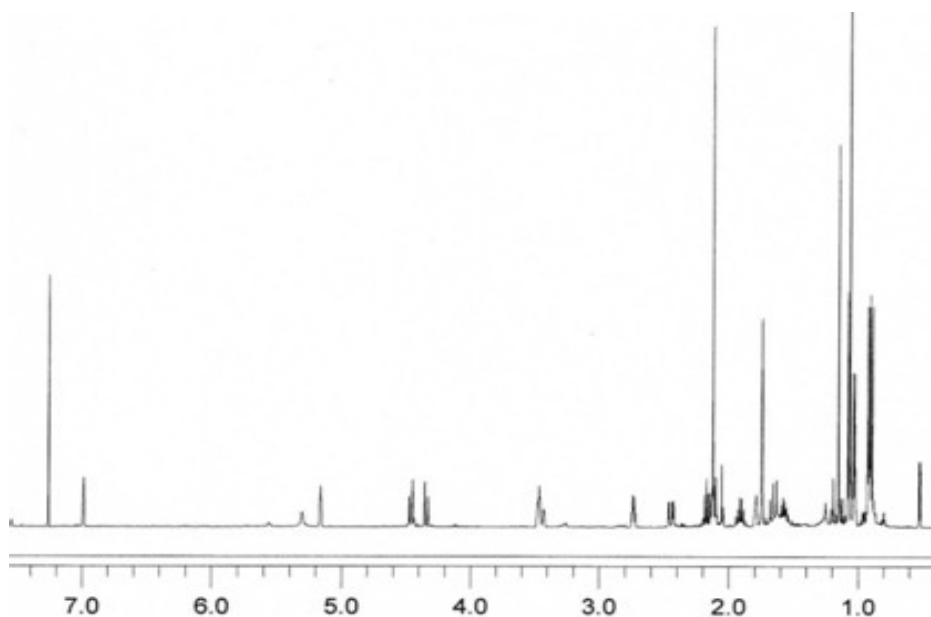
^1H NMR spectrum (500 MHz) of compound **93** in CDCl_3 .



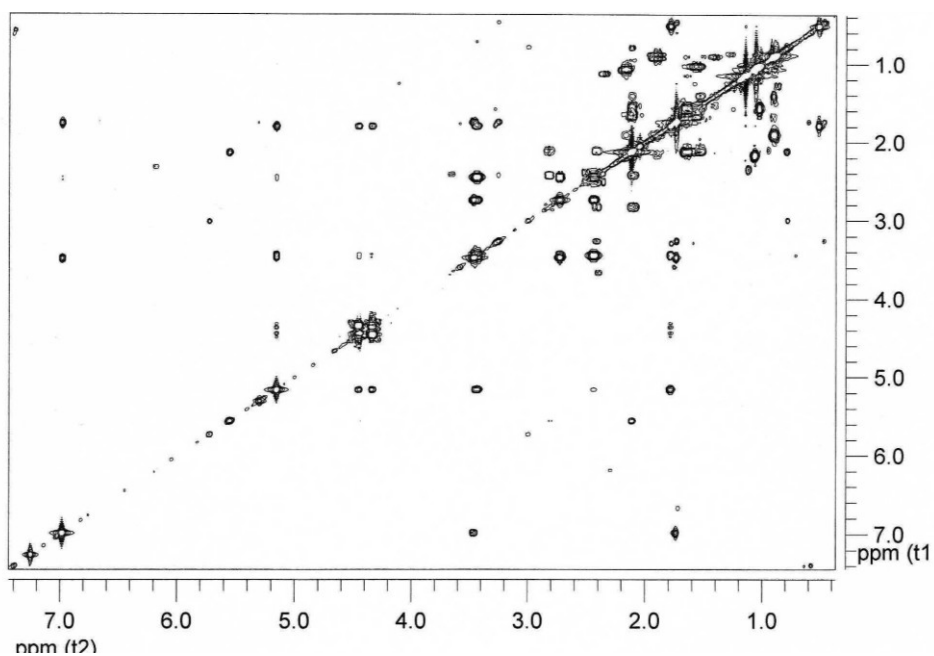
^1H NMR spectrum (500 MHz) of compound **94** in CDCl_3 .



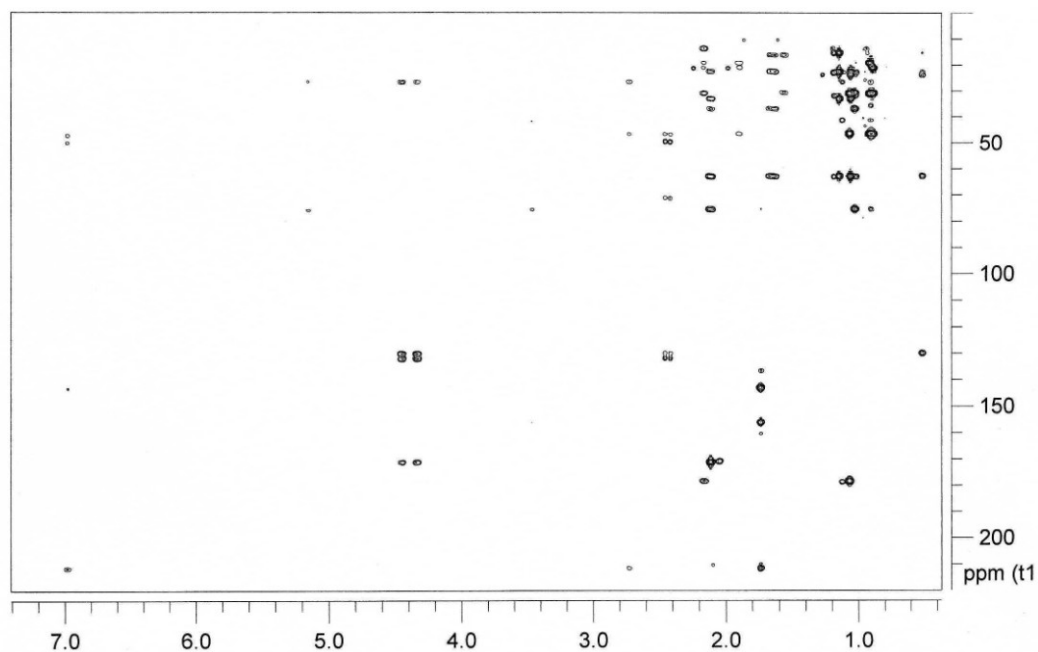
^1H NMR spectrum (500 MHz) of compound **97** in CDCl_3 .



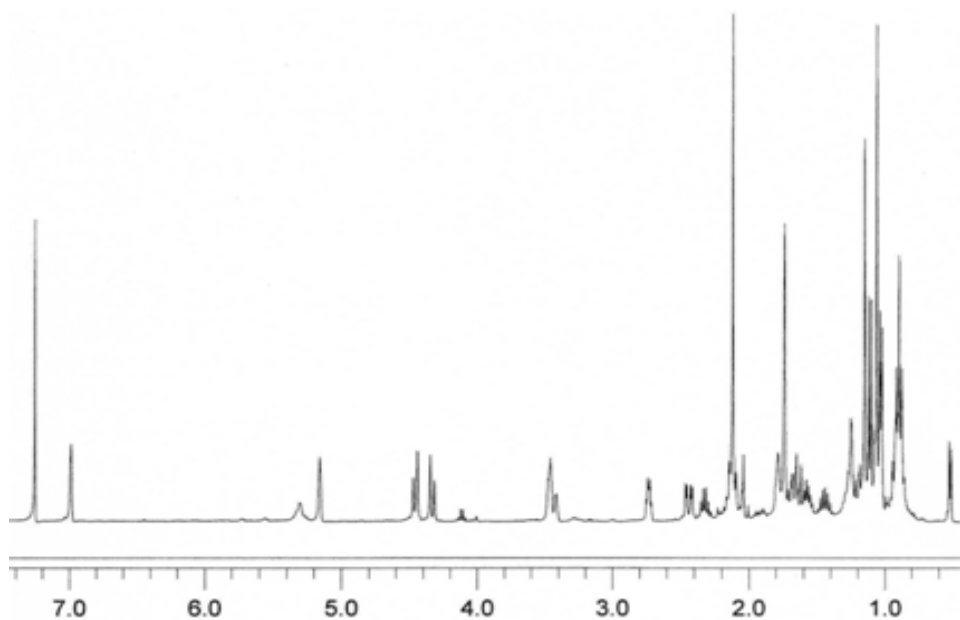
COSY 2D NMR spectrum (500 MHz) of compound **97** in CDCl_3 .



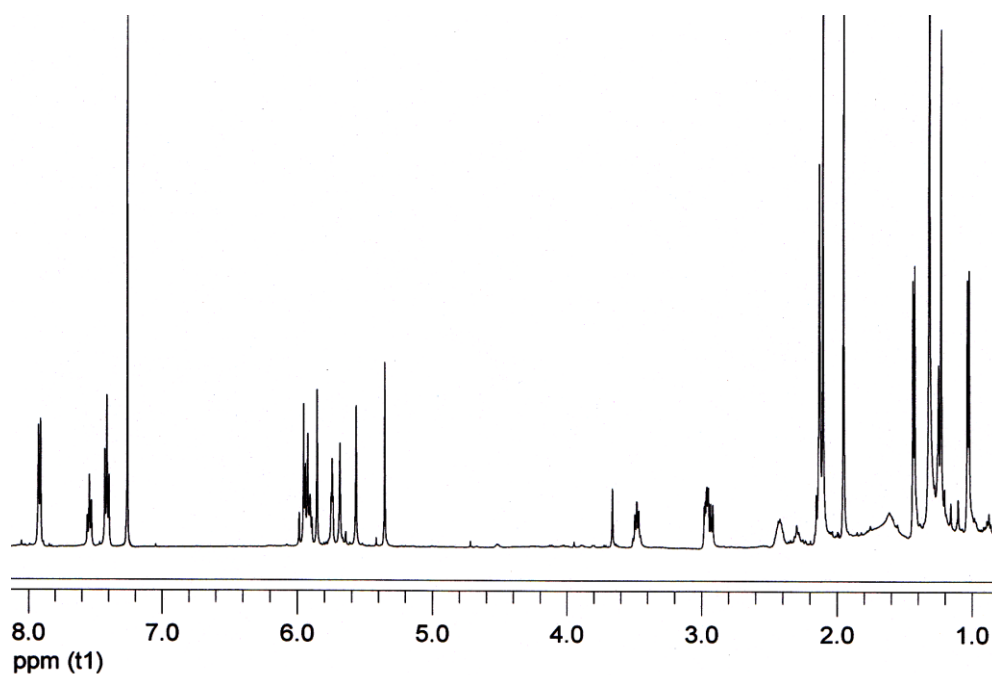
HMBC 2D NMR spectrum (500 MHz) of compound **97** in CDCl₃.



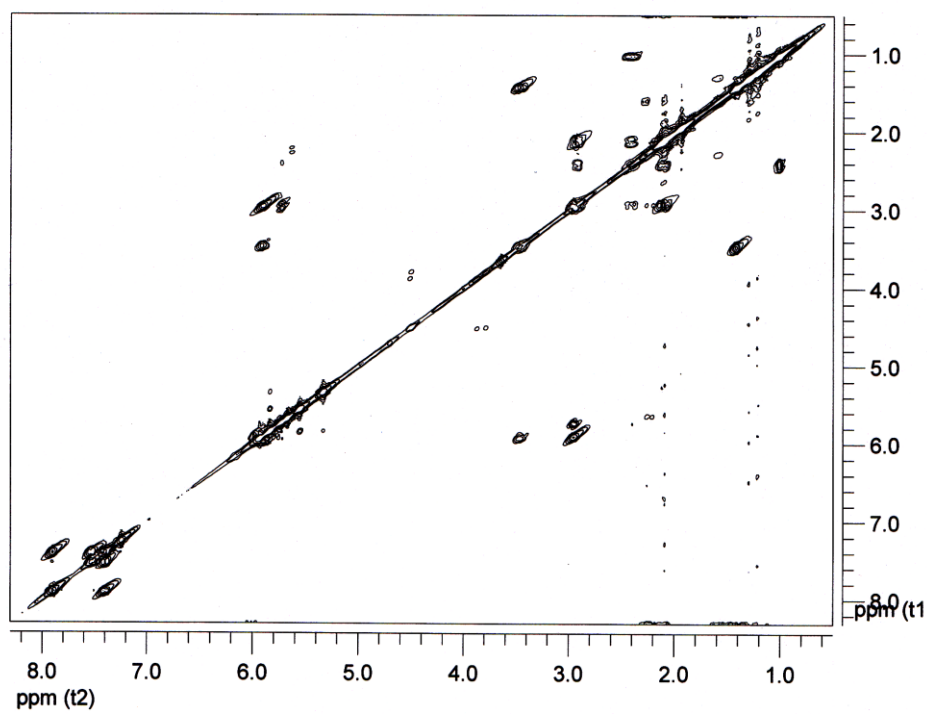
¹H NMR spectrum (500 MHz) of compound **98** in CDCl₃.



^1H NMR spectrum (500 MHz) of compound **101** in CDCl_3 .



COSY 2D NMR spectrum (500 MHz) of compound **101** in CDCl_3 .



5.3. Computational details of compounds 57-63

Table 5.1. Occurrence rate (%) of 1,2-dioxane ring conformations of **8-14** considering PM6 conformers within 5 Kcal/mol from the global minimum

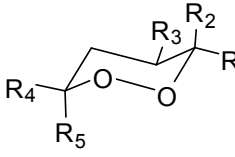
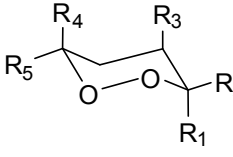
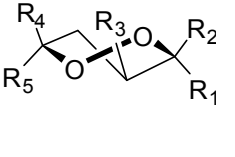
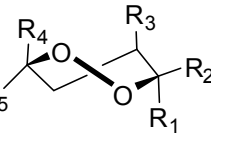
	Chair A	Chair B	Skew Boat A	Skew Boat B
Cm p				
57	48	13	26	13
58	43	13	34	10
59a	60	6	30	4
59b	49	17	29	5
60a	54	4	38	3
60b	58	4	35	2
60c	61	9	23	7
60d	52	16	25	7
61a	72	2	21	5
61b	62	4	28	6
61c	77	4	17	2
62a	67	5	26	2
62b	53	15	30	2
63a	71	2	25	2
63b	66	6	24	4

Table 5.2. Occurrence rate (%) of PM6 conformers within 5 Kcal/mol from the global minimum owning interatomic distances suitable for a radical shift from O1 or O2 ($\leq 3\text{\AA}$) and steric accessibility of the endoperoxide oxygens lone pairs.

Cmp	C3 axial alkyl side chain		C3 equatorial alkyl side chain		C6 axial alkyl side chain		C6 equatorial alkyl side chain	
	1,4H- shift	1,5H- shift	1,4H- shift	1,5H- shift	1,4H- shift	1,5H- shift	1,4H- shift	1,5H- shift
8	0	0	0	0	0	0	0	0
9	0	0	32	0	0	0	0	0
10a	0	0	24 ^a	3 ^a	0	0	0	0
10b	17	1	0	0	0	0	0	0
11a	0	0	0	0	0	0	18 ^a	6 ^a
11b	0	0	0	0	21 ^a	3 ^a	0	0
11c	0	0	0	0	0	0	22 ^a	3 ^a
11d	0	0	0	0	20 ^a	3 ^a	0	0
12a	0	0	30 ^a	2 ^a	0	0	20	5
12b	0	0	23 ^a	5 ^a	20	1	0	0
12c	30	0	0	0	0	0	22 ^a	4 ^a
13a	0	0	0	0	14 ^a	3 ^a	16 ^a	4 ^a
13b	0	0	0	0	22 ^a	1 ^a	20 ^a	4 ^a
14a	0	0	13 ^a	4 ^a	9	0	16	2
14b	17	1	0	0	11 ^a	0	18 ^a	4 ^a

^a Putative bioactive conformations.

5.4. Computational details of compound 76.

Table 5.3. Conformational Analysis of **14** in the Gas

	ΔE^a	ΔG^b	P% ^c
76A	0.00	0.00	65.00
76B	0.42	0.37	35.00

^aRelative energy (kcal/mol). ^bRelative Gibbs free energy (kcal/mol).

^cConformational distribution calculated at the at the B3LYP/6-31G(d) level in the gas phase.

Table 5.4. Optimized Z-Matrices of **76** in the Gas Phase (A).

1				2			
C	-0.070760000	-2.050208000	-0.274246000	C	-0.075803000	-2.048953000	-0.186025000
C	-3.913568000	0.046237000	0.152298000	C	-3.910849000	0.046667000	0.290581000
C	-4.810933000	0.625830000	-0.653821000	C	-4.081294000	0.301917000	1.592557000
C	-4.165775000	-0.073315000	1.638590000	C	-5.031886000	0.239315000	-0.702356000
C	0.856030000	-2.825262000	0.296794000	C	0.856893000	-2.818340000	0.382839000
C	-0.296527000	3.833596000	-0.392523000	C	-0.263921000	3.832228000	-0.417017000
O	2.106351000	2.407140000	-0.336890000	O	2.127545000	2.384919000	-0.434473000
C	1.574426000	0.077759000	1.626604000	C	1.641581000	0.115066000	1.617300000
C	3.054420000	-0.216214000	1.628428000	C	3.118380000	-0.192959000	1.581927000
C	3.581752000	-0.406334000	0.407341000	C	3.606284000	-0.420324000	0.350826000
C	2.506450000	-0.266220000	-0.606165000	C	2.501319000	-0.297833000	-0.632658000
O	2.599698000	-0.479117000	-1.799055000	O	2.555793000	-0.543938000	-1.821576000
C	4.986977000	-0.729736000	0.012673000	C	4.996042000	-0.766249000	-0.078075000
H	-0.073335000	-0.320574000	-1.477810000	H	-0.105400000	-0.344111000	-1.422688000
H	-1.347444000	-0.144187000	1.283738000	H	-1.299576000	-0.108954000	1.370763000
H	-2.308758000	2.072938000	0.085809000	H	-2.266014000	2.101371000	0.197464000
H	-2.605762000	-0.298270000	-1.488073000	H	-2.612162000	-0.282624000	-1.370447000
H	-2.637361000	-2.356110000	0.778330000	H	-2.637157000	-2.301468000	0.919173000

H	-3.476062000	-2.496864000	-0.767142000	H	-3.490372000	-2.475955000	-0.611589000
H	-1.297472000	-3.748963000	-0.772517000	H	-1.325755000	-3.747907000	-0.624765000
H	-1.310589000	-2.459780000	-1.976209000	H	-1.347628000	-2.485860000	-1.856962000
H	-4.643076000	0.720718000	-1.724113000	H	-3.289218000	0.169516000	2.324852000
H	-5.750560000	1.020733000	-0.274689000	H	-5.033948000	0.654951000	1.979180000
H	-3.403093000	0.456064000	2.224769000	H	-4.765349000	0.996672000	-1.452447000
H	-5.140077000	0.346679000	1.905433000	H	-5.235496000	-0.687188000	-1.256441000
H	-4.147701000	-1.118160000	1.972477000	H	-5.959681000	0.553199000	-0.214424000
H	1.770656000	-2.446118000	0.736906000	H	1.782160000	-2.436272000	0.797453000
H	0.734961000	-3.905890000	0.313430000	H	0.729417000	-3.897551000	0.424176000
H	0.134865000	4.102095000	-1.363491000	H	0.367207000	4.364906000	0.303164000
H	0.299414000	4.357998000	0.362904000	H	-1.287610000	4.210589000	-0.339185000
H	-1.325938000	4.201891000	-0.351151000	H	0.128499000	4.079548000	-1.409893000
H	1.351629000	0.990110000	2.195225000	H	1.444566000	1.044620000	2.167246000
H	1.010259000	-0.731800000	2.106742000	H	1.085120000	-0.675139000	2.136966000
H	3.617572000	-0.272150000	2.557204000	H	3.709240000	-0.229291000	2.494302000
H	5.402330000	0.072712000	-0.608725000	H	4.996797000	-1.689586000	-0.668935000
H	5.633461000	-0.866367000	0.884736000	H	5.401092000	0.019500000	-0.727033000
H	5.014930000	-1.641232000	-0.595771000	H	5.666449000	-0.892500000	0.777323000

Table 5.5. Frequencies of **76** at the B3LYP/6-31G* Level in the Gas

76A	42.2907	47.6641	58.4454	63.3436	87.2221	114.5908	120.2151
	124.547	136.468	164.525	179.3605	195.3316	197.4674	211.7265
	221.3312	258.4839	261.8258	276.0028	292.44	301.5613	322.8498
	338.7079	359.9033	366.5604	390.0987	400.6622	457.6766	477.0069
	493.1077	506.7708	530.321	561.7681	601.7547	647.7869	656.0384
	661.8678	674.4815	707.3434	724.4083	744.2789	756.6094	775.0509
	829.3904	835.0724	849.2338	862.296	901.8237	916.2502	924.4245
	933.6563	939.8286	947.8196	956.0303	987.5944	990.0369	1008.2543
	1028.8456	1030.2146	1039.3976	1046.3244	1063.1193	1072.8041	1072.8041
	1077.3564	1081.5512	1086.1222	1093.1754	1102.4072	1123.4503	1123.4503
	1145.4719	1166.3199	1188.3065	1220.5579	1233.6207	1250.9439	1250.9439
	1260.0417	1271.1844	1293.0659	1306.6538	1311.457	1335.9208	1335.9208
	1339.2221	1356.2095	1362.5401	1375.9573	1377.6923	1388.8397	1388.8397
	1401.9142	1407.7623	1442.3338	1443.8204	1445.8063	1479.306	1479.306
	1486.8753	1502.6772	1503.3955	1512.0612	1514.4399	1515.6168	1515.6168
	1516.4056	1517.6075	1521.6609	1528.7934	1712.5058	1716.229	1716.229
	1725.0077	1732.1592	1749.5169	1812.0345	2983.6497	3000.341	3000.341
	3016.8478	3023.6982	3040.6049	3044.8273	3045.5841	3052.2372	3052.2372
	3055.9831	3073.7577	3086.1064	3090.1059	3092.992	3107.6916	3107.6916
	3112.7198	3129.8892	3134.5196	3136.1322	3155.7446	3164.0639	3164.0639
3170.4858	3195.5639	3231.9488	3259.5264				
76B	36.4624	42.7754	52.9919	62.9927	89.0895	110.8221	117.4908
	127.7412	140.8402	157.1063	179.7207	194.8828	203.2207	212.2353
	221.3514	256.0121	260.7923	275.9933	293.4209	299.3921	312.9682
	340.3318	359.9515	367.2302	387.169	401.4726	452.1482	478.7054
	484.1783	510.3931	530.0829	556.1544	600.6975	648.0219	654.8333
	662.609	674.7846	708.7558	721.8678	730.8519	757.713	774.9311
	833.8788	841.665	860.0717	864.6116	902.0668	917.4658	921.9904
	923.7945	939.3075	947.5559	956.4659	983.8215	988.5362	1002.8369
	1028.9326	1029.4597	1038.0781	1043.8545	1061.2735	1071.7843	1071.7843
	1077.0966	1081.0541	1086.2537	1094.5006	1101.0214	1125.0682	1125.0682
	1145.5555	1166.5133	1187.4177	1222.7026	1234.4904	1246.4951	1246.4951
	1256.5293	1267.6352	1276.0575	1293.6704	1311.7978	1335.6897	1335.6897
	1348.6194	1356.2668	1362.1969	1376.7278	1384.4323	1391.7043	1391.7043
	1404.6474	1411.0028	1439.5295	1442.0153	1443.5456	1473.267	1473.267
	1486.5035	1502.2716	1503.1142	1508.2355	1513.1116	1514.351	1514.351
	1516.4773	1516.9964	1520.5199	1523.9366	1712.5363	1715.1377	1715.1377
	1730.5573	1732.8016	1749.6701	1812.1789	2986.7384	2997.2034	2997.2034
	3009.0043	3016.754	3030.9268	3043.7845	3045.47	3052.3365	3052.3365
3055.9235	3073.9689	3076.3456	3083.9187	3090.8322	3107.8497	3107.8497	
3112.8119	3127.5734	3134.5213	3135.4914	3162.8547	3170.6582	3170.6582	
3171.6506	3195.4086	3235.7317	3260.1101				

ACKNOWLEDGMENTS

This work is the result of a multidisciplinary research project. The contribution of the following researchers from other Universities has been of key importance:

- ✚ Prof. Giovanni Appendino (Dipartimento di Scienze Chimiche, Alimentari, Farmaceutiche e Farmacologiche, Università del Piemonte Orientale, Novara, Italy) for collaboration on the projects on *Cannabis sativa*, *Euphorbia macroclada* and *E. bungei*.
- ✚ Prof. Vincenzo Di Marzo (Endocannabinoid Group and Cybernetic Institute, Pozzuoli (NA), Italy) for the evaluation of interaction on CB receptors.
- ✚ Prof. Claudio Trombini (Dipartimento di Chimica “Giacomo Ciamician”, Università di Bologna, Bologna, Italy) for the design and the development of the synthesis of antimalarial 1,2- dioxanes.
- ✚ Prof. Caterina Fattorusso (Dipartimento di Chimica delle Sostanze Naturali, Università di Napoli “Federico II”, Napoli, Italy) for computational studies.
- ✚ Prof. Donatella Taramelli (Dipartimento di Sanità Pubblica-Microbiologia-Virologia, Università di Milano, Milano, Italy) for *in vitro* antimalarial test.
- ✚ Prof. Annette Habluetzel and Prof. Fulvio Esposito (Scuola di Scienze del Farmaco e dei Prodotti della Salute, Università di Camerino, Camerino (MC), Italy) for *in vivo* antimalarial test and for the sample of *Azadirachta indica*.
- ✚ Prof. Werner E.G. Müller (University Medical Center of Johannes Gutenberg University Mainz, Germany) for providing us extracts of *Jatropha curcas* and for antiproliferative tests on the isolated diterpenoids.
- ✚ Dr. Paolo Luciano (Dipartimento di Chimica delle Sostanze Naturali, Università di Napoli “Federico II”, Napoli, Italy) for quantum mechanical TDDFT calculations.

It is a pleasure to convey my gratitude to them all in my humble acknowledgment.

I would like to express my sincere gratitude to my supervisor, Prof. Orazio Tagliatela Scafati, who has been a great intellectual support with his expertise

and research insight. He gave me a constant encouragement and enriched considerably my Ph.D. experience.

I would also like to thank prof. Ernesto Fattorusso, all professors, researchers and PhDs of Department of Natural Products Chemistry. In particular I wish to thank Dr. Masteria Yunovilsa Putra, my funny colleague and my best friends Dr. Roberta Teta and Dr. Cristina Perinu for helping me during PhD period and for the nice moments spent together.

I am grateful to all students, who spent a period in laboratory 513, with love I will remember all of them.

I wish to thank my boyfriend Alessandro for his support, strong encouragement and for believing in me. Thanks, in particular, for the patience accorded me during the my thesis-writing period.

Lastly, and most importantly, I wish to thank my entire extended family for providing a loving environment for me. Thank to my mother for her unconditional support and attentive care. A thought and a thanks to my father, my strength. To him I dedicate this thesis.

Thanks all

Giuseppina Chianese